UNIVERSITAT DE BARCELONA

Deciphering the mechanisms of neuroblastoma metastasis by multi-omics analysis

Jara Martín Serrano

Universitat de Barcelona *Facultat de Medicina*

PhD Program in Biomedicine

Molecular and cellular biology of cancer program

"Deciphering the mechanisms of neuroblastoma metastasis by multi-omics analysis"

Jara Martín Serrano

Developmental Tumor Biology Laboratory

Institut de Recerca Sant Joan de Déu (IRSJD) – Pediatric Cancer Center Barcelona (PCCB)

PhD Candidate

Jara Martín Serrano

Thesis directors **Thesis Tutor**

Silvia Mateo-Lozano, PhD Jaume Mora, MD, PhD Alfons Navarro, PhD

Abstract

Neuroblastoma (NB), a heterogeneous pediatric cancer originating from neural crest cells, presents significant clinical challenges due to its high propensity for metastasis. Approximately 60% of patients show widespread disease at the initial diagnosis, with metastasis being the primary cause of NB-related deaths. Understanding the molecular mechanisms underlying metastasis is crucial for the development of targeted therapies for patients with high-risk NB. The metastatic process involves complex interactions between tumor cells and their surroundings, with the tumor microenvironment (TME) playing a key role. Current in vivo models for NB metastasis have limitations, including incomplete replication of metastatic stages and difficulties in tumor tracking and removal. To address these issues, we established a spontaneous metastasis *in vivo* model, allowing surgical removal of the primary tumor, ensuring animal survival, and enabling metastatic cells to colonize distant organs. Our primary objective was to identify a metastatic signature by multi-omics analyses, comparing primary tumors and metastatic masses from the *in vivo* model. Whole-genome expression analysis revealed that the most differentially expressed genes (DEGs) were linked to lymphatic metastasis. Data integration emphasized the crucial role of the tumor microenvironment (TME) in NB metastasis, particularly the TGF-β signaling pathway, suggesting a potential interaction between TME and NB mesenchymal (MSN) phenotype induction. Podoplanin (PDPN), a transmembrane glycoprotein, has emerged as a metastatic marker for NB. It exhibited distinct cellular localization in NB cells, with a prominent cytoplasmic location in metastasis. Notably, the membrane localization of PDPN in NB cells was linked to higher lymph node infiltration rates in NB patients. By generating NB stable cell lines overexpressing PDPN, we demonstrated that elevated levels were correlated with increased metastatic potential. Since PDPN expression is known to be induced by interactions with stromal and immune cells, we confirmed that NB cells can promote the polarization of fibroblasts into cancer-associated fibroblasts (CAFs) and that PDPN is induced in NB cells through interactions with CAFs, suggesting a potential feedback loop. Furthermore, PDPN expression was also induced by low oxygen conditions and cytokines exposure, confirming significant regulation by TME. Notably, NB cells released PDPN via exosomes to facilitate the establishment of pre-metastatic niches by inducing stromal cell polarization.

Altogether, our data provide further insight into the mechanisms underlying metastasis in NB and identify a novel NB metastatic driver to target, crucial to improve patients' outcome.

Index

INTRODUCTION

1. A brief introduction to cancer

In 2018, the World Health Organization (WHO) estimated that cancer was the second leading cause of death worldwide, resulting in approximately 9.6 million deaths globally (1). Cancer is widely recognized as a disease characterized by abnormal and uncontrolled cell growth that can affect almost any tissue in the body. Furthermore, these abnormal cells can invade neighboring tissues and spread throughout the body, a process known as metastasis (1).

In recent years, a substantial proportion of adult cancers, ranging from 90% to 95%, have been linked to lifestyle factors, such as smoking, dietary habits, exposure to ultraviolet light, and various pathogens (2). Environmental factors throughout an individual's lifetime can result in increased cellular stress, leading to higher mutation rates, which, in turn, contribute to the development of cancer. Notably, most adult cancers are associated with aging, which causes the accumulation of mutations over many years or decades, thereby increasing the risk of developing cancer (3). In addition, most adult tumors originate from epithelial cells that undergo malignant transformation, a process known as carcinogenesis (3). This leads to the formation of carcinoma tumors that have a high tendency to invade distant organs. The remaining cancer cases are linked to genetic predispositions and inherited mutations that significantly increase the risk of developing cancer. In these cases, individuals may carry specific genetic mutations through generations, accounting for a low percentage of cases, typically ranging from 5% to 10% (4).

2. Childhood cancer

Childhood cancer is a rare disease that emerges during childhood, adolescence, and young adulthood (5). According to the WHO, cancer is the leading cause of death among children aged 14 years and younger in developing countries (2). Every year, approximately 400.000 individuals aged 0 to 19 years are diagnosed of cancer (2).

In contrast to adult tumors, much less is known about the origins of childhood cancer. Knowledge about the cell of origin is limited, however, it is known that most tumors arise due to an impairment in fetal cell differentiation, leading to the excessive production of undifferentiated cells (5). Consequently, each childhood tumor exhibits biological characteristics that resemble its tissue ontogeny and behaves similarly to the embryonic cells from which it originates (5). Pediatric cancer typically exhibits a low mutation rate, in addition, some childhood tumors may be related to genetic predisposition syndromes like the Li-Fraumeni syndrome, as the WHO described in its childhood cancer report in 2021 (6). The origin of childhood tumors usually arises from non-epithelial cells, with hematological and neural cell linages being the most affected during embryogenesis (2, 5). As a result, tumors such as leukemia, central nervous system tumors, lymphoma or neuroblastoma have a higher global incidence compared to others (**Figure 1**)(7).

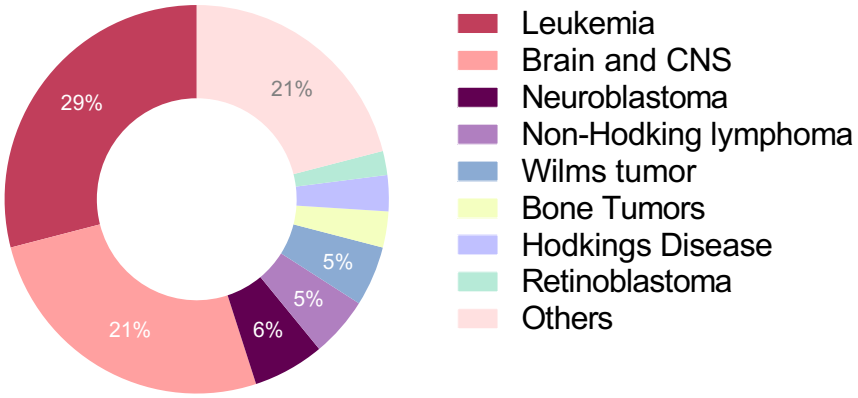

Figure 1. Childhood tumors global incidence. The incidence of pediatric tumors varies depending on histology and type, with diagnoses made annually for patients aged 0 to 19 years. Among these tumors, leukemia is the most frequent, impacting pediatric patients at an alarming rate, followed closely by brain and central nervous system (CNS) tumors. Neuroblastoma is categorized as the third most common pediatric tumor globally. Adapted from (7)

2.1. Neuroblastic tumors

Neuroblastic tumors, which originate from neural crest precursor cells (NCCs), are among the most common pediatric malignancies and contribute substantially to the overall mortality rate of childhood cancers. The presence of considerable heterogeneity in these tumors poses difficulties in both the diagnosis and the development of effective treatment strategies (8). Neuroblastic tumors, which includes ganglioneuroma (GN), ganglioneuroblastoma (GNB) and neuroblastoma (NB), are the most common extra-cranial solid tumors in the first five years of life. Approximately 95% of GNB and NB occur in patients under the age of five, while GN presents in older children (9). These tumors frequently appear in the adrenal medulla (40%), the mediastinum (25%), the retroperitoneum (25%) and the cervical sympathetic ganglia (3-5%)(9).

It is important to emphasize that neuroblastic tumors display a wide range of clinical outcomes. NB, in particular, is a highly malignant tumor that is linked to the stage of cellular differentiation (10). The lack of cellular differentiation contributes to the tumor's ability to invade surrounding tissues, grow faster, and resist conventional treatments. On the other hand, neuroblastic tumors with a higher degree of cellular differentiation may have a more favorable prognosis. For instance, GN are characterized by well-differentiated ganglion cells and behaves as a benign tumor (11). Understanding the relationship between the malignant potential of neuroblastic tumors and the stage of cellular differentiation is crucial for developing effective therapeutic interventions. This understanding can help in developing therapies that can benefit patients with these rare and challenging tumors.

3. Neuroblastoma

NB is the most prevalent extra cranial childhood tumor, and accounts for 15% of all childhood cancer-related deaths. This type of cancer primary affects children under the age of five, with a median age at diagnosis of 18 months (8). Epidemiological data from international registries indicate a disproportionately higher incidence of NB in high-income countries than in low- and middle-income nations, which may reflect disparities in healthcare accessibility and diagnostic capabilities (**Figure 2**)(12). In Spain, approximately 66 annual cases are diagnosed in children under the age of five, while it drops to 1.7 among children aged 10 to 15 years (13).

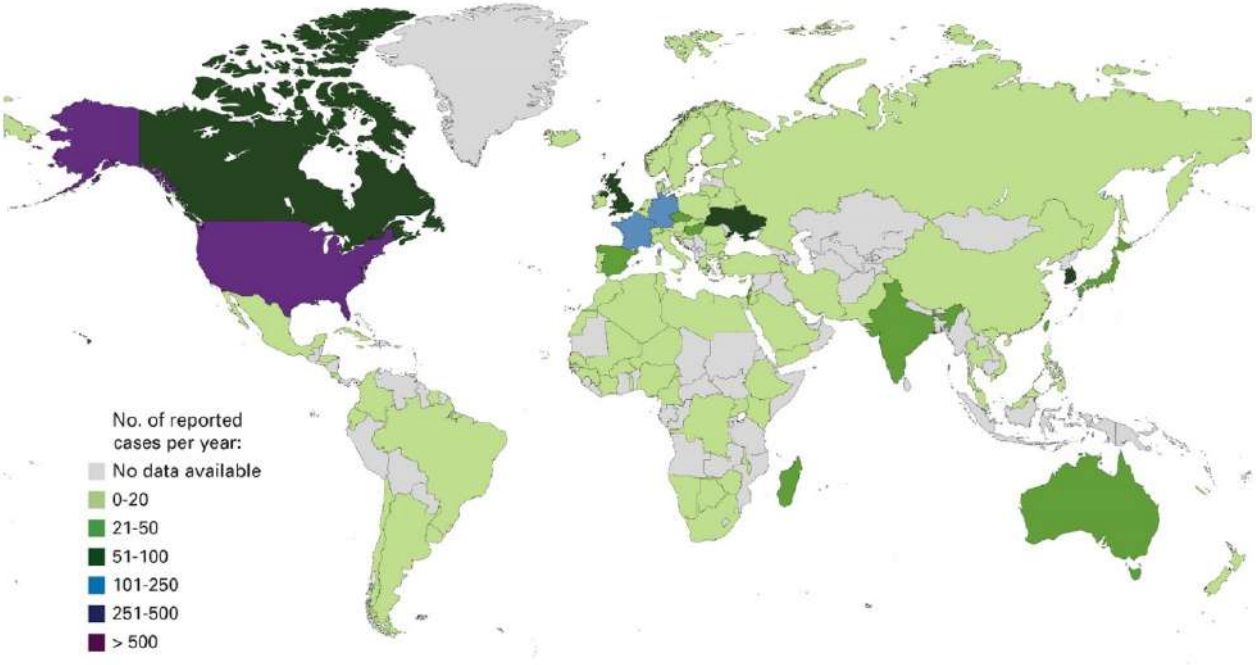

Figure 2. Global incidence distribution of NB. The map illustrates the number of NB cases reported annually in various countries. The color-coded map indicates that the incidence levels varied, with light green representing low incidence (0-20 cases), medium green (21-50 cases), dark green (51-100 cases). Light blue signifies an incidence of 101-250 cases, and dark blue, 251-500 cases per years. Purple represents more than 500 cases. Gray regions indicate areas in which data were not available. Highest incidence rates of NB are found in North America and certain parts of Europa and Asia (12).

Notably, patient prognoses typically demonstrate a negative correlation with age at diagnosis, as infants under 18 months show a remarkable 88% overall survival rate (OS). It is worth mentioning that certain NB tumors exhibit spontaneous regression without any therapeutic intervention (14). However, survival rates decline to 49% for infants aged 18 months to 12 years and plummet to less 10% for adolescents and young adults (15). The increase in survival rate is associated with increased cellular differentiation. Conversely, NB with higher levels of undifferentiated cells exhibit higher aggressiveness and metastatic potential compared to those affecting younger patients (16).

3.1. Clinical presentation

NB arises anywhere along the sympathetic nervous system, as it originates from the sympathoadrenal lineage. NB presents in the adrenal gland in almost 50% of cases, followed by the retroperitoneum in 20%, and the mediastinum in 16% (17). NB can manifest in two clinical formats: localized and disseminated.

Localized NB usually present as solitary primary lesions without any accompanying symptoms (18). However, in some cases, the compression of adjacent organs and tissues due to tumor volume can lead to early diagnosis. Most localized tumors are diagnosed in newborn children, who tend to have a better prognosis and higher survival rates (18). However, approximately 50% of NB patients present with disseminated disease at the time of diagnosis (19). The most common site of metastasis is the bone marrow (BM; 70%), followed by bone (56%), and lymph nodes (31%)(10). Unlike localized tumors, primary symptoms of disseminated NB are frequently related to the primary tumor site or metastatic location. For instance, systemic symptoms such as abdominal distension, bone pain and/or orbital ecchymosis, commonly known as "*raccoon eyes*", are only observed in patients with metastatic tumors (17)(**Figure 3**).

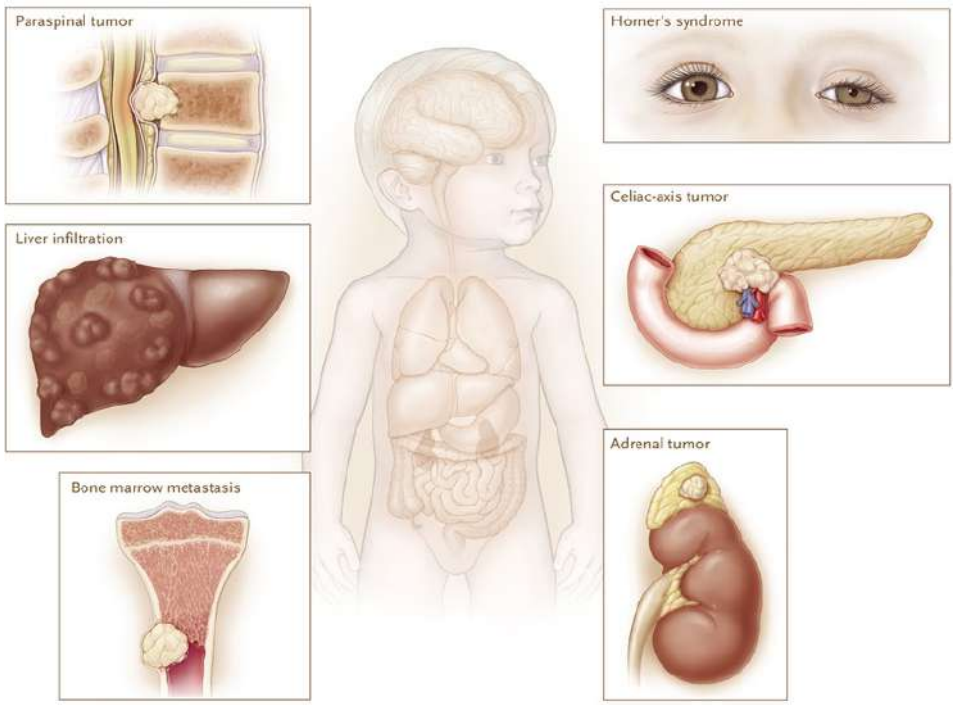

Figure 3. Clinical presentation of NB. The diverse presentations of NB emphasize the intricacy and heterogeneity of this malignancy in pediatric patients. It can manifest as a paraspinal tumor, leading to spinal cord compression; liver infiltration resulting in hepatomegaly and nodules, BM metastasis and as a celiac-axis tumor, affecting nearby abdominal organs. Adrenal tumors are prevalent due to NB's origin. Additionally, NB patients can present Horner's syndrome, characterized by ptosis, miosis and anhidrosis, as consequence of cervical sympathetic chain involvement.

NB is a complex disease well known for its diverse range of symptoms and ability to exhibit different behaviors as it progresses, resulting in various NB disseminated subtypes. The 4S (S for Special) subtype primarily affects children under 18 months of age and often undergoes spontaneous regression without aggressive therapeutic intervention (14). Tumor masses can be numerous and are typically detected in the liver, the skin, and/or BM but with no skeletal involvement (20). This subtype is characterized by a favorable disease course, leading to a long-term survival rate of 65-92% (14). As previously described for localized tumors, one of the main complications of tumor masses is compression of adjacent organs, which is also a frequent clinical complication of 4S-NB. Although conventional treatments are usually not necessary due to spontaneous regression, the excessive size of some masses can compress the lungs, kidneys, or parts of the circulatory system. In these cases, intervention with chemotherapy may be necessary to reduce tumor volume (21).

Another of the NB subtypes is characterized by the exclusive dissemination to lymph nodes (22). This subset of patients are categorized as stage 4N (N for Nodal) and are associated with a more differentiated cellular stage, leading to a more favorable outcome (22). Initially, this subgroup was identified within a cohort of patients who had not received treatment, primarily affecting children over 1 year old, and exhibiting an improved event-free survival (EFS). In the 2000s, a retrospective study observed that this subgroup, when receiving less intensive treatment, had significantly better EFS and OS compared to other stage 4 cases (22).

3.2. Clinical assessment: diagnosis and monitoring

Imaging methods are currently the primary approach for identifying tumor lesions either at diagnosis or disease evolution. Various techniques are employed, including sonography, computed tomography, bone scintigraphy, and I-metaiodobenzylguanidine (I-MIBG) (**Table 1**). Although these approaches have proven to be effective in detecting neuroblastoma tumors, they face limitations when dealing with more differentiated cell states or when tumor cells lose their distinctive properties as the disease progresses (23, 24).

To accurately diagnose NB tumors, a biopsy or surgical resection must be performed to obtain a representative sample from the primary or metastatic location. The histopathological features are assessed based on the neuroblastic tumor classification system, including the examination of synaptophysin, chromogranin A, and neuron-specific enolase (10). In addition, liquid biopsies, such as urine, plasma or even bone marrow aspirates, are analyzed to determine levels of catecholamine metabolites (dopamine, homovanillic and/or vanilylmandelic acids) and other biomarkers (10, 25). Notably, high concentrations of serum

lactate dehydrogenase, ferritin or chromogranin are detected in patients with high-risk neuroblastoma (HR-NB) (26). However, these concentration levels are non-specific and non-independent predictors of disease outcome (8, 26).

Table 1. Imaging techniques most commonly used for the diagnosis of NB.

Technique	Technology	Detection
Sonography	High-frequency sound waves	Abdominal mass, adenopathy and congenital NB
Computed tomography	Computerized X-Ray	Calcifications
Bone scintigraphy	Phosphates or diphosphonates labeled with technenitum (99m)	Bone abnormalities
Positron emission tomography (PET)	Radiotracers	Changes in metabolic process
Radiologic I-metaiocobenzylguanidine (I-MIBG)	Radiotracer similar to norephinephrine/noradrenaline	Neuroendocrine cells

Additionally, molecular and histological techniques are necessary to determine the status of minimal residual disease (MRD). Different types of samples can be used for MRD assessment, with BM aspirates being the most commonly used in the case of NB. MRD status, in NB, is evaluated using real-time quantitative polymerase chain reaction (RT-qPCR) by analyzing the expression levels of NB specific markers, such as Cyclin D1 (*CCND1*), GD2 synthase (*B4GALNT1*), Paired-like homeobox 2b (*PHOX2B*) or Tyrosine Hydroxilase (*TH*).

3.3. Risk stratification system and histology

The continuous improvement of the NB features and behavior have led to various stratification systems. In the past, the histological characteristics of NB had been the most crucial factors in the evaluation of NB stratification. More recent classification systems have included biological characteristics.

The International Neuroblastoma Pathology Classification (INPC) is based on a previous classification method proposed by Shimada H *et al*. (27). The INPC classifies NB tumors into four groups based on their neuroblastic maturation grade and the presence of Schwannian stroma, distinguishing NB (stroma-poor), GNB (stroma-rich), GN (stroma-dominant) and GNB nodular (composite). Additionally, the INPC system includes a subclassification of NB tumors associated to histological characterization. Of note, NB is characterized as a small, blue, round cell tumor, consistent with an undifferentiated cellular stage. Therefore, three main sub-groups are distinguished based on their cellular differential stage, including undifferentiated (U), poorly differentiated (PD) and differentiated (D)(**Figure 4)**. Moreover, the INPC also considers

other biological and histological characteristics, such as patient age at diagnosis and the Mitosis-Karyorrhexis Index, to differentiate between favorable and unfavorable histology (28).

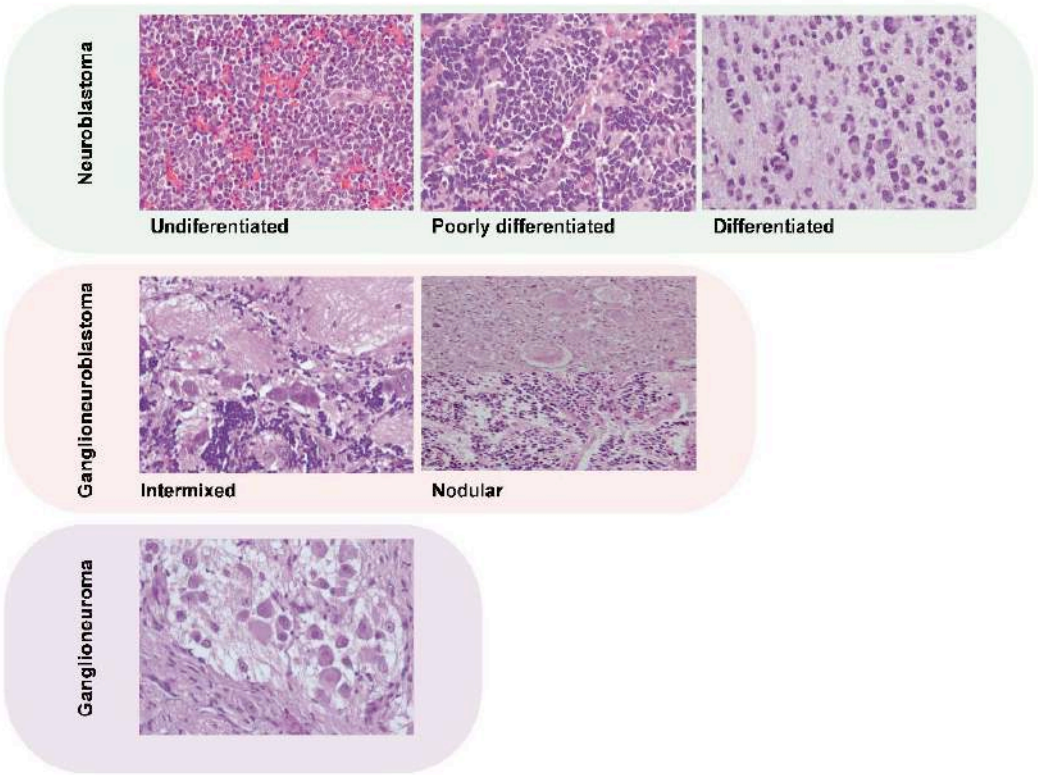

Figure 4. Histology of neuroblastic tumors. Histological examples of neuroblastic tumors in HE staining at 40x magnification included NB (undifferentiated, poorly differentiated and differentiated), GNB (intermixed and nodular), and GN.

Since the original INPC system was established in 1999 by Shimada *et al.*, several other classification systems have been implemented. However, it is important to note that the International Neuroblastoma Staging System (INSS) has been in use since 1986. Despite its widespread adoption across numerous countries, the INSS faces challenges in accurately distinguishing between NB tumor stages because of its reliance on the extent of surgical resection, as showed in **Table 2** (29). Furthermore, the INSS encounters difficulties in properly staging patients with localized tumors that exhibit tumor regression and assessing extra-regional regional lymph node involvement (29).

Table 2. INSS classification system for NB (29)

Stage	*Definition*
Stage 1	Localized tumors are confined to the area of origin. Complete gross resection with or without microscopic residual disease; identifiable ipsilateral and contralateral lymph node negative for tumor. Adherent lymph nodes in direct continuity with and removed with the tumor may be positive for the tumor. A grossly resected midline tumors without ipsilateral (with: Stage 2A) or contralateral (with: Stage 2B) lymph node involvement is considered Stage 1.
Stage 2A	Unilateral with incomplete gross resection; identifiable ipsilateral and contralateral lymph node negative for tumor.
Stage 2B	Unilateral with complete or incomplete gross resection; with ipsilateral lymph node positive for tumor identifiable contralateral lymph node negative for tumor.
Stage 3	Tumor infiltrating across midline with or without regional lymph node involvement; or unilateral tumor with contralateral lymph node involvement or midline tumor with bilateral lymph node involvement.
Stage 4	Dissemination of tumor to distant lymph nodes, bone marrow, liver, or other organs except as defined in Stage 4S.
Stage 4S	Localized primary tumor as defined for stage1 or 2 with dissemination limited to liver, skin, and bone marrow (<10 % of nucleated marrow cell are tumor cells)

In 2004, NB experts developed the International Neuroblastoma Risk Group (INRG) Staging System (INRGSS) to enhance the classification criteria of the INSS system. INRGSS aimed to compare risk-based clinical trials across various global regions by establishing consistent patient cohorts prior to treatment (29). This was accomplished by utilizing standardized tumor imaging assessments, including preoperative and diagnostic imaging as shown in **Table 3**. INRGSS system serves as a risk classification tool that is applied before initiation and during reassessments (29).

Table 3. INRGSS classification system of NB risk before treatment.

INRG Stage	Age (months)	Histologic Category	Grade of Tumor Differentiation	*MYCN*	11q Aberration	Ploidy	Pretreatment Risk Group
L1/L2		GN maturing; GNB intermixed					A Very low
L1		Any, except GN maturing or GNB intermixed		NA			B Very low
				Amp			K High
L2	< 18	Any, except GN maturing or GNB intermixed		NA	No		D Low
					Yes		G Intermediate
	≥ 18	GNB nodular; neuroblastoma	Differentiating	NA	No		E Low
					Yes		H Intermediate
			Poorly differentiated or undifferentiated	NA			
				Amp			N High
M	< 18			NA		Hyperdiploid	F Low
	< 12			NA		Diploid	I Intermediate
	12 to < 18			NA		Diploid	J Intermediate
	< 18			Amp			O High
	≥ 18						P High
MS	< 18			NA	No		C Very low
					Yes		Q High
				Amp			R High

In addition, as many other tumors, NB is risk-categorized based on patient outcome, comprising low-risk NB (LR-HR), encompassing localized tumors with a favorable prognosis; intermediated-risk NB (IR-NB), including both localized and multi-focal tumors with varying outcomes; and HR-NB, predominantly presenting as disseminated disease and associated with an unfavorable prognosis. Considering the diverse systems of classification for NB, it is noteworthy that a significant number of biological factors are shared among them. These includes age at diagnosis, histology, and some genetic alterations. The latter have garnered interest and have been linked to patient outcomes, thus making their implementation crucial for NB stratification (30).

3.4. Biological features

Similar to other pediatric tumors, NB has an etiology that is not yet fully understood. Nevertheless, certain biological features have been associated with its development, including genetic alterations, chromatin remodeling, and chromosomal copy number abnormalities. While these characteristics have been identified, it is important to acknowledge that the ultimate cause of NB remains unclear.

3.4.1. Genetic alterations

3.4.1.1. *MYCN* amplification

Gene amplification involves an increase in the copy number of a specific gene or chromosomal region. This process often arises from genetic alterations such as duplication or

rearrangement, leading to the presence of multiple copies. Amplification of a gene can result in the overexpression of its encoded protein, leading to abnormal cellular functions and contributing to various diseases, including cancer. In cancer, gene amplification is frequently associated with oncogenes, which promote cell proliferation and survival, thereby driving tumor growth and progression (31). The first gene discovered to be amplified in tumor cells was *MYC*, which was identified in neuroendocrine cells derived from different carcinomas (31). This gene belongs to a family of transcription factors, which play a crucial role in regulating cellular processes associated with tumor initiation and progression (32). Notably, *MYC* plays a significant role in the early stages of embryogenesis, disappearing in adulthood, particularly in neuroectodermal tissues (32).

In the early 1980s, amplification of the *MYCN* oncogene was observed in the undifferentiated phenotype of NB tumors. Since then, this amplification has been classified as the principal genetic anomaly associated with poor prognosis in NB patients; hence, HR-NB (32). Different studies, including genetically engineered mouse models of NB, have demonstrated that *MYCN* amplification in NB is associated to tumorigenesis and malignancy, promoting invasive and metastatic behavior. It contributes to all metastatic characteristics required by a tumor cell, such as adhesion, motility, invasion and degradation of the surrounding matrices (32). Notably, at the time of diagnosis, 20% of NB patients exhibit more than four-fold increase in the *MYCN* signal number and increased up to 50% when patients with disseminated disease are analyzed exclusively (8).

Unfortunately, targeting *MYCN* as a therapeutic option faces challenges due to the limited availability of small molecules that can effectively bind to its α-helix surface (32). Moreover, its inherent function as a transcription factor complicates this process. Currently, many therapeutic strategies focus on targeting this pathway using compounds such as Aurora Kinase A (AURKA) or bromodomain and extra-terminal motif inhibitors (BET)(32).

3.4.1.2. ALK alterations

The anaplastic lymphoma kinase (*ALK*) gene is a proto-oncogene that encodes a receptor tyrosine kinase involved in growth and proliferation. In NB, amplification or mutations of *ALK* are commonly associated with an aggressive tumor behavior and poor prognosis. Additionally, gain-of-function mutations in the receptor tyrosine kinase *ALK* have been linked to a rare form of NB known as familial NB, which accounts for approximately 1-2% of diagnosed cases and is inherited in an autosomal-dominant manner within families. Approximately 50% of cases exhibiting *ALK* mutations are associated with familial NB (33). Additionally, single-base missense mutations cluster in the regulatory regions of the kinase domain of ALK is also

frequently found in sporadic NB, presenting different mutated domains compared to familial NB. Notably, most NB tumors express full-length *ALK* (33).

Studies have shown that the incidence of ALK mutations is increased in relapsed NB tumors. In certain situations, mutations were found present at extremely low allele frequencies in the primary tumor, but others emerged as the *novo* mutations (34).

3.4.1.3. LIN28B polymorphism

Patients with HR-NB frequently exhibit overexpression of the protein-coding gene *LIN28B*. This protein is essential for regulating the expression levels of the let-7 family of microRNAs (miRNAs). Overexpression of *LIN28B* suppresses the expression of let-7 miRNAs, resulting in derepression of their target genes (35). Among its various functions, the protein has been observed to contribute to the maintenance of a more pluripotent state in embryonic stem cells by repressing let-7 (35). Several studies have demonstrated the involvement of *LIN28B* in NB by enhancing the dissemination capacity of NB cells to initiate and sustain metastatic colonization and outgrowth, among other functions (35). Additionally, the expression levels of *LIN28B* have been associated with *MYCN*, which acts as a positive regulator of this protein (35).

3.4.2. Chromatin remodeling

3.4.2.1. ATRX and TERT mutation

NB does not exhibit a high mutation rate, but approximately of 8.6% of HR-NB patients display loss-of-function mutations or deletions of the Alpha Thalassemia/Mental Retardation Syndrome X-Linked (*ATRX*) gene, which encodes an SWI/SNF-like protein that regulates DNA-histone interactions, facilitates chromatin remodeling during transcription, DNA replication, and repair; and plays a role in restructuring the nucleosome (36). Intragenic deletions of ATRX are linked to early disease progression and relapse, among other factors. In NB, ATRX alterations have been associated with poor prognosis, particularly in older patients, with mutations being the most frequent alteration in HR-NB (36).

Notably, mutations in *ATRX* and *MYCN* amplification are mutually exclusive, and they do not occur simultaneously with Telomerase Reverse Transcriptase (TERT) rearrangements (36). TERT is involved in telomere maintenance and is associated with deregulated DNA methylation (58). Peifer *et al.* (2015) described a subgroup of HR-NB characterized by *MYCN* amplification and TERT rearrangement; however, these tumor cells did not display any changes in telomerase length. Conversely, patients with exclusive TERT rearrangements exhibit significant upregulation of their transcriptional levels, resulting in an unfavorable prognosis (36).

3.4.3. Segmental chromosomal copy number alterations

A subset of NB display alterations in regions of the genome, particularly caused by copy number variation (CNVs), which has been associated with different outcomes depending on CNVs type and affected region (8). Two different types of CNVs modifications can be observed in cancer, distinguishing numerical CNVs, which result in gains or losses of entire chromosomes; and structural CNVs which involve gains and losses of specific portions of chromosomes (37). Numerical CNVs are frequently observed in localized tumors of LR-NB, whereas structural CNVs are more prevalent in HR-NB.

3.4.3.1. Gain of segmental chromosomal copy number

In NB, gains of segmental chromosomal copy numbers are frequently observed in the 1q, 2p and 17q regions (8). Among them, the most prevalent cytogenetic alteration in NB is the gain of chromosome arm 17q, which accounts for 46 % of the cases (37). Patients presenting this gain usually harbor an advanced stage of the disease (37).

3.4.3.2. Loss of segmental chromosomal copy number

Remarkably, the most frequent chromosomal alterations linked to unfavorable outcomes in NB involve segmental deletions in arms 1p and 11q. Deletions of 1p are the most prevalent, occurring in 30-45% of cases, and are strongly associated with *MYCN* amplification. In addition, this deletion has been associated to a poor treatment response and unfavorable outcome. Although the significance of chromosomal alterations is still being studied, the affected regions typically contain tumor suppressor genes such as *CHD5*, *CAMTA1*, *CASZ1*, *KIF1B*, and miR-34a (38). Conversely, deletions of 11q are observed in 30 % of the cases and are mostly detected in older patients, which are classified as HR-NB. The relationship between 11q deletions and *MYCN* amplification is either inverse or absent, unlike 1p deletions (39).

3.5. Treatment

Treatment approaches vary depending on the risk stratification of the tumor, ranging from tumors that spontaneously regress to highly aggressive tumors that rapidly progress despite intensive therapy. Patients with favorable prognosis often benefit from conservative protocols involving surgery only with/without chemotherapy. In some cases, surgical intervention alone may be sufficient. In contrast, HR-NB patients require a combination of multimodal therapies, including chemotherapy, surgery, high-dose chemotherapy with autologous stem cell transplantation, radiotherapy, and immunotherapy (40). Treatments are typically associated with tumor stages, as illustrated in **Figure 5**, which also presents the different treatment phases conducted in NB patients depending on tumor stage.

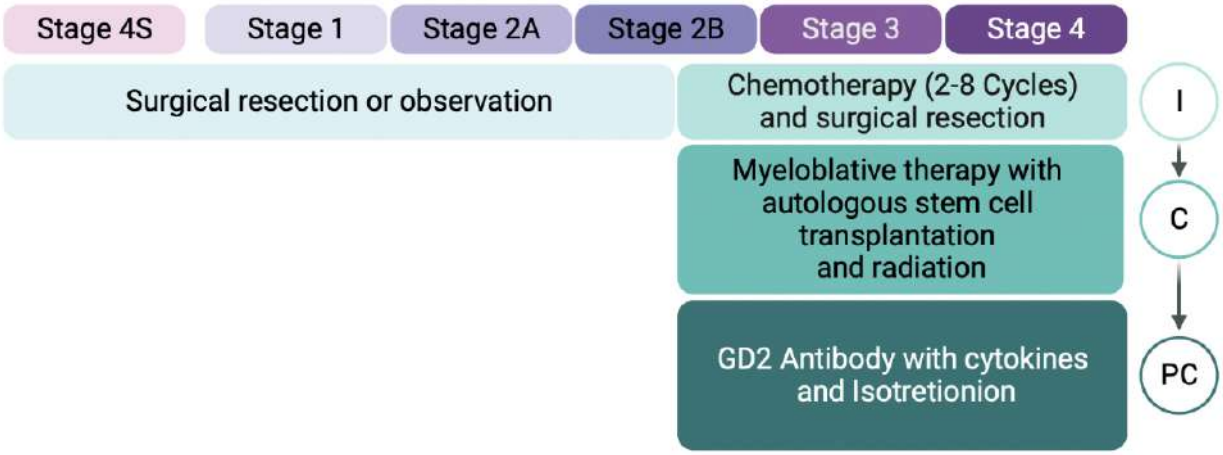

Figure 5. Overview of treatment protocol for various NB risk classifications. LR-NB patients (stage 1-2B) are typically managed with clinical observation or surgical resection, as asymptomatic tumors often regress spontaneously (stage 4S). Intermediate-risk patients received moderate-dose chemotherapy and surgical removal of the primary tumor. In contrast, HR-NB patients require intensive multimodal therapy which is divided into three phases: induction (I), consolidation (C), and post-consolidation (PC). The first phase involves intensive chemotherapy and primary tumor resection, whereas the second includes radiotherapy, high-dose ablation chemotherapy and autologous stem cell transplantation. The final phase, maintenance or post-consolidation, involves anti-GD2 immunotherapy and differentiation agents.

After confirming the diagnosis of HR-NB, the initial phase of treatment is known as induction chemotherapy (I). This phase aims to reduce the tumor's size an eliminate any cancer cells that may have spread beyond the primary site. It usually entails chemotherapy, occasionally combined with surgery or radiation therapy, depending on the tumor location and disease spread. Notably, surgical resection of the primary tumor is often performed either before or after induction chemotherapy, depending on the tumor response and surgical feasibility. Of note, surgeons strive to remove as much of the tumor as possible, while minimizing damage to the surrounding healthy tissues. Subsequently, the consolidation phase (C) is initiated in order to eradicate any remaining cancer cells and minimize the risk of recurrence. This treatment may involve high-dose chemotherapy with autologous stem cell rescue and radiation therapy. Finally, patients with a high risk of relapse receive maintenance therapy (PC) to help prevent cancer recurrence. PC phase involves mainly anti-GD2 immunotherapy (40). After completing active treatment, patients attend regular follow-up visits to monitor for any signs of recurrence or late effects of treatment. Follow-up care include physical examinations, imaging studies, and blood tests to ensure timely detection of disease recurrence or late effects.

Unfortunately, establishment of new strategies such as autologous stem cell transplantation along with chemotherapy during consolidation phase is not enough to improve OS of NB patients (41). For instance, patients who have achieved complete remission through standard protocols often experience a recurrence of NB, which is characterized by a more aggressive form of cancer that has spread to metastatic sites, as well higher resistance to chemotherapy

(42). Therefore, numerous approaches trying to incorporate immunotherapy in the previous phases in order to increase OS had been performed. Immunotherapy works by stimulating the patient's inherent immune system to fight cancer. In NB, the uniform presence of the ganglioside GD2 on the cellular surface makes it a great candidate to be targeted by immunotherapy (43). The implementation of anti-GD2 immunotherapy has demonstrated significant survival results in NB, however, it is worth mentioned that expression in normal tissues, particularly in unmyelinated type C nerve fibers is associated with neuropathic pain (42). Of note, monoclonal antibodies against GD2 (mAbs) trigger antibody-dependent cell-mediated cytotoxicity (ADCC) conducted by natural killer cells, granulocytes and macrophages, which activity has been proven to be boost by cytokines stimulation. Hence, combination of anti-GD2 mAbs with granulocyte macrophages colony-stimulating factor (GM-CSF) exhibited enhances ADCC response *in vitro* and *in vivo* (42). Last year, researchers from Hospital Sant Joan de Déu achieved promising outcomes by combining chemotherapy with anti-GD2 mAbs and GM-CSF in primary refractory patients. These patients exhibited a complete response to the treatment during I phase (44). Notably, their results emphasized the relevance of implementing immunotherapy in early phases of treatment, considering chemo-resistant capacity of the tumor. Since they demonstrated that a lack of response to chemotherapy is linked to an absence of ADCC response, which is more likely to occur in NB tumors after I phase (44).

Although significant advances have been made in the fields of immunotherapy, further investigation and development of new treatments are still necessary (40). Nonetheless, NB tumors are known for their low immunogenicity, which is characterized by a limited presence of immune cells within the tumor, often referred to as a "cold tumor" (45). Due to the immature system of pediatric patients, the effectiveness of treatment is complicated. In addition, to develop new therapies for NB other obstacles must be overcome such as metastatic disease at the time of diagnosis and a lack of knowledge of NB origins. Nevertheless, whereas chimeric antigen receptor T-cell (CAR-T) therapy has shown promising results in other tumors, NB studies have revealed limited benefits due to the immunosuppressive nature of the tumor microenvironment (TME), which prevents the infiltration of T-cells at the tumor site (40). Briefly, CAR-T development for NB has been challenging due to absence of specific targets on tumor cells. Some common molecular targets, such as GD2, CD171, and B7 homolog 3 protein (B7H3), has shown some improvement in patient prognosis in clinical trials. **Table 4** shows the most relevant clinical trials conducted in NB so far.

Table 4. Current clinical trials in NB tumor using immunotherapies against GD2 and different CAR-T.

Clinical Trail	Phase	Status	Target	Country	Outcome	REF
NTC05489887	II	Recruiting	GD2 mAb (Naxitamab)	USA and Canada	The proportion of patients with a complete response or partial response to naxitamab with standard induction therapy for subjects with newly-diagnosed HR-NB according to INRC.Collected by the presence of radiologically assessable disease by cross-sectional CT or MRI imaging and/or by MIBG or PET scans and bone marrow response.	
NCT03786783	II	Active, not recruiting	GD2 mAb with GM-CSF	USA, Australia and New Zealand	To assess the feasibility and tolerability of administering ch14.18 (dinutuximab) and sargramostim (GM-CSF) in combination with a multi-agent chemotherapy regimen during cycles 3-5 of the Induction phase for patients with newly-diagnosed high-risk neuroblastoma.	
NCT03294954	I	Recruiting	GD2-CAR NKT cells	USA	Maximum tolerated dose of autologous NKTs expressing a 2nd generation GD2-specific chimeric antigen receptor administered to patients with relapsed or refractory neuroblastoma.	(46)
NCT03373097	I/II	Recruiting	GD2-CART01	Italy	Phase I - Identification of the dose limiting toxicity (DLT) Phase II - Antitumor effect	(47)
NCT05650749	I	Recruiting	GPC2 CAR T cells	USA	Determine the Maximum Tolerated Dose of GPC2 CAR T cells Frequency of Adverse Events Following GPC2 CAR T cell administration	
NCT01460901	I	Completed	GD2 CAR modified Tri-virus specific cytotoxic t-cells	USA	Number of Participants With Immediate and Short Term Toxicity of Infusion Over 8 Weeks. Peak Transgene Copy Number Per 1000ng PBMC DNA Death Within 8 Weeks of Infusion	(48)
NCT04483778	I	Active, not recruiting	B7H3 CAR T Cell	USA	Assess the safety and tolerability of cellular immunotherapy utilizing ex-vivo expanded autologous T cells genetically modified to express B7H3-specific CAR (Arm A), as well as, a bispecific B7H3xCD19 CAR (Arm B) with or without the combination with pembrolizumab (Arm C), and so on	(49)

3.6. Origen of Neuroblastoma

Childhood tumors are believed to arise from precursor cells during embryonic or early postnatal development. Studies have suggested that pediatric tumors originate from failures in the development and differentiation of stem or progenitor cells, as demonstrated using *in vivo* models (5). NB originates from precursor cells of the NCCs within the developing sympathetic nervous system. The neural crest is a complex organ comprising multipotent and migratory cell populations that gives rise to various tissues during embryogenesis, such as components of the peripheral nervous system, including neurons and ganglia of the sympathetic nervous system as well as the adrenal medulla (50). During embryogenesis, NCCs from the dorsal region undergo epithelial-mesenchymal transition (EMT), which involves loss of cellular polarity and adhesion properties (**Figure 6A**)(51). Additionally, EMT process enables delamination, migration, and subsequent differentiation into diverse cell types contributing to the distribution of the cell to various anatomical structures. As mentioned before, pediatric tumors arise from an alteration of the differentiation program, and therefore, if the program is disrupted at this stage, undifferentiated cells may migrate to different locations within the fetus, leading to multi-focal disease. Furthermore, dysregulation of these processes can induce changes in cell specification leading to neoplastic lesions, potentially culminating in neuropathic syndromes or different childhood tumors such as neuroblastic or sarcoma tumors (50).

Recent studies have shed light onto the intricate origin of NB, revealing the cellular and molecular dynamics contributing to the initiation and progression of NB. Even though single-cell data from different studies exhibited contradictory information regarding the cell of origin, all studies agree that NB emerged from early differentiation stages of the neural crest which presents a migratory capacity, hence, the undifferentiated cells could settle into different location of the embryo, emerging as multi-focal disease, as previously described (52-54). The use of genetic linage-tracing during the adrenal tissue development, has demonstrated that there are two waves of migrating NCCs responsible for the development of sympathoadrenal lineages, distinguishing between early and late NCCs giving rise to different cell lineages and arriving at different anatomical structures within the embryo (**Figure 6B**) (53, 55, 56).

Moreover, alterations in neural crest development are correlated with the metastatic rate of NB. *Delloye-Bourgeois* and Castellani propose that NB cells derived from neural crest cells hijack embryonic programs, transitioning from physiological migration to metastatic dissemination (20). This hypothesis underscores the dynamic nature of NB metastasis, as tumor cells exhibit adaptability when exploring developmental pathways. This phenomenon reveals a complex interplay between tumor cells and molecular programs reminiscent of

embryonic development. In addition, it is hypothesized that during neural crest formation, NB cells migrate towards sympathoadrenal derivatives, where they remain dormant until their presentation, displaying distinct foci for primary tumors (**Figure 6C**)(20). Despite this developmental theory, several studies have demonstrated that NB cells exhibit an aggressive phenotype, enabling tumor cells to metastasize from their primary location.

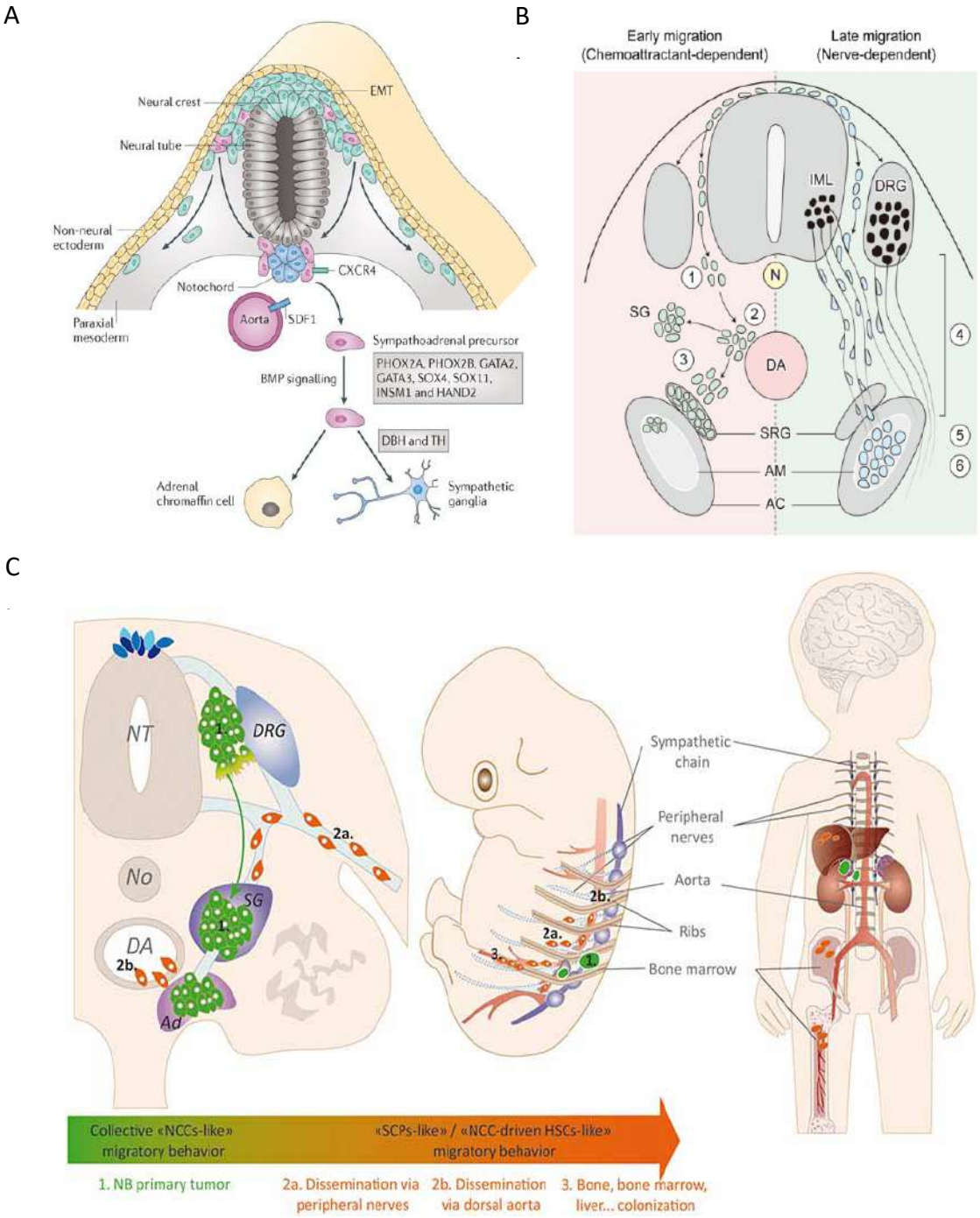

Figure 6. Theories on the origin of NB: exploring potential pathways. **A.** NB development from neural crest (51). **B.** Distinct developmental modes of the different cell linages related to NCCs (53). **C.** NCCs/SCPs migratory strategies potentially used or hijacked by neuroblastoma (NB) cells (20).

4. The metastatic process in cancer

Metastasis is a hallmark of cancer characterized by the spread of cancer cells from the primary tumor site to distant organs or tissues, where secondary tumors or metastases can develop. The capacity of tumor cells to metastasize is the primary cause of death, accounting for over 90% of cancer-related deaths. Notably, only a small fraction (less than 0.01%) of tumor cells have the ability to metastasize, at least in adult tumors (57). This is because, in order to complete the entirely metastatic process, a tumor cell must leave the primary tumor site, navigate the circulatory system, overcome immune checkpoints, and establish themselves at secondary sites where they can proliferate to form a secondary tumor mass, leading to numerous adaptive changes in each phase (**Figure 7**)(58). Understanding the dynamics of this process is crucial to identify molecular targets for therapy (57).

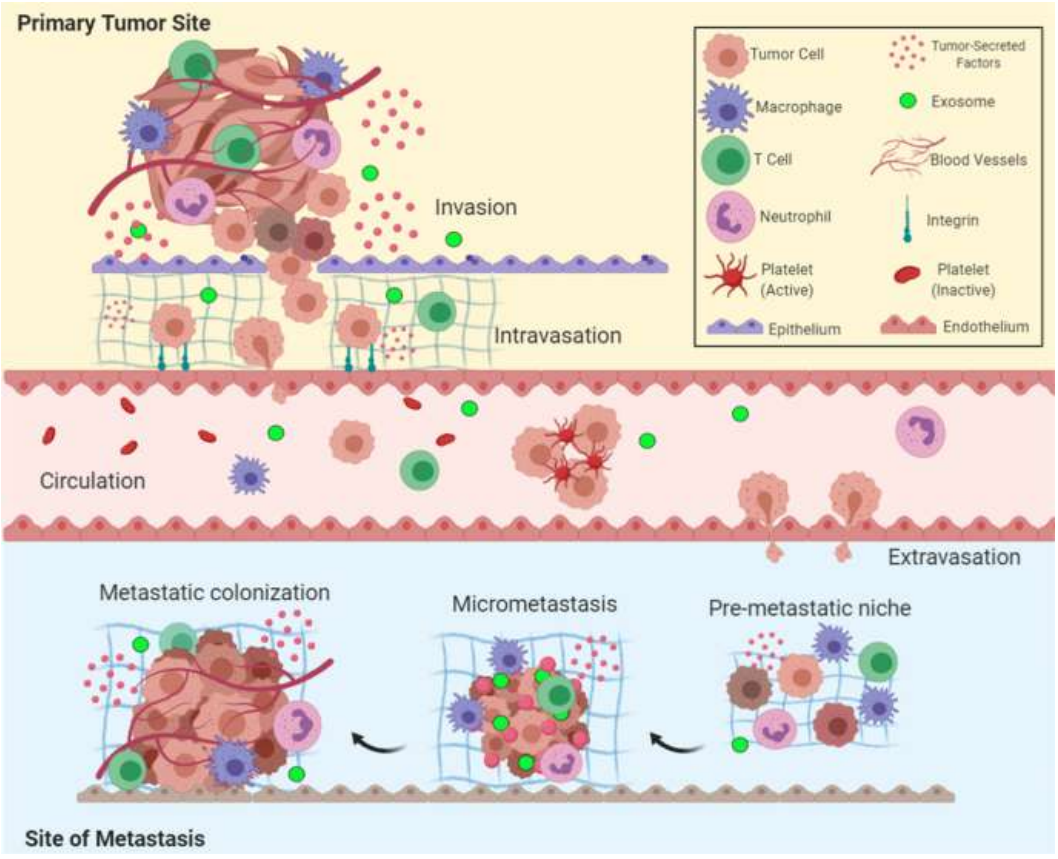

Figure 7. Schematic overview of the metastatic process described in adult tumors. Metastasis is a complex process that includes several critical steps, each of which is essential to the process. First step is invasion, in which cancer cell penetrate the surrounding extracellular matrix and invade adjacent tissues. Second step is intravasation, in which these cells enter the bloodstream or lymphatic system by breaching the endothelial lining of blood or lymph vessels. Then, cancer cells travel through the circulatory system, often encountering shear stress and immune surveillance. Extravasation is the fourth step, in which cancer cells exit the bloodstream or lymphatic system by adhering to and penetrating the vessel walls in a secondary tissue. Finally, cells establish new tumors at secondary sites by proliferating and adapting to the microenvironment, known as colonization step (58).

Most studies investigating the mechanism of metastasis have been conducted on adult tumors, which are primary epithelial in nature. However, the understanding of the mechanisms of pediatric tumor metastasis is incomplete, since few studies have been conducted in this area. Additionally, some pediatric tumors often develop as multifocal disease, which further complicates the understanding of the metastasis process. Therefore, in the following section, the process of metastasis is discussed in the context of adult tumors, although it could help to shed light onto the mechanisms of metastasis in childhood cancer.

As previously mentioned, tumor cells undergo a series of steps during the metastatic process, the first of which involves leaving the original tissue. In order to do so, the cell must undergo genetic changes and acquire a new cellular phenotype with the ability to migrate, in the process of EMT (57). Of note, only a low percentage of cells, which exhibit high cell plasticity ability, can undergo EMT process. Cell plasticity refers to the capacity of cells to change their phenotype or functional characteristics in response to internal or external cues, is known as cell plasticity (59). Hence, the initiation of EMT process in cells, specifically epithelial cells of adult tumors, is triggered by the exposure to various factors such as cytokines, growth factors, or hypoxic factors (60). Nonetheless, EMT is not a linear process; recent studies have determined that this transition is not permanent, and tumor cells can switch between stages as required in each step of the metastasis process, in the inverse process known as mesenchymal-to-epithelial transition (59).

Numerous studies on the metastatic process have described that transition processes occur at various steps. Depending on the requirement on each step, the tumor cells switch between phenotypes, including transitional stages. As mentioned before, these cellular changes are triggered by external factors, hence, both processes have been associated with a variety of microenvironments within the tumor. In addition, phenotypes not only determine cellular abilities, but also displayed changes in the microenvironment by releasing certain factors. In particular, the mesenchymal (MSN) phenotype is observed near endothelial and inflammatory cells, and promotes an inflammatory response by releasing chemokines and proteins to attract immune cells and stimulate angiogenesis (59).

Over the years, more than 100 genes have been discovered to predict invasive potential, suggesting that primary tumor cells exhibit a metastatic signature associated to each metastatic step. The main genes are summarized in **Table 5** (57). Interestingly, not all of them are related to physical modifications in the cellular phenotype; some are also influenced by tumor conditions, such as the prevalence of hypoxic conditions, which can lead to metabolic changes and the promotion of angiogenesis, thereby promoting the spread of cancer cells (57). Due to the elevated number of studies in this area, it has been possible to identify the

distinct capabilities of cancer cells at various stages of EMT (**Figure 8**). This underscores the significance of establishing a metastatic signature to assess the aggressiveness and overall condition of the tumor.

Table 5. Most frequently altered genes during each step of the metastatic process.

Mechanism in the metastatic process	*Gene*	*Underlaying mechanism*
Initiation of tumorigenesis	*RAS*	Activation of MAPK signaling pathway
Local Intravasation and Infiltration	*ROCK*	Actin remodeling and cell migration
Local Intravasation and Infiltration	*AKT*	Cell growth
Local Intravasation and Infiltration	*RAF*	Activation of MAPK/ERK pathway
Local Intravasation and Infiltration	*CDC42*	Actin filaments depolymerization
Bloodstream circulation	*FMS*	Modulation of macrophages activity and tumor invasion
Bloodstream circulation	*BCL2*	Inhibits apoptosis
Intravascular arrest	*CD44*	Interaction with endothelial selectins to facilitate arrest
Intravascular arrest	*ITGB1*	Interaction with endothelial ligands to promote adhesion
Immune escape	*PD-L1*	Inhibit immune response via PD-1 interaction on T cells
Immune escape	*CTLA-4*	Inhibits T cell activation
Distant dissemination	*MMP9*	Facilites invasion by degradation of extracellular matrix
Distant dissemination	*CXCR4*	Interacts with CXCL12, promoting homing to distant organs
EMT	*TWIST1*	Induce EMT
EMT	*ZEB1*	Repressed epithelial markers
EMT	*Snail*	Inhibits E-cadherin expression
EMT	*Slug*	Repressed E-Cadherin

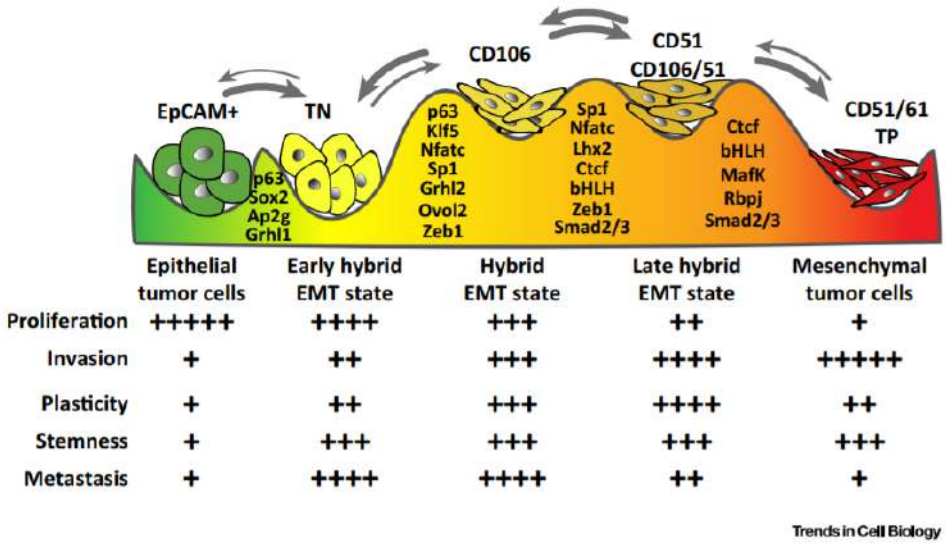

Figure 8. EMT transition states exhibit different functional characteristics. Schematic representing EMT transition states and the transcription factors driving each transition. The thickness of the arrows signifies the flexibility of plasticity of the various EMT states. A summary of the proliferation, invasion plasticity, stemness, and metastatic capacity of the different EMT transition states is provided, with the scale ranging from low (+) to very high (++++) (59).

Upon reaching their metastatic capacity through genetic alterations, tumor cells infiltrate the bloodstream. By undergoing intravasation, they gain access to the lumen of the vasculature. This process can occur actively or passively, depending on the type of tumor cell, microenvironment, and vasculature (57, 58). Additionally, research has shown that cancer cells can enter blood vessels either singly or in groups that included various cell types, such as stromal and immune cells, along with the tumor cells themselves.

Once inside the circulatory system, circulating tumor cells (CTCs) may endure the interactions presented by the microenvironment in circulation and eventually extravasate to distal organs (58). The suppression of leukocyte activation by neutrophils or the formation of a coating shield by platelets can contribute to the prevention of CTC detection by immune cells and shielding tumor cells from the physical stresses of circulation (57, 58).

Conventional studies of metastasis are focused on the dissemination of cells through the blood system, but it is known that the same tumor cells are able to disseminate via lymphatic system (57, 61). In this case, a change in fatty acid oxidation is induced in tumor cells invading the lymph nodes by the yes-associated protein (YAP) transcription factor, demonstrating the capacity of some tumor cells to invade by lymphatic pathways (61).

Upon arrival at the capillaries, CTCs become stucked. They can either migrate through the endothelial wall or proliferate within the vessel, which can result in the rupture of microvessels before extravasation and colonization (57). The rate of extravasation depends on the permeability of the organ; organs with sinusoidal vessels have high permeability and,

therefore, higher rates of metastasis (57). In contrast, organs with tight barriers require molecular modifications, primarily related to integrins, for tumor cells to extravasate (57).

Additionally, before tumor cells arrive at a secondary site, the microenvironment of the distant organ is altered to facilitate tumor colonization after extravasation. This alteration involves the release of various secretory factors and vesicles related to vascular leakage, ECM remodeling, and immunosuppression, collectively known as the pre-metastatic niche (PMN) (62). Despite these modifications, tumor cells may enter a state of dormancy because they need to acclimatize to the secondary site. This state is regulated by crosstalk between the environment and mechanisms that control transcriptional programs, resulting in the inhibition of WNT protein-driven signaling pathway, slowing down their division rate, and downregulating the expression of immune cell-recognizable molecules to avoid an immune response (57). The activation of tumor cells from their dormant state remains largely unknown. Some researchers believe that persistent inflammation in the host organ shifts the cellular state into an aggressive one, while others have proposed that the host microenvironment activates cells (57).

It is noteworthy that some studies suggest that the nature of the primary seeding cancer cell is a determining factor in its metastatic properties, including growth and response to therapy (57). This hypothesis suggests that the primary tumor cells present an organotropism condition.

4.1. Epigenetic changes associated to the metastasis process

Comprehending the molecular changes that facilitate metastasis is vital for understanding this process. Therefore, both genetic and epigenetic factors are considered as key players in the progression of tumors. Unlike permanent genetic events such as mutations, epigenetic modifications are dynamic and tissue-specific. Consequently, it would be intriguing to consider how primary tumor cells utilize these mechanisms to acquire metastatic properties. There are two primary epigenetic mechanisms described to be involved, DNA methylation and non-coding RNAs, including miRNAs.

4.1.1. DNA methylation

DNA methylation is a biochemical process that involves the addition of a methyl group to the DNA molecule, specifically to cytosine residues within CpG dinucleotides (63). The methylation of DNA is mediated by different types of methyltransferases (DNMTs) which absence has been demonstrated to be lethal (63). These enzymes possess the ability to act at various locations along the DNA strand, however, the most significant modifications are linked to promoter and enhancer regions. The methylation status of these regions plays a crucial role in the regulation of gene transcription. When these regions are hypomethylated,

the transcriptional machinery is able to reach the DNA strand, whereas hypermethylation repress gene transcription (**Figure 9**)(63).

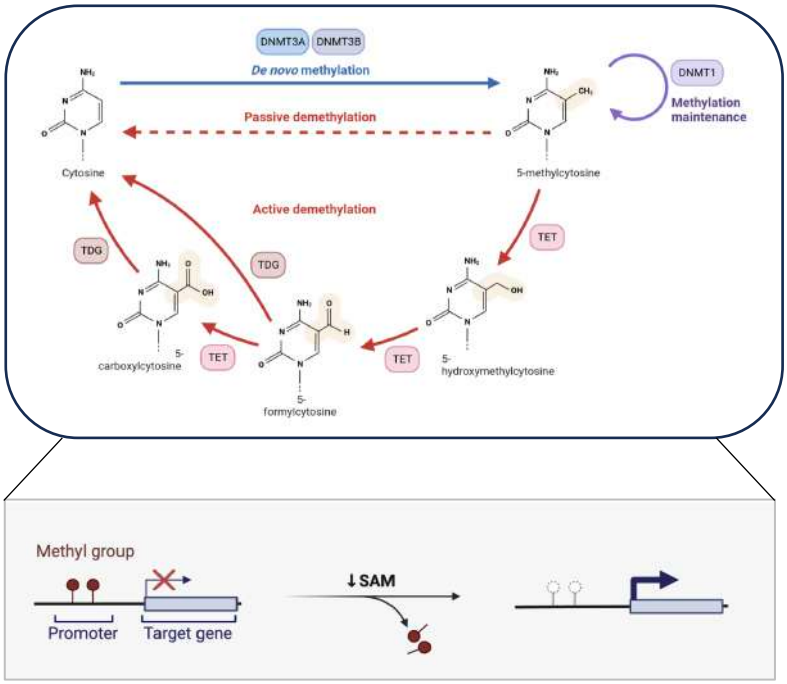

Figure 9. Overview of DNA methylation mechanism. Methylation is a chemical process in which a methyl group (CH3) is added to a molecule, often to the cytosine base on DNA. This addition occurs at CpGs dinucleotides where the methyl group is covalently bonded to the carbon 5 position of the cytosine ring. This process is catalyzed by DNA methyltransferases, resulting in a stable modification that can alter gene expression by affecting DNA structure and interaction with transcription factors. DNA methylation can silence gene activity and is crucial for the regulation of various biological processes, including development and genomic stability. Image generated with Biorender.

In cancer, abnormal DNA methylation patterns are often observed, leading to changes in gene expression that contribute to the development and progression of tumors (64). Broadly, the hypermethylation of promoter regions can result in the silencing of tumor suppressor genes and the control of regulatory proteins, whereas hypomethylation of regulatory regions activate oncogenes and is associated with genomic instability and cell transformation (64). The first evidence of the epigenetic effect in metastasis was described in retinoblastoma patients, where focal hypermethylation was found in a promoter associated CpG island of the retinoblastoma suppressor gene (65). Over the years, DNA methylation status in cancer has been studied in depth. Recent studies have identified non-genetic heritable epigenetic alterations associated with tumor progression and distinct metastatic phenotypes including DNA methylation and histone tails modifications (64). Even though DNA methylation is a significant epigenetic driver, studies have also focused in the histone modifications which can also regulate gene transcription depending on their methylation status.

Histone modifications are associated with chromatin remodeling which has become a relevant field of study due to its implication promoting tumorigenesis by regulating gene expression (64). They can be methylated during post-transcriptional modifications, resulting in another epigenetic driver. Its methylation status can lead to either activation or repression of gene transcription, depending on the specific histone residue that is methylated and the degree of methylation (64). Considering the entire regulatory machinery of methylation, in **Table 6** we summarized the most studied regulatory proteins, including DNMTs which enables DNA and histones methylation.

Regarding the metastatic process, primary tumors exhibit a low frequency of mutations in epigenetic regulating proteins. In contrast, metastatic tumors carry epigenetic modifications that could be associated to their tumor initiating onco-genotype (64). Some studies suggest that modulation of epigenetic modifications can be induced by TME throughout the metastatic process. For instance, secreted factors could be affecting plasticity of tumor cell in EMT, being tumor growth factor β (TGF-β) the most abundant factor in the stroma. The long-term stimulation by TGF-β has been associated to different histone modifications promoting active transcription (64). Similarly, in metastatic tumors of breast cancer, elevated levels of DNMT3B are found due to continuous exposure to inflammatory cytokines, such as interleukin 6 (IL-6) and prostaglandin E2 (64). Furthermore, some studies revealed that the exposure to different mechanical conditions during the metastatic process leads to epigenetic modifications. These signals influence the location or expression of transcriptionally enhanced associated-domain transcription factor, which mediate metastasis to multiple organs (64).

Table 6. Epigenetic modifiers and their regulatory proteins including writes, readers and erasers. *Adapted from (64).*

Epigenetic mark	*Writers*	*Readers*	*Erasers*	*Molecular Function*
H3K4Me	MLL1–5 (KMT2A-E), SETD1A/B (KMT2E-G), SMYD1/2, SET7, PRDM9	CDH1, BPTF, TAF3, ING4, CFP1, PHF2/KDM7C, SPIN1, PHF23, PYGO2, KDM5A/B	KDM1A/B, KDM5A/B/C/D, NO66	Marker of active transcription
H3K27Ac	CBP/p300 family	BRD containing proteins, some PhD domain containing proteins	HDACs	Marks active enhancer regions
H3K27Me	EZH1/2	CBX7, EED, BAHD1, NSD2	KDM6A/B/C, KDM7A/B	Transcriptional repression with increasing methylation
H3S28p	MSK1/2, PCAF	PRCs, HDACs	PP1	Regulates binding ability of other regulatory complexes (i.e. HDACs, PRCs)
H3K36Me	NSD1/2/3, ASH1L, SETD2/3, SETMAR	DNMT3A, LEDGF, NBS1, KU70, MRG15, ZMYND11	KDM2A/B, KDM4A/B/C	Marker of euchromatin regions, promotes novel DNA Me sites
DNAMe	DNMT3A/B, DNMT1*	MeCP1, MeCP2, other proteins containing MBDs with the exception of MBD3	Oxidation, passive replication loss	Transcriptional regulation & regulating transcription factor binding site accessibility

4.1.2. miRNAs

Non-coding RNAs are a category of RNA molecules that do not code for proteins but play important roles in a variety of cellular processes (66). One type of non-coding RNAs are the miRNAs, which are molecules of approximately 22 nucleotides in length that regulate gene expression post-transcriptionally.

The biogenesis of these small non-coding RNAs can occur through canonical and non-canonical pathways. In the former, the RNAse polymerase II transcribed a long primary miRNA transcript (pri-miRNAs) from genomic DNA, which typically features a hairpin structure. However, the non-canonical pathway can generate miRNAs from short hairpin intronic sequences or small nucleolar RNAs, instead of transcribing from genomic DNA. Then, the precursor miRNAs (pre-miRNAs) are obtained in both pathways by the cleavage inside the nucleus of the pri-miRNA. (67).

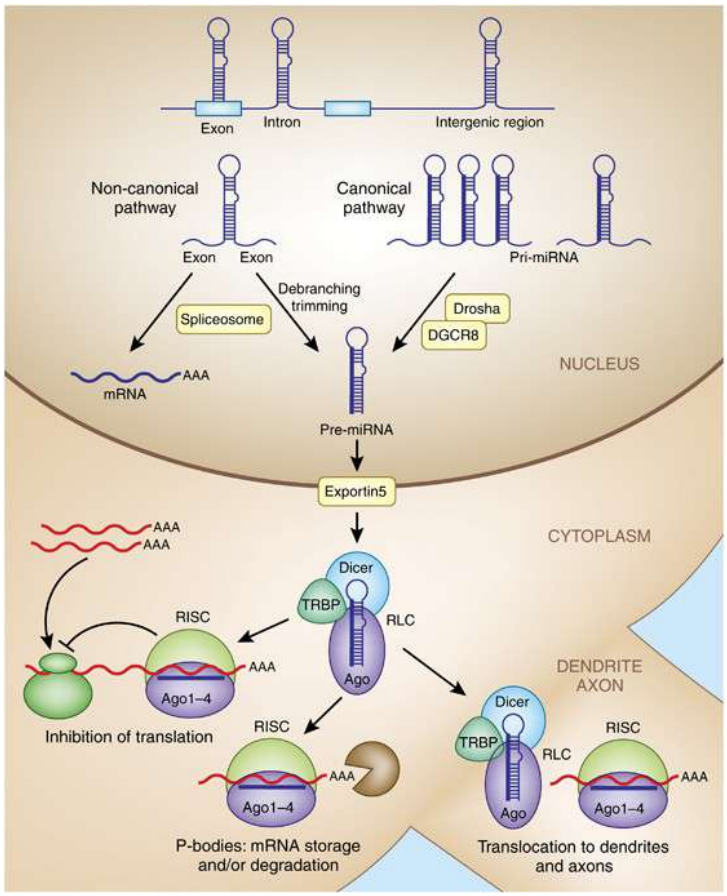

Figure 10. Overview of miRNA biogenesis and their functions in the cytoplasmatic compartment. The canonical miRNA pathway generates pri-miRNA transcripts from miRNA genes located in exonic, intronic, or intergenic regions, which are then processed into pre-miRNAs by Drosha/DGCR8. In contrast, the non-canonical mirtron pathway forms intronic pre-miRNA hairpins through splicing, debranching and trimming of short introns without Drosha processing. Both canonical and non-canonical pre-miRNAs are exported from the nucleus via Exportin5 and then cleaved by Dicer within the RISC loading complex (RLC). The miRNA/miRNA* duplex is unwound by Argonaute, and the loaded miRNA is transported into the RISC. The binding of target mRNAs to miRNAs in the RISC leads to the inhibition of translation and/or mRNA degradation within p-bodies in the cytosol (67).

In addition, miRNAs can undergo post-transcriptional modifications like phosphorylation (phosphate group incorporation into a protein which modifies its function), ubiquitylation (attaching ubiquitin to a protein, which frequently signifies its degradation) and sumoylation (addition of SUMO proteins to a target, affecting its stability and interactions) affecting RNA expression and cell signaling pathways (68). Then, they become an integral part of the effector RNA-induced silencing complex, or RISC, which allows them to link to its complementary messenger RNA (mRNA) target as shown in **Figure 10**. They bind to complementary sequences in the 3' untranslated region (UTR) of target mRNA molecules, resulting in either the inhibition of translation or the promotion of degradation of the target mRNAs.

Notably, the abundance of miRNA is significantly lower than their target genes, however, it is sufficient to substantially repress them. A single miRNA has the capacity to target multiple genes, and conversely, a gene can be targeted by various miRNAs, resulting in a complex regulatory network. Over the years, several studies have demonstrated that miRNAs are involved in processes such as development, differentiation, proliferation, and apoptosis (66). Therefore, an imbalance of miRNA expression levels have been linked to various diseases, including cancer, in which miRNAs can act as oncogenes or tumor suppressors (69). Consequently, they have become promising targets for diagnostic and therapeutic interventions.

As mentioned previously, several roles have been associated with miRNAs in tumorigenesis, including angiogenesis, cell death, cell cycle control or invasion. Remarkably, many of them have been identified to engage in the communication between tumor cells and the surrounding TME cells, regulating expression of genes involved in the metastasis process (66). In brief, some miRNAs secreted by tumor cells associated to the metastatic process are listed in **Table 7**.

Table 7. miRNAs related to the metastasis process in several tumors. OSCC, oral squamous cell carcinoma; GBM, glioblastoma multiforme; HCC, hepatocellular carcinoma; CRC, colorectal cancer; BMM, bone marrow macrophages. Adapted from (66)

miRNA	Cancer	Receptor cells	Target
miR-9	Breast	Fibroblast	E-cadherin
miR-15b-5p	GBM	Non-tumor brain cells	MAPK/ERK
miR-20a-5p	Breast	BMMs	SRCIN1
miR-21	Lung, GBM, HCC	Pre-osteoclasts, macrophages, non-tumor brain cells, tumor cells	PTEN, TLR8, MAPK/ERK
miR-25-3p	CRC	Endothelial cells	KLF2/KLF4
miR-103a-3p	HCC	Endothelial cells	VE-Cadherin
miR-210	Breast	Endothelial cells	Ephrin A3; A3/PTP1B
miR-210-3p	HCC	Endothelial cells	SMAD4/STAT6
miR-211	Melanoma	Fibroblasts	IGF2R
miR-218-5p	Breast	Pre-osteoblasts	Collal
miR-301a-3p	Pancreatic	Macrophages	PTEN
miR-934	CRC	Macrophages	PTEN
miR-939-5p	Breast	Endothelial cells	VE-cadherin
miR-1246	OSCC	Low-metastatic cells	DENND2D
miR-1247-3p	HCC	Fibroblasts	B4GALT3

4.2. The metastatic process in NB

As described before, NB is a highly metastatic malignant tumor with approximately 70% of patients presenting with metastasis at the time of diagnosis (70). NB mainly spreads to BM and bones, liver, and regional lymph nodes (8). To metastasize, NB tumor cells must undergo an adaptive and dynamic process that depends on various structural, molecular, and microenvironmental conditions (71).

In 1973, it was reported that NB cells display diverse morphological and biochemical properties *in vitro* with two distinct phenotypes: neuroblast and substrate-adherent types (72). A third phenotype was described later, identified as intermediate. Afterwards, it was discovered that NB cells could interconvert bidirectionally *in vitro* between these phenotypes. More recently and because of technological advances, researchers were able to distinguish between noradrenergic (NOR) and MSN phenotypes based on epigenetic and transcriptomic landscapes. In case of NOR cells, they displayed a sympathetic identity with noradrenergic properties, whereas MSN cells presented a NCC-like phenotype. Of note, another phenotype has always been considered instead of NOR, which is the adrenergic phenotype characterized by the presence of phenylethanolamine N-methyltransferase (PNMT) enzyme, which converts

noradrenaline to adrenaline. However, some studies have shown that NB cell lines do not express PNMT at the mRNA or protein levels (73, 74).

The transition capacity between the two phenotypes suggests that NB cells possess a high degree of plasticity. Furthermore, the transition from NOR to MSN phenotype has been defined as noradrenergic-to-mesenchymal transition (NMT), which is similar to, but distinct from, EMT. As previously described, EMT occurs only in epithelial cells, whereas NB cells are neuroendocrine. Additionally, like EMT, NB cells can undergo the inverse process known as mesenchymal-to-noradrenergic transition (MNT) and can also exhibit intermediate stages with different cellular properties and genetic signatures.

Regarding their genetic profile, NOR phenotype is characterized by high levels of *TH*, dopamine bet-hydroxylase (*DBH)*, *PHOX2B* and *MYCN*, among other molecules. However, identifying the signature of MSN phenotype has proven challenging, and it is characterized by low levels of NOR genes and the presence of *CD44*, fibronectin type 1 (*FN1)*, collagenases, and runt-related transcription factor 2 (*RUNX2*) (75, 76). Gene set enrichment analysis (GSEA) of their signature highlighted the hallmark of EMT as being enriched in MSN cell lines, which exhibited high levels of vimentin (*VIM*) and *FN* (76, 77). However, it is worth noting that NB cells lack the main genes of the epithelial signature, such as E-cadherin, claudins and occludins (76).

An exhaustive study of their signature revealed the association of these phenotypes with immune markers, such as the loss of GD2 expression in the MSN phenotype, along with metabolic programs (78). Moreover, recent research has highlighted the importance of microenvironment interactions in NMT, as it has been shown that the immune system plays a critical role in determining the presence of each phenotype (79). Additionally, single-cell transcriptomic analyses performed on patient biopsies in PDX models have revealed that the MSN phenotype clusters with ECs, CAFs and Schwann cells, whereas the NOR phenotype clusters individually (75).

As previously mentioned, these phenotypes exhibited distinct cellular capacities, similar to EMT. Broadly, the NOR phenotype is indicative of a more differentiated cellular state characterized by limited proliferation and a more favorable prognosis (76). In contrast, the MSN phenotype is associated with a more undifferentiated and aggressive state, featuring enhanced migratory and invasive properties (76). Additionally, NMT exhibits different transition stages that have recently been described to present distinct genetic signatures in neuroblastic tumors, including NB (**Figure 11**).

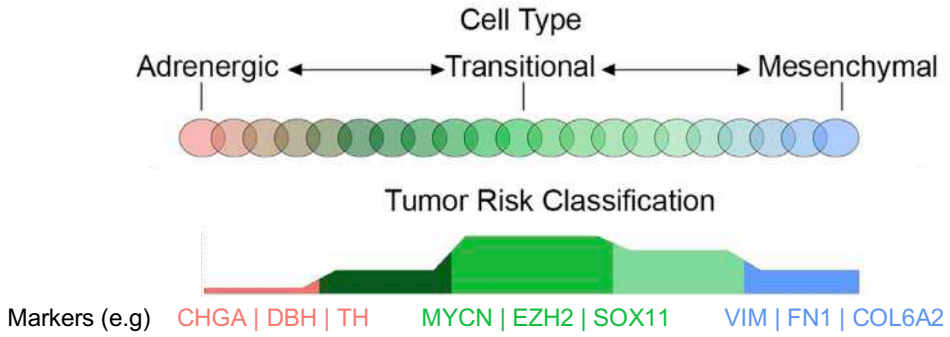

Figure 11. NMT process in neuroblastic tumors, including NB. A continuum of cell types, with color gradients representing each phenotype: adrenergic cells (pink), transitional cells (green) and mesenchymal cells (blue), is associated with the tumor risk classification, as well as the gene expression profiles that are characteristics of phenotype. Key markers genes are labeled for each stage. *Adapted from (80)*

In this study, it was established that tumors exhibiting the transitional neuroblast signature were associated with poor prognosis (80). By bulk mRNA expression, they distinguished both NB phenotypes, NOR and MSN, considering the pre-established genetic signature. However, it was observed that the transitional phenotype lacked the typical genes found in the extreme phenotypes and exhibited an increased expression of Neuronal Differentiation 6 (*NEUROD6*), Enhancer of Zeste 2 Polycomb Repressive Complex 2 Subunit (*EZH2*), SRY-Box Transcription factor 11 (*SOX11*) and MYCN (80). Research has shown that transitional stages are the most aggressive, and have the worst prognoses (80). However, further in-depth studies are needed to enhance our understanding of the process and its implication in NB progression. Moreover, several genes associated with various processes that have been linked to metastasis in NB have been thoroughly investigated and are listed in **Table 8** (81).

Table 8. Genes related to the metastasis process in NB

Gene	*Function in Metastasis*	*Preferential metastasis*
HIF-1α	Induce proliferation, migration and invasiveness	Lymph Node
V-CAM	Cell-cell adhesion	Gut and liver
MMP9	Extracellular matrix (ECM) protease	Gut and liver
VEGF	Promotes angiogenesis	Gut and liver
CDH1	Associated with cell adhesion	Gut and liver
TWIST1	Tumor growth and ECM disruption	Lung
SNAIL1/2	EMT and invasion	Gut, liver and pararenal area

In brief, non-coding RNAs, with a particular focus on microRNAs, have been identified as key regulators of various processes involved in tumorigenesis, including the cell proliferation, differentiation, adhesion, angiogenesis, migration, and invasion pathways (82). Most studied miRNA in NB metastasis are summarized in **Table 9**. Despite the extensive data available on these genetic and non-coding markers, our knowledge of the metastatic cascade in NB remains an area of ongoing research.

Table 9. miRNAs related to the metastatic process in NB and their function. Adapted from (79)

miRNAs	*Function*	*Target gene*
miR-145	Reduced cell viability	*MTDH*
miR-92	Stimulate or inhibit the canonical wnt pathway	*DKK·*
miR-1247	*Suppress cell proliferation, induce cell cycle G0/G1 phase arrest*	*ZNF346*
miR-149	Inhibits cells proliferation and enhances chemosensitivity	*CDC142 and BCL"*
miR-205	*Inhibits tumor growth*	*CREB1*
miR- 3934-5p	Induce apoptosis and inhibits cell viability	*TP53INP1*
miR-34a	*Inhibitory effect on proliferation, migration, invasion and autophagy*	*ATG5*
miR-129	Inhibits tumor growth and potentiates chemosensitivity	*MYO10*
miR-362-5p	*Suppresses cell growth and motility*	*(PI3K)-C2b*
miR-203	Role in malignant progression	*Sam68*
miR-338-3p	*Suppresses proliferation, invasion and migration*	*PREX2a*
miR-145	Represses migration, invasion and angiogenesis	*HIF-2a*

To gain a comprehensive understanding of the complete metastatic process, the deployment of *in vivo* preclinical models is necessary. Syngeneic, transgenic, xenografts, and humanized models are among the most commonly utilized *in vivo* models in the study of NB metastasis (71)(**Table 10**).

Intravenous injection of tumor cells into the tail vein or intracardiac injection are the most frequently used methods to study the metastatic process in NB (83). These models are named experimental metastasis models because of the high rate of metastatic tumor generation, but they skip the first steps of the process (84). In these models, the cells do not acquire the modifications needed to escape from the primary tumor and reach the bloodstream. On the other hand, orthotopic models recapitulate each step of the process and exhibit the same metastatic pattern (85). However, there are some limitations of this models as well such as tumor monitoring and resection, as it is performed in patients (83). Therefore, to better understand the metastatic signature of NB tumors it is imperative to establish an *in vivo* model in which the same monitorization and treatment as used in the clinic is reproduced.

Table 10. Mouse models used to study the metastatic process in NB.

In vivo model	*Infiltrated organs*	*Advantages*	*Limitations*	*REF*
Syngeneic mouse model	BM and Liver	Reproducible, easy to handle, with an intact immune system and high metastatic capacity.	Do not mimic biology and genetics characteristics of human NB. No human cells are used.	(86, 87)
Transgenic mouse mode	Abdominal and ganglion*	Orthotopic tumor can be established which reproduces genetic aberrations of NB, with an intact immune mouse system and high metastatic capacity.	Do not mimic biology and genetics characteristics of human NB. No human cells are used, and do not reproduce metastatic pattern.	(85)
Human xenograft mouse model	Peritoneum, lungs, kidney, adrenal gland and BM	Reproduces genetics complexity. It is reproducible and easy to handle. NB human cells are used.	Immunocompromised models are used, lacking tumor microenvironment complexity and presenting a low metastatic capacity (subcutaneous or intraperitoneal injection).	(85)
Patient-derived xenograft mouse model (PDX)	Lungs, liver and BM	Reproduces genetics complexity. It is reproducible and easy to handle. NB human cells are used. Orthotopic transplanted tumor retains high metastatic capabilities.	Immunocompromised models are used, presenting a low metastatic capacity with subcutaneous transplantation. Time-consuming.	(85)
Immune mouse model		Varying degrees of human tumor-human immune system interactions. Suitable for screening and studying mechanism of action of checkpoint blockers	Highly labour intensive and time-consuming. Low rate of successful human immune system transplantation	(88)

4.3. The role of TME in metastasis

Despite the genetic and epigenetic changes that occur in the tumor cell, it is now well accepted that these modifications alone are insufficient to explain the whole process of tumorigenesis. Over the years, numerous research groups have focused on studying the complex ecosystem of cancer, which involve a wide range of non-tumoral cells and their interactions within the tumor, known as TME (89). The ecosystem comprises a vascularized matrix and a diverse mix of non-tumoral cell types including different immune cell types, cancer-associated fibroblasts (CAFs), endothelial cells (ECs), pericytes and other cell types that vary by tissue (89). Principal components of TME and their functions are summarized in **Table 11**. Additionally, the composition and functional state of TME can differ among patients with the same cancer type, due to individual variations such as age, gender, lifestyle, body mass index, microbiome and the organ in which the tumor arises (89).

Briefly, tumor cells manipulate their environment to create supportive conditions for their growth and proliferation. This is achieved by recruiting and reprogramming non-tumoral host cells, as well as remodeling the vasculature and extracellular matrix (ECM). To modify their environment, tumor cells utilize intercellular communication methods such as cell-to-cell contact and paracrine signaling (89). The first method is facilitated by adhesion molecules, including integrins, cadherins and immunoglobulin superfamily members, among others. Paracrine signaling is mediated by cytokines, chemokines, growth factors, proteases and extracellular vesicles (EVs). These molecules and vesicles are secreted in response to cancer-intrinsic features and cellular stress, and can be derived from various cell types within the TME, including tumor cells, to exert both direct and indirect effects on target cells by binding to their receptors or through ECM remodeling (89).

During tumor initiation, tumor cells employ two different mechanisms of interactions within TME in order to succeed (89). The first mechanism involves the ability of tumor cells to evade immune-checkpoints of the adaptive immune system, resulting into a full-blown tumor. The second mechanism relates to chronic inflammation favoring immune suppressive conditions, characterized by the accumulation of CD4+ Th2 subtype of T-cells and myeloid cells with an immunosuppressive functional state. Under prolonged inflammatory signaling, conditions such as hypoxia, low pH, and altered metabolite levels, lead to an increase in secreted molecules (89).

Table 11. Major cellular and non-cellular components of TME. Adapted from (153)

	Cell type	*Function in TME*	
		Anti-tumorigenic	Pro-tumorigenic
Adaptative immune cells	CD8+ T cells	Destroy target cells. In tumors, different stated are observed, including dysfunctional or exhausted phenotype.	
	CD4+ T cells	*Th1 subtype* kills cancer cells via interferon γ (IFN-γ) and TNF-α; and contribute to effective CD8+ T cells responses.	*Th2 subtype* secretes anti-inflammatory mediators that exert pro-tumoral functions.
	Regulatory T cells (Tregs)	Gatekeepers of immune homeostasis	Suppress effective anti-tumor immunity.
	B cells	ACDD and complement activation	Promotes inflammation and immunosuppression via secretion of anti-inflammatory and pro-angiogenic mediators
Myeloid immune cells	Macrophages	Direct phagocytosis of cancer cells or activation of anti-tumor immune responses.	TAMs: Promotes angiogenesis, immunosuppression, metastasis formation and therapy resistance.
	Neutrophils		Systemic accumulation contributes to immunosuppression and ECM remodeling in distant organs, promoting PMN formation.
	Monocytes	Produce tumoricidal mediator and stimulate natural killers (NK) cells.	Immunosuppression, ECM remodeling, angiogenesis, and cancer cell intravasation. Can differentiate into tumor-supporting TAMs.
	Dendritic cells (DCs)	Antigen-presenting cells, mostly to T cells	
	Myeloid-derived suppressor cells		Suppress T cells, NK cells, B cells, and DCs via paracrine and cell-cell contact mechanism
	Platelets		Promotes CTCs survival by shielding them from physical stress and immune attack; and modulate angiogenesis and vascular integrity by binding to ECs. Activate myeloid cells.

Intermediate immune cells*	NK cells	Recognized and kills stressed cells that lack MHC class I expression	
	Invariant NK T cells (iNKT)	Direct tumor cell killing and anti-tumorigenic immune cells orchestration	Pro-tumorigenic immune cells orchestration
	γδT cells	Citotoxicity mediated by TCR- and NK-receptor interactions or productions of effector molecules	Promotes progression by suppressing anti-tumor immune responses via the production of cytokines, including IL-17
Stromal cells and	CAFs		Synthesize and remodel the ECM, altering the behavior of tumor cells and immune cells. Impacts angiogenesis, and immunomodulate TME contributing to immune evasion of tumor cells
Vascular cells	Blood vascular ECs		Tumor ECs express lower levels of adhesion molecules, which causes an impaired barrier function, and they express increased levels of inhibitory immune checkpoint molecules.
	Lymphatic ECs (LECs)		Provides dissemination route for tumor cells in addition to blood vessels.
	Pericytes		Modulation of TME via paracrine

Considering the numerous cell types conforming the TME, tumor initiation is not the only process in which they are involved. Additionally, processes such as ECM remodeling and angiogenesis are being promoted and modulated by TME, mainly through paracrine signaling. Both are mainly orchestrated by CAFs, which are the main component of many tumors, and they are also responsible for the fibrosis or desmoplasia (89).

Several factors involved in angiogenesis such as VEGF-A and VEGF-C, are also involved in lymphangiogenesis (90). As a result of the vascularization processes, both endothelial cells (ECs) and lymphatic ECs (LECs) dampen T cell responses through multiple mechanisms like expression of immune checkpoint molecules and antigen presentation in the absence of co-stimulatory molecules.

Subsequently, tumor cells undergo EMT changes in order to metastasize, as previously described. The initiation of the process is triggered by cytokines, mainly TGF-β which is secreted by CAFs (89). Then, once the tumor cells reach the vasculature, the main population involved in TME interactions are the TAMs, which play a key role activating RhoA signaling in tumor cells, inducing invadopodia formation and subsequent extravasation, along with stemness reprogramming (89). Afterwards, a small proportion of CTCs will survive in the bloodstream, because of their association with specific immune cells, such as neutrophils or platelets, which help them to evade NK cells (89). Finally, metastatic seeding at secondary sites involves a complex interplay between tumor dormancy and outgrowth depending on the tissue, which is mainly orchestrated by host cells (89). A comprehensive overview of the entire process, highlighting its intricacy and multiple interactions is illustrated in **Figure 12.**

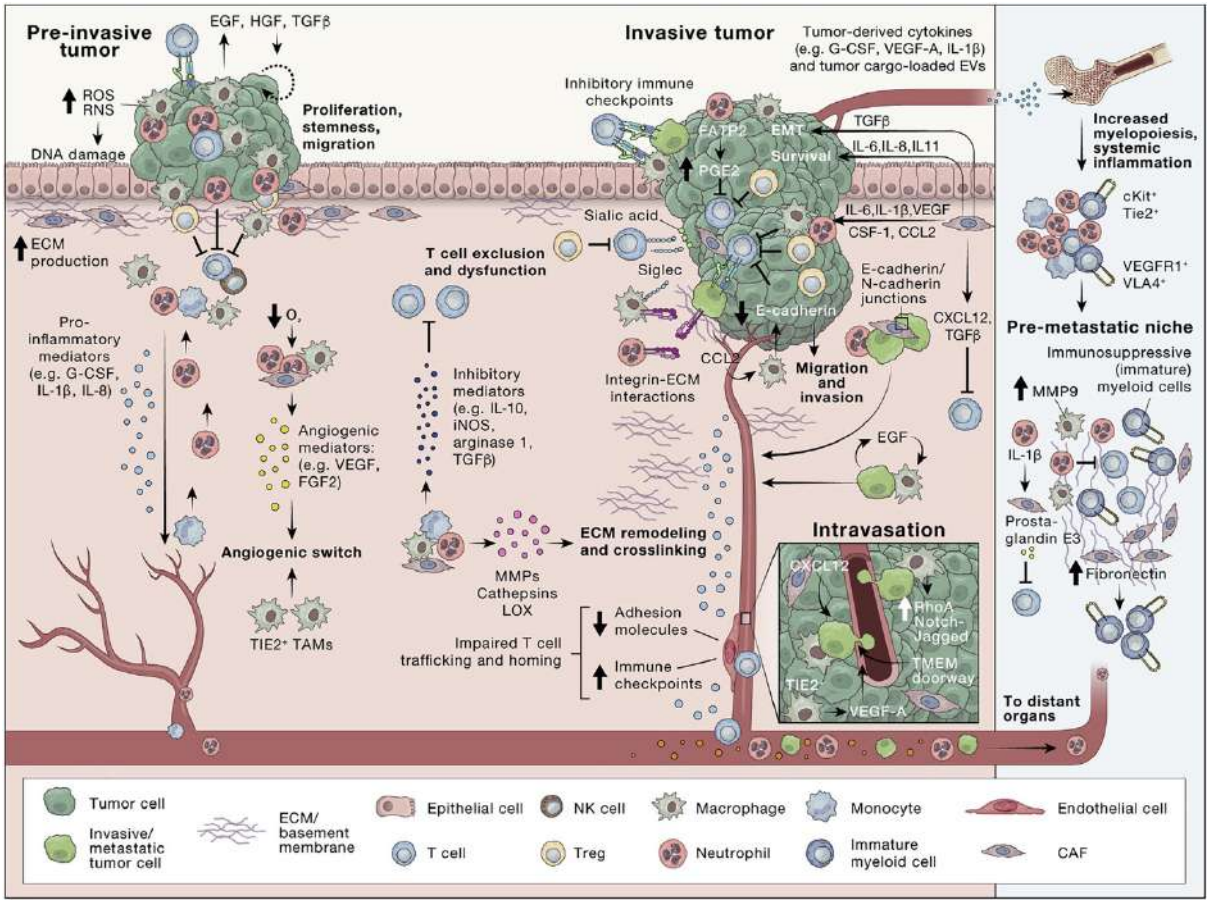

Figure 12. Overview of primary tumor progression and the complex interplay within the TME. The primary tumor TME is supported by various stromal and immune cells. Early on tumorigenesis, cancer cells may be targeted for destruction by the immune system, as well as fibroblasts and macrophages that can initially help suppress tumor growth. Eventually, both cell lines may be influenced by the developing cancer to gain pro-tumorigenic functions. For instance, tumor-associated macrophages (TAMs) can promote angiogenesis and invasion by secreting growth factors, cytokines, and proteases, whereas CAFs can become activated to secrete ECM proteins and angiogenic factors including VEGF-A, which further contribute to the complex interconnected TME. During intravasation step, macrophages locate to perivascular niches, where they can help cancer cells cross vessels barriers though the TME of metastasis. Additionally, in order to success in metastasis, pre-metastatic niche is previously formed, resulting in immunosuppressive environment induced by different factors secreted by cancer cells and pro-tumoral cells (89).

In recent years, several studies examining the landscape of TME in NB tumors have been published using diverse technologies. Based on these investigations, significant differences in the TME landscape have been described in relation to *MYCN status (91)*. When *MYCN* is amplified, NB tumors present high infiltration of stromal cells, particularly CAFs, and some TAMs are also observed. These tumors are classified as “cold-tumors” given the low rate of immune cell infiltration. In contrast, non-amplified *MYCN* tumors exhibit higher infiltration of different cell types including immune cells such as T and B cells, and other types like NK cells, among others (**Figure 13**). Additionally, *MYCN* amplified tumors exhibit a higher vascularization compared to non-amplified tumors, given the control of hypoxia -inducible factor - α (HIF-α) by *MYCN* that consequently increases VEGF (91). Of note, in *MYCN*

amplified tumors, it has been observed that ECs covered with pericytes can originate from NB tumor cells, a vasculomimicry that can contribute to 70% of the tumor vascularization (91).

Considering the technological advancements, such as spatial and single-cell transcriptomics, and the limited understanding of the TME interactions in NB, it is crucial to gain insights into the role of the different cell types involved in the progression of NB. By doing so, we can develop novel therapies specifically targeting the TME, thereby preventing tumor cell adaptations.

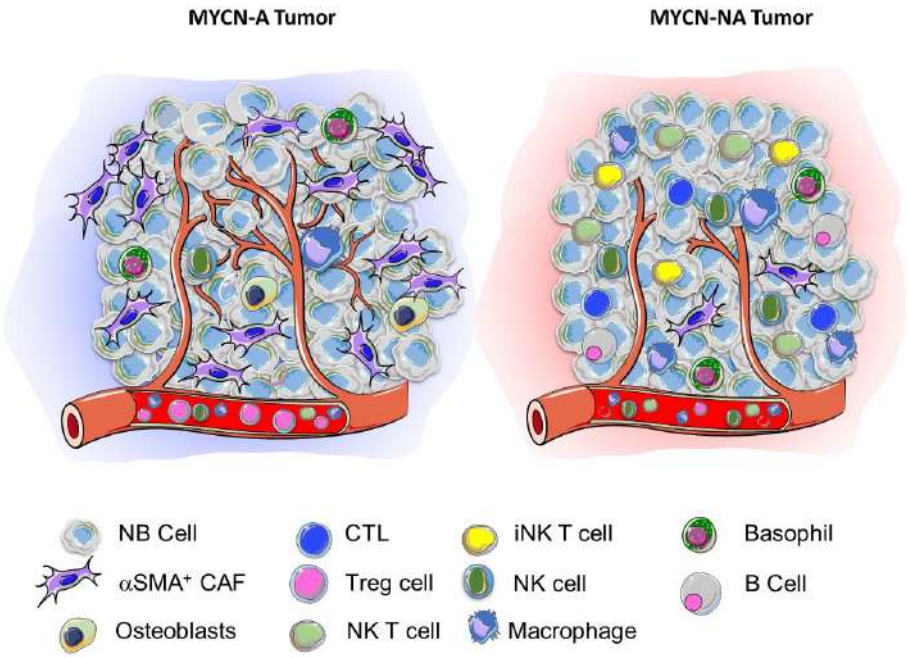

Figure 13. The landscape of the TME in NB based on the MYCN amplification status. Low levels of immune cells are commonly found in NB tumors with *MYCN* amplification (MYCN-A), known as cold-tumors. These tumors are frequently infiltrated with cancer-associated fibroblast (CAFs), macrophages, osteoblast and basophils. In contrast, tumors without *MYCN* amplification exhibit infiltration of several immune cells such as Treg cells, NK T cells, iNK T cells and B *cells (91).*

4.3.1. CAFs

Among the different cell types conforming the TME, CAFs require special attention because they present a wide range of functions depending on the tumor types, as well as being the main TME component of HR-NB. CAFs have been proven to play a critical role in promoting tumor growth, angiogenesis, and the recruitment of inflammatory cells (92, 93). However, under physiological conditions the main component of the microenvironment are normal fibroblasts instead of CAFs. Likewise, fibroblasts present numerous functions such as secretion of MMP, contraction of wound edges, and activation of inflammatory responses (94).

During tumorigenesis, inflammatory responses are time delayed, resulting in the activation of tissue-resident fibroblasts to be transformed into CAFs. Over the years, several studies have

demonstrated that CAFs polarization is not exclusive of fibroblasts but other stromal cells present the ability. CAFs subtypes can originate from cells such as epithelial, adipocytes and mesenchymal stem cells, and can polarize under appropriate conditions (**Figure 14**). The different populations exhibit different transcriptomic profiles and different intra-tumoral locations. Notably, several changes affecting their composition, population density and function are observed during tumor progression. Despite the fact that CAFs are an heterogeneous cell population, there is agreement regarding their genetic signature. They are characterized by an increased levels of α-smooth muscle actin (α-SMA) and fibroblast activation protein α (FAP). However, specific CAF genes are observed depending on cancer tissues.

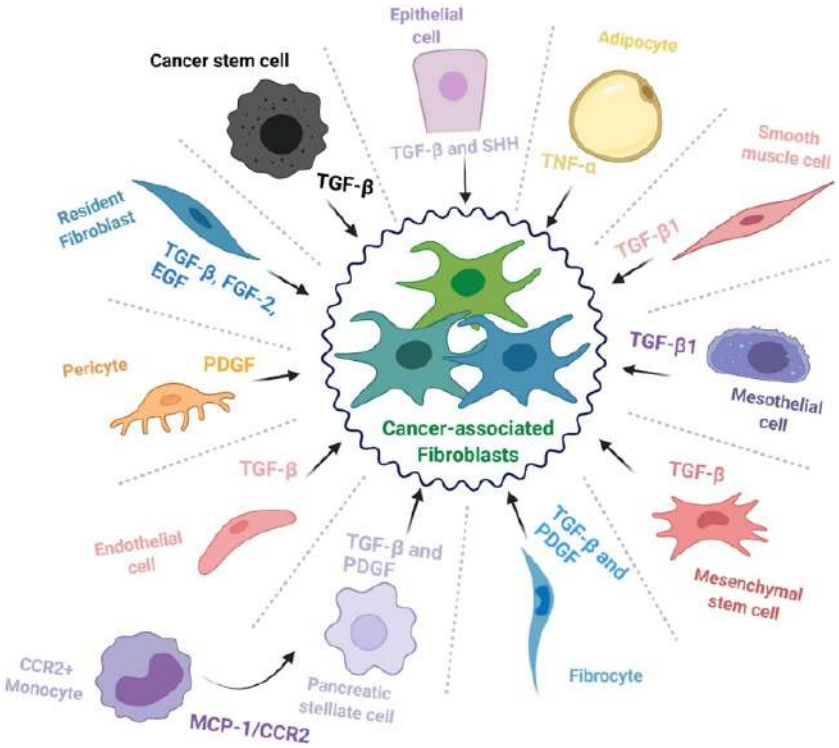

Figure 14. The cellular origins of CAFs. The various origins of CAFs, includes resident fibroblasts, mesenchymal stem cells (MSCs), epithelial cells, smooth muscle cells, endothelial cells, pericytes, fibrocytes and adipocytes among others. Additionally, cancer stem cells can be transformed into CAFs. Principal factors and signaling pathways involved in this process, such as TGF-β, platelet-derived growth factor (PDGF), or TNF-α, are represented (95).

Regarding NB tumors, various studies have highlighted the significance of CAFs, as well as TAMs, in the progression of the tumor. On the one hand, Hashimoto *et al*. demonstrated that different cell types, including peripheral blood mononuclear cells and mesenchymal stroma cells (MSC) from the BMs, are recruited to the tumor site and contribute to forming the TME of NB and promoting tumor progression (95). Additionally, the group lead by JY Declerck showed that a subset of CAFs in NB originates from MSC, which exhibit an immune-independent effect and possess pro-tumorigenic activity through the JAK2/STAT3 pathway

(96). Notably, a significant amount of tumor fibroblasts correlates to diminished responses to immune therapies including anti-PD-L1 or anti-CTLA-4. In brief, anti-PD-L1 immunotherapy works by targeting and inhibiting the Programmed Death-ligand 1 (PD-L1) protein found on cancer cells, thereby enhancing the immune system's ability to attack tumors, whereas anti-CTLA-4 blocks the Cytotoxic T-Lymphocyte Antigen 4 (CTLA-4) protein on T cells, which enhances the immune response against cancer cells. As numerous studies have shown, this particular cell type is present in NB tumors. Uncovering their function and identifying potential targets could lead to the development of innovative targeted therapies and enhance existing ones.

4.4. The formation of Pre-Metastatic Niche

As previously mentioned, metastasis is a complex process that extends beyond mere alterations in tumor cells to enable their spread to distant organs. According to various studies, it is essential for tumor progression to bring about microenvironmental modifications in distant tissues, thereby creating a hospitable environment for tumor cells prior to their arrival, known as pre-metastatic niche (PMN) (62). To establish the PMN, a series of molecular and cellular changes must occur within the host microenvironment, often referred to as the "fertile soil", which prepares the path for the colonization of metastatic tumor cells, thereby facilitating their settlement (90). The modifications during PMN formation are not exclusively conducted by tumor-secreted factors, in addition, non-tumoral secreted factors are involved, as well as independent pathological and physiological processes, like surgery, infection and ageing effects (62).

Regarding the cellular mechanisms responsible for promoting PMN formation, six key characteristics have been identified, including immunosuppression, inflammation, organotropism, cellular reprogramming, lymphangiogenesis, angiogenesis and vascular permeability (90). These characteristics are processes triggered by various factors and secreted molecules, which can be differentiated based on their cellular origin, including tumor-derived, tumor/stroma-derived and stroma-derived molecules. The principal factors and secreted molecules involved in the initiation, polarization, and establishment of PMN are summarized in **Table 12**. Notably, the process of PMN formation initiates with local modifications, including the induction of vascular permeability, alterations in the stroma and ECM, which subsequently result in significant systemic consequences on the immune system (62).

Initially, tumor-derived secreted factors remodel the vasculature of PMN, altering its integrity, enhancing its permeability, and generating aberrant morphology of the vascular endothelium.

Furthermore, several factors contribute to the destruction of the vascular basement membrane, primarily through the action of the metalloproteinase (MMP) family of enzymes (62). In addition, some proteins from the MMP family possess the ability to remodel ECM and contribute to the formation of a proliferative, immunosuppressive and inflamed PMN (62). Another described mechanism involved in PMN formation is the increase of blood clots, which is mediated by tissue factors that recruit immune cells such as macrophages. This process is also facilitated by the interaction between platelets and tumor cells, which results in the formation of blood clots and the secretion of various factors that promote PMN formation and metastasis (62). Additionally, increased levels of VEGF are found in the first steps of the process, along with other pro-angiogenic factors, secreted by monocytes and ECs (**Figure 12**) (90). Consequently, a pro-angiogenic microenvironment is generated leading to an increase of the vascularization, also promoted by VEGF-A and placenta growth factor (PLGF) (62, 90). Notably, other secreted factors from tumor cells also contribute to the creation of an inflammatory microenvironment in the PMN, leading to the recruitment of immune cells with pro-tumoral functions, such as neutrophils and monocytes (90). In addition, hypoxic conditions of the primary tumor triggers the secretion of HIF-α a key factor in the PMN formation, which promotes protein and EVs secretion involved in the tumor formation process, and also in the metastasis (62, 90). Concerning EVs, studies have shown that tumor cell-derived EVs fuse with resident cells, transferring their cargo, including genetic material, metabolites and proteins. This fusion process leads to cellular modifications that promote a pro-tumoral phenotype of host cells (62). The intricate aspects of EVs are described in-depth in the next section.

Considering the different processes involved in the PMN and the metastatic process, it can be stated that metastasis involves a series of pathological events that unfold over time (90). In NB tumors, there is limited information available regarding PMN. Yves A DeClerck's group demonstrated the role of EVs promoting the seeding of NB cell lines in lung and liver (21). However, this study has some limitations, since these organs are not the most common sites of NB metastatic spread.

Table 12. Principal factors and secreted molecules involved in the initiation, polarization, and establishment of PMN. LLC, Lewis lung cancer; ML, melanoma; CC, Colon cancer; BC, Breast carcinoma; GC, Gastric carcinoma; PA, Pancreatic adenocarcinoma; PC, Pancreatic cancer

	Niche-promoting molecules	*Underlying mechanism*
Tumor-derived	VEGF	Recruits VEGFR1$^+$ BMDCs to the lung for niche formation
	PIGF	Recruits VEGFR1$^+$ BMDCs to the lung; redirects cancer cell metastasis to the pre-metastatic niche
	S100A8/A9	Recruits Mac1$^+$ myeloid cells and cancer cells to the inflammatory niche
	TIMP-1	Creates a liver pre-metastatic niche and drives cancer cell homing to the liver
	CD44/CD44v6	Regulates cancer stem cell behavior and allows exosomes to modulate niche cells for cancer embedding and growth
	Osteogenic and N-cadherin	Promotes bone micro-metastases and tumor cell proliferation in the niche
	MIF $_{TE}$	Recruits to the liver pre-metastatic niche and induces fibronectin via TGF for niche formation
Stroma-derived	ECs: AND-2	Recruits macrophages and induces inflammatory, angiogenic response of endothelial cells for niche formation
	ECs: periostin	Creates and immunosuppressive niche and promotes breast cancer cell outgrowth within the niche
	Fibroblast: fibronectin	Determines the location of niche formation by recruiting VLA-4$^+$BMDCs; increases metastatic seeding into the niche
	CAFs: HSF1	Reprograms CAFs and cancer cells via TGF- β and SDF-1 signaling to promote tumor metastasis into the niche
	CAFs: girdin	Promotes ECM remodeling for niche formation and promotes tumor growth
Tumor/stroma-derived	TGF-β	Lung niche: induces S100A8/A9; remodels lung parenchyma for niche formation; accumulates TAMSs and Treg cells
	TNF-α	Induces lung expression of S100A8/A9 and remodels lung parenchyma for niche formation
	G-CSF	Mobilizes MDSCs to the lung niche and promotes metastatic cancer cell seeding in the lung
	SDF-1/CXCL12	Recruits VEGFR1$^+$ and CD11b$^+$ BMDCs; regulates angiogenesis and promotes the outgrowth of CXCR4-expressing cancer cells in the PMN
	MCP-1/CCL2	Recruits monocytes and BMDCs for niche formation, enhances metastasis capacities and promotes angiogenesis via VEGF
	MMPs	Promotes ECM degradation and tissue remodeling for niche formation, promotes metastatic cancer cell outgrowth in the niche
	HIFs	Recruits BMDCs to promote angiogenesis, induces arginase and NO to support cancer cell invasion
	LOX	Promotes ECM remodeling and recruits CD11b$^+$ cells for niche formation, enhances colonization of CTCs to the niche
	Microvesical PDGF	Cancer cells-ECs crosstalk to promote the formation of a pro-metastatic vascular niche through Art6 upregulation
	RANK/RANKL	Promotes niche formation via RANKL/c-Met feedforward loop and reprograms tumor cells for bone colonization

4.5. Extracellular-vesicles (exosomes) in the metastatic process

Given that the majority of TME components comprise immune cells capable of eliciting an anticancer response, cancer cells must establish mechanisms to interact and alter the microenvironment prior to their arrival. Several studies have shown that EVs, particularly exosomes, are used as a mode of communication in this process. Exosomes are microvesicles ranging in size from 30 to 100 nm in diameter and are generated by most cell types through intracellular multivesicular body formation and subsequent release via exocytosis into the extracellular space as shown in **Figure 15A** (97). Although numerous studies have been conducted on the biogenesis of exosomes, there is limited information on how the cells regulate their exosomal-cargo. However, it is believed that exosomes are specifically charged with a wide range of genetic messengers, such as DNA, mRNA, miRNAs, cytosolic proteins, and lipids, as shown in **Figure 15B** (97). Additionally, some specific exosomal markers have been identified, such as tetraspanin proteins CD9, CD63, and CD81, facilitating their study (97).

A. B.

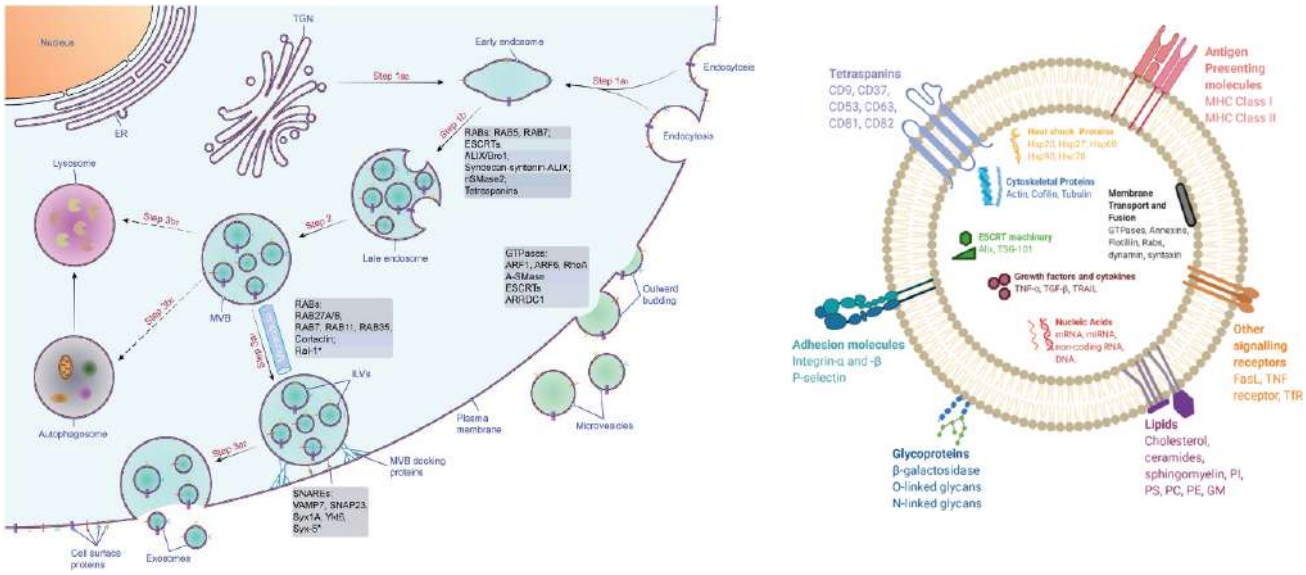

Figure 15. Overview of exosomes biogenesis and cargo A. Initially, early endosomes are formed from the plasma membrane, which is facilitated by endocytosis. Afterwards, immature endosomes develop into either late endosomes or multivesicular bodies (MVBs), which contain intraluminal vesicles (ILVs) that incorporate several cytoplasmic components. MVBs can either fuse with lysosomes for degradation or with the plasma membrane to release ILVs as exosomes into the extracellular space. The process involves the participation of crucial molecular players, including ESCRT complexes, Rab GTPases, and tetraspanins***. B.*** Exosomes transport a wide range of biomolecules, including but not limited to proteins, lipids, RNA and DNA. Common proteins found on the exosomal surface included tetraspanin (such as CD63, CD81 and CD9), heat shock proteins (such as HSP70 and HSP90), and MHC class I and II. The lipid components of exosomes include cholesterol, sphingomyelin, and phosphatidylserine. Exosomal RNA cargo consists of various types of RNA, including mRNA, miRNAs and non-coding RNAs, which can be transferred to recipient cells, affecting different physiological and pathological processes.

As previously mentioned, tumor-derived exosomes are involved in cell-to-cell communication, inducing phenotypic changes on cells conforming the PMN (97, 98). Particularly, they are involved in immune evasion mechanisms of tumor cells (98). To do so, exosomes can interact with a significant number of cell types in order to promote tumorigenesis and metastasis processes, which include lymphocytes, macrophages, fibroblast, and NK cells, among others (99). Some studies have demonstrated the ability of tumor-derived exosomes to induce macrophages to polarize to pro-tumoral M2 phenotype under hypoxic conditions (99). In addition, increased levels of exosomes have been associated with angiogenesis and pro-angiogenic microenvironment within TME and PMN (62, 90, 97, 99). For instance, the levels of factors such as proteases or miRNAs have been demonstrated to be modified in the exosomal-cargo under hypoxic conditions, leading to an accumulation of HIF1-α in ECs, which results in the release pro-angiogenic factors (97, 99). Nonetheless, exosomes released to promote tumorigenesis and metastasis can also occur under normoxic conditions. For instance, colon cancer cells show increased levels of miR-1246 in their cargo exosomes, triggering M2-phenotype polarization and increased TGF-β activity, which also promote cancer progression (100).

Lately, exosomes have emerged as promising biomarkers for monitoring cancer and assessing treatment efficacy (98, 99). Broadly, as exosomes are conformed by a lipid bilayer, their proteins are protected from being degraded. In addition, they exhibit specific components that can reflect the physiological state of their originating cells (97, 98). Considering all their properties, exosomes can be used as disease biomarkers, frequently detected in blood and showing higher sensitivity than protein detection of liquid biopsies (97). Therefore, *in vivo* detection of exosomes is highly sensitive and allows early-stage cancer diagnosis. Even, as carriers, exosomes may represent a new class of drug delivery system because they can cross biological barriers without concerns associated with drug toxicity, immune responses, biodistribution and targeted delivery (99). However, it is not fully understood which exosomes are safe and bio-compatible for drug delivery system, and there is a need to improve drug-loading methods and targeted modification technology.

In NB tumors, some studies have revealed that NB exosomes present specific cargo. The proteome analysis of two distinct commercial cell lines, with and without the amplification of *MYCN*, identified over 900 proteins that differed between them (101). Additionally, a different study analyzed the proteome of primary tumors and metastasis identifying 15 and 6 differential express proteins, respectively. Notably, these sets of

proteins were related to neuron development and extra-cellular matrix processes (102). However, the role of NB-exosomes in TME modification is not completely understood.

Thus, by elucidating the underlying molecular mechanisms driving cell-to-cell communication will provide valuable insights into disease biology and help to identify new biomarkers and novel potential therapies.

5. Podoplanin

Podoplanin (*PDPN*) is a small cell-surface mucin-like glycoprotein receptor that plays a crucial role in platelet aggregation, among others (103). Interestingly, PDPN derives its name from its initial discovery in podocytes of the kidney glomerulus, where it was first identified as a marker of these specialized cells (104). Since it was described, several names have been given to it such as Glicoprotein 36 (GP36) and T1α for human protein, whereas its homologues in mice are known as Gp38 or antigen PA2.26, among others (103).

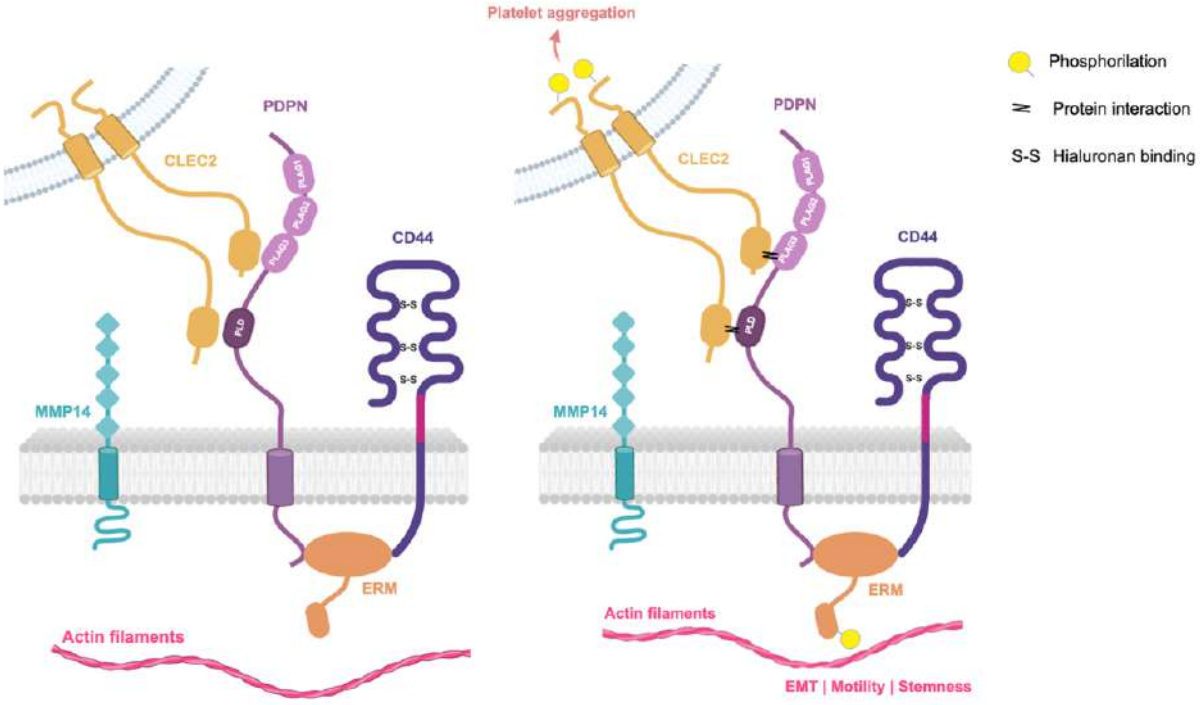

Figure 16. The molecular structure and main ligands of PDPN related to its principal physiological functions. PDPN is a type I transmembrane glycoprotein that consists of an extracellular domain, a transmembrane portion, and a short cytoplasmic tail. This extracellular domain includes PLAG1-3 (PL1, PL2, and PL3) domains and a PLAG-like domain (PLD). C-type lectin-like receptor 2 (CLEC-2), a platelet receptor, recognizes both the sialylated PLAG3 domain and PLD with adjacent PDPN peptides, leading to CLEC-2 tyrosine phosphorylation and platelet aggregation. The intracellular domain of PDPN includes basic residues, which act as binding sites for ezrin, radixin, and moesin (ERM) family proteins that regulate RHO GTPase activity and promote actin cytoskeleton reorganization to promote cell migration, motility, and EMT. PDPN interacts with hyaluronan receptor CD44 and matrix metalloproteinase 14 (MMP14), promoting hyaluronan-binding and extracellular matrix (ECM) degradation, respectively. Image generated with Biorender.

Like a mucin-type protein, PDPN is comprised of three different domains: N-terminal extracellular domain, which presents various O-glycosidic chains, a single transmembrane domain and a short cytoplasmic tail (103). Three tandem repeats are found in the extracellular domain, known as the PLAG1 to PLAG3 (Platelet aggregation-stimulating domains) and a PLAG-like domain (PLD), which carries the O-glycosidic chain. Thus, is in the extracellular domain where its main ligand, C-type lectin-like receptor 2 (*CLEC-2*), is going to bind (103, 105). Despite its short intracellular domain, it presents binding site to ezrin-radixin-moesin complex (ERM proteins) that activates the Rho GTPase and its effector kinase ROCK promoting actin cytoskeleton reorganization, cell migration and EMT (**Figure 16**)(105). Since it was discovered, no enzymatic function or specific domain has been identified for this protein. Nevertheless, it has been observed to interact with other proteins, thereby influencing various signaling pathways (105).

Under physiological conditions, PDPN is found in numerous cell types with different origins. The main functions of PDPN related to each cell type are summarized in **Table 13.**

Table 13. PDPN expression in various cell types under physiological conditions and its function (105).

Cell type	*Function*
Lymphatic endothelial cells	Separating the lymphatic vessels from the blood vascular system during development
Type-I pneumocytes	Differentiation
Glomerular podocytes	Maintaining normal podocyte morphology and glomerular homeostasis
Peritoneal mesothelial cells	Differentiation
Osteocytes	Cell shape construction such as dendrite elongation
Reticular cells	Contractility
Dendritic cells of lymphatic organs	Post-natal blood filling of lymphatic system and dendritic cell migration
Fibroblast	Increase migratory capaticies

Numerous investigations have attempted to identify the transcription factors responsible for inducing PDPN expression across different cell types. Notably, these efforts have focused on the activation of its promoter associated to CpG islands, and proteins containing domains for it, like Prox1 and Sox2 (105, 106). However, the available information regarding promoter activation remains limited. Additionally, in 2012, a study revealed the transcriptional regulation of PDPN expression through the activation of TGF-β signaling pathway via Smads in neonatal human keratinocytes (103).

Furthermore, other cytokine interactions or pathways have been described to induce the expression of PDPN, as illustrated in **Figure 17.** Over the years, associations with additional cytokines, such as IL-7, IL-1B and IL-12, have emerged.

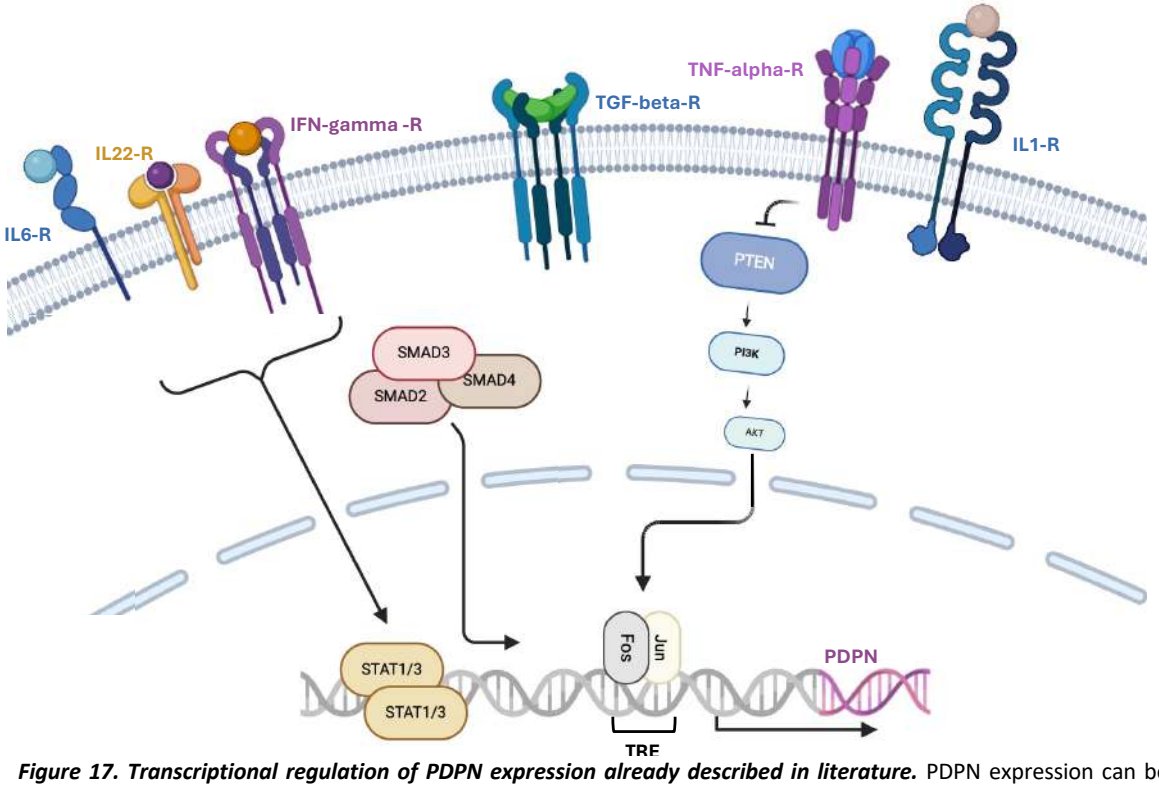

Figure 17. Transcriptional regulation of PDPN expression already described in literature. PDPN expression can be increased by various pro-inflammatory cytokines, such as IL-22, IL-6, IFN-γ, TGF-β, IL-1β, and TNF-α, but the specific signaling pathways involved are not well understood. For instance, TGF-β-induced PDPN upregulation requires Smad2/3 and 4 activity, while IFN-gamma-induced upregulation depends on STAT1 and STAT3, and IL-6 and IL-22-induced upregulation depends on STAT3. In addition, the PI3K-AKT-AP-1 pathway can also stimulate PDPN expression in brain tumors that have lost the normal negative regulation provided by PTEN. The AP-1 transcription factor, composed of Fos and Jun proteins, binds to the tetradecanoylphorbol acetate-responsive element (TRE) in the PDPN promoter, which is heavily methylated. Image generated with Biorender.

5.1. The mechanism of PDPN-protein interaction

As previously mentioned, the principal function of PDPN is through protein-protein interactions and signaling cascade. PDPN is the main endogenous ligand for CLEC-2, a non-classical C-type lectin expressed on platelets, dendritic cells and neutrophils (103). The CLEC-2/podoplanin axis promotes the separation of vessels during embryonic development, along with maintenance of lymph node vascular integrity and optimization of adaptive immune responses (107). The interaction of both proteins induces platelet activation among other functions like inflammatory regulation (103, 107). Other ligands are described to link to the extracellular domain of PDPN, such as Galectin-8 and C-C motif chemokine ligand 21 (CCL21) chemokine. Different to CLEC-2 function, Galectin-8 induces an increase of lymphangiogenesis, whereas CCL21 is mainly implicated in immune system functions such as immune response and development of Tregs (107).

Notably, protein interactions within extracellular domain depend on glycosylation status allowing for the correct conformation (105).

The intracellular domain of PDPN also lacks traditional signaling motifs, but interacts with ERM proteins, which are essential for cell polarity, adhesion, and migration. ERM proteins, which act as cytoskeletal adaptors, connect PDPN to the actin cytoskeleton and modulate small Rho GTPases, such as RhoA, Rac1, and Cdc42, which regulate cytoskeletal dynamics. Thus, this interaction orchestrates actin rearrangement, which is crucial for cell migration and invasion. Therefore, the PDPN-ERM interactions play a pivotal role in coordinating signaling events that govern cell behavior, particularly in cancer progression and metastasis (103, 105, 108). **Table 14** provides a summary of the proteins that interact with PDPN under physiological conditions.

Table 14. Physiological roles of PDPN related to their protein binding (105)

Binding sites with PDPN	*Ligands*	*Function*
Extracellular Domain	CLEC-2	Platelet activation
		Thrombosis
		Blood vascular integrity
		Lymphangiogenesis
		Immune response
	CCL21	Immune response
		Development of Treg cells
	Galectin-8	Lymphangiogenesis
Transmembrane Domain	CD9	Inhibition of PDPN-CLEC-2 interaction
	CD44	Modulation of cell migration
Cytoplasmic Tail	ERM	Embryonic development
		Immune response

Despite extensive studies on the role of *PDPN*, further investigation is required to gain a comprehensive understanding of the molecular function of PDPN under physiological conditions.

5.2. The role of PDPN in embryogenesis

During mouse embryogenesis, different locations and expression levels of *PDPN* are observed in association with stages of embryo development. Initially, *PDPN* is prominently expressed in the epithelium of pulmonary alveoli. However, in the final stages, its presence is limited to type-I neumocytes (109). Likewise, variations in its levels are observed in the CNS, being highly expressed at the beginning, and subsequently decreased during fetal development (103).

In 2003, the phenotypic characterization of mice lacking *PDPN* revealed significant physiological consequences. These knock-out mice exhibited respiratory failure shortly after birth, leading to mortality. Necropsy findings revealed abnormalities in the structure of terminal respiratory units, resulting in impaired lung inflation and function (103, 105). Additionally, the absence of PDPN led to lymphedema in these mice, likely attributed to increased migration and adhesion of ECs to fibronectin and type-I-collage within the lymphatic system (105). Studies have also demonstrated PDPN's involvement in vascular development, as its inhibition was associated with perturbations in capillary tube formation, as mentioned previously (103).

Furthermore, knock-out mice displayed increased fetal mortality linked to abnormal heart development. Morphological abnormalities such as hypoplasia, alterations in coronary vessels, and ventricular septal defects were observed (103). These cardiac anomalies are believed to be the results of impaired EMT processes due to the absence of PDPN. Notably, the loss of PDPN was associated with an increase in E-cadherin expression, suggesting a potential regulatory role through PDPN (104). These findings underscore the critical role of PDPN in various physiological processes during embryogenesis including lung and lymphatic function, vascular development, and cardiac morphogenesis.

5.3. Role of PDPN in tumor progression

Elevated levels of PDPN have been detected in a range of human cancers, particularly carcinomas, which exhibit a correlation with higher metastatic potential, mostly in tumors affecting the central nervous system like glioblastoma multiforme (108, 110). Nonetheless, PDPN expression has been observed across other types of tumors such as germinoma and melanoma (111). In addition, metastasis of these tumors exhibited higher levels of PDPN expression than the primary tumors, suggesting an association between elevated PDPN expression and a more unfavorable prognosis, similar to central nervous system (CNS) tumors (111). Notably, some studies have connected the expression of PDPN to cancer cells forming the invasive front of the primary tumor, and to CD45-positive inflammatory cell infiltration in the tumor (110, 112, 113).

Conversely, certain investigations have failed to establish a stable relationship between elevated PDPN levels and negative outcomes. Instead, these studies identified PDPN as a protective factor against tumor invasion, associating it with a favorable prognostic indicator (114). Moreover, diminished PDPN expression in the primary tumor of uterine cervix cancer has been linked to an unfavorable prognostic factor, characterized by an increased rate of lymphatic vessel invasion (114, 115). Even though there is controversy

between studies, it is widely accepted that PDPN expression can be influenced by tumor promoters such as 12-O-tetradecanoylphorbol-13-acetate (TPA), RAS, and Scr (116-118). These promoters have been linked to poor prognosis in different tumors. Additionally, other ligands such as epidermal growth factor (EGF) have shown to upregulate PDPN expression in tumors (118). Broadly, the majority of studies have linked the increased expression of PDPN in cancer cells to poor outcome.

Nevertheless, the function of PDPN among different tumors is not yet comprehensively understood. Many functions have been attributed to PDPN in relation to its potential role in the progression of cancer (**Figure 18**). In the 1990s, various studies demonstrated a correlation between aggregated blood platelets and metastatic potential when this protein was present on the surface of different mouse tumors (119-121). Its association was validated when antibody assays against PDPN inhibited the formation of tumor cell-platelet aggregates and lung metastasis (122). Similar results were observed in other mouse models (123). As previously described, one critical step in the metastatic cascade β involves the infiltration of cancer cells into blood vessels, where a significant portion of cells face elimination, either through immune system activity or mechanical damage induced by factors associated with blood flow. A protective mechanism against immune recognition and hemodynamic influences involves cancer cell aggregation, stemming from adhesion among cancer cells themselves and/or between cancer cells and blood components, particularly platelets (124). This aggregation is thought to enhance metastasis by promoting the adhesion of cancer cell clusters to vascular endothelium. This process is specifically known as intravascular arrest (125). Additionally, platelet-derived factors boost the proliferation potential of cancer cells and facilitate extravasation β by inducing the retraction of ECs. The binding of PDPN to blood platelets occurs through CLEC-2, resulting in platelet degranulation and oligomerization of CLEC-2 (123, 126).

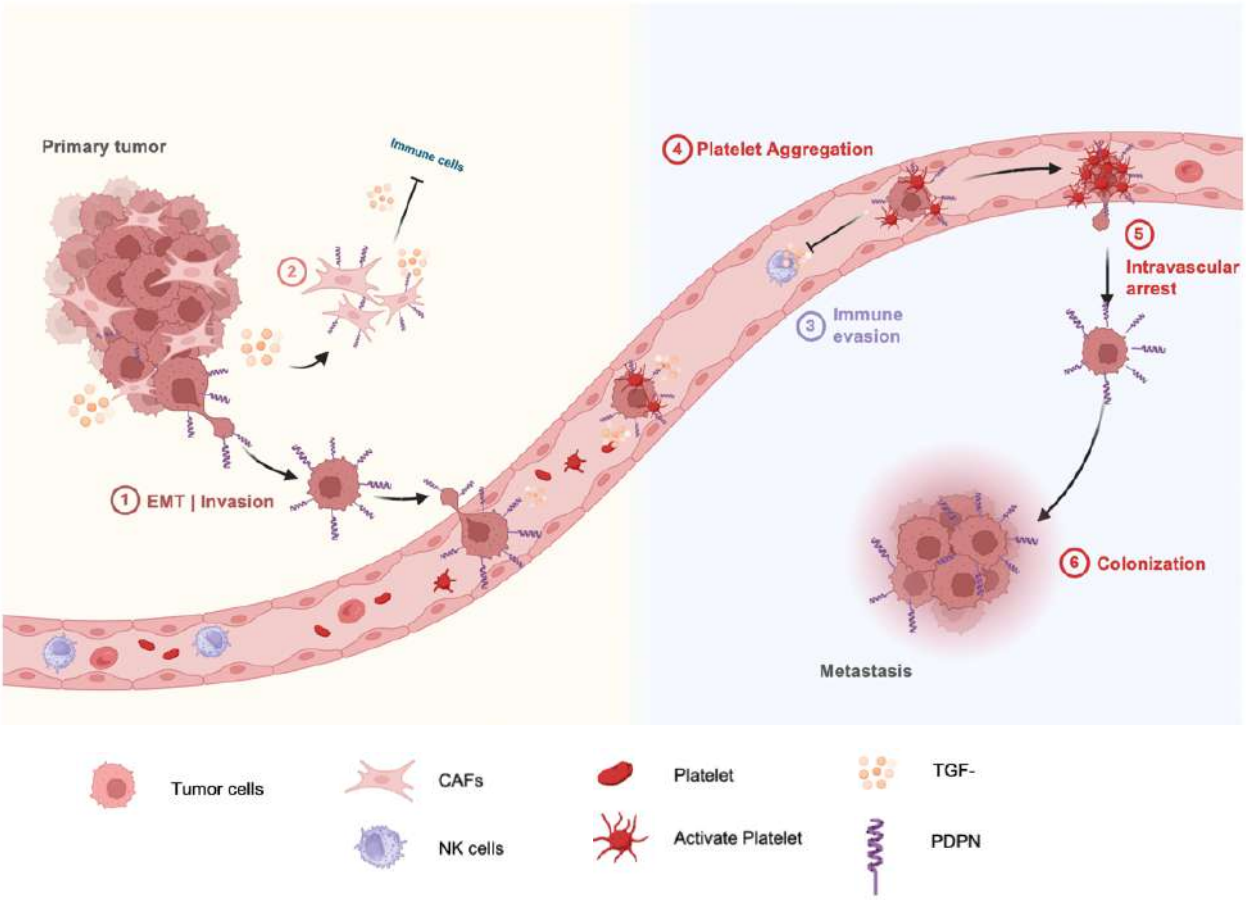

Figure 18. Involvement of PDPN during the metastatic cascade described in adult tumors. PDPN plays a crucial role in tumor metastasis process by inducing epithelial-to-mesenchymal transition (EMT), which reduces the levels of E-cadherin and promotes the spread of cancer cells from primary sites. PDPN recruits CD44 and MMP14 at filopodia, lamellipodia, and invadopodia, respectively, and stimulates hyaluronan-binding and extracellular matrix (ECM) degradation. Additionally, PDPN reorganizes the intracellular actin cytoskeleton, promoting cell motility. These events contribute to the migration/invasion phenotype and stimulate intravasation. Additionally, PDPN expression is observed at the invasive front of the tumor's collective invasion, which implies the importance of tumor-stroma interaction. Moreover, +PDPN CAFs construct the immunosuppressive tumor microenvironment (TME) by producing TGF-β, a potent immunosuppressive cytokine. PDPN-mediated platelet aggregation promotes the survival of shear stress and immune attacks in the circulation. Furthermore, platelet-derived factors (PDGFs and TGF-β) also promote tumor cell survival and plasticity. PDPN confers stemness, probably through the Rho-ROCK pathway, and promotes colonization in a distant organ. Thus, PDPN is involved in multiple steps of the invasion-metastasis cascade. Image created with Biorender.

PDPN interacts with migration- and invasion-promoting membrane proteins, including CD44 and MMP14 (105). The former is a highly glycosylated type I transmembrane glycoprotein with multiple isoforms that co-localize at cell-surface protrusions with PDPN. Direct interaction between both molecules has been associated to migration induction in different tumor types (127, 128). Additionally, specialized cell-surface protrusions, known as invadopodia, recruit glycoproteins involved in tumor cell invasion such as PDPN and CD44. The recruitment of PDPN to the adhesion ring of invadopodia relies on its binding to ERM proteins and its association with lipid rafts, which plays a dual role promoting

maturation and stabilization of the different components. Furthermore, PDPN/CD44 interaction has been linked to elevated MMP14 levels, hence, potentially playing a role in ECM degradation promoting the assembly of invadopodia (129-131). However, the precise details of the PDPN/CD44 interaction and its specific role in the assembly and maturation of invadopodia require further in-depth investigation.

On the other hand, PDPN has been linked to another form of cell movement known as ameboid migration in melanoma (132). Rounded cell morphology and the continuous formation of protruding membrane blebs are characteristic of this cell movement, which allow the cell to squeeze through the ECM (133). This phenomenon involves the phosphorylation of ERM proteins by PDPN, leading to characteristic cell blebbing and protrusions of ameboid migration type. Moreover, the rapid and high actomyosin contractility is associated with other interacting factors of PDPN, including RhoA, ROCK and myosin II (132).

Over the years, many articles have been published regarding the role of PDPN in many tumors, including two in NB. Both publications described the correlation of PDPN expression in NB cells with clinicopathological features. Studies show how elevated levels of PDPN expression associate with an aggressive disease phenotype, including advanced stage, high-risk features, and poor prognosis (134, 135). In addition, they also determined that PDPN was being expressed by LECs within the tumor tissue, and its expression was directly proportional to lymph-vessels density (135). It is worth mentioning that neither of the two studies determine the examined the role of PDPN in NB, and that PDPN expression extends beyond tumor cells and includes stromal components such as LECs, but also, CAFs and TAMs, implying its involvement in shaping the TME.

5.4. PDPN in the TME

Besides PDPN function in tumor cells, it is demonstrated that various cells conforming the TME express PDPN in their membrane, playing a critical role in cell-to-cell interaction. Among the different cell types in TME, PDPN is upregulated in pro-tumoral phenotypes of immune and stromal cells, highlighting TAMs and CAFs, among others (103). Investigations have particularly focused on the role of PDPN in TAMs, which promotes lymphangiogenesis and cellular invasion via the lymphatic system (136). In addition, several studies have demonstrated that the expression of PDPN is significantly associated with macrophage polarization towards a pro-tumoral phenotype.

In contrast to its role on macrophages and TAMs, the observation in CAFs show opposite functions depending on the tumor type, and the cell from which CAFs originate. Studies demonstrate that PDPN expression in this cell type enhances the invasion capacity of tumor cells by facilitating matrix digestion attributed to the activation of the Rho-ROCK pathway (137, 138). Recent studies observed an increase in TGF- β due to PDPN up-regulation, resulting in an inflammatory and pro-tumoral microenvironment. Conversely, an immunosuppressive role has also been described (139). No evidence of CAFs expressing PDPN has been described in NB. Studying its role in NB will increase our understanding of NB. In addition, it could potentially lead to the development of new target therapies by directly targeting CAFs.

5.5. PDPN in exosomes

As PDPN is a transmembrane glycoprotein, it is implicated in various biological processes, including EVs biogenesis and function. PDPN's role in exosomes is multifaceted, as evidenced by its involvement in the release of EVs and the modulation of recipient cell behavior. Cells expressing PDPN can release EVs containing PDPN in two distinct ways: either as mRNA and protein, which are then incorporated into both micro-vesicles and exosomes (140). Exosomes rich in PDPN have the ability to impact cellular processes like angiogenesis and lymphangiogenesis, with specific effects mediated by PDPN on the surface of the exosomes (140). Interestingly, it was demonstrated that PDPN-positive cells post-myocardial infarction release exosomes that can alter the physiology and structure of healthy hearts, suggesting a paracrine signaling role in cardiac pathology (141). Furthermore, in the myocardial infarction context, it has also been described that particularly the PDPN+ MSCs release exosomes that contribute to cardiac amyloidosis, highlighting a role post-injury cardiac remodeling (141). On the other hand, in glioblastoma tumors, elevated levels of PDPN expression have been linked to an increased risk of venous thromboembolism, which aligns with its primary function of stimulating platelet aggregation (142). Notably, in this situation, researchers demonstrated that it is not the tumor cells expressing PDPN that trigger platelet activation, but rather the EVs containing PDPN that play a crucial role (143). While the general role of exosomes in intercellular communication and cancer is well established, PDPN's specific contribution to these processes through exosomes underscores its potential as a therapeutic target in various pathologies, including cancer (144-146). In summary, PDPN is potentially integrated into the biogenesis and functional cargo of exosomes, influencing the behavior of host cells and contributing to pathological processes such as tumor progression, thrombosis, and cardiac remodeling.

5.6. Targeting PDPN

As insights into the relevance of PDPN have grown, various strategies have been developed to target it. The extracellular domain can be targeted by agents such as Maackia amurensis seed lectin (MASL) to inhibit tumor cell migration and viability (117, 147). In addition, antibodies have shown to disrupt the PDPN-CLEC-2 interaction, leading to decreased tumor burden in xenografts models of glioma, mesothelioma, and lung cancer (148-150). Broadly, this interaction is linked to intravascular arrest which promotes metastasis, as previously described. A derivate of 4-O-benzoyl-3-methoxy-beta-nitrostyrene (BMNS), compound “2CP”, binds to CLEC-2, preventing it from binding to PDPN, and demonstrating decreased PDPN-mediated platelet aggregation and tumor cell-induced platelet activation in PDX models (151).

On the other hand, the intracellular domain of PDPN contains various residues that can be phosphorylated, which alters the conformation of its amino acids, preventing tumor motility. Different compounds have been proved to target the intracellular domain of PDPN. Particularly, 8-br-cAMP, disulfiram and CARP-1 functional mimetics were shown to phosphorylate serine residues and inhibit PDPN-mediated cell migration (152-154).

In brief, innovative therapies such as near-infrared photoimmunotherapy (NIR-PIT), have been developed to directly target PDPN-expressing cells, including cancer cells and CAFs, with the goal of selectively eliminating them (155). Moreover, CAR-T cells targeting PDPN are being generated to treat glioblastoma, which have demonstrated encouraging *in vitro* activity effectively lysing tumor cells (156). Remarkably, the *in vivo* results showed a 60% decrease in tumor growth (157). Furthermore, cancer-specific monoclonal antibodies have been developed to exclusively target specific cancer cells (158).

In summary, PDPN serves as a critical target for the development of novel therapeutic strategies aimed at inhibiting cancer progression and metastasis. The multifaceted role of PDPN in various cellular processes underscores its potential as therapeutic target, with current research focusing on both intracellular and extracellular interventions to modulate its function (117, 147, 155, 157-160).

HYPOTHESIS AND OBJECTIVES

NB is a pediatric malignancy originating from neural crest cells, characterized by its heterogeneity in clinical presentation and outcomes. Notably, approximately 50% of patients present with metastatic disease at the time of diagnosis, significantly impacting prognosis and treatment. Despite advances in treatment modalities, survival rates vary widely depending on factors such as age at diagnosis, tumor stage, and genetic aberrations, with metastatic disease correlating with poorer outcomes. Over the years, numerous studies have been conducted to elucidate the molecular mechanism underlying NB metastasis by using different *in vitro* and *in vivo* models. Notwithstanding, there is still a lack of understanding in this area, which leads to a failure to improve patients outcome. Notably, immunotherapy has significantly improved prognosis of HR-NB patients. However, it is important to recognize that not all patients benefit from these advancements. Therefore, deciphering the mechanism of NB metastasis is critical to develop new therapies that can increase survival of HR-NB patients.

Metastasis is a highly intricate phenomenon that has been extensively studied in the context of adult tumors. However, it is important to remember that the cells of origin of pediatric cancers often exhibit inherent migratory capabilities due to their undifferentiated state. Thus, a comprehensive understanding of the diverse transformations that NB cells undergo to disseminate to other organs holds promise for more targeted and successful therapeutic strategies.

The main hypothesis, of this thesis, is based upon the idea that elucidating the molecular changes that NB cells undergo to infiltrate distant organs will not only advance cancer knowledge, but also unveil new therapeutic options for patients. Therefore, the main objective of this thesis is to develop a comprehensive genetic and epigenetic signature of NB cells with the potential to migrate and invade within the intricate heterogeneity of the primary tumor cells. To achieve this objective, we plan the following specific aims:

> ***Aim 1.*** To generate a NB spontaneous metastasis *in vivo* model, and obtain diverse genetic material (DNA, RNA, and noncoding RNAs) and protein from primary tumors and metastatic masses. We aim to demonstrate that NB tumor cells have the capacity to invade other organs at early stages of the disease.
>
> ***Aim 2.*** To define the genetic and epigenetic signature by multi-omics analyses. Analyses will be performed by comparing samples from the generated primary tumors to the newly formed metastasis. Data integration will enable the identification of the most robust set of genes involved in the process, and uncover the most altered pathways, providing a comprehensive understanding of the underlying mechanisms.

Aim 3. *In vitro* and *in vivo* validation of the metastatic signature. By generating isogenic systems in NB cells, we will explore the role of the most differentially expressed genes in our analysis. Different functional assays will be performed including wound healing assays, viability assays, and proliferation assays, among others.

Aim 4. Validation of the metastatic signature in patient cohorts. The signature will be validated in cohorts of patients by immunohistochemistry of available Tissue Microarrays (TMA) or patients biopsies.

MATERIALS AND METHODS

1. Cell culture

1.1. Cell lines

The NB cell lines used in this project are summarized in **Table 15** and were obtained from the repository at the *Institut de Recerca Hospital Sant Joan de Déu* (Barcelona, Spain). In addition, non-tumoral cell lines were used including human kidney embryonic cells 293T, human foreskin fibroblast (HFF-1) and human Mesenchymal stem cell (hMSC). HFF-1 and hMCS were kindly provided by Dra. Alexandra Avgustinova (PCCB-IRB), whereas 293T were obtained from the repository at the *Institut de Recerca Hospital Sant Joan de Déu* (Barcelona, Spain). Cells were cultured in Roswell Park Memorial Institute (RPMI)-1640 medium (Gibco) supplemented with 10% fetal bovine serum (FBS; Invitrogen), 2nM L-glutamine, penicillin (100 U/mL, Thermo Fisher Scientific) and streptomycin (100 µg/mL, Thermo Fisher Scientific), at 37 ^{o}C in 5% CO_2 and 95% relative humidity. During culture maintenance, cell medium was changed every 3-4 days. Exceptionally, HIFF-1 cell line was cultured in Dulbecco's Modified Eagle (DMEM) medium (Thermo Fisher Scientific) supplemented with 15% FBS and 2nM L-glutamine, and hMSC cell line was cultured in Mesenchymal Stem cell Growth Medium 2 (PromoCell) under low oxygen condition (5% CO_2 and 3% O_2). Cell passages were performed by enzymatic dissociation with Trypsin-EDTA 0.25% (Thermo Fisher Scientific) before cells reached 90% of confluence.

Table 15. Biological features of NB cell lines. A:Amplified; NA: Non-amplified; wt:wild-type; mut: mutated

Cell line	*MYC-N status*	*TP53 status*	*Tissue Origin*	*Tumor status*	*Sex*	*Age (years)*
LA-N-1	A	mut	Bone Marrow	Metastatic	M	2
LA1-55n	A	wt	Bone Marrow	Metastatic	M	2
SK-N-JD	A	wt	Bone Marrow	Metastatic		
IMR-5	A	wt	Abdomen	Metastatic	M	1
IMR-32	A	wt	Abdomen	Metastatic	M	1
SK-N-AS	NA	mut	Bone Marrow	Metastatic	F	6
SH-SY5Y	NA	wt	Bone Marrow	Metastatic	F	4

After dissociation, cells were suspended in fresh regular media and transferred to a new flask (Corning) or were counted with Cell Counter Luna (logos, Labtech), and cultured in

appropriated plates in preparation for the assay. Mycoplasma polymerase chain reaction (PCR) test was performed monthly. Notably, it is worth mentioning that NB cells were incubated in a low oxygen environment, alongside hMSC cell lines, when required.

For long-term storage, cells were kept frozen in liquid nitrogen or –80ºC. To this end, cellular pellets, were resuspended in 1 mL of FBS with 10% of Anhydrous Dimethyl Sulfoxide (DMSO, Sigma-Aldrich) and aliquoted in cryovials (Corning). The process for thawing cryopreserved cells entailed resuspending 1 mL of medium at 37ºC within the frozen cryotube, followed by manual mixing until the cells were fully thawed.

1.2. Primary cell culture derived from NB patients

PDX-derived NB models were generated by the group of Dr. Ángel M. Carcaboso from patient biopsies obtained at diagnosis or during different treatment stages at Hospital Sant Joan de Déu, Barcelona (15). PDX models used in this thesis are summarized in **Table 16.**

Table 16. Summary of molecular, biological and clinical features of each PDX cell lines used. A: Amplified; NA: Non-amplified; wt: wild-type; mut: mutated; MT: Metastatic; RF: Refractory; M: Male; F: Female BM: Bone marrow

PDX	*MYC-N status*	*TP53 status*	*Tissue Origin*	*Tumor Status*	*Sex*	*Age (years)*
HSJD-NB-002	A	mut	BM	MT	M	2
HSJD-NB-004	A	mut		RF	F	2
HSJD-NB-005-A	A	mut	kidney	MT	F	2
HSJD-NB-005-B	A	mut	BM	MT	F	2
HSJD-NB-007	NA	wt	Bone	RF	M	6
HSJD-NB-011	A	wt	Abdomen	RF	M	2
HSJD-NB-012	A	wt	Shell	MT	F	4
HSJD-NB-016	NA	wt	Spine	RF	F	3

1.3. Establishment of primary cell cultures from NB tumors originated in a spontaneous metastasis mouse model

Briefly, primary cell cultures were established from primary tumors and metastatic masses obtained from the spontaneous metastasis *in vivo* model. Tumor samples were mechanically dissociated using two scalpels, and centrifuge at 300 g for 3 min. Disaggregated samples were cultured in two different mediums: tumor stem medium (TSM; Gibco) and RPMI-1640 supplemented with 10% FBS, 2nM L-glutamine, penicillin (100 U/mL), and streptomycin (100 µg/mL). TSM was reconstituted in a 50:50 mixture of DMEM/F12 (Dulbecco's Modified Eagle Medium/Nutrient Mixture F-12) and Neurobasal medium (Invitrogen), HEPES buffer solution 10mM, 1% Sodium pyruvate MEM 100 nM,

1% MEM non-essential aminoacids 10 mM, 1% glutamax-I supplement and antibiotic-antimycotic (Gibco™), all purchased from Fisher™. Furthermore, the medium was completed with B-27™ supplement minus vitamin A (Gibco™), heparin (2 µg/mL, H3149-10KU, Sigma), h-EGF (20 ng/mL), h-FGF (20 ng/mL), h-PDGF-AA (10 ng/mL) and h-PDGF-BB (10 ng/mL). All human factors used for TSM reconstitution were purchased from Preprotech. Cell cultures were incubated under the same conditions of humidity, temperature and CO_2, as described before for cell lines culture. The media was refreshed every 2-3 days. When cells reached 90-95% confluence, were transferred to new flask for maintenance. Of note, a mixture of cells growing attached and in suspension was observed, known as semi-adherent cell culture. Cells grown in suspension were precipitated and mechanically dissociated following the replacement of 75% of the medium with fresh medium.

Additionally, fresh bone marrow (BM) aspirates were obtained from each mouse. This process was carried out in a sterile environment within the operating room, where the procedure was conducted under a closed cabinet. At endpoint, the BM was harvested from two different bones, the hindlimb where the primary tumor was established, and the backbone. For both, we harvested the BM by introducing a needle inside the bones and collecting the RPMI-1640 medium in an Eppendorf tube. Previously, bones were carefully peeled to avoid muscle contamination. The BM was centrifuged immediately at room temperature at 300 g during 3 min. The pellet was resuspended in TSM before culture in T-25 flask (Corning).

1.4. Stable transduction of PDPN

Overexpression of human *PDPN* was achieved using MISSION technology (Sigma-Aldrich) and lentiviral particles in LA-N-1 and SH-SY5Y NB cell lines. Before lentiviral transfection, a total of $7.5x10^5$ 293T cells were seeded in a six-well plate. After 24 hours, cells achieved a 90% of confluence, approximately, then, they were transiently transfected with lentiviral packaging vectors (1.5 µg D8-933 and 0.5 µg VSV-G), kindly provided by Dra. Alexandra Avgustinova (PCCB-IRB), and the corresponding plasmid (Vector Builder) using Lipofectamine 3000 (Thermo Fisher Scientific), following manufacturer's instructions. Lentiviral particles were collected from medium at 24-48 h post-transfection and stored at 4°C. The day prior to cell infection with lentivirus, NB cells were seeded in a six-well plate to achieve a 40% confluence at the time of transfection. Collected lentiviral particles were filtered, after centrifugation for 5 min at 250 g at RT, using a 0.2 µm filter to avoid cellular contamination. The whole particle concentration was added to NB cells within 5 µg/mL of polybrene to promote binding of the viral

envelope with cell membrane increasing infection efficacy. After 24 h, cell media containing lentivirus particles was removed and fresh medium with 1 µg/mL of puromycin (Sigma-Aldrich) was added to select transduced cells. The selection of cells was achieved after 10 days of puromycin exposure. All plasmids information used in this thesis is summarized in **Table 17**, along with nomenclature of the generated cell lines.

Table 17. Lentiviral plasmids used to generate stable cell lines during this thesis

Nomenclature	***Vector description***	***Source***	***ID***
Cell line_control	EGFP/Puro-EF1A>ORF_stuffer	VectorBuilder	VB010000-9389rbj
Cell line_^{High}PDPN	EGFP:T2A:Puro-EF1A>hPDPN	VectorBuilder	VB900136-2824wmf
Plasmids	***Vector Backbone***	***Source***	***ID***
D8-933	pCMVR8.2	Addgene	#12263
VsV-G	pCI	Addgene	#14888

1.5. Co-culture and cell culture medium conditions

To explore whether PDPN expression in tumor cells is induced by interactions with stromal cells or vice versa, various co-cultures and conditioned medium experiments were conducted. For co-culture, NB cells were cultured with the HFF-1 cell line. To mimic the proportions within the tumor, different concentration ratios were used, with cells seeded at 1:1 and 2:1. Moreover, a time course of *PDPN* expression analysis was performed, spanning intervals of 3, 6, and 24 h, with subsequent assessments made every 12 hours following the 6-hour time point. In a 96-well plate, 500 or 1000 cells, depending on the ratio of tumor cells to fibroblasts, were seeded at different time points. Once the assay was stopped, the cells underwent immunofluorescence (IF) in the same plate, following the same protocol as described in section 5.

For conditioned medium (CM), we obtained CM separately from NB cell lines (CM-NB) and a human fibroblast cell line (CM-FBL). To remove any residual cells, the CMs were spun at 300g for three minutes. The NB cell lines were then exposed to CM-FBL at various time points, while the human fibroblast cell line was exposed to CM-NB during the same timeframe. Both assays underwent IF as described to evaluate PDPN expression in section 5.

2. Molecular Biology techniques

2.1. RNA and miRNA extractions

Total RNA was isolated from tissue and cell samples using TRI Reagent (Invitrogen) following the manufacturer instructions. For cryopreserved tissue, we performed mechanistical disaggregation of the samples using two scalpels and samples placed in a safe-lock microtube (Eppendorf) containing steel beads 0.9-2 mm (Next Advance) and 150-300 µL of TRIzol ™ (Thermo Fisher Scientific). Tissue samples were homogenised using a Bullet Blender Storm 24 (Next Advance) at maximum speed at 4ºC, for 5 min until an homogenous mixture was obtained. The homogenous mixture was collected and transferred to a new tube to complete the manufacturer protocol.

For cell pellets, RNA and miRNAs extraction was conducted resuspending cells in 500 µL of TRIzol ™ followed by the addition of 100 µL of chloroform (Sigma-Aldrich) and manually agitated the sample to mix it thoroughly. After 10 min of incubation at room temperature (RT), tubes were centrifuged at 12000 rpm for 10 min. Top-phase was collected, transferred to a new tube and 250 µL of 2-propanol (Sigma-Aldrich) was added. In order to increase the efficiency of miRNA isolation, we flipped the tubes 6-8 times and incubated overnight at -20ºC. Next day, samples were centrifuged at 12.000 rpm for 10 min at 4ºC, and the obtained pellet was washed with 75% ethanol (VWR^{BDH} Chemicals). Consecutively, a centrifuge at 12.000 rpm for 5 min was performed and ethanol was removed using pipette. To avoid contamination, samples were left to dry in the bench until there was no visible ethanol in the tube. The final pellet was resuspended in 30 µL of purified water. RNA was quantified using NanoDrop ™ ND-1000 device (Thermo Scientific).

2.2. Reverse transcription and quantitative reverse transcription PCR (RT-qPCR)

Reverse transcription reaction was performed using 1 µg of purified RNA in order to obtain the complementary DNA (cDNA). Then, a mixture comprising random hexamers (0.5 µM, Thermo Fisher Scientific), random primers or dNTPS (0.2 mM, ABI), retro-transcriptase buffer (Thermo Fisher Scientific) and a transcriptase enzyme (100 u/µL, ABI) was added into the sample. For microRNA retro-transcription, manufacturer's protocol was followed (Thermo Fisher Scientific). In brief, RT-qPCR was performed using gene specific assay on demand and TaqMan® universal PCR Master Mix (Thermo Fisher Scientific) or specific forward and reverse primer pairs and SYBR Green PCR Master Mix (Thermo Fisher Scientific), as summarized in **Table 18-19**, in a QuantStudio

6 Flex (Applied Biosystems). The relative expression of mRNA was determined using the $2^{-(\Delta\Delta Ct)}$ quantification method and normalized to *β-ACTIN* as housekeeping gene in case of cDNA. T-test was used to compare differences between two groups using GraphPad Prism 10.

To assess miRNA expression levels, we followed the manufacturer protocol for each specific assay on demand (Thermo Fisher Scientific). The miR-23-3b was used as housekeeping. Used miRNAs are summarized in **Table 18**.

Table 18. Human TaqMan™ probes used to assess the expression levels of each gene, purchased at ThermoFisher Scientific, excepting PHOX2B probe (Sigma).

Gene/miRNA	*Assay ID*
PHOX2B	VC0021N/VC0023N
PDPN	Hs00366766_m1
GRIK3	Hs00168182_m1
DBH	Hs01089840_m1
PROM1	Hs01009259_m1
LUM	Hs00929860_m1
SEMA3A	Hs00416565_m1
NFL	Hs00196245_m1
ASCL1	Hs00269932_m1
SNAI1	Hs00195591_m1
β-actin	Hs99999903_m1
GAPDH	Hs02786624_g1
miR-629-5p	002436
miR-6780-3p	467339_mat
miR-149-3p	002255
miR-23-3b	245306_mat

Table 19. List of primers (SYBR Green technology) used to assess gene expression levels were purchased in Sigma

Gene	*Forward sequence*	*Reverse sequence*
NF	TGTCAGTGCATAACCTCTTGC	AGTGCCATCACTCTTTTCTGAAG
VIM	TACAGGAAGCTGCTGGAAGG	ACCAGAGGGAGTGAATCCAG
SLUG	*AACGCCTCCAAAAAGCCAAA*	*GGTTGTGGTATGACAGGCATGG*
TWIST1	AAGGCATCACTATGGACTTTCTCT	GCCAGTTTGATCCCAGTATTTT
hTGFB1	*CTGGAGAGGGCCCAGCATCT*	*CGCACGCAGCAGTTCTTCTC*
hTBP	GAACATCATGGATCAGAACAACAG	ATTGGTGTTCTGAATAGGCTGTG
α-SMA	*CCGCGATCTCACCGACTACC*	*GGGCCACGTAGCACAGCTTC*
mFAP	CTCGTCCAATTCAGTATCTATG	GCATTTCCTCTTCATAAACCC
mCD68	*TGCTCAGCTGCCTGACAAGG*	*GGAGGACCAGGCCAATGAT*
mCD163	AGTCTGCTCACGATACATAG	TCCTTCTGGAATAGATTGGG
mTGFB1	*GGAGCCCGAAGCGGACTACT*	*TTGGTTTTCTCATAGATGGCGTTG*
mTBP	TGCTGACCCACCAGCAGTTC	GGAGAACAATTCTGGGTTT

2.3. Protein Extraction

For tissue samples a piece of frozen tumor was cut using two scalpels and homogenized in safe-lock microtubes with stainless steel beads 0.9-2 mm and 150-200 µL of commercial RIPA 1X buffer (25 mM Tris·HCl pH 7.6, 150 mM NaCl, 1% NP-40, 1% sodium deoxycholate, 0.1% SDS, Thermo Fisher Scientific) completed with proteases Inhibitors Cocktail Tablets X25 (Roche). Using Bullet Blender Storm 24 at 12000 rpm, at 4ºC, for 5 min until homogenous mixture was obtained. The homogenous mixture was collected and transferred to a new tube. Afterwards, samples were incubated for 30 min at 4ºC, vortexing every 10 min, and centrifuged for 20 min at 13.000 rpm.

For cell pellets, samples were directly incubated with 30-60 µL of commercial RIPA 1X buffer completed with Proteases Inhibitors Cocktail Tablets X25. For exosomes, different methods were employed based on the isolation protocol. In the case of exosomes isolated from serum samples, 2,5 µL of the total concentration of exosomes were incubated with 30 µL of commercial RIPA 1X buffer supplemented with Proteases Inhibitors Cocktail Tablets X25. For ultracentrifuge (UC)-isolated samples, another UC was performed to obtain a second pellet for protein extraction. From the total concentration of exosomes, 20 % of the final volume was used to obtain the protein pellet, which was incubated with 30 µL of commercial RIPA 1X buffer supplemented with Proteases Inhibitors Cocktail Tablets X25. The protocol for both sample types was executed using the same procedures as those employed for tissue samples. The protein extracts were quantified with Bradford Reagent (Bio-Rad) by measuring the absorbance at 560 nm using a TECAN INFINITE FNANO^{+} (Mannedorf).

2.4. Western Blot

For Western Blot (WB) electrophoresis, 30 to 60 µg of protein were mixed with Lammeli buffer in a 1:5 proportion and incubated for 5 min at 95 ºC before loaded in 8-12 % polyacrylamide gels. Subsequently, proteins were transferred into a nitrocellulose membrane (GE Healthcare Lyfe Science) and blocked in 3% Bovine Serum Albumin (BSA, Sigma-Aldrich or 5% skim milk power (Sigma) solved in Tris-buffer saline, 0.1 %Tween 20 (TBS-T) depending on the primary antibody, for 1 h at RT in agitation. Primary antibodies were incubated overnight at 4ºC (**Table 20**). In general, membranes were incubated with fluorescence labelled secondary antibodies (IRDye anti-rabbit IgG and IRDye anti-mouse IgG), for 1 hour at RT in agitation. The different secondary antibodies used are summarized in **Table 21**. After three washed with TBS-T for 10 min, fluorescence was detected using LI-COR Odyssey Classic Infrared Imaging System (LI-COR Inc.). Relative levels of protein expression were measured by Image J Software (161).

Table 20. Antibodies used for protein detection during this thesis. WB: Western Blot; IF: Immunofluorescence; IHC: Immunohistochemistry.

Protein	*Technique*	*Working solution*	*Reference*	*Source*
PDPN	WB/IF FC	1:500/1:100 1:100	HPA007534	Merck
D2-40	IHC	1:200	IR07261/2	Agilent
PHOX2B	IHC	1:200	ab183741	Abcam
GRIK3	IHC/WB	1:100/1:500	PA598452	ThermoFisher Scientific
LUM	IHC	1:500	HPA001522	Merck
SEMA3A	IHC	1:50	HPA029447	Merck
LYVE-1	IHC	1:100	MA532512	ThermoFisher Scientific
CD31	IHC	1:100	ab28364	Abcam
FAP	IHC/IF	1:100	PA5-99458	ThermoFisher Scientific
α-Tubulin	WB	1:30.000	T6199	Sigma Aldrich
Laminin-β1	WB	1:2.000	ab16048	Abcam
Anti-human Nuclei	IHC/IF	1:200	MAB4383	Millipore
TSG101	WB	1:100	ab125011	Abcam
CD63	WB	1:100	ab134045	Abcam
CD81	WB	1:100	ab109201	Abcam
CD9	WB	1:100	ab263019	Abcam
CD9	FC	1:100	10626D	ThermoFisher

For exosomes, modifications of the protocol were conducted. The initial modification involved excluding Dithiothreitol (DTT) from the Lammeli Buffer to prevent any interference with tetraspanin proteins. Furthermore, the polyacrylamide gels were prepared without the addition of SDS to their composition to avoid the alteration of exosome specific proteins. Final modifications are related to protein quantification, which was performed using iBright Imagine System 1500 (Invitrogen), to improve signal specificity, after bathing the membrane with chemiluminescent HRP Substrate (Millipore; 1:1) for 1-2 min. Therefore, for hybridization of the membrane with secondary antibodies, we added non-fluorescently labelled secondary antibodies (**Table 22**). Imaging acquisition of the membrane was obtained with multi-exposure method including different time expositions from 30'' to 15'. Relative levels of protein expression were measured by Image J Software as previously described (161). Secondary antibodies information is available in **Table 22**. T-test was used to compare differences between two groups using GraphPad Prism 10.

Table 21. Secondary antibodies used to detect primary antibodies during this thesis. WB: Western Blot; IF: Immunofluorescence; FC: Flow Cytometry.

Secondary antibody	*Technique*	*Conjugated to*	*Reference*	*Source*
IRDye anti-rabbit IgG	WB	680LT	925-68023	LI-COR
IRDye anti-mouse IgG	WB	800CW	926-32211	LI-COR
Goat Anti-rabbit IgG(H+L)	IF	Alexa flour™ 488	A11034	Invitrogen
	IF	Alexa flour™ 594	A11012	Invitrogen
	IF/FC	Alexa flour™ 647	A21244	Invitrogen
Goat Anti-mouse IgG(H+L)	IF/FC	Alexa flour™ 488	A32723	Invitrogen
	IF	Alexa flour™ 594	A11035	Invitrogen

3. Multi-omics techniques

3.1. Genome-wide array profiling

Total RNA (2 μg) was extracted from primary tumors (T) and metastatic masses (M) generated in the spontaneous metastasis *in vivo* model and PDX-derived NB cells (Cp) using TRI Reagent. For quality control, tissue samples were previously included in OCT, and the percentage of tumor cells assesed by a Board certified Pathologist at the Department of Pathology, *Hospital Sant Joan de Déu.* Only samples with > 80% of tumor cells content were selected for further analysis. In addition, assessment with Agilent 2100 Bioanalyzer (Agilent Technologies, Santa Clara) was performed before microarray experiments. Genome-wide analysis was performed using Affymetrix Clariom™ D Assay for human samples (Affymetrix, Santa Cruz) at *Servei d'Anàlisi de Microarrays (MARGenomics, Institut Hospital del Mar d'Investigacions Mèdiques* (IMIM), Barcelona, Spain.. Amplification, labelling and hybridization were performed according to the GeneChip WT PLUS Reagent kit and the samples hybridized to Clarion D Human (ThermoFisher Scientific) in a GeneChip Hybridization Oven 640. Washing and scanning were performed using the Expression Wash, Stain and Scan Kit (Affymetrix Inc). Gene expression array data was analysed at the Sarcoma Research Group, *Institut d'Investigacions Biomèdica de Bellvitge* (IDIBELL), Barcelona, Spain. Bioinformatic analysis included quality control of raw data (aroma.affymetrix package)(162) and normalization using the robust multi-chip average (RMA) and comparative analyses by the Linear Models for Microarray package (*limma* package)(163) as shown in **Figure 19A**. Principal component analysis (PCA) was performed before DEGs detection (**Figure 19B**). Probes were considered significantly differentially expressed when the adjusted false discovery rate (FDR) was <0.05. Differentially expressed genes (DEG), with p-value < 0.05 and LogFC > 0.58 (absolute value), were selected as significant. The list of DEGs was used for a gene set enrichment analysis against the Gene Ontology (GO) using Enrichr (164). For the analyses, we included paired samples, T (N_A=6; N_B=6) and M (N_A=5; N_B=4), of both

HSJD-NB-005 models. Three different RNA extractions from PDX-derived NB cells from the passages before animal inoculation were included in the analysis.

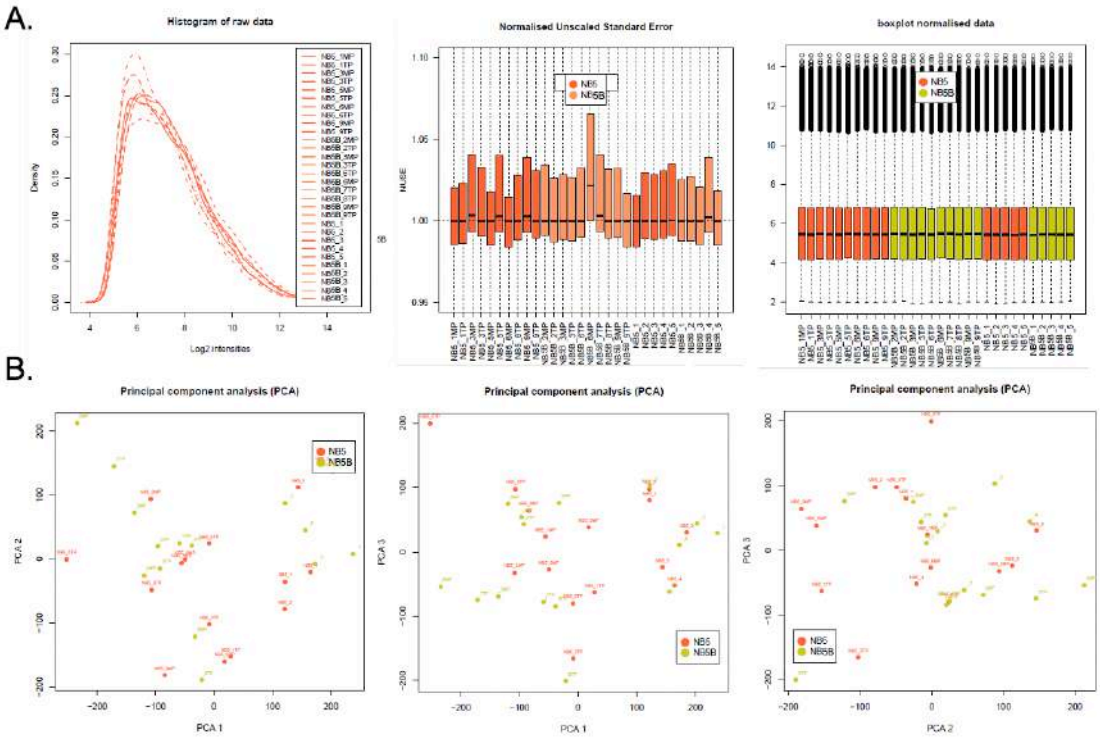

Figure 19. Raw data processing of Clariom-D samples. **A.** Quality control and data normalization of individual samples. **B.** PCA analysis of both NB models included in the analysis.

3.2. miRNA array profiling

Total RNA containing miRNAs was extracted from tumor samples of HSJD-NB-005-B (NB016) *in vivo* model, including same samples as in the previous array (T=6, M=4 and Cp=3; referred as 6_sample_TP; 6_sample_MP; and NB16_replicate in bioinformatic analysis, respectively). Extraction of miRNA was conducted following NucleoSpin miRNA kit instructions (Cultek). Affymetrix GeneChip miRNA 4.0 Array (Affymetrix, Santa Cruz) was used following the manufacturer protocol in the Microarray Department of Institut Josep Carreras (IJC, Barcelona). As before, bioinformatic analysis included quality control normalization (RMA) and comparative analyses using R (*limma* package; F**igure 20A**). Principal component analysis (PCA) was performed before differential expressed miRNAs detection (**Figure 20B**). Differentially expressed miRNAs (p-value < 0.05 and LogFC > 0.58) were obtained by comparing primary tumors to metastasis. For the enriched pathways analysis and the targets associated to miRNAs, we used different tools from miRTarBase (165). Gene targets described for differentially expressed miRNA were used to conduct a gene enrichment analysis against the Gene Ontology using Enrichr (164). Figures were generated using ggplot2 package and RColorBrewer package. All analyses were performed in R (v3.5.2, http://www.R-project.org/).

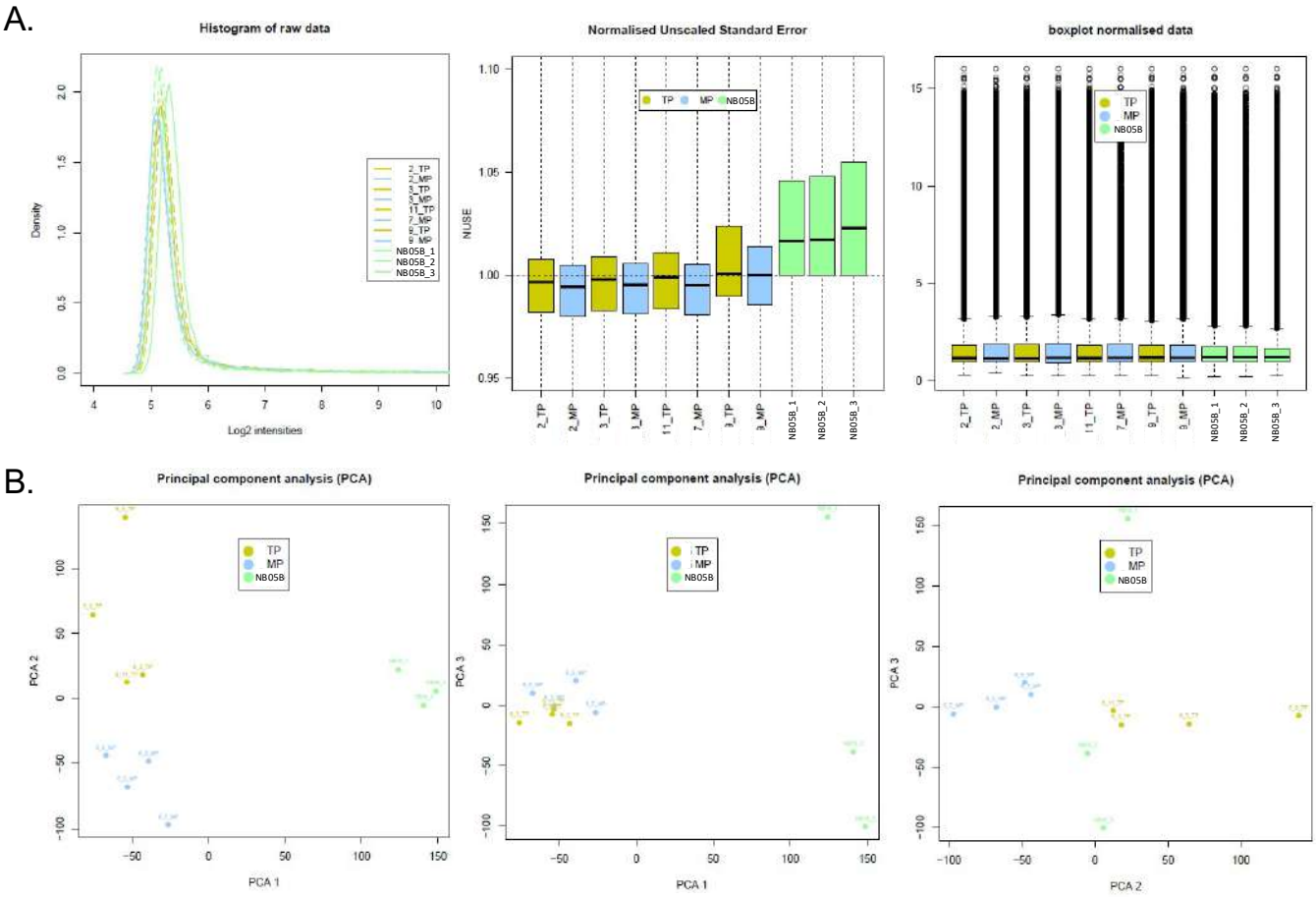

Figure 20. Raw data processing of samples included in miRNA 4.0 array. **A.** Quality control and data normalization of individual samples. **B.** PCA analysis.

3.3. Methylation array profiling

Tumor and Metastasis samples (T=3, M=3 and Cp=3) obtained from the NB spontaneous metastasis mouse model generated by inoculation of HSJD-NB-005-B were included in the methylation analysis. Genomic DNA (gDNA) was extracted following DNA extraction protocol established in the laboratory. In brief, mechanical disaggregation was performed in cryopreserved tissue samples by using two scalpels. Cell lysis solution (#158908, Qiagen) supplemented with proteinase K (Sigma), was used overnight in agitation at 37ºC. Next day, protein precipitation buffer (#58912, Qiagen) was added in our samples before centrifuging for 10 min at 2000 g at RT. Isopropanol and ethanol were used consecutively to purify and washed gDNA. Samples were resuspended in hydration solution (#158914, Qiagen). Methylation array was processed at the Genomic unit of the *Institut de investigació Josep Carreras* (IJC). Total gDNA (500 ng) was converted by sodium bisulfite using the EZ DNA Methylation kit (Zymo Research), following the manufacturer's protocol. The bisulfite-converted DNA was hybridized to the Infinium MethylationEPIC BeadChips (Illumina) which covers over 850000 CpG sites

along the human genome. Whole-genome amplification and hybridization were performed, followed by single-base extension and analysis on a HiScan (Illumina) to determine the cytokine methylation states. The methylation data was processed in the R statistical environment using RnBeads 2.0. Raw data intensity data files (IDATs) were imported into RnBeads 2.0 for quality control and preprocessing. To filter out low-quality probes, a greedycut algorithm was used. Probes overlapping with SNPs and probes whose sequences mapped to multiple genomic locations were removed. IDATs obtained in the array were normalized using the beta-mixture quantile (BMIQ) method. The DNA methylation level was represented as the average β-value, which was calculated as the radio of the fluorescent signal intensity of the methylated probe of those of total (methylated and unmethylated) probes. Average β-values were used to calculate the mean methylation difference between groups. Hierarchical linear models performed wigh RnBeads 2.0 were used to obtain the methylation differences between groups. P-values were corrected for multiple testing (FDR) using Benjamini-Hochberg method and a threshold of p-value <0.05 was selected for significance. As a first step, quality control and normalization of the data were performed (IDIBELL; **Figure 21A**). PCA analysis and supervised hierarchical clustering heatmaps of β-values were generated using the prcomp

function and Complex Heatmap package, respectively (**Figure 21B**). The enrichment analysis of biological pathways was evaluated using Enrichr software (164) .

3.4. Proteome cytokine profiler array

In order to explore the potential role of cytokines in the metastatic process, a cytokine profile proteome array (Mouse cytokines array panel A, R&D Systems) was conducted, enabling simultaneous detection of multiple cytokines in a single sample. Cytokine levels were assessed in new primary tumor protein extraction (N=4) from HSJD-NB-005-B, as described in the manufacturer protocol. The chemiluminiscent signal of each membrane was detected using iBright Imagine System 1500 (Invitrogen) and quantified with Image J Software (161).

3.5. Spatial transcriptomics analysis

The spatial transcriptomics (ST) analysis was performed on FFPE samples obtained from two distinct patients, including HSJD-NB-005. From the NB cohort at Hospital Sant Joan de Déu, we undertook intensive research to identify two patients with the same tissues affected at the

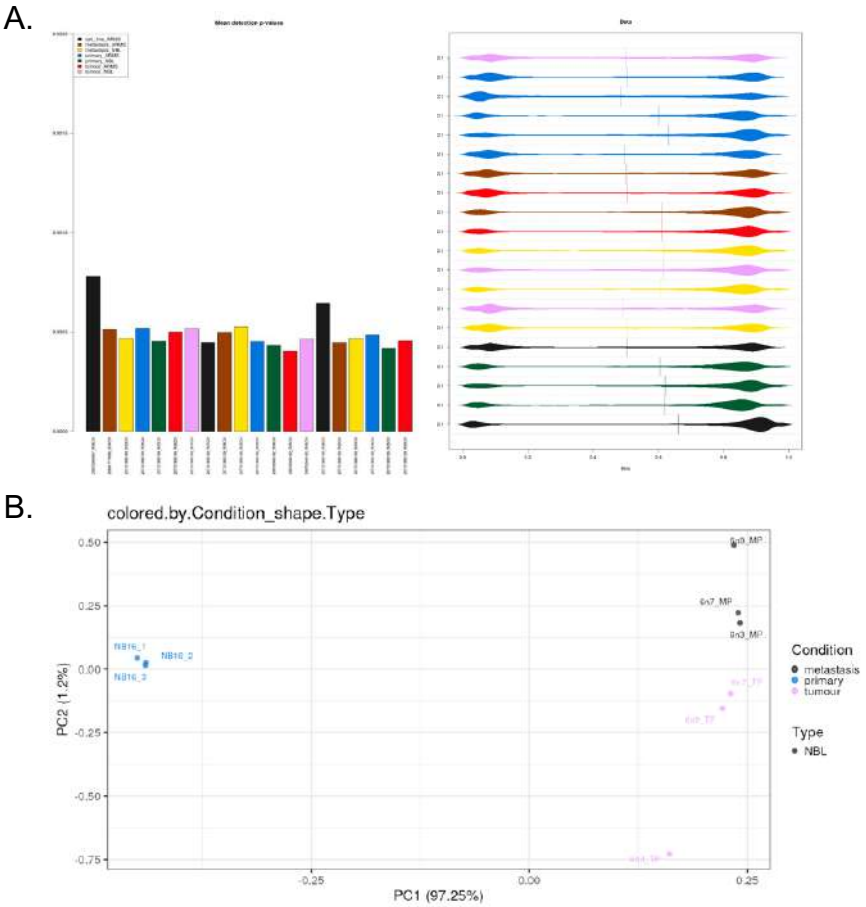

initial diagnosis and the final stages of the disease. Using the same tissue will enable the

Figure 21. Data processing of methylation analysis. **A.** Quality control (left) and data normalization (right) of NB tumor samples. **B.** PCA from NB sample, referred as NBL, distinguishing between primary tumor (pink; referred as tumour), metastatic mass (dark grey, named as metastasis) and cell culture samples (blue, annotated as primary). (NBL=neuroblastoma)

comparative analysis of the spatial distribution of the tumor and the stroma components. After the selection of patient samples, a preliminary pathological analysis was conducted by a board certified pathologist to select the tumor region and the stroma components. A 6.5 mm area was selected from each sample, comprising both tumor cells and surrounding stroma.

Subsequent procedures were carried out at the Cancer Immunogenomics Group at the IJC. Prior to initiating the analysis, a quality control of the RNA was conducted according to the manufacturer's protocol of the Cytassist. Samples with a DV200 value higher than 25% were included in the study. Afterwards, Visium CytAssist for FFPE Spatial Gene Expression for human samples was conducted following manufacturer's protocol. Then, the barcoded library, generated after tissue permeabilization, was subjected to standard NGS short-read sequencing on Ilumina sequencers at Macrogen. The Space Ranger analysis software was employed for the analysis and visualization of the data. The SCTRansform package was used for data normalization across dimension data samples, and FindMarkers (min.pct = 0.8; LogFC.Threshold = 0.25) was carried out to identify specific markers. Harmony algorithm was used to integrate spatially resolved transcriptomic data with next generation sequency data, considering primary tumor and metastasis (only.pos = TRUE, min.pct = 0.4, logfc.threshold = 0.25)(**Figure 22**).

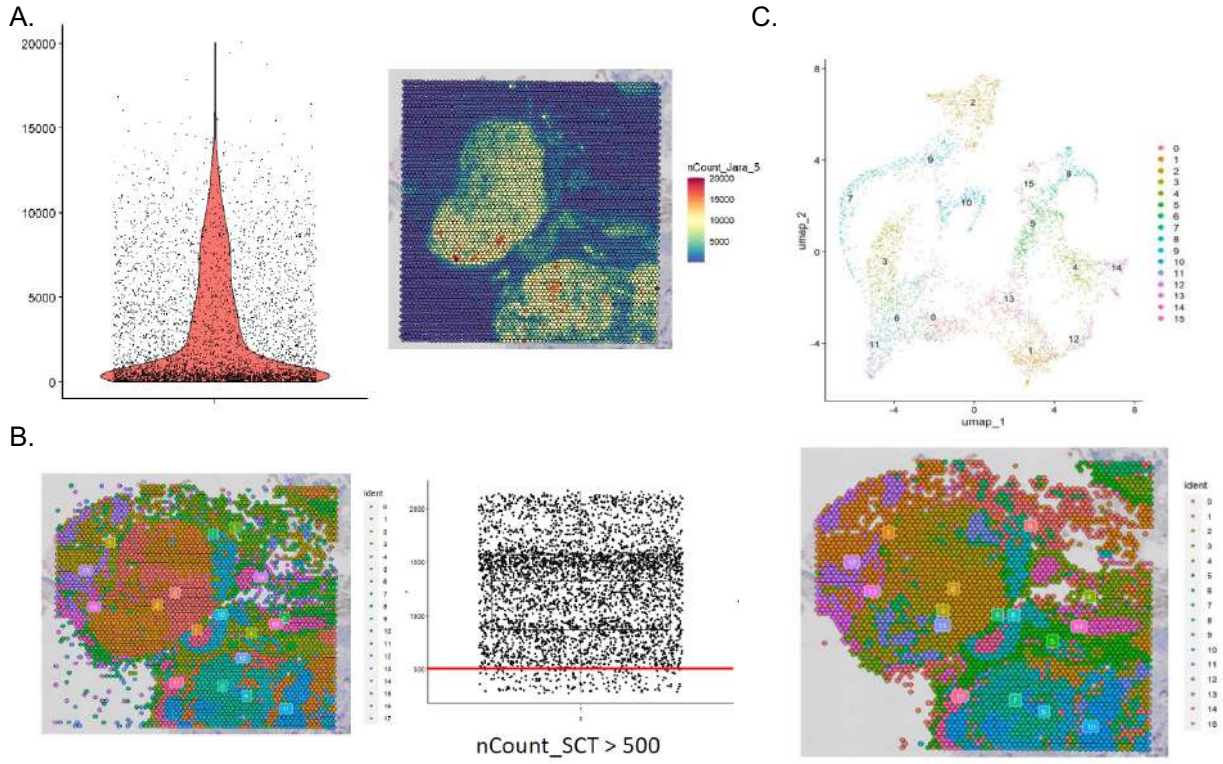

Figure 22. Example of data processing of spatial transcriptomics analysis. A. Data preprocessing of FFPE sample, resulting in high number of nCounts. Each count represents the number of genes in each spot. **B.** Quality control of data samples. **C.** Unsupervised clustering of FFPE samples represented using a U-map (top) and spatial map (bottom)

4. Immunohistochemistry (IHC)

Transversal sections from collected tumors were included in a histology cassette and preserved in formol for at least 24 hours. Tumor sections were included in paraffin in the Department of Pathology (AP) at *Hospital Sant Joan de Déu* following standard protocols. Formalin-fixed paraffin embedded (FFPE) samples were sectioned using a microtome and included into histological slides. Sections (3 µm) were deparaffinized in a hot chamber for at least 30 minutes and dried before each staining or immunohistochemistry (IHC) for different protein markers. Then, sections were subjected to a series of decreasing alcohol dilutions. At this point, all procedures were executed either automatically using a AutostainerLink 48 (DAKO) or manually within the laboratory. Sections were immunostained with Novolink polymer detection system (Leica) according to manufacturer's protocol after antigen retrieval with 10 mM citrate buffer pH 6. The sections were incubated with primary antibodies at 4ºC, overnight using BOND primary antibody diluent (#AR9352, Leica). After incubation, slides were washed and IHC was developed with 3.3'-diaminobenzidine (DAB, Sigma) until the signal was visible. The counter staining with hematoxylin-Eosin (HE) was carried out in Tissue-Tek Prima(r) automated slide stained using an HE staining kit. To determine the specificity of primary antibodies that had not yet been established in our laboratory, negative and positive controls were tested (**Figure 23)**. The primary antibodies used during this thesis are summarized in **Table 21**.

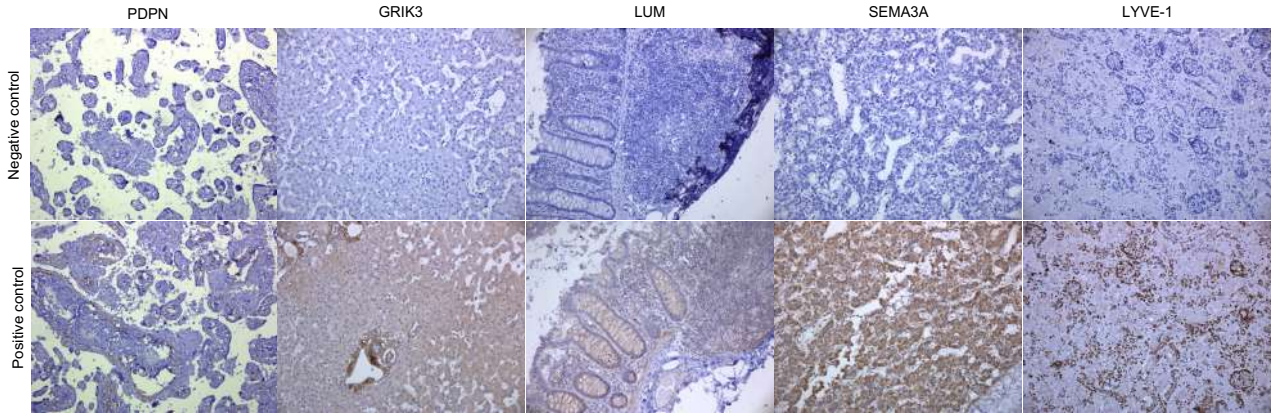

Figure 23. Technical controls of IHC. Non-pathologic tissues were used as positive controls for each Ab, which has not been previously employed in the laboratory. Negative controls were not exposed to any Ab in order to determine Ab specificity. Specific tissues used for each Ab were: placenta (PDPN using D2-40 Ab); pituitary gland (GRIK3); colon (LUM); Liver (SEMA3A) and Kidney

5. Immunofluorescence (IF)

5.1. IF on primary culture cells

Adaptations from the same protocol were performed based on whether the cells were adherent or growing in suspension. In case of adherent cell cultures, such as NB commercial cell lines, cells were grown on glass coverslips and fixed with 4% formaldehyde (PFA) in PBS for 20 minutes at room temperature (RT). For non-adherent cell cultures, including primary cell lines from the *in vivo* model, pellets of cells were embedded in OCT in the Pathology Department (*Hospital Sant Joan de Déu, Barcelona)*. Afterwards, cut sections were placed into slides for fixation with 4% PFA for 20 min. Going forward, the protocol was standardized for both cell types. Of note, previous to fixation, cells were labeled with Wheat Germ Agglutinin conjugated to Alexa Fluor ® 647 (Thermo Fisher Scientific) at a concentration of 0.5 µg/mL for 10 min at 37ºC.

After fixation, samples were washed in PBS for 10 minutes at RT. Then, permeabilization and blocking steps were combined. Cells were incubated for 120 minutes in solution A (5% BSA diluted in PBS and 0.05% of Tween) at RT in a humidified chamber. Once blocked, cells were incubated with primary antibodies overnight at 4ºC (**Table 21**). Next day, samples were washed 3 times with PBS for 10 minutes at RT and incubated 2 hours with secondary antibodies diluted 1:1.000 in Solution A at RT (**Table 22**). After 3 washes with PBS for 10 minutes at RT, cellular nuclei were counterstained with DAPI (1:2.000, Thermo Fisher Scientific). Additionally, phalloidin (1:2.000, Thermo Fisher Scientific) staining was added at the same time as DAPI, both resuspended in PBS, and the incubation time was extended up to 30 min. Finally, the coverslips were mounted on a slide using Vectashield mounting medium (Vector laboratories). Images were taken under a Thunder Imager Leica DM6 B. Each IF procedure was performed, including negative controls for each antibody, as shown in **Figure 24A**.

5.2. For formalin-fixed paraffin-embedded (FFPE) Blocks

Paraffin block samples were cut into sections of 3 µm. After dewaxing using established protocols, the samples underwent antigen retrieval with a target retrieval solution in a hot water bath at 95°C for 30 minutes. The samples were then incubated in the retrieval solution pH 6 Novocastra (Leica Biosystems) at RT on the bench for 20 min, followed by a 5-minute rinse with running tap water. A hydrophobic pen (Vector Laboratories) was used to draw a closed barrier around the sections to reduce incubation volume. The samples were then washed with PBS for 30 min and incubated with Solution A for 120 min at RT. At this stage, the IF protocol was similar to cell culture protocol, with a modification in the duration of the washing steps,

which was extended to at least 30 min. Negative controls were included (**Figure 24B**). In order to identify the location of PDPN, it was necessary to establish the best cellular marker. Various markers, including those for the nucleus (Histone-1) and cell membrane (WGA and α-actin) were tested in FFPE samples due to their high background signal. As shown in **Figure 24C**, none of these markers emitted sufficient signal when compared to the PDPN marker.

In general, samples were sealed with nail varnish after excess of mounting medium was removed. Eventually, samples were stored at 4ºC prior to picture assess, and at -20 ºC for long term storage.

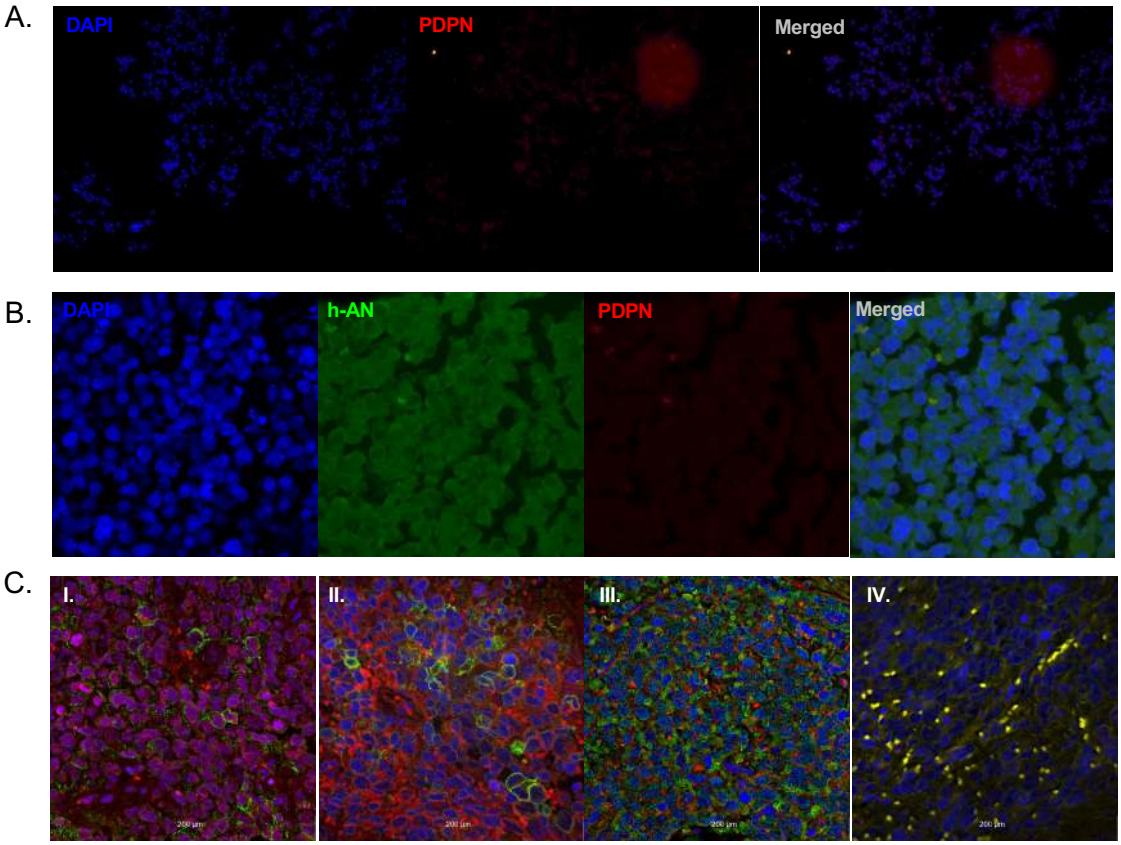

Figure 24. Technical controls of IF. **A-B**. Negative controls of PDPN and h-AN of cell culture and tissue samples included in FFPE, respectively. **C.** Various surface markers used in order to identify PDPN location in FFPE samples. (I.) Histone 1; (II.) WGA; (III.) alpha-actin; and (IV.) negative control.

6. Enzyme-linked immunosorbent assay (ELISA)

The levels of TGF-β1 and IFN-γ cytokines were quantified in protein samples obtained from tissue extracts using the Quantikine ELISA kit (Biotechne), following the manufacturer's protocol. To quantify IFN-γ (# MIF00), a specific kit for mouse cytokines was used. The TGF-β1 kit (#DB100C), on the other hand, is capable of recognizing different species, including humans, mice, and rats, among others. Following the manufacturer's instructions, the reaction was terminated using a specific buffer, and the absorbance at 490 nm was measured using a

TECAN INFINITE FNAno+ (Mannedorf). T-test was used to compare differences between two groups using GraphPad Prism 10.

7. Exosomes isolation

Different isolation methods were implemented based on the type of samples, with a distinction made between serum obtained from our *in vivo* model and cell culture samples. As the volume of serum samples was a limitation, exosome isolation was performed using the Total Exosomes isolation Kit for serum samples (Invitrogen). For long-store, serum samples were kept at -80ºC, and were thawed under tap water as recommended in the protocol. Since sample volumes varied heterogeneously across different time points, the same volume was used, with the smallest sample serving as the reference within a minimum of 10 µL. Exosome isolation was conducted following manufacturer's protocol.

For cell culture exosomes isolation, the conventional method of ultracentrifuge (UC) was performed at the *Institut d'Investigació Biomèdica de Bellvitge* (IDIBELL) facilities. NB cells (LA-N-1 and SH-SY5Y) achieved a 90% confluence when supernatant was collected. Supernatant, from one T-125 Flask or five T-75, was collected after three days of cells being cultured in RMPI-1640 without FBS. At that time, 30 mL of the supernatant was collected and centrifuged at 300 g for 10 min at 4ºC. The pellet was discarded, and the supernatant was further centrifuged at 15.000 g for 20 min at 4ºC using a Beckman centrifuge. Once again, any pellet obtained was discarded, and the supernatant was carefully filtered using 0.2 µm filter. The samples were stored in the freezer at 4ºC for 24 h. The following day, an ultracentrifugation was conducted at 27.000 rpm for 70 min at 4ºC. The supernatant was finally discarded, and a non-visible pellet was resuspended in 100 µl of PBS using vortex to lift it. The total volume was divided into two parts for further processing. The first part was stored safely at -20ºC until it was used for further experiments. The second part underwent ultra-centrifugation at 26.000 rpm for 70 minutes at 4ºC, using the F50L rotor. The resulting pellet was preserved at -80ºC until protein extraction was performed.

8. Cell viability assay

Assays were conducted by seeding a total of 1.000 NB cells in each well of a 96-well plate, with 4-6 replicates per plate. Five plates were seeded to analyse cell viability every 24 h, for 5 consecutive days. At the time of seeding, cell Titer 96R Aqueous Non-Radiactive Cell Proliferation Assay (MTS, Promega) was added into the wells (1:10) from one plate to measure time 0 in case of cells growing as tumorspheres. For adherent cells, MTS was added once cells were fixed to the plate. Once MTS was added to the wells, 3 hours of incubation

was carried out at 37 ^{o}C in 5% CO_2 and 95% relative humidity. Absorbance quantification at 490 nm using TECAN INFINITE FNANO+ was directly proportional to the number of living cells in each well. Of note, each plate contained 3-6 wells with the medium from day 0 to be used as background measure for normalization purposes. T-test was used to compare differences between two groups using GraphPad Prism 10. In this case, each time point was compared to initial time.

9. Colony formation assay

NB cells were seeded onto six-well plates at a density of 10.000 cells per well and incubated until the colonies were visible to the naked eye, 7-10 days depending on the NB cell line. The medium was refreshed every two or three days. Once visualized macroscopically, colonies were fixed with 4% PFA (Sigma-Aldrich) at RT, for 20 min. Then, cell colonies were stained with 1% crystal violet (2% w/v, 20% methanol in PBS, Sigma-Aldrich) at RT for 20 min. Finally, plates were rinsed with tap water to eliminate crystal violet excess and scanned using iBright 1500 Imaging System (Invitrogen). Quantification was measured with Image J software (161). T-test was used to compare differences between two groups using GraphPad Prism 10.

10. Cell migration analysis: adherent and non-adherent cells

10.1. Wound Healing Assay: adherent cells

Genetically modified NB cell lines (LA-N-1 and SH-SY5Y) were cultured in 6-well plates until 90-95% confluence. Before scratching, cells were treated with 5 µg/mL of mitomycin-C (Santacruz) for 2 hours to inhibit cell proliferation. To generate a wound, the cell surface monolayer was mechanically scratched with a sterile p-200 pipette tip. Then, cells were washed with sterile PBS and incubated at 37 ^{o}C in 5% CO_2 and 95% relative humidity. The photographs of the wound were captured using a microscope (DM 5000 B Leica) at various time points, specifically at the initial time point and every 24 hours until the wound was fully healed in one condition, with the aim of quantifying the rate of cellular migration. The size of the wound was measured using the Wound Healing Tool Plugin in Image J by RIO Imaging (161). T-test was used to compare differences between two groups using GraphPad Prism 10.

10.2. Transwell Assay: non-adherent cells

To analyse the migration capacity of non-adherent cells, we used 24-well Falcon Cell Culture transwell Inserts with 0.8 µm pore membranes (Corning). Firstly, the cell pellets were manually disaggregated, and 30.000 cells seeded and suspended in 300 µL of RPMI -1640 medium

supplemented with 10% FBS, 2nM L-glutamine, penicillin (100 U/mL) and streptomycin (100 µg/mL) in the upper chambers, whereas the lower compartment were filled with 500 µL of RPMI supplemented with 15% FBS, as a chemoattractant. The experiment was stopped at different time points depending on the cell line. Then, the membranes were fixed with 4% PFA (Sigma-Aldrich) at RT, for 20 min, and stained with 1% crystal violet at RT for 20 min. The quantification was performed using pictures taken in the microscope with Image J software (161). T-test was used to compare differences between two groups using GraphPad Prism 10.

11. Cell Invasion Assay

Cell culture transwell Inserts (Falcon) were pre-coated with 70 µL Matrigel (10% in RPMI-1640 media) and allowed to polymerize up to 30 minutes at 37ºC. On the top of the invasion chamber, 200.000 cells were seeded in suspension with in 200 µL of RPMI-1640 media in case of adherent cells. For non-adherent cells we seed 50.000 cells on the top of the invasion chamber, after mechanical disaggregation, using same volume of RPMI-1640 media. Lower chamber was filled with 500 µL of RPMI-1640 supplemented with 15% FBS, as chemoattractant. Invasion capacity was quantified at 48 hours. For adherent cells, colorimetric quantification method with 1 % crystal violet was used, as described before. In case of non-adherent cells, the lower medium was collected and cells were count using Cell Counter Luna (logos, Labtech). T-test was used to compare differences between two groups using GraphPad Prism 10.

12. Inflammatory cytokines treatment

The day before cytokine treatment, wild-type NB cells lines (1-1.5x10^6), including LA-N-1 and SH-SY5Y cell lines, were seeded in a six-well plate using completed RPMI-1640 at 37 ^oC in 5% CO_2 and 95% relative humidity. After 24h, cells were treated with recombinant human TNF-α (10 ng/mL, 300-01A), TGF-β_1 (2 ng/mL, 100-21) and IFN-γ (50 ng/mL, 300-02). All the recombinant human cytokines were purchased from Gibco. Different time exposure was conducted depending on the experimental conditions, ranging from 16 to 48 hours. In case of long exposure treatment, meaning more than 48 hours, the medium with cytokines was refreshed every 24 h.

13. Exosomes treatment

Exosome concentration was assessed using a Nanosight Nanotrack System at the Institute of Materials Science of Barcelona (ICMAB-CSIC). A total of 50.000 cells, comprising hMSC and

HFF-1 cells were resuspended in 200 µL of medium, and seeded onto coverslips the day before treatment. The medium used was specific to each cell line, as previously described. Cells were treated with 1 × 10^7 exosomes previously extracted from control and ^{HIGH}PDPN cell lines, for 17h. Subsequently, the cells on the coverslips underwent IF, as previously described for cell culture.

14. *In vivo* studies

14.1. Spontaneous metastasis mouse model generation without primary tumor resection

Five-week-old female athymic nude Fox$^{nu/nu}$ and BALB/c$^{OlaHsd\text{-}Foxn1nu}$ mice were inoculated with LA-N-1 NB cell line. Cells were injected into the right gastrocnemius muscle of each mouse as previously described (1). Briefly, NB cells were harvested and counted to obtain a final concentration of 1 × 10^6 cells suspended in 100 µL of PBS. Due to the pandemic, the first experimental procedure was modified. Our protocol originally stipulated that tumor resection should be performed when the tumor reached a size of 800 mm. However, due to the COVID lockdown, it was necessary to modify the protocol. Particularly, no tumor resection was performed, and animals were kept until the tumor reached 1800 mm^3 (used formula: Volumen = (Length x $Width^2$)/2). A digital calliper was used to monitor tumor growth once per week. The athymic nude Fox nu/nu strain was selected for further experimentation.

14.2. Spontaneous metastasis mouse model generation

Different cellular concentrations of PDX-derived NB cells were inoculated into the right gastrocnemius muscle of mice (athymic nude Fox$^{nu/nu}$ strain), including 7.5x10^5 and 1.5x10^6 cells in 100 µL of PBS, as well as previous described concentration, to determine the optimal concentration. The PDX-derived NB cells were generated from different PDX models, including HSJD-NB-005-A; HSJD-NB-005-B and HSJD-NB-002. A digital calliper was used three times per week to monitor tumor growth. Once the tumor volume reached 800 mm^3, it was surgically removed, without amputation. After surgery, the mice survived long enough to develop metastasis to distant organs. Mice were euthanized based on specific criteria, including signs of illness, appearance of hind limb tumor relapse, appearance of tumor mass in the peritoneal zone, or time criteria after six months. Organs were collected and placed in cassettes for subsequent embedding in FFPE blocks. Organs suspected of infiltration were cut into pieces and immediately placed in an N_2 tank for freezing. Frozen samples were stored long-term at -80°C.

For PDX generation, written informed consent was obtained from patients/parents/legal guardians and procedures approved by the Institution Review Boards. All animal experiments were carried out under procedures approved by the Institutional Animal Research Ethics Committee and followed European Guidelines (EU directive 2010/63/UE).

14.3. *In vivo* blood extraction

In order to obtain blood samples from our *in vivo* model to study various metastatic biomarkers and exosomes in the bloodstream, two different techniques were used. To investigate potential biomarkers through the metastasis process, a longitudinal experiment was performed, resulting in four different time points for blood collection: before tumor cells inoculation (T0); 14 days after tumor cells inoculation (T1); 14 days, after primary tumor resection (T2); and at endpoint (TF). It is essential to follow established guidelines when extraction blood *in vivo*, which stipulate that no more than 10% of the mouse's weight can be collected. Consequently, the blood volume range obtained at different time points was between 20-100 µL, except for TF. Additionally, two-week breaks are needed between different time points according to guidelines. Blood was obtained from the mandible vein suing a sterile lancet (VWR).

At endpoint, we managed to gather up to 1 mL of blood by performing exsanguination through intracardiac bleeding. In this instance, the animals were administered an intraperitoneal injection of 300 µL of a combination of ketamine (120 mg/kg) and xylazine (10 mg/kg) prior to the procedure. After the animal reached the appropriate levels of anaesthesia, we opened the thoracic cavity to have a direct access to the heart. An intracardiac puncture was conducted to obtain a blood sample, the animal was euthanized after blood collection. Each blood sample was divided into two separate tubes, based on their intended use, with one tube containing heparin and the other tube without heparin. The samples were stored at -80 ^{o}C until required.

RESULTS

1. Generation of spontaneous metastasis *in vivo* model

1.1. Interactions between mouse immune cells and human NB cells influence tumor engraftment

To understand the molecular mechanism behind NB metastasis, a model that recapitulates all the steps of the metastasis process is needed. As described before for Ewing Sarcoma by Lopez-Alemany *et al*., we established a NB spontaneous metastasis *in vivo* model (166). Inoculation of LA-N-1 cells in two different mouse strains, Athymic $Fox^{nu/nu}$ (N=5) and BALB/$c^{OlaHsd\text{-}Foxn1nu}$ (N=5), resulted in an unexpected engraftment rate. While Athymic $Fox^{nu/nu}$ presented 80% tumor engraftment (N=4), no tumor engraftment was observed in BALB/$c^{OlaHsd\text{-}Foxn1nu}$ mice (**Figure 25A**). It is worth mentioning that the animals were sacrificed 4 months after tumor cell inoculation, and we are unsure if additional time would have allowed the development of a primary tumor. On the other hand, athymic $Fox^{nu/nu}$ mice developed tumors that reached 1500 mm^3 volume between 90 and 135 days after inoculation (**Figure 25B**). In addition, metastatic masses were found at different anatomical locations such as the peritoneum (20%) and the peri spinal region (20%). The human origin of NB masses was confirmed by human anti-nuclei stanning in the collected tumors, as well as in the micro-metastasis detected by IHC in the collected organs (70 % of liver, 50% of kidney and 50% of lung) (**Figure 25C**). Of note, this experiment was conducted during the COVID-19 lockdown, which prevented the surgical resection of the primary tumors. Animals were sacrificed once the tumor volumes reached 1800 mm^3.

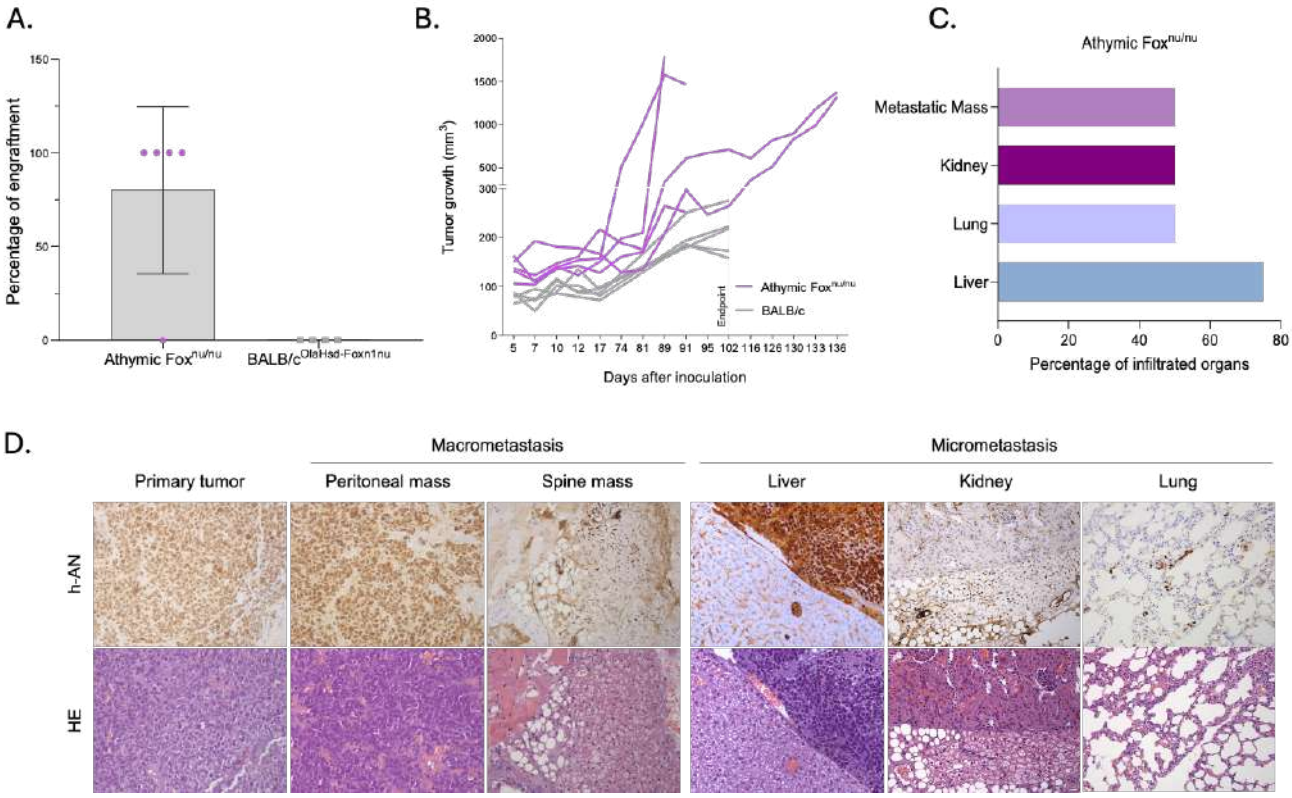

Figure 25. Generation of spontaneous metastatic model using LA-N-1 NB cell line. **A.** Percentage of engraftment of both mouse strains: Athymic Foxnu/nu presented 80% of tumor engraftment (N=4), no tumor engraftment was observed in BALB/cOlaHsd-Foxn1nu mice. **B.** Tumor growth representation of both mouse strains (Athymic Fox$^{nu/nu}$. purple; BALB/ c$^{OlaHsd\text{-}Foxn1nu}$, gray). **C.** Percentage of infiltrated organs in Athymic Fox$^{nu/nu}$ *in vivo* model (N=4). **D.** IHC images showing positive staining for human anti-nuclei (h-NA) confirming the human origin of peritoneal masses and infiltrated organs. H&E staining of consecutive sections. Scale bars, 100 µm.

1.2. The number of inoculated NB cells and tumor volume determine the frequency of local relapse

Once selected the mouse strain, different concentrations of the PDX-derived cell line HSJD-NB-005-A were inoculated into the gastrocnemius muscle of mice: 1,5x10^6 (N=10), 1x10^6 (N=5) and 7,5x10^5 (N=5). The primary cell lines from PDX-NB were previously established in our laboratory. This approach aimed to determine the optimal cell number for establishing the model. Despite inoculating different cell numbers, a consistent 100 % engraftment was achieved across conditions. Notably, diverse times of tumor engraftment were observed in relation to cell concentrations. Specifically, the higher the concentration the earlier engraftment, which occurred 10-15-days post-inoculation. Conversely, medium and low concentrations exhibited a wider range of tumor engraftment, from 10 to 20 days after inoculation (**Figure 26A**). Interestingly, a lower incidence (20%) of local relapses was observed with less number of inoculated cells compared to higher concentrations ranging from 50 to 70%. These results suggest a correlation between cell number inoculum and relapse

occurrence (**Figure 26B**). Considering our findings, it was determined that the optimal NB cell count for the spontaneous metastasis *in vivo* model generation was 1x10^6 cells.

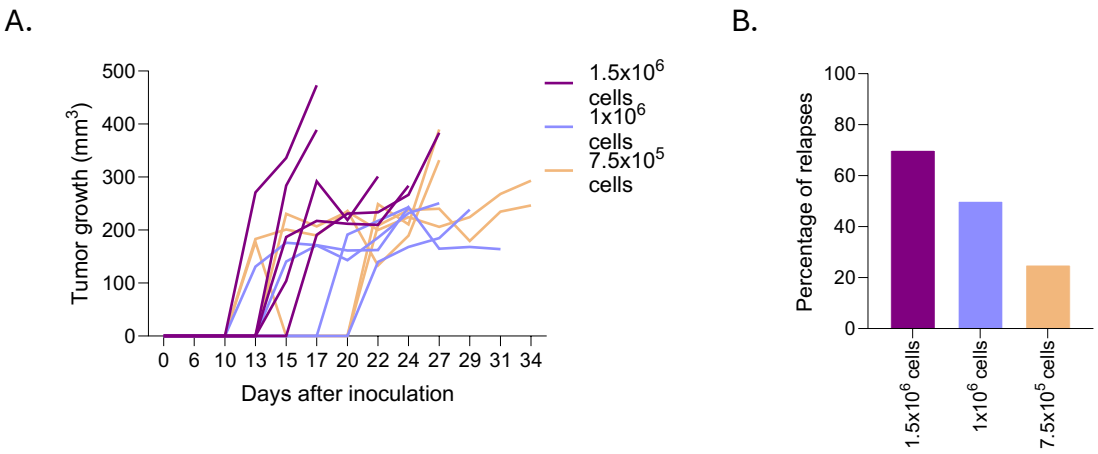

Figure 26. Optimizing NB PDX-derived cell concentration for spontaneous metastasis model generation. **A.** Tumor growth (tumor volume) for each cellular concentration of HSJD-NB-005-A model used**. B.** Percentage of local relapses found in each PDX cell concentration inoculated after primary tumor resection.

1.3. The NB spontaneous metastasis *in vivo* model exhibits a similar pattern of dissemination as observed in patients

Following the establishment of the model, three different PDX-derived NB cells (HSJD-NB-005-A, HSJD-NB-005-B and HSJD-NB-002) were inoculated into the gastrocnemius muscle of mice (N=10). Each PDX model exhibited a similar tumor growth rate, with each sample reaching 800 mm^3 at comparable time points, leading to a similar timeframe for resection (**Figure 27A**). A high percentage of engraftment, ranging from 90 to 100%, was observed in all models, being the median time for primary tumor appearance 3 weeks after inoculation. Remarkably, the results varied among the different models regarding the percentage of macro-metastasis, ranging from 29 to 42%. Macro-metastasis, defined as a visible tumor mass, was commonly observed in the peritoneum of mice at the endpoint. However, the development of relapsed masses in the primary site exhibited disparate results among the models; only the HSJD-NB-005-B showed a < 50% of relapses (**Figure 27B**). Given the fact that we administered 1x10^6 of tumor cells and observed similar relapse rates than 1.5x10^6 highlights that the percentage of relapses at the primary tumor site may not only be influenced by the number of inoculated cells but also by the biology of the tumor cells and technical aspects of the procedure. As previously described, the human NB origin was validated by the human anti-nuclei stanning (**Figure 27C**).

Distant organ infiltration rate was complemented by micro-metastasis analysis. Among all the experimental groups, the endpoint of the experiment ranged from 1 month after tumor resection to > 150 days, at which time the experiment was concluded. In non-relapsed

animals, the most infiltrated organs were the kidneys (80%), lung (60%) or bones (100%) for the models HSJD-NB-005-A, HSJD-NB-005-B and HSJD-NB-002, respectively (**Figure 27D**). We observed that those animals that did not relapse presented a higher number of infiltrated distant organs compared to those animals that were sacrificed because of relapsed local tumor achieving 1500 $mm^{3.}$ Animals presenting local relapses showed a distinct pattern of dissemination among the three models, with notable lung infiltration in HSJD-NB-002 model reaching 100%. For HSJD-NB-005-A, a consistent 20% infiltration in the liver and bones, with higher percentages up to 30-80 % observed in lung, brain and kidneys. Conversely, HSJD-NB-005-B displayed a more consistent infiltration percentage across organs, 40-60 % in the organs examined (**Figure 27D**). To evaluate BM infiltration, Paired Like Homeobox 2B gene (*PHOX2B*) mRNA expression levels were analyzed using LA-N-1 cells as a positive control. As a negative control, we used mRNA extracted from BM of mouse non-inoculated with tumor cells (BMc-). Comparable mRNA expression levels of *PHOX2B* were observed between the positive control and the BM samples from the *in vivo* models. A BM extraction from each inoculated model was obtained to validate PHOX2B levels (**Figure 27E**). Unfortunately, most BM cell cultures were lost before RNA extraction because of bacterial contamination. As previously performed for macro-metastasis, we detected micro-metastasis dissemination of NB cells human anti-nuclei by stanning collected organs. A representative image of different infiltrated organs are shown in **Figure 27F**.

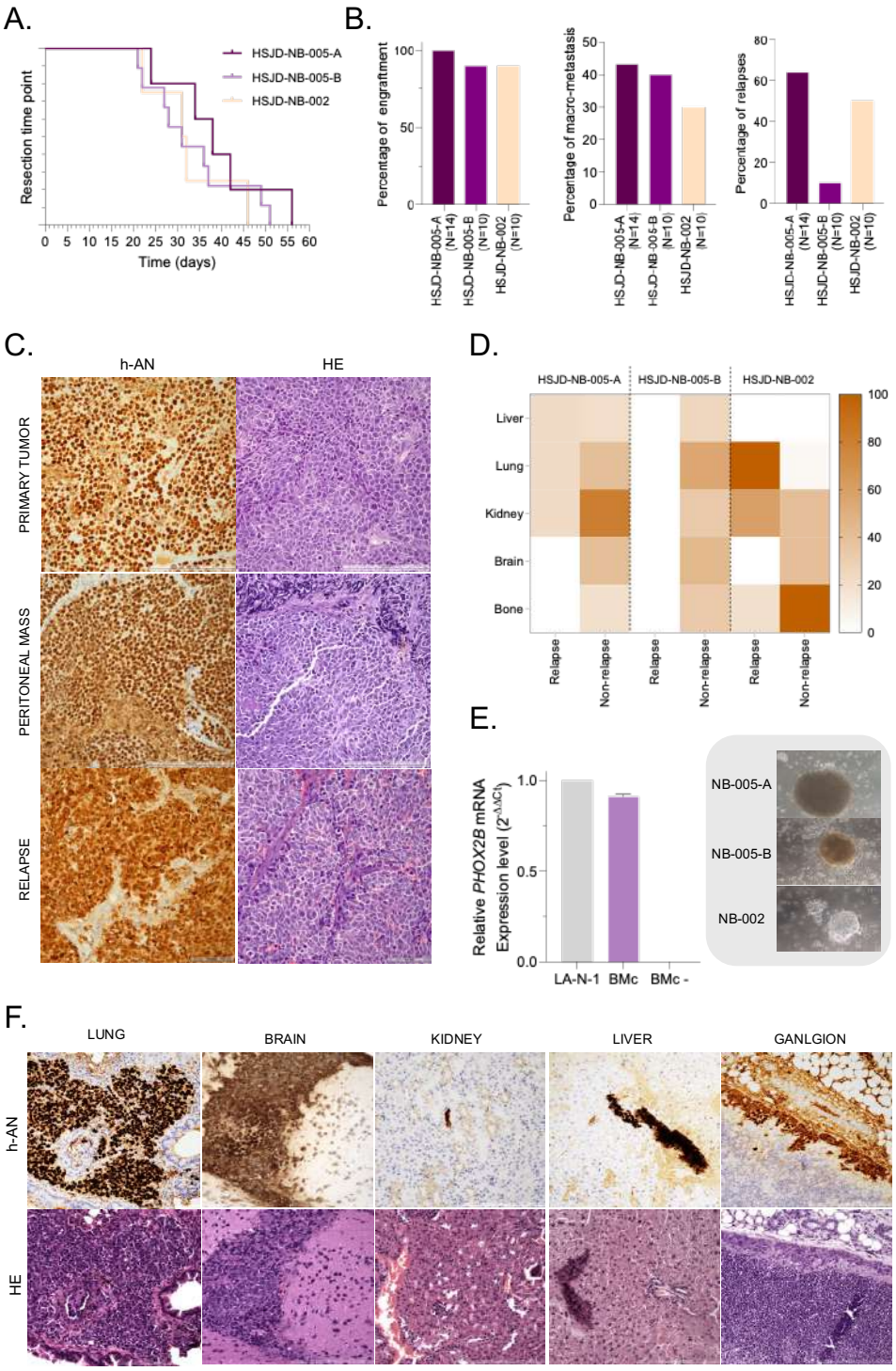

Figure 27. Spontaneous metastasis NB mouse model generation by injection of PDX cells. **A.** Time points of primary tumor resection in the *in vivo* models. Each model is represented with different colors. **B.** Percentage of primary tumor engraftment, metastatic masses generation and local relapses found in three different models. **C.** Representative pictures of IHC staining with human antinuclei antibody (h-NA) and hematoxylin and eosin (H&E) in tumor masses and collected organs, among models. Scale bars, 150 µm. **D.** Heatmap showing the percentage of micro-metastasis generated in our *in vivo* models, comparing animals exhibiting relapsed tumors with those without relapse. **E.** Representative images showing primary culture of NB cells isolated from bone marrow of the three *in vivo* models. PHOX2B mRNA levels were assessed by RT-qPCR to confirm NB cells infiltration in BM. LA-N-1 cells and bone marrow from non-inoculated mouse were used as a positive and negative control, respectively. **F.** Representative pictures of IHC staining with human antinuclear antibody (h-NA) and hematoxylin and eosin (H&E) in tumor masses and collected organs, among models. Scale bars, 150 µm.

1.4. Characterization of primary cell cultures derived from the spontaneous metastasis in vivo model reveals a transitional state.

As previously described, NB cells undergo NMT during the metastatic process, which confers cellular abilities, such as migration and invasion capacity. We investigated specific phenotypic markers in NB cells derived from primary and metastatic masses generated in the spontaneous metastasis model, which have been traditionally classified as either adrenergic or mesenchymal. Additionally, given the similarity in metastatic behavior between NB and epithelial tumors, we also examined some EMT transcription factors (EMT-TFs) which are associated with different metastatic capacities. For the noradrenergic phenotype, we analyzed *NFL* and *ASCL1*, while *FN* and *VIM* levels were assessed to determine the mesenchymal phenotype. Moreover, three different EMT-TFs genes were studied: *SLUG*, *SNAI1* and *TWIST1*. A comparison between primary cell cultures derived from primary tumors and those derived from metastatic masses did not yield definitive results. No differences were found with NOR and MSN in both models. It is important to note that each data point represents a different pair of samples established from the *in vivo* model. Notably, *PHOX2B* expression displayed low levels in two samples from HSJD-NB-005-A (**Figure 28A-B**). Conversely, the samples from HSJD-NB-005-B showed a slight increase of *PHOX2B* expression in the metastatic mass compared to the primary tumor. Significant results were observed for *SLUG* and *VIM* in both models, with the former displaying a 50-90% decreased expression in the metastatic mass, and the latter showing a 2-fold increase (p-value < 0.003). Additionally, *FN* exhibited a significant decrease of approximately 80% in the metastatic mass of HSJD-NB-005-A, with an heterogeneous expression observed in HSJD-NB-005-B. For *TWIST1*, more than 5-fold increase was observed in HSJD-NB-005-B model. **Figure 28C** displays the global expression results for both models combined, exhibiting an increase in MSN markers, along with the EMT-TFs, *SNAI1* and *TWIST1*, suggesting that tumor cells from the metastatic masses acquire this phenotype to increase their invasion capacity. However, a slight increase of the NOR markers were also observed. These findings show that no distinct phenotype distinguish the two sample types, primary and metastatic cell culture samples, suggesting the possibility of a transitional phenotype as described in the literature. Additionally, the variations in the mRNA expression levels indicates the heterogeneity of the NB tumors.

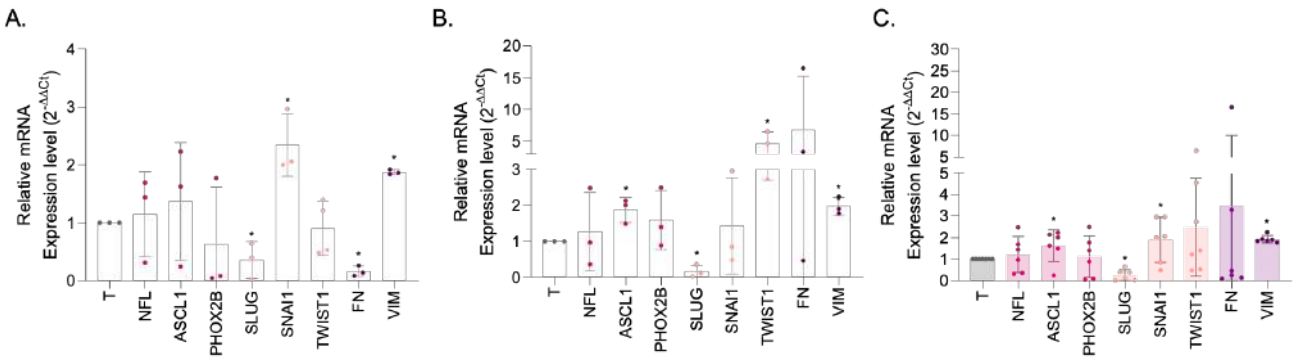

Figure 28. Gene expression levels of NOR and MSN markers in metastatic samples compared to paired primary tumor samples from our in vivo model. **A.** Heterogeneous pattern is exhibit in HSJD-NB-005-A model. **B.** HSJD-NB-005-B showed higher levels of MSN markers (*FN* and *VIM*). **C:** Overall analysis of both models presented increase levels of MSN markers, as well as EMT-factors (*SNAI1* and *TWIST1*). In addition, *PHOX2B* displayed an increase in metastatic samples. *p-value* < 0.003. Each point represents a biological replicate for each primary cell culture.

2. Deciphering the NB metastatic signature by multi-omics analyses

2.1. Transcriptomic signature of NB metastasis

2.1.1. Transcriptomic analysis uncovers a diverse transcriptional pattern across different *in vivo* models comparing primary tumors and metastases

As many other pediatric tumors, NB possesses a stable genome with only a limited number of recurrent mutations. Consequently, we started our multi-omic analysis with a transcriptomic approach, since most alterations might rely on post-transcriptional modifications affecting RNA levels. To decipher the molecular intricacies underlying NB metastasis, we started the omics characterization with a transcriptomic approach using the Affymetrix GeneChips Clariom-D^{TM} human analysis. Clariom-D array is a comprehensive gene expression platform designed to detect and quantify gene expression levels of over 20.000 genes across the entire transcriptome. Using material obtained from our spontaneous metastasis mouse model, we analyzed the transcriptomic profile of primary and metastatic tumors generated in the HSJD-NB-005-A (N_A) and HSJD-NB-005-B (N_B) *in vivo* models (Primary tumors: N_A= 5, N_B= 6; Metastatic tumors: N_A= 5, N_B= 4). Cells from the inoculation time were included in the analysis for both models (N=3). Although all tissues used were generated from the same NB cell line, cellular modulations within the *in vivo* model led to changes in their transcriptomic profile. Supervised hierarchical clustering showed two well-differentiated groups, cell cultures and tissue samples. Notably, different transcriptomic signatures were also identified for primary tumors versus metastases (**Figure 29A**). A low astringency analysis ($p < 0.05$ and absolute fold change <0.58) identified 203 differential expressed genes (DEG) when comparing primary tumors versus metastases considering both models. Previously published literature unveiled that the majority of DEG, identified through combined analysis, were associated with

metastasis and lymphatic dissemination across different cancer types like *GRIK3*, *PDPN*, *ID1* and *RUNX1*, among others (167-169). Reactome enrichment analysis showed that the most significant up-regulated biological pathways involved cellular attachment, whereas downregulated pathways involved cytoskeleton remodeling. Notably, upon conducting analysis using the *MSigDB Hallmark 2020 Data-base*, most prominently up-regulated pathways in metastases were associated with inflammatory response, followed by the TGF- β signaling pathway. Conversely, down-regulated pathways were associated with myogenesis, and EMT, as expected (**Figure 29B**).

190 and 949 DEGs were identified for HSJD-NB-005-A and HSJD-NB-005-B models, respectively. To identify common targets between the individual analysis of both models, we compared their DEGs. The study unveiled a limited number of common DEGs; in particular, one up-regulated and nine down-regulated genes were identified (**Figure 29C**). It is important that although the number of DEGs was 190 and 949 for each model, as previously mentioned, there was a reduction in their total count due to the exclusion of some probes with a "not available" (NA) ID. Afterwards, we analyzed the altered pathways of the individual data. Surprisingly, no significant altered pathways were found in the HSJD-NB-005-A model (data not shown), while similar results to the combined data were observed in the individual analysis of the HSJD-NB-005-B model (**Figure 29D**). Henceforth, subsequent work will focus on the HSJD-NB-005-B model. Due to the large number of DEGs identified, the following data was obtained after screening based on the standard deviation of the sample, using a more restrictive analysis (SD < 0.7). Afterwards, DEGs were significantly reduced to 17 and 52, up-regulated and down-regulated, respectively in the metastatic masses.

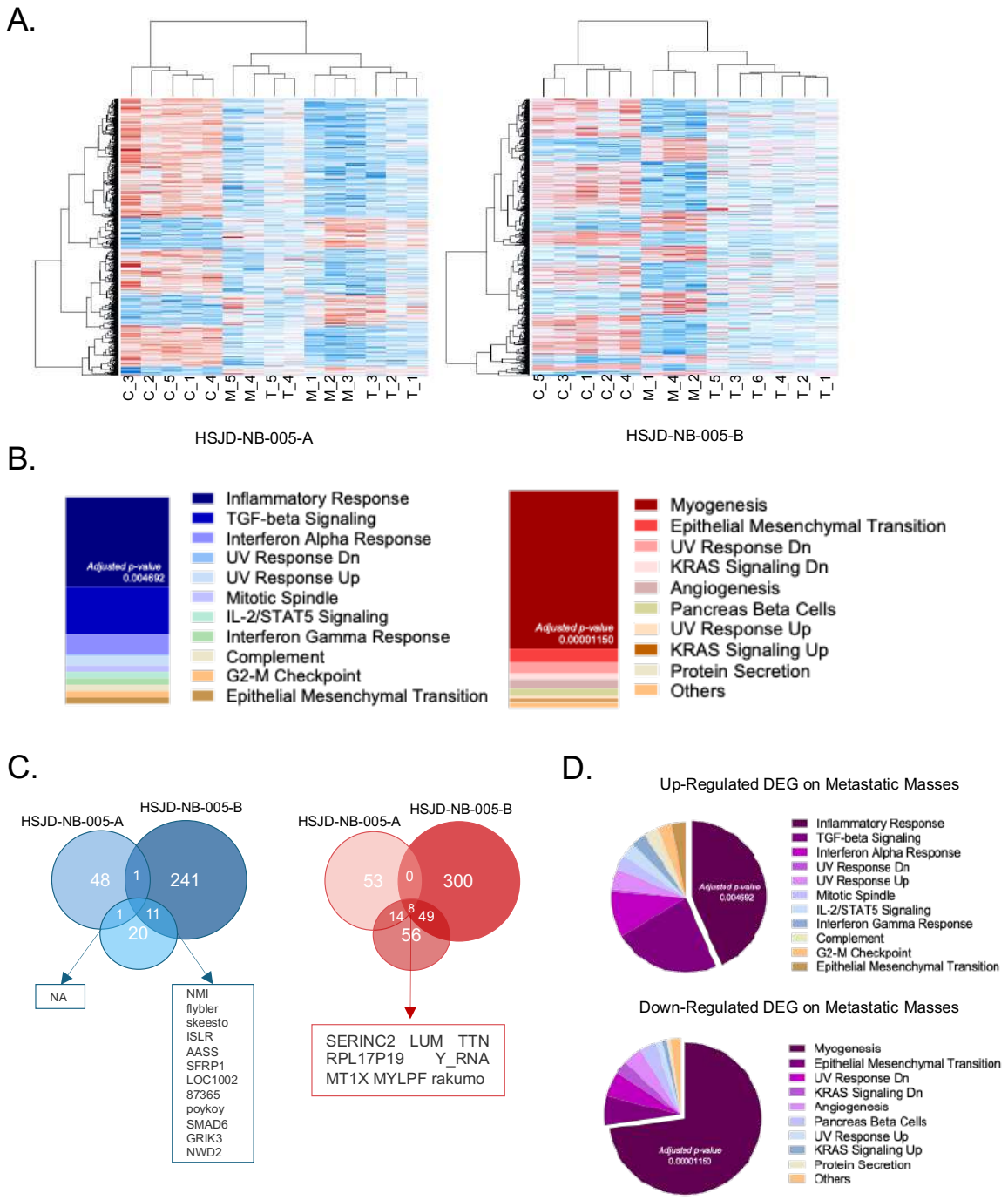

Figure 29. Transcriptomic analysis using Clariom-D array of our in vivo models. **A.** Hierarchical clustering of the supervised analysis performed of both models, HSJD-NB-005-A and B. Clariom-D analysis showed different gene expression pattern between cell culture and tissue samples, and identified 203 differential expressed genes (DEG) ($p < 0.05$ and absolute fold change < 0.58). **B.** Overall analysis of integrated DEGs of both models showed a significant alteration of inflammatory responses in the up-regulated DEGs (adjusted p-value = 0,004692); and myogenesis process in down-regulated DEGs (adjusted p-value = 0,00001150) in the metastatic masses when compared to primary tumors. **C.** Genes overlap analysis of individual DEGs from both models and the overall dataset reveals a limited number of common DEGs. Among the up-regulated DEGs, no overlap was observed across all three analyses. However, the comparison between HSJD-NB005-B and the overall dataset identified 11 common genes. For down-regulated DEGs, 9 overlapping genes were identified between all analysis. **D.** Pie chart showing the most altered pathways in HSJD-NB-005-B exhibiting significant results for inflammatory responses (p-value < 0.005) and various cytokines signaling pathways, including TGF-β (p-value 0.087). Analyses of enriched pathways was performed by using MSignHallmarks_2020 database in the Enrichr software.

To provide a more in-depth analysis, we sought to uncover any relevant information regarding the potential cells of origin from our analyzed samples. Fortunately, the Enrichr software offers the *HuBMAP ASCTplusB augmented 2022 DataBase,* which allowed to determine the possible origin of cells based on their genetic expression. Therefore, by using transcriptomic profiles of both primary and metastatic tissues, it is feasible to identify the origin of the cells. After consulting the *HuBMAP ASCTplusB augmented 2022 DataBase,* we observed that the combined values showed a strong association with lymph node origin, whereas individual analysis showed a more heterogeneous relationship. For instance, HSJD-NB-005-A model displayed a higher similarity to the genetic profile of brain cells, whereas HSJD-NB-005-B model revealed a stronger association with the genetic profile of cells conforming the lymph node (**Figure 30**). These findings are consistent with our previous array results, in which DEGs were associated with lymphatic dissemination and with high rate of lymph node infiltration observed in NB patients.

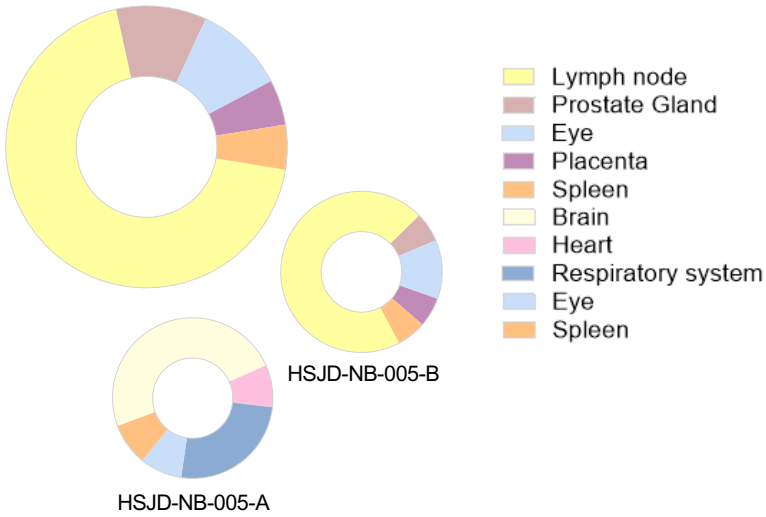

Figure 30. Transcriptomic profile from Clariom-D array revealed lymph node tissue as the tissue of origin of the metastatic masses of our in vivo model. Of note, HSJD-NB-005-A exhibited a different pattern from HSJD-NB-005-B and overall dataset analyses. HuBMAP ASCTplusB augmented 2022 DataBase was used to determine the cell of origin of the tissues.

2.1.2. DEGs are correlated with an unfavorable prognosis in NB

As mentioned earlier, the most DEGs identified have been associated with different mechanisms of dissemination in other types of cancer. To elucidate the metastatic signature of NB, we singled out specific DEGs, previously associated to the metastatic process, for further investigation. The volcano plot displayed the DEGs on both sides, distinguishing between the down-regulated on the left and up-regulated on the right in the metastatic masses. Genes that were selected for study were chosen based on their involvement in metastasis or their role in NB progression. These genes were labeled on the volcano plot, and included

SEMA3A, *LUM*, *GRIK3*, *PDPN*, *DBH* and *PROM1* (**Figure 31A**). To evaluate the potential relevance of these genes in tumor survival, an overall survival analysis of NB patients was conducted using the *Tumor Neuroblastoma public database, Kocak "R": Genomics Analysis and visualization platform* N=649, 2013). Kaplan-Meier (KM) analysis revealed that patients with poor prognosis exhibited significantly higher levels of *PDPN* (p-value = 1.96e-08). While the distinction among groups for *GRIK3* (p-value = 0.330) and *DBH* (p-value = 0.383) expression was less pronounced, differences were observed for both prior day 60 and 30, respectively. No association between *PROM-1* expression levels and overall survival was shown. Higher expression levels of *LUM* and *SEMA3A* were associated with adverse prognostic outcomes (**Figure 31B**).

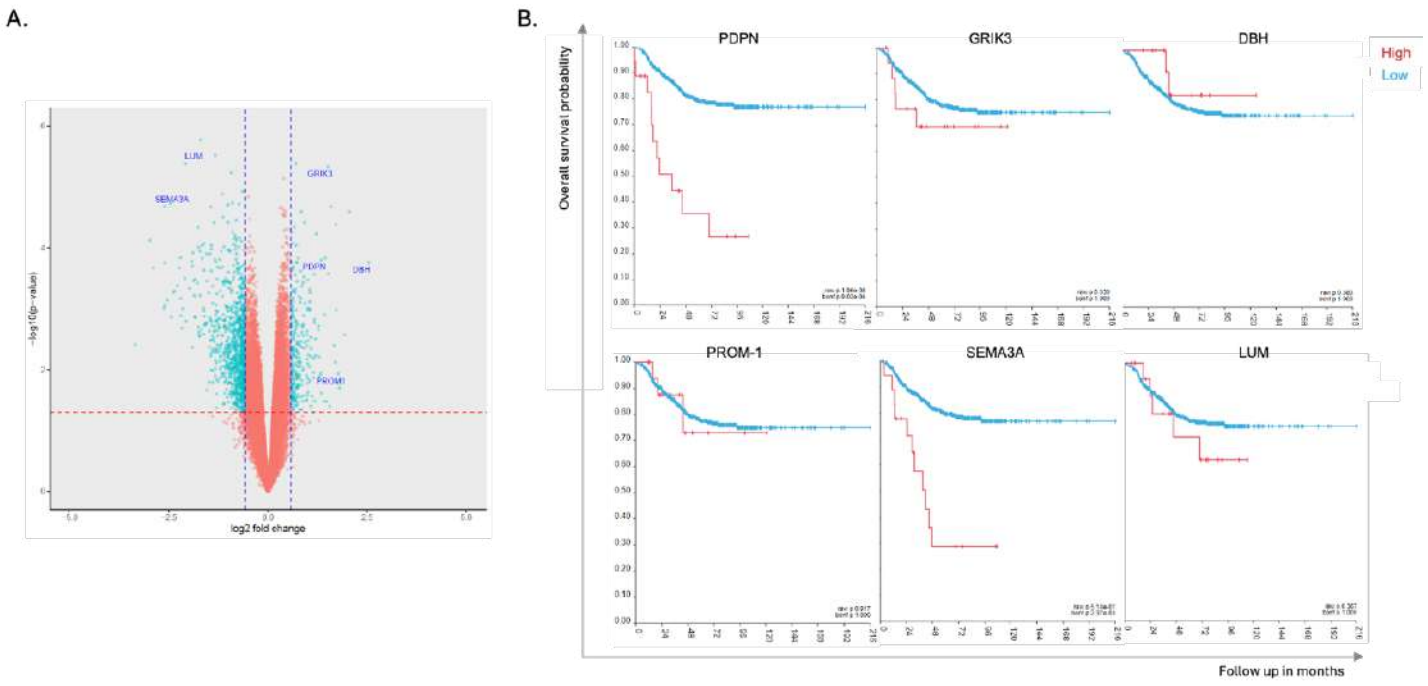

Figure 31. In dept analysis of DEGs of our in vivo model. **A**. Volcano plot showing results of differential expression analysis comparing primary tumors vs metastatic masses. In blue are represented DEGs (p-value < 0.05 and LogFC |0.58|). Labeled genes were selected to continue the study, including four up-regulated (*PDPN, GRIK3, PROM1* and *DBH*) and two down-regulated (*LUM* and *SEMA3A*). **B.** Kaplan-Meier graphics obtained from Kodak DataBase (N=649) of the most DEG up-regulated and down-regulated.

2.1.3. Metastatic transcriptional signature validation

The results obtained from the array were validated by RT-qPCR using the three independent spontaneous metastasis models established (**Figure 32A**). The results obtained, comparing the primary tumor samples with metastases, were dependent on the model. In model HSJD-NB-005-A, *PDPN* and *DBH* showed a 2-fold increase in expression, whereas in model HSJD-NB-005-B, it was *GRIK3* exhibiting an increase of over 3-fold in the metastases (p-value <

0.05). Despite the increased expression of *DBH*, it was not statistically significant given the heterogeneity in expression across the samples. In agreement with KM results, *PROM-1* did not exhibit differential changes in expression when compared to primary tumors in model HSJD-NB-005 but showed an increase in model HSJD-NB-002, albeit with heterogeneous levels. Conversely, the expression levels of down-regulated genes in HSJD-NB-005-B demonstrated a substantial reduction of 50%, including *SEMA3A* and *LUM* (p-value < 0.04). The HSJD-NB-002 model showed uncertain and non-significant results for the different DEGs validated. Despite up-regulated genes displayed higher levels in metastatic masses than in primary tumors, they all showed significant fluctuation in the fold increase. Furthermore, down-regulated gene *SEMA3A* presented inverse expression levels. Moreover, considering the different models collectively, significant results were observed for *PDPN, GRIK3* and *DBH* (p-values < 0.005). These genes exhibited more than 2-fold increased expression in the metastases compared to primary tumors, suggesting potential involvement in the metastatic process (p-value < 0.005; **Figure 32B**).

It is important to highlight that examination by IHC in paired-patient samples, revealed an association between protein expression levels and previously validated DEGs by mRNA ($N_{patient}$=10). Elevated expression of PDPN and GRIK3 were observed in metastases compared to primary tumors. However, expression levels of LUM and SEMA3A were undetectable in NB tissues (**Figure 32C**). Of note, specific staining was observed in the positive controls including placenta and liver, respectively (**Figure 23**). Our findings indicate a set of genes that could be participating in the NB metastatic process. Nevertheless, we could verify protein expression of only 4 of the selected genes suggesting that SEMA3A and LUM might not play a functional role, whereas PDPN and GRIK3 might be much more relevant.

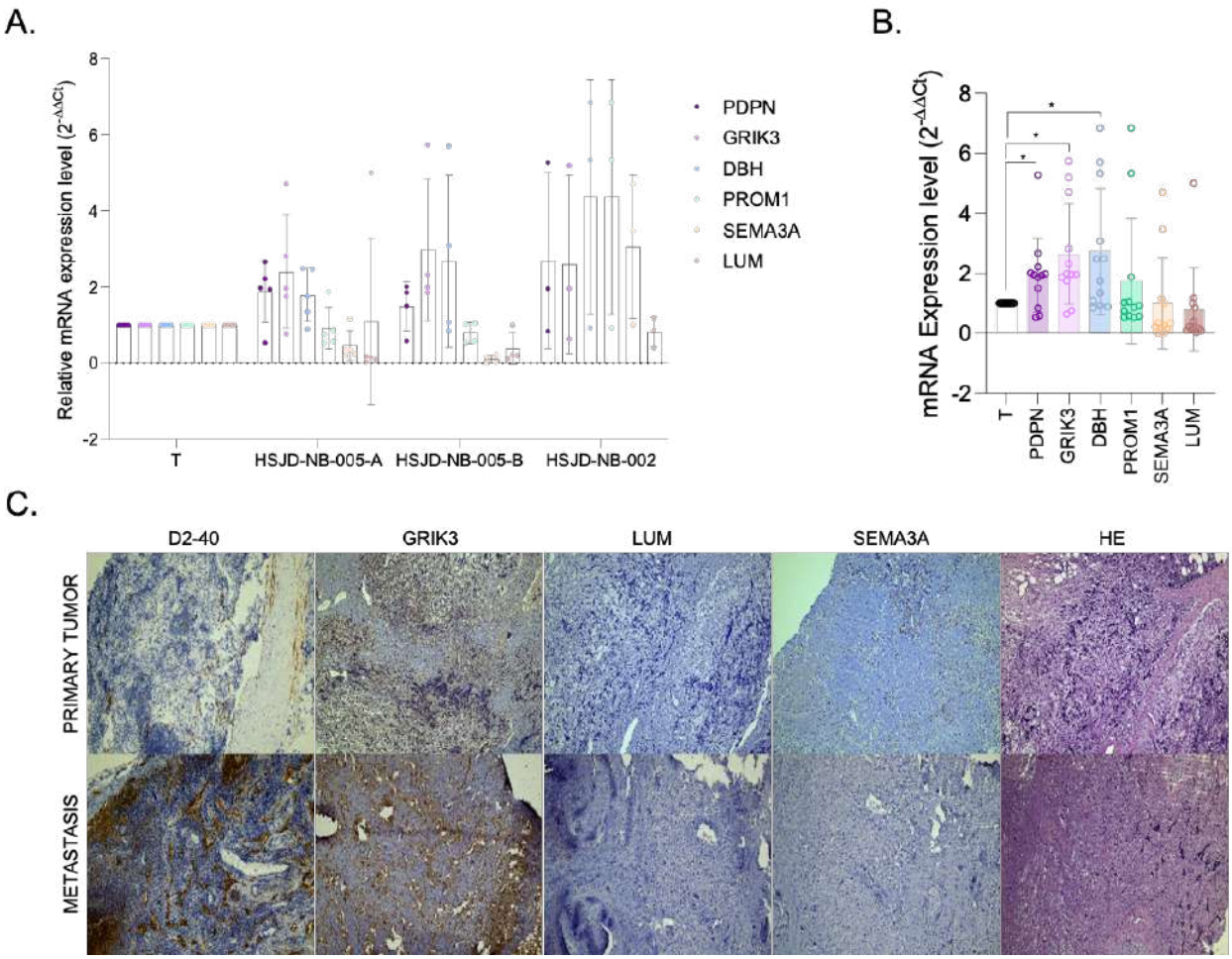

Figure 32. Validation of DEGs in our in vivo models. **A**. Relative mRNA expression levels of *PDPN*, *GRIK3*, *DBH*, *PROM1*, *SEMA3A* and *LUM* relative to each primary tumor (T) using RT-qPCR. Paired samples were compared, and normalization was achieved relative to *β-ACTIN* expression. **B.** Global relative mRNA expression levels of selected DEGs in spontaneous metastasis NB *in vivo* model. Mean values were obtained by comparing samples from the three generated mouse models, (p-value < 0.005). **C**. Representative images of Protein analysis by IHC of DEG-associated proteins in our cohort of NB patients, including PDPN (D2-40), GRIK3, LUM, SEMA3A and hematoxylin and eosin (HE).

2.2. Epigenetic signature of NB metastasis

2.2.1. DNA methylation status may not be associated with the metastatic process in NB

To complete the metastatic signature of NB, we conducted a study to examine the DNA methylation status using the Infinium MethylationEPIC platfom (Illumina). This methylation screening array includes more than 900000 CpG sites of the human genome, providing a unique opportunity to decipher the methylation changes in the metastases compared to primary tumors. Following our previous findings comparing the two models included in the Clariom-D array, we selected HSJD-NB-005-B as the most appropriate model for analysis because of its distinct genetic profile when comparing the primary tumor with the metastasis. Hence, DNA from primary tumor (N_1; N=4), metastasis (N_2; N=4) and cells (N_0; N=4) was extracted and profiled. As previously shown, after quality control, PCA showed excellent

segregation of the samples (culture/tissue) where the origin of the sample accounts for most of the variation observed (**Figure 21**). However, although some segregation was observed among tissues, the differences were not significant as demonstrated by the hierarchical cluster (**Figure 33A)**, in which all tissue exhibited a similar methylation pattern.

Genome-wide DNA methylation was investigated in the context of both differentially methylated positions (DMPs) and differentially methylated regions (DMRs). After p-value thresholding (<0,05), no significant differences in the DMPs were observed when comparing tissue samples (N1-N2 tissue) indicating that alterations in the methylation status of DNA are not contributing to the metastatic process of NB. Subsequently, a new comparative analysis including the PDX-derived NB cells along with tissues was conducted (N0-N1+N2), identifying significant DMPs (134 hypermethylated and 65 hypomethylated). This analysis aimed to determine methylation changes in PDX-derived NB cells after they were inoculated in mice. More importantly, the analysis exhibited 3723 hypermethylated and 1976 hypomethylated DMPs when comparing primary cell culture and primary tumors. A more detailed examination of the regions of the genome where the differentially methylated CpG sites were found showed that approximately 50% were in the body region of genes (**Figure 33B**). In addition, the largest proportion of DMPs mapped to open-sea regions (**Figure 33C**).

Moreover, differential methylation can affect several loci within a region, resulting in differentially methylated regions (DMRs). The analysis of DMRs showed a different methylation profile between primary tumors and metastases (p-value < 0.01 and FDR < 0.05). We observed 65 hypomethylated DMRs and 57 hypermethylated DMRs, which related to 101 genes. Even though, the methylation status of the DMR could not be associated with an alteration of their integrated genes, we investigated which pathways could be altered. In alignment with previous results, cytokine signaling pathways were found to be altered in both methylated statuses. Notably, TNF-α signaling via NK-kB was significantly altered in the hypomethylated DMRs (p-value < 0.01), and more highly altered in the hypermethylated DMRs. Other cytokine pathways were observed to be altered in the hypomethylated DMR, principally involving interleukins such as IL-6 or IL-2. In addition, both statuses shared other altered pathways such as hypoxia and mitotic spindle. Remarkably, hypermethylated DMR did not show significant altered pathways (**Figure 33D**).

Our findings suggest that DNA methylation is not primarily involved in the metastatic process of NB. However, differences were observed between cell cultures and primary tissues, highlighting the relevance of the microenvironment of tumor cells.

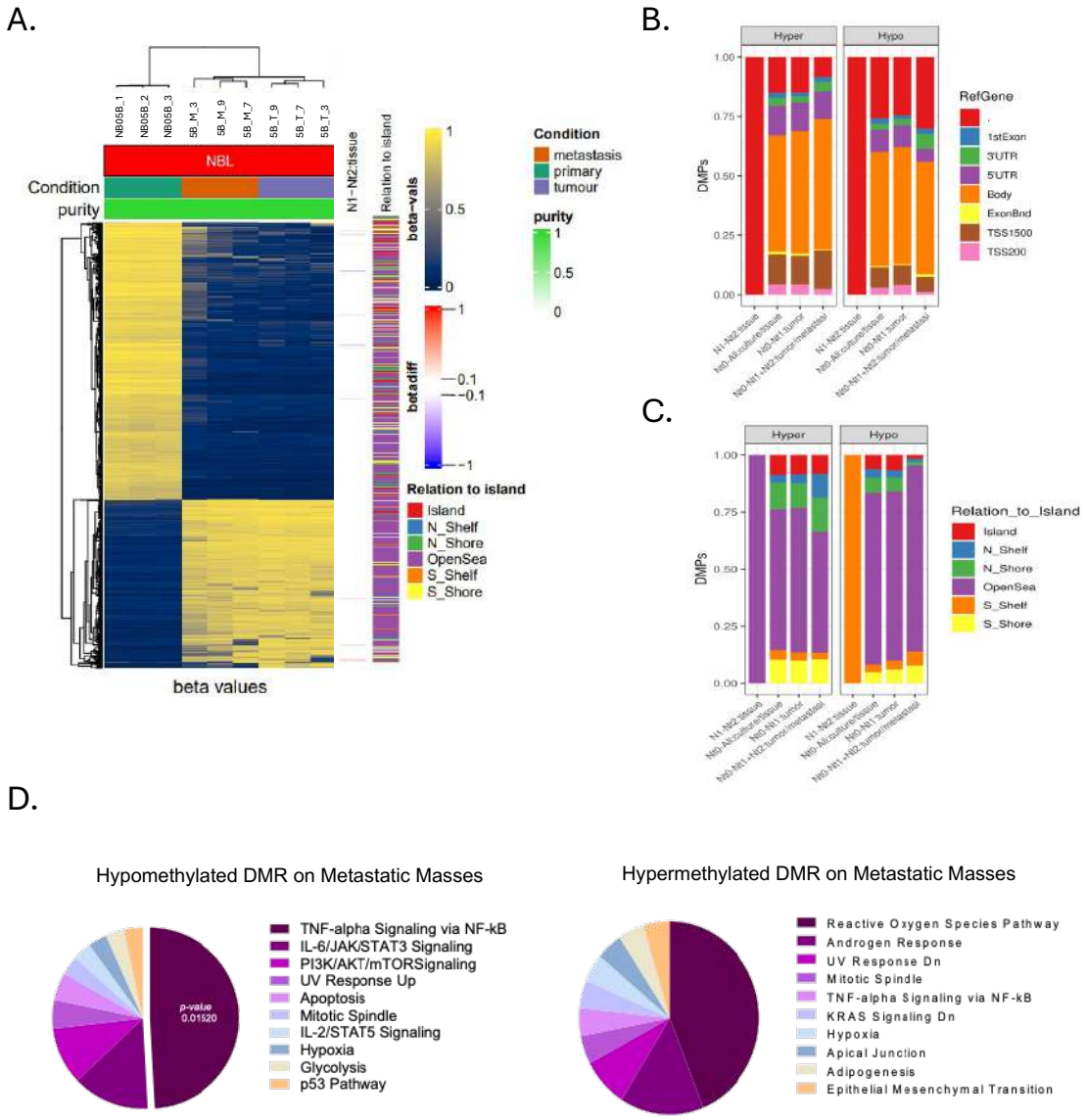

Figure 33. Methylation analysis of HSJD-NB-005-B in vivo model revealed no DMPs between primary tumor and metastatic samples. **A.** Hierarchical clustering of included samples: cell culture, primary tumor and metastatic samples. Different patterns were observed between cell culture and tissue samples. **B.** Analysis of DMPs in the different comparison among samples. No differences were observed when primary tumor (N1) was compared to metastatic mass (N2). Remaining analysis revealed a higher percentage of genes situated in body regions. **C.** Analysis of DMPs regarding CpG island, exhibited a higher percentage in opensea regions among different compared conditions. **D.** Most altered pathways of genes included in DMRs showed TNF-α signaling via NK-kB in the top of hypomethylated processes (p-value = 0,015) in the metastatic masses, and hypermethylated signaling altered in for genes included in DMRs did not present any statistically significant results. Analysis of enriched pathways was performed by using MSignHallmarks_2020 database in the Enrichr software

2.2.2. miRNA analysis highlights the relevance of TME interactions with NB cells

As previously described, the epigenetic signature encompasses various characteristics and mechanisms. In addition to DNA methylation, the post-transcriptional gene silencing by miRNAs is an important regulator of gene expression. Therefore, to complete the metastatic signature of NB at epigenetic levels, a GeneChip™miRNA 4.0 array was conducted in HSJD-NB-005-B samples. As expected, PCA analysis exhibited primary cells and tissue samples clustering separately, like previous PCA analysis of transcriptomic and methylation arrays (**Figure 20**). Using Ward's method, which is an unsupervised clustering technique based on the optimal value of an objective function, the statistical analysis revealed a clear distinction between cell and tissue samples, highlighting the relevance of the microenvironment within the metastatic signature (**Figure 34A**). Thereby, cell samples were excluded in the following analysis to prevent the identification of differential expressed miRNA related to the absence of TME. Afterwards, supervised hierarchical clustering showed distinct expression patterns of miRNAs between primary tumor and metastases (**Figure 34B**). Due to sample limitations regarding the primary tumor, we included two different pieces from the same primary tumor, referred to as T_2B. Additionally, including these two pieces enabled the study of tumor heterogeneity.

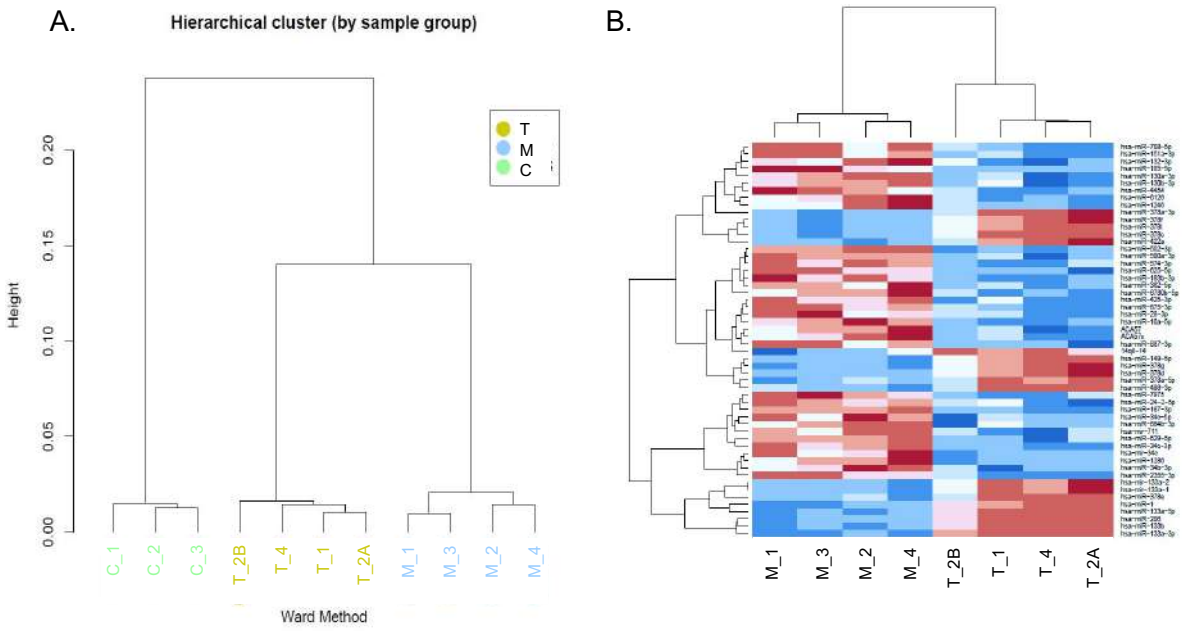

Figure 34. miRNA 4.0 array showed different miRNA expression levels between primary tumor and metastatic mass in HSJD-NB-005-B in vivo model. **A.** Unsupervised clustering showed differential expression of miRNA between cell culture and tissue samples. (C= Cell culture; T=Primary tumor; and M=Metastatic mass) **B.** Hierarchical clustering of primary tumor and metastatic mass presented different expression patterns of miRNAs. **C.** Pathways associated to miRNAs expression. At the top its represented processes associated with up-regulated miRNAs in the metastatic mass compared to primary tumor. At the bottom, it is shown pathways from down-regulated miRNAs. Analyses of enriched pathways was performed by using mirPathDB.

Differential expression analysis revealed 55 probe sets with altered expression when compared to tissue samples (primary tumors N=4, and metastasis N=4) using an adjusted p-value < 0.05 and a fold change < 0.64. Among them, we identified 34 and 18 up-regulated and down-regulated miRNAs, respectively, when comparing metastases to primary tumors.

To identify signaling pathway-associated microRNAs, we used miRPath database (miRPathDB) applying only strong interaction parameters in our analysis. Notably, in accordance with the previous analysis, TGF-β signaling was observed among the most altered pathways of the up-regulated miRNAs (**Figure 35**; top). In addition, different functions associated with SMAD proteins were found in the analysis, which are regulated by TGF-β family, reinforcing its role in NB. The principal miRNAs involved in these pathways were miR-130a-3p, miR-574-3p, and miR-675-3p. Broadly, the immune system appeared as one of the pathways being regulated by miR-574-3p, miR-34, miR-132-3p and miR-193b-3p. We observed individual regulation of Toll-like receptor (TLR) mediated cascade which is associated with inflammatory response, and it was regulated by miR-10. Additionally, pro-tumoral functions such as DNA damage, RAS regulation or TP53 degradation were found to be modulated by miR-132-3p, miR-130a-3p and miR-708-5p among others. Like previous analysis, down-regulated miRNAs exhibited a regulation of various cytokines and growth factors, such as the IL-12 family and VEGF (**Figure 35**; bottom). Among the miRNAs detected, miR-133a-3p and miR-206 were regulating those pathways. Remarkably, platelet activation signaling, a pro-tumoral mechanism, was observed in the analysis, regulated by miR-486-3p. In addition, a negative regulation of various fibroblast growth factor receptors (FGFR) was regulated by miR-378a-3p, which may be modulating the TME.

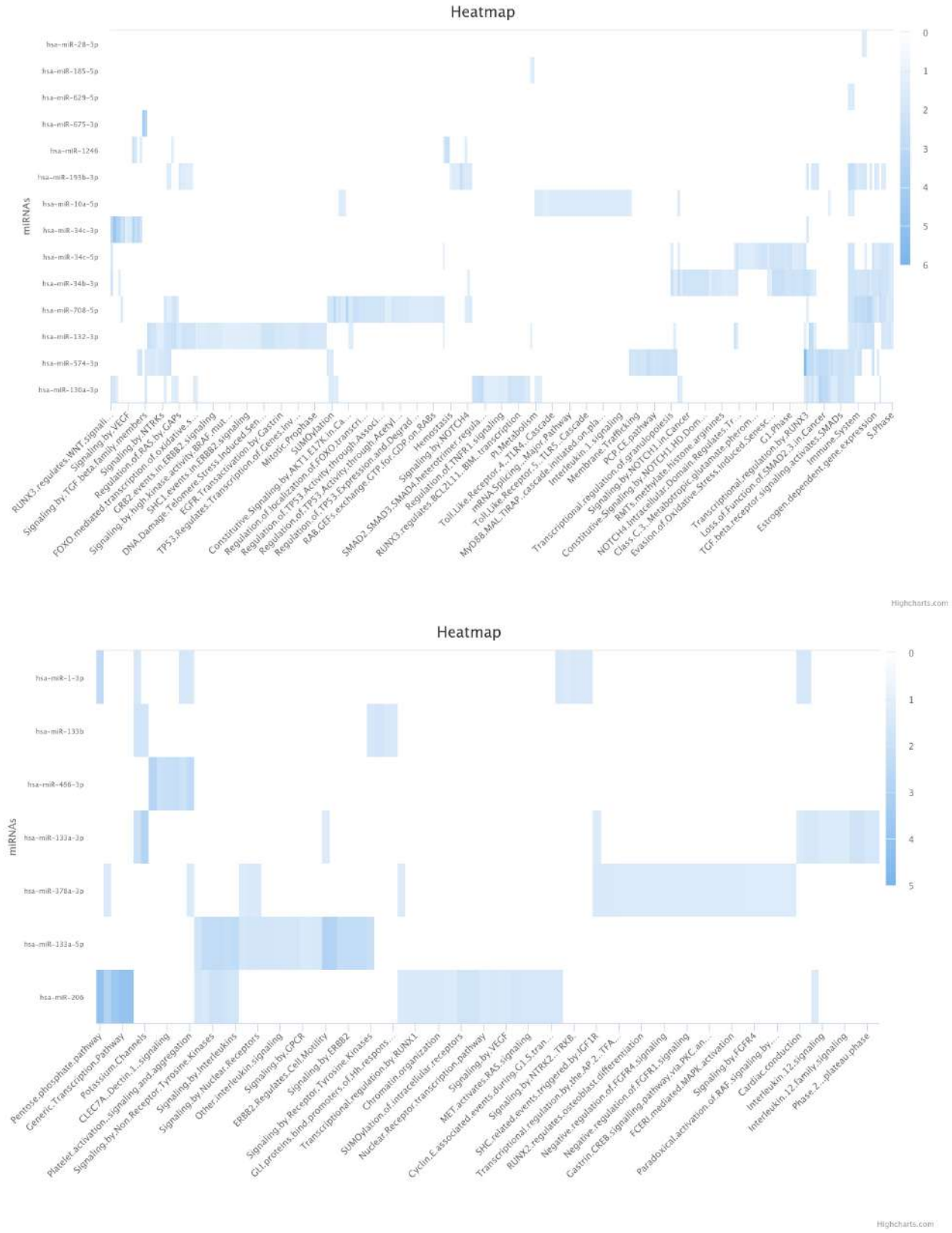

Figure 35. Pathways associated to miRNAs expression. At the top its represented processes associated with up-regulated miRNAs in the metastatic mass compared to primary tumor. At the bottom, it is shown pathways from down-regulated miRNAs. Analyses of enriched pathways was performed by using mirPathDB.

Identification of genes whose expression is regulated by miRNAs provides a hint for the functional roles of the miRNAs. To gain a comprehensive understanding of the function of the differentially expressed miRNAs, it is essential to know that high miRNA expression levels are typically correlated with the suppression of their target genes, and conversely. First, we compared the most altered pathways related to their predicted target genes, more than 6.000 and 15.000 targets for up and down-regulated miRNAs respectively. In accordance with previous results, there was a significant enrichment of the inflammatory response and cytokines signaling when we analyzed targets associated to down-regulated miRNA in the metastases (*adjusted p-value* < 0.005; **Figure 36A;** *top*). Notably, upon scrutinizing the predicted target genes of up-regulated miRNA, which are anticipated to be down-regulated in the metastases, we observed that cytokine signaling and the inflammatory response emerged as the most affected pathways (**Figure 36A;** *bottom*). In addition, we observed that one of the most significantly altered pathways was related to the cell cycle. Of note, the same database utilized for the transcriptomic analysis was employed for this study. These results strongly suggest a significant role of these pathways in the metastatic process, both seen by transcriptomics and epigenetics.

To validate our findings, we selected different miRNAs based on a brief review of published data that has previously demonstrated their involvement in the metastatic process. Among the list of differential expressed miRNAs, we selected miR-629-3p, miR-6780b-5p and miR-149-5p. Both up-regulated miRNAs have been briefly studied, demonstrating their role increasing invasion capacity and inducing EMT, respectively (170, 171). In contrast, miR-149-5p has been long studied describing its role in different human cancers, as a tumor suppressor (172). Considering the HSJD-NB-005-B model, we observed consistent results with the analysis for miR-629-3p and miR-149-5p, when comparing primary tumors and metastases (**Figure 36B**). A 4-fold-increase was observed in miR-629-3p, although not statistically significant. Moreover, miR-149-5p exhibited approximately a 90% decreased expression in the metastases, which was statistically significant (p-value < 0.05). However, miR-6780b-5p exhibited an heterogenous expression among samples from this model. In contrast, the HSJD-NB-005-A model presented an inverse expression of miR-629-3p and miR-149-5p in the metastases. Like HSJD-NB-005-B, miR-6780b-5p exhibited non-homogeneous levels in the metastases.

Overall, our findings suggest that dysregulated miRNAs are involved in the metastatic process of NB, potentially being regulated by the cytokines signaling, or vice versa. Once more, and in concordance with our previous results, miRNA analysis highlights the relevance of cytokines during metastasis. In addition, validation of array results related a heterogeneous expression

of different miRNA, making difficult to use as biomarkers. However, study of these miRNAs is needed to understand their role and distribution during NB progression.

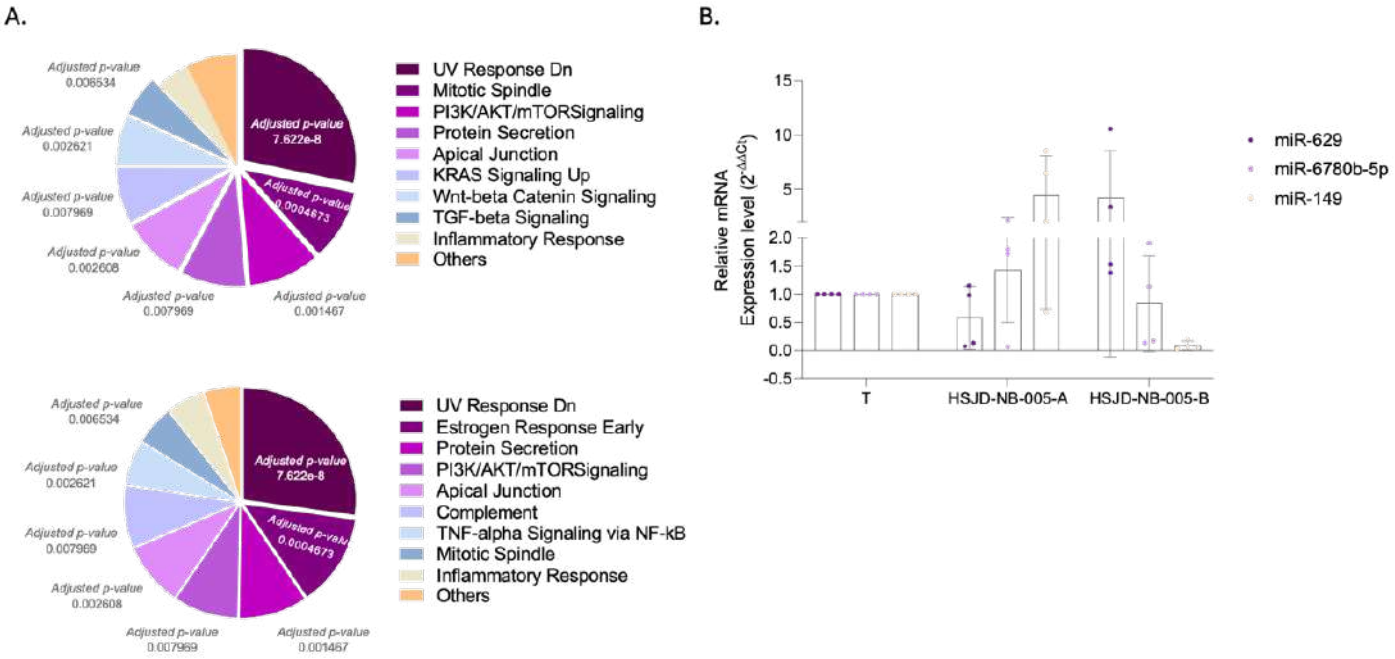

Figure 36. Analysis of target genes of differential expressed miRNAs and validation of miRNA 4.0 array results. **A.** Enrichr analysis of targets from down-regulated miRNAs (top) and up-regulated miRNAs (bottom) revealed inflammatory response as one of the most significant altered processes in both analysis (adjusted p-value < 0.002) in accordance with previous results Analysis of enriched pathways was performed by using MSignHallmarks_2020 database in the Enrichr software. **B.** Expression levels of miR-629, miR-6780b-5p and miR-149 in HSJD-NB-005-A and B by Rt-qPCR. Similar results to miRNA 4.0 array were obtained in HSJD-NB-005-B. In contrast, HSJD-NB-005-A exhibited inversed expression levels of miR-649 and miR-149. Each point represents a miRNA extraction from different *in vivo* sample (T=Primary tumor).

2.2.3. Exploratory analysis of mouse miRNA expression highlights the significance of TME interactions in NB progression

Given the findings from various molecular analysis that highlight the significance of the microenvironment within NB tumor cells, we investigated the mouse microenvironment to gain a deeper understanding of the underlying mechanisms of NB metastasis using miRNA 4.0 analysis since it contains probes for human and mouse.

Conducting the same bioinformatic analysis as for human probes, we obtained two clearly different expression patterns when comparing primary tumor and metastasis (**Figure 37A**). The hierarchical clustering exhibited 30 differentially expressed miRNAs using an adjusted p-value < 0.004 and a fold-change > 0.64 and < -0.75. Afterwards, we analyzed which signaling pathways were associated to these miRNAs, distinguishing between up-regulated and down-regulated. Notably, cell differentiation pathway (GO:0030154) emerged as the most significantly enriched, along with various cellular proliferation pathways in the metastasis (*p-value* < 0.03; **Figure 37B;** top). Remarkably, upon analyzing the down-regulated miRNAs, we

observed enrichment in pathways associated with immune system activation, including innate and adaptative responses, as well as the response to cytokines (GO:0034097). Additionally, pathways related to fibroblast migration and proliferation were particularly noteworthy, suggesting the relevance of mouse immune system interaction with the primary tumor and its potential to disseminate (**Figure 37B**; bottom).

We identified the predicted target genes of the altered miRNAs, more than 6.000 genes, and performed an enrichment pathways analysis using the same database as before, the *MSigDB Hallmark 2020 Data-base*. We included only those targets that exhibited strong interactions with the miRNAs. No significant values were obtained when analyzing the down-regulated targets (**Figure 37C;** *top*). However, TGF-β signaling stood as one of the altered pathways when processing, down and up-regulated targets genes. Regarding down-regulated target genes, protein secretion and apical surface signaling were found among others for their potential involvement in tumor progression (**Figure 37C;** *bottom*).

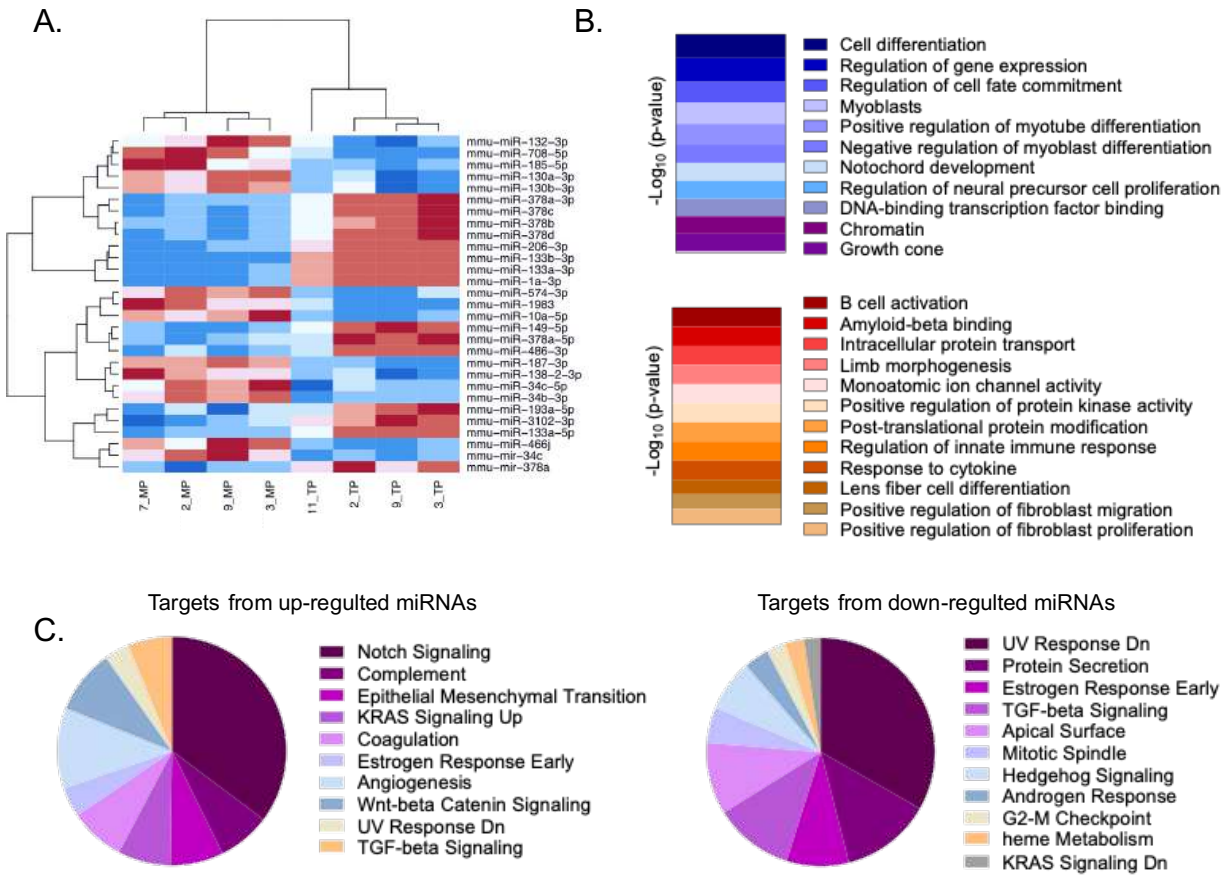

Figure 37. Analysis of mouse miRNA from miRNA 4.0 array showed differential patterns between primary tumor and metastatic mass. **A.** Hierarchical clustering exhibited 30 differentially expressed miRNAs (adjusted p-value < 0.004) using a fold-change > 0.64 and < -0.75 for up-regulated and down-regulated miRNA, respectively. **B.** Predicted processes associated to differential expressed miRNAs. **C.** Enrichr analysis of targets from up-regulated miRNAs (left) and down-regulated miRNAs (right) revealed TGF-β pathways as one of the most significant altered processes in both analysis in accordance with previous results.

These findings underscore the crucial role of the TME and cytokines in the metastasis process, and more significantly, their potential role during the early stages of metastasis while in the primary tumor. Additionally, it provides insights into the potential involvement of stromal cells in the initiation of the metastatic process within the primary tumor, highlighting the role of fibroblasts.

2.3. Multi-omics data integration underscores the role of TME in NB metastasis

To shed some light into signaling pathways and specific targets that could be important for NB biology, it is essential to take an integrative approach that combines multi-omics data. Thus, data integration of transcriptomic and epigenetic analysis was performed using different methods including cross-checking of identified DEGs, miRNAs targets, and genes in DMRs from the methylome array.

2.3.1. Comparing methylome and transcriptomic results

Bioinformatic analysis was performed to integrate methylation and transcriptomic data, including the combination of the two different *in vivo* models.

Since no DMPs were uncovered in the methylation analysis, we opted to incorporate the genes associated with DMRs to assess whether there was any overlap with DEGs. As anticipated, no overlap was observed between the up-regulated genes and hypomethylated regions or vice versa. These findings further imply that DNA methylation does not play an important role in NB metastasis.

2.3.2. Integration of transcriptomic and miRNAs data identified common TME-related genes

We compared the list of DEGs with the predicted target genes of differentially expressed miRNAs obtained from the transcriptomic and miRNA arrays. The Venn Diagrams revealed overlapping genes, up-regulated DEGs and target genes from down regulated miRNAs and vice versa. In total, 15 and 11 genes, respectively, were found in the overlaps (**Figure 38A**). Notably, the identified targets aligned with the validated targets from the Affymetrix GeneChip Clariom-D™ array, including *PDPN*, *GRIK3* among the up-regulated genes, and *LUM* among the down-regulated. These results reinforced the potential role of these genes in the metastatic process of NB.

Not surprisingly, pathway analysis showed an enrichment of genes associated with TGF-β signaling pathway (*p-value*=0.028), including SMAD6 protein, in the metastatic samples **Figure 38B,** *top***)**. Relevant pathways when using the down-regulated genes showed angiogenesis among the significant ones, regulated by *LUM* (**Figure 38B,** *bottom***)**. Considering the integration of the multi-omics data, along with individual results suggests that TME interactions play a crucial role in NB metastasis, particularly through cytokine signaling. Additionally, data integration highlights the relevance of angiogenesis in the primary tumor which is in line with the literature.

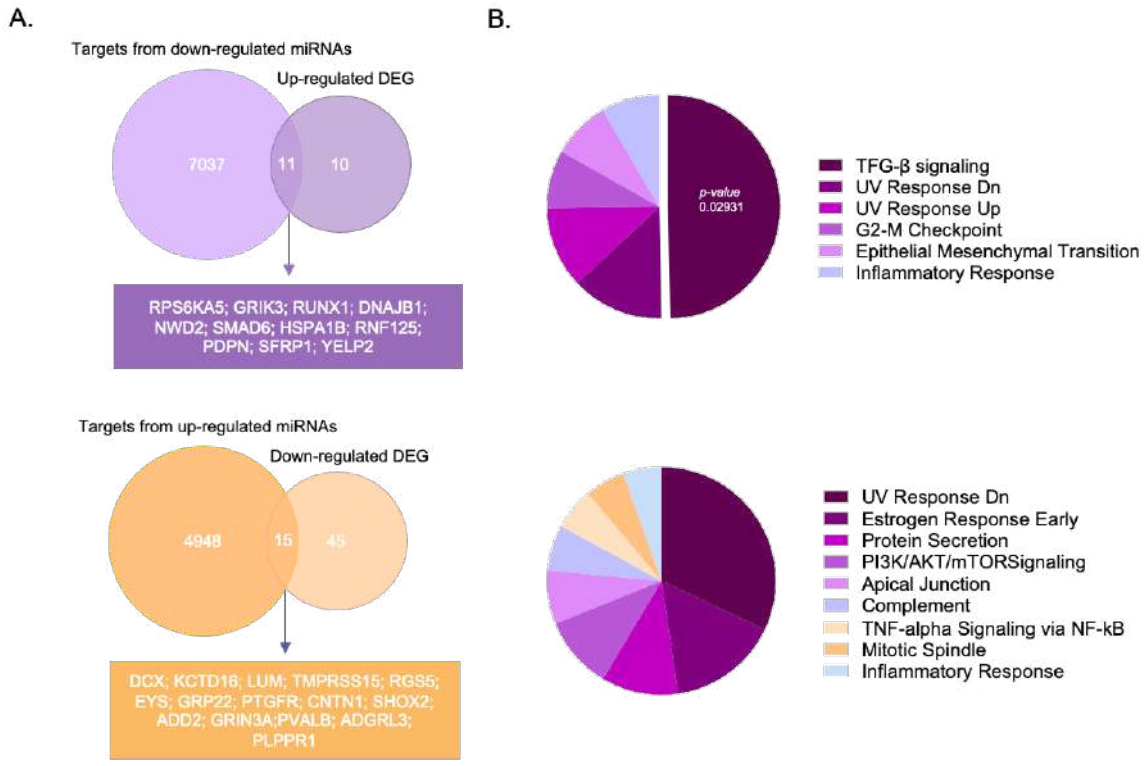

***Figure 38. Data integration from Clariom-D and miRNA 4.0 array showed common genes*. A.** Overlap analysis between DEGs and targets from differential expressed miRNAs revealed 11 up-regulated, such as *GRIK3*, *RUNX1* and *PDPN*, and 15 down-regulated common genes, including *LUM*. **B.** Most altered pathways from common genes exhibited TGF-β signaling as the most altered (p-value = 0.028) in the up-regulated common genes. Remarkably, inflammatory response was observed in analyses from up and down regulated common genes.

2.4. Relevance of TGF-β signaling in NB metastasis

In line with individual analyses, results of data-integration suggested TGF-β signaling as one of the most enriched pathways. In accordance, we observed a significant difference of TGF-β_1 levels, with 15%-fold-increase in the metastasis compared to primary tumors (*p-value* < 0.005) (**Figure 39A**). As cytokine-mediated modulation of the metastatic process gained significance, we assessed the cytokines levels in the primary tumors of animals that did not develop metastasis throughout the duration of the experiment (T_Non-Met), compared to those animals that had developed metastasis at endpoint (T_Met). We noted a slight increase

in TGF-β_1 levels among primary tumors of animals with higher macro-metastasis rate, suggesting a potential role of TGF-β_1 promoting NB metastasis (**Figure 39B**).

Following the assessment of TGF-β_1 expression levels, we determined which cells conforming the TME were secreting the cytokines. In addition to the human *versus* mouse TGF-β_1 comparison, we analyzed the expression of primary tumor samples *versus* metastasis (**Figure 39C**). The results revealed a significant increase of over 40-fold of mouse TGF-β_1 in the metastasis (p-value < 0.003). A 20% decrease was observed for the human TGF-β_1 probe in the same samples (p-value < 0.05). These findings suggest that tumor cells secrete TGF-β_1 in the primary tumor, whereas TGF-β_1 secreting mouse cells may be more involved in the metastasis.

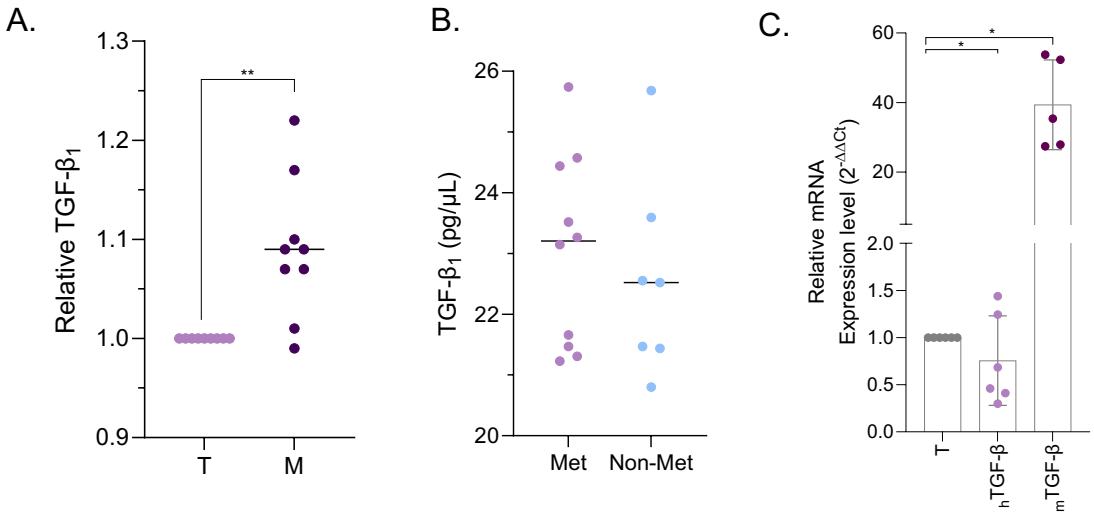

Figure 39. TGF-β1 arises as a potential metastatic factor in our in vivo model. **A**. Relative TGF-β1 expression levels in primary tumor and metastatic samples from our *in vivo* models. Significant elevated levels are observed in metastatic masses compared to paired primary tumors by ELISABlot. (T=Primary tumor; M=Metastatic mass) **B.** A slightly increase of TGF-β1 was observed in primary tumor from metastatic animals (Met) when compared to non-metastatic animals (Non-Met). **C.** mRNA expression levels of human and mouse TGF-β1. A decrease of human TGF-β1 ($_h$TGF-β1) is observed in the metastatic samples compared to primary tumors. Inverse results were observed for mouse TGF-β1 ($_m$TGF-β1) levels. *p-value < 0.05; **p-value < 0.002.

3. Tumor microenvironment enhances NB metastasis

3.1. Cytokines secreted by mouse cells may be involved in NB tumor progression

Our previous results suggested that TGF-β_1 is being secreted by NB cells in the primary tumor promoting metastasis. In addition, results from multi-omics analyses pointed to the relevance of cytokines in the early steps of tumorigenesis. Furthermore, the examination of mouse miRNA differential expression indicated the potential role of the TME, which aligns with the literature describing the role of immune and stromal cells enhancing tumor development (89).

Therefore, to gain a broader understanding of the cytokines implicated in the metastatic process, we performed a proteome profile of mouse cytokines in primary tumor samples from HSJD-NB-005-*B in vivo* model. As for TGF-β_1 analysis, we included samples from mice that did (N=2) and did not (N=2) develop metastasis. Inflammatory cytokines such as I-CAM, IL-1α and CXCL12 were differentially expressed, with more than a two-fold increase in expression observed in the primary tumor compared to the metastatic group (**Figure 40A**). Unexpectedly, cytokines identified in the previous array analysis, such as TNF-α and IFN-γ, did not show significant differences, probably because the previous arrays used human probes. For data validation, levels of IFN-γ and IL1α were obtained by ELISABlot. No significant differences were found (**Figure 40B**). Overall, these findings suggest that cytokines produced by cells within the TME may contribute to enhancing the metastatic capabilities of NB cells.

As previously described, cytokines are released by cells conforming the TME, including immune cells and cells that regulate them, such as TAMs and CAFs (89). To determine whether these mouse cells were involved in the interaction with NB cells, we assessed the mouse mRNA levels of their specific markers. Hence, we measured the expression levels of macrophage markers (*CD68*), macrophages polarized to a pro-tumoral phenotype (*CD163*), and CAFs (*FAP* and *α-SMA*) in the metastasis (**Figure 40C**). Our findings showed that both CAFs markers were significantly decreased, approximately 80% and 50% in *α-SMA* and *FAP, respectively,* in metastasis (p-value < 0.05). Furthermore, the expression of specific markers of polarized macrophages like *CD163*, significantly decreased in the metastasis (p-value < 0.003). Overall, our results suggest that CAFs and polarized macrophages such as TAMs, are

increased in the primary tumors and potentially being involved in the metastatic process by promoting tumorigenesis.

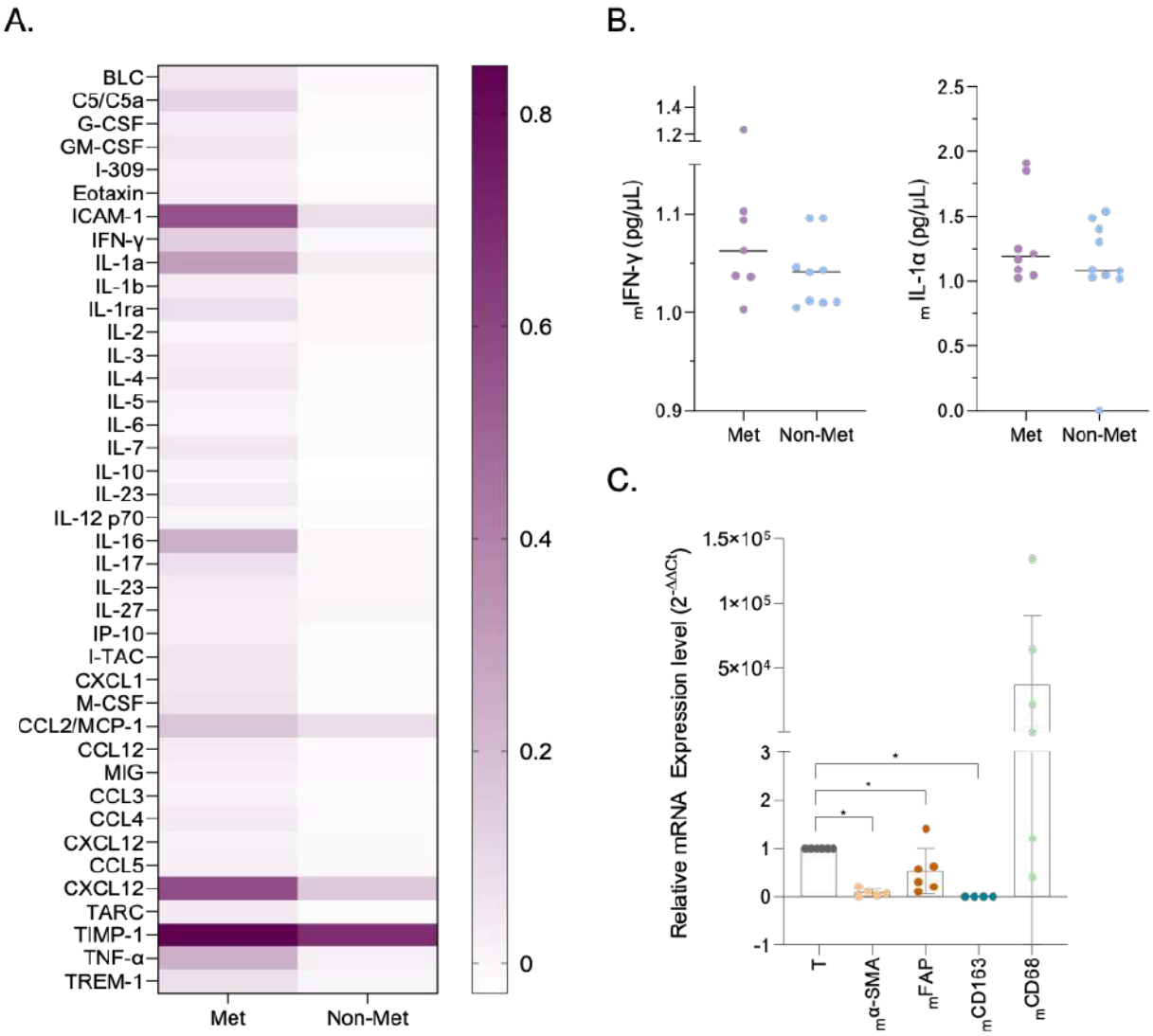

Figure 40. Tumor microenvironment is involved in NB progression. **A.** Proteome profiler for mouse cytokines revealed different expression patterns between primary tumors from metastatic (Met) and non-metastatic (Non-Met) animals. **B.** ELISA Blot validated previous results for IFN-γ expression in the primary tumors from our *in vivo* model. Each point on the graph represents a distinct primary tumor sample. **C**. mRNA expression levels of specific markers for CAFs (α-SMA and FAP), macrophages (CD68) and TAMs (CD163) using mouse sequencing by RT-qPCR. Significant decrease of expression was observed in CAFs and TAMs markers in metastatic samples compared to paired primary tumor (T; *p-value < 0.05).

3.2. Spatial transcriptomics analysis reveal selective distribution of the NB phenotypes and the population conforming the TME

To gain understanding of the interactions between the TME and NB cells, we conducted spatial transcriptomic analysis of two HR-NB patients. This analysis allows for the discovery of specific cellular populations and their gene expression patterns within their native spatial setting, providing insights into the cellular diversity and the function of the different cell types within the TME. This analysis included the original tumor from which the HSJD-NB-005 cell line was derived (referred as patient_1). Our analysis covered primary tumors or initial biopsies

at our institution (T_#), as well as secondary tumor masses, which we recognized as metastasis (M_#). The results revealed a distinct spatial distribution for the different cell subtypes discriminating between stromal and tumor tissue, in agreement with the histological analysis. Of note, various quality controls assessed for each sample as described in materials and methods (**Figure 22**). Considering the limited sensitivity of this method and the absence of single-cell sequencing, our spatial transcriptomic results revealed multiple specific gene signatures from the different cell types in a single spot, which makes it challenging to distinguish between individual populations. Consequently, a combination of various cell types is typically identified. Nevertheless, the transcriptomic signature analyzed can differentiate between NB cells (annotated as NE_cells), ECs, CAFs, and macrophages (referred as MQs) (**Figure 41A**). Notably, other populations such as lymphoid (lymphTissue) or BM subtypes were observed in the metastatic samples. As previously described, *MYCN* amplified NBs are categorized as “cold tumors”, characterized by absence of immune cells but increased presence of CAFs and TAMs (91). Interestingly, most spots containing these cell types are localized surrounding tumor cells in primary tumor samples.

In depth analysis of data integration of the different samples of both patients, revealed 12 main clusters covering primary tumors and metastasis (**Figure 41B**). Additional annotation of NB cells was included, distinguishing between NOR (NA_cells) and MSN (MSC_cells) phenotypes. Main NB phenotype was NOR cell, even found conforming individual spots. MSC phenotype was always detected in combination with other populations such as ECs, CAFs or/and macrophages. Analysis of the proportion of these clusters revealed significant differences between primary tumors and metastasis (**Figure 41C**). These results were quite surprising, as the population of both NB phenotypes in the metastasis decreased more than 50% compared to the primary tumor. However, we noticed a 1.5-fold increase in the combination of NOR phenotype with CAFs. A new population (5%) was observed in the metastasis, conformed by both NB phenotype and CAFs. Additionally, other populations such as CAFs, macrophages and MSN mixture showed a 2-fold increase, whereas ECs with MSN phenotype exhibited more than 5-fold increase in metastasis. The results suggest that the MSN phenotype is more frequently adjacent to stromal cells than the NOR phenotype. There may be a set of interactions among CAFs, TAMs, ECs and NB cells that are exclusive to the primary tumors, suggesting their relevance in promoting metastasis, as previously described

in the literature (91, 95). In summary, there is evidence of heterogeneity regarding CAFs and TAMs population among NB samples, which warrants further study.

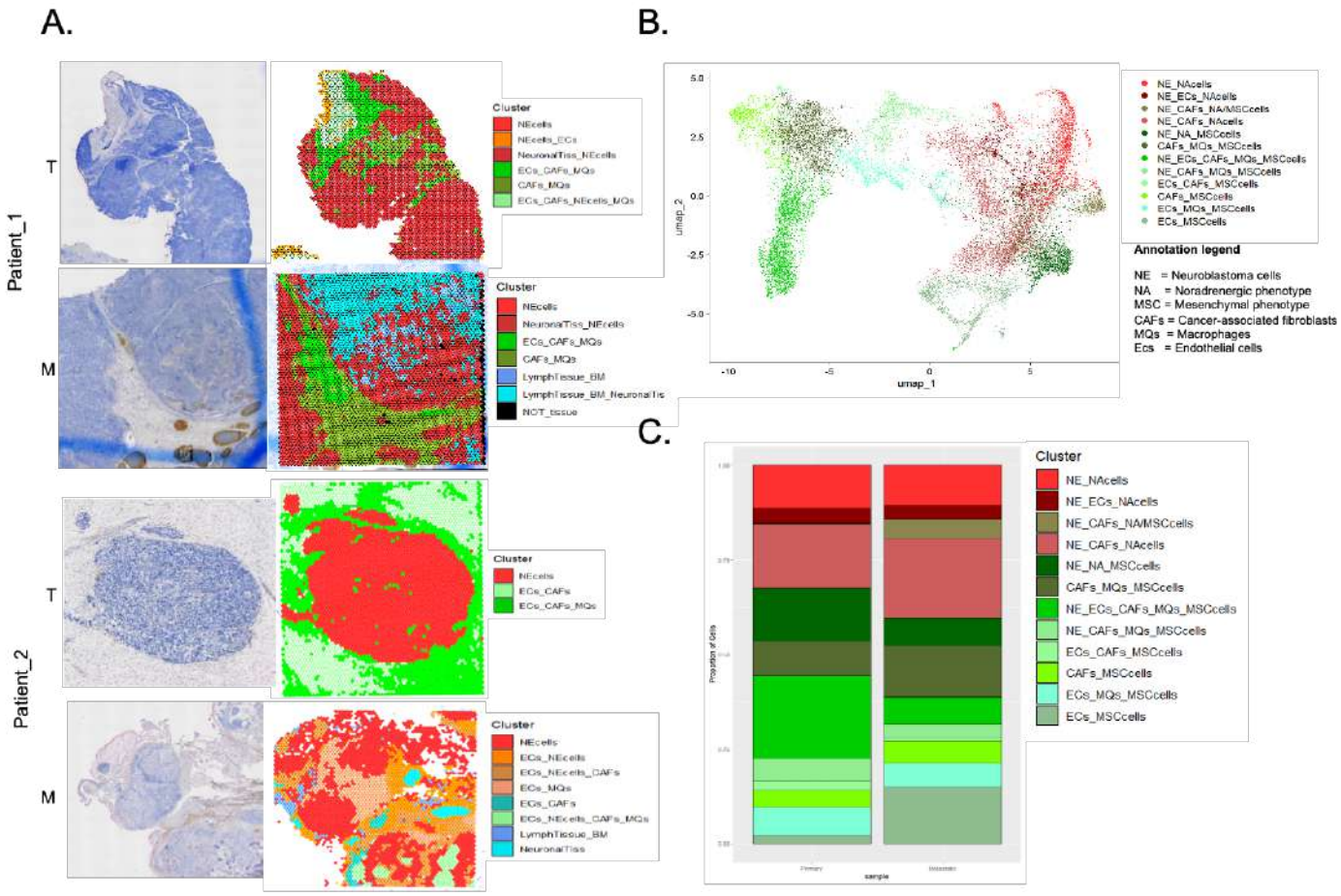

Figure 41. Tumor microenvironment is involved in NB progression. **A.** Spatial transcriptomic analysis of different cell population conforming NB-TME in two different patients. FFPE samples were used for the analysis. **B.** U-MAP clustering of integrated data from primary tumors and metastatic masses revealed 12 different clusters**. C.** Analysis of cell population percentage in the integrated data exhibited different rates between populations.

3.3. CAFs and TAMs emerge as populations of cells promoting NB metastasis

Given that CAFs and macrophages were identified as the predominant non-tumoral cell types in the spatial transcriptomic analysis, we investigated their role in NB. Of note, as macrophages can polarize into a pro-tumor or anti-tumor phenotype, we included only their activated status as TAMs. Thereby, specific genes from both cell types, such as *FAP, ACTA2* for CAFs, and *CD163* for TAMs, were analyzed spatially (**Figure 42A**). Previously, the expression levels of these markers, represented with different color intensities was found concentrated at the periphery of the tumors. The expression values varied depending on the samples, ranging from 0 to over 3. However, few positive spots with half-intensity, meaning 50% lower gene expression, were observed within each tumor mass. Of note, the expression levels for each gene differed among samples, leading to different color scales. Hence,

clustering using U-MAP was performed to determine the distribution of different markers in primary tumor sand metastasis.

Initially, we examined each patient's tumor individually to identify specific populations. As shown in **Figure 42B**, distinct pattern was found among cell populations with an increase in the mixed population (ECs, CAFs, macrophages and the NB-MSN phenotype) in the metastasis compared to primary tumors. The NB-NOR phenotype exhibited a variable pattern of expression among patients. Specifically, patient_1 exhibited an increase of the number spots in the metastatic mass, whereas patient_2 showed decrease. This discrepancy could be attributed to tumor heterogeneity, as evidenced by significant interpatient differences observed in our initial population analysis. Specifically, patient_1 presented a more heterogeneous tissue composition, whereas patient_2 exhibited a more homogeneous tissue sample.

Subsequently, we analyzed the distribution of specific markers for CAFs and TAMs, including *FAP*, *ACTA2* and *CD163,* across different populations. For this analysis, data from both tissue samples (primary tumor and metastasis) were integrated from each patient individually. In both patients, the expression of these genes was observed on the left side of the U-MAP analysis, where mixed populations were found, confirming the expression of these populations. Additionally, some spots were detected in the NB-NOR phenotype clusters, suggesting potential infiltration of these cells or the potential capacity of NB cells to express these markers.

To gain insight into TME interactions, we examined the expression of cytokines that were up-regulated in our previous multi-omic analysis focusing particularly on *TGF-β*, *IFN-γ,* and *TNF-α.* Unexpectedly, only *TGF-β* gene was expressed among the different samples, with notably heightened expression observed in primary tumor samples. Notably, U-MAP clustering was conducted integrating data expression from primary tumors from both patients (T) on one side, and the integration of the metastatic (M) data from both patients on the other (**Figure 42C**). Broadly, we observed that gene expression was higher in mixed populations, but also, few positive spots were observed on the right side of the U-MAP in both samples, where NB signature was increased, particularly the NB-NOR phenotype. In addition, although, the expression levels of *TNF-α and IFN-γ* was barely detectable, some spots were observed in individual NB clusters, specifically in the primary tumor samples.

Our previous results, in conjunction with these findings, suggest the potential involvement of these cytokines in the early stages of tumor development. Furthermore, it is possible that CAFs and TAMs secrete these cytokines within the primary tumor to facilitate metastatic progression. This is supported by the increase of these cells in the metastasis, despite the lack of corresponding cytokine levels. Alternatively, NB cells may also secrete these cytokines, potentially contributing to the modulation of the TME promoting disease progression.

Considering the spatial transcriptomic findings, CAFs and TAMs raised as two relevant populations with potential to induce NB progression. Subsequently, to determine whether their expression was associated with NB prognosis, we explored their expression in the Tumor Neuroblastoma public database, Kocak "R": Genomics Analysis and visualization platform" (N=649, 2013) (**Figure 42D**). Specific markers for each cell type, *FAP* and *CD163*, were associated with poor prognosis. We validated the presence of CAFs in our *in vivo* samples (**Figure 42E**). CAFs, marked by the FAP protein, displayed higher expression levels in the edges of those primary tumors that developed experimental metastasis. The expression in paired metastasis showed CAFs throughout the tumor. Our findings suggest that the presence of CAFs within the primary tumors could be promoting NB metastasis, reinforcing the role of TME interactions during the metastatic process.

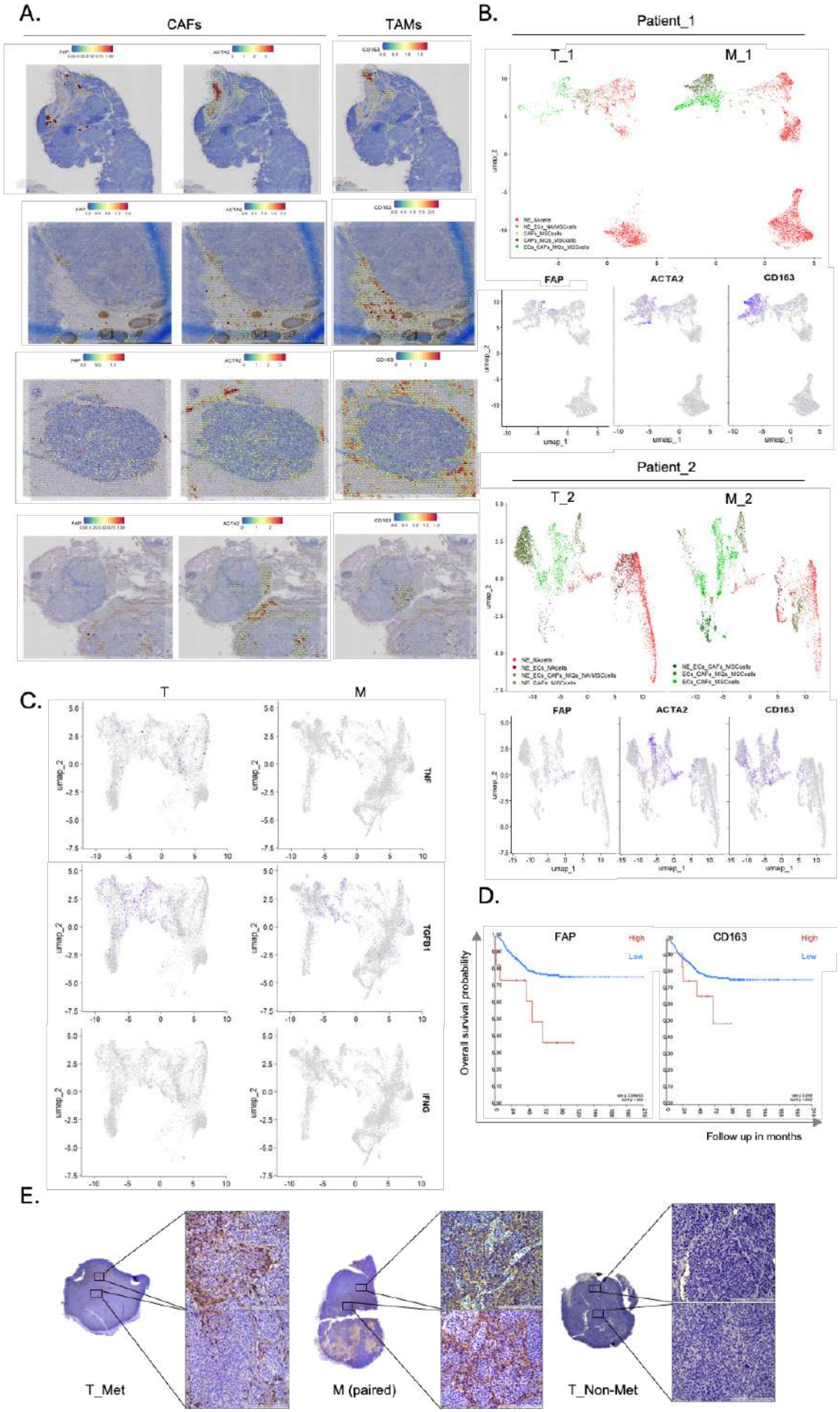
A.
CAFs
TAMs
B.
Patient_1
T_1
M_1
FAP
ACTA2
CD163
Patient_2
T_2
M_2
C.
T
M
TNF
TGFB1
IFNG
D.
FAP
CD163
High
Low
Overall survival probability
Follow up in months
E.
T_Met
M (paired)
T_Non-Met

Figure 42. Analysis of CAFs and TAMs population in NB samples. **A.** Spatial distribution of CAFs and TAMs are frequently found in the edges of tumor masses. **B**. U-MAP clustering revealed different population rates between primary tumor and metastatic samples, highlighting mixed populations including CAFs, TAMs, ECs and MSN-NB phenotype. Specific markers showed an increase of their expression in the mixed populations. **C.** U-MAP of the principal cytokines related to our mouse model exhibited low levels in the metastatic mass. TGF-β displayed highest levels in mixed clusters in primary tumors of NB patients. (T=Primary tumor; M=Metastatic mass) **D**. Kaplan-Meier graphics for FAP and CD163 using Kodak Database (N=629). Elevated levels of both markers were associated with poor prognosis in NB. **E.** IHC analysis of FAP protein revealed different staining patterns between primary tumor and paired metastatic mass (T_Met and M). No expression was observed in primary tumor from non-metastatic animals (T_Non-Met)

3.4. NB phenotypes exhibited specific spatial distribution in the TME

For spatial transcriptomic annotation of both NB phenotypes different genes were assessed. To determine the NOR phenotype *PHOX2B*, *MYCN*, *DBH*, and *TH* genes were included, whereas MSN signature was determined by *CD44 and FN1* expression and the absence of NOR markers. The spatial distribution of the various NB markers in patient_1 is shown as representative of both patients (**Figure 43A).** The expression data reveals the presence of NOR markers within the tumor mass, while the MSN phenotype is seen along the periphery of samples. Notably, spatial distribution was similar between primary tumors and metastasis. Further analysis using U-MAP clustering, exhibited NOR markers being expressed in NB clusters. However, it is worth mentioning that MSN markers were mostly found within mixed populations (**Figure 43B**).

These results support the hypothesis of the NB-MSN phenotype interacting with the TME, and potentially being induced by populations that enhance the metastatic potential of NB, or vice versa.

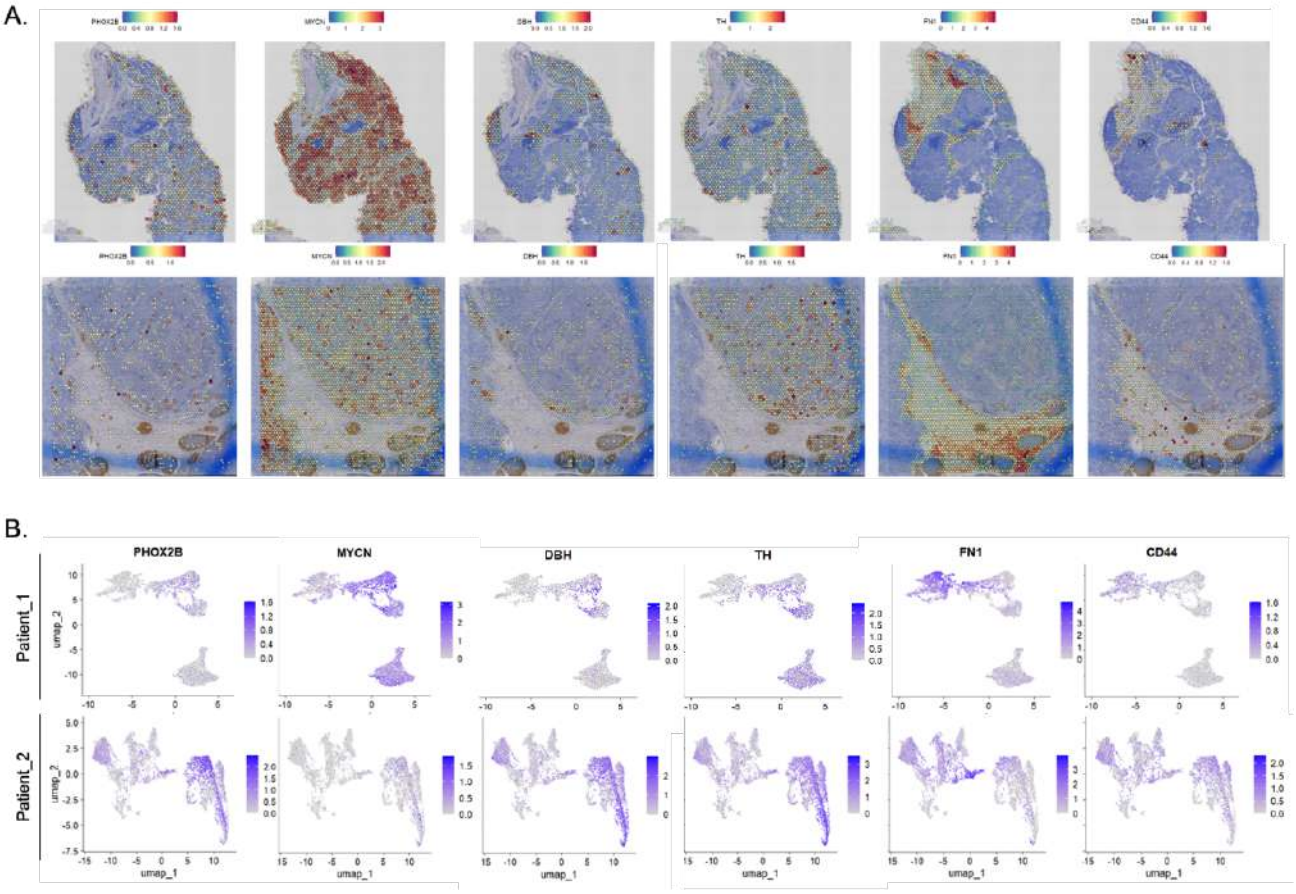

Figure 43. Analysis of NOR and MSN-NB phenotypes using spatial transcriptomics. **A.** Spatial distribution of NOR (PHOX2B, MYCN, DBH and TH) and MSN (FN1 and VIM) phenotypes. NOR phenotype was observed conforming the center of tumor mass. In contrast, MSN phenotype was located in the edges. Patient_1 was used as a representative result. **B.** U-MAP clustering for both patients exhibited RNA levels of each marker through different population.

4. Multi-omics data integration reveals PDPN as a potential marker of NB metastasis

Approximately 60% of patients with NB present with metastatic disease. Indeed, metastatic spread is the leading cause of NB-related deaths. Thus, understanding the molecular mechanisms driving metastasis and identifying novel biomarkers for therapeutic purposes may help much-needed precision therapy strategies for HR-NB. From integrated data of multi-omics analysis, including differential expressed genes and miRNAs, 11 common genes were revealed when compared overexpressed genes and downregulated miRNAs targets as previously shown. Among the different genes, *PDPN* has garnered particular attention due to its role in promoting cell motility, lymphangiogenesis and metastasis to lymph nodes. Additionally, PDPN has been associated with poor prognosis and increased lymph node infiltration rate in NB; however, its role has not been thoroughly studied. As shown in the transcriptomic analysis, *PDPN* exhibited a 2-fold increase in metastasis compared to primary tumors in our *in vivo* HSJD-NB-005-A model (p-value < 0.05; **Figure 44A**). It is important to

highlight that both models, HSJD-NB-005-B and HSJD-NB-002, showed high levels of *PDPN* in the metastasis, although not statistically significant. In accordance with these findings, an increase in protein expression was detected in the metastasis, ranging from 40 to 120% among the different models (p-value < 0.04). A representative image of the WB results is shown in **Figure 44B**.

Of particular significance is the different *PDPN* expression levels observed in those primary tumors generating experimental metastasis (T_Met) compared to those who did not (T_Non-Met). As shown in **Figure 44C**, animal tumors with higher levels of *PDPN* underwent surgical intervention at an earlier time. More importantly, those animals developed macro-metastasis, suggesting that higher levels of *PDPN* may be related to increased tumor aggressiveness. Conversely, animals that underwent later surgical intervention, indicating slower primary tumor growth, exhibited lower levels of PDPN. These findings support the potential role of *PDPN* in NB metastasis. Based on these results, we studied whether there were any differences in *PDPN* mRNA expression in primary tumors related to study endpoint. We distinguished four different endpoints: experimental time endpoint (>150 days); local relapse; signs of disease and metastatic mass detection (**Figure 44D**).

Although not statistically significant, higher *PDPN* expression levels were observed in primary tumors that developed metastasis or local relapses. The results of our study suggested that increased levels of PDPN are associated with a more aggressive form of NB. Nevertheless, the potential for an heterogeneous distribution of PDPN may introduce a confusing bias in our analysis.

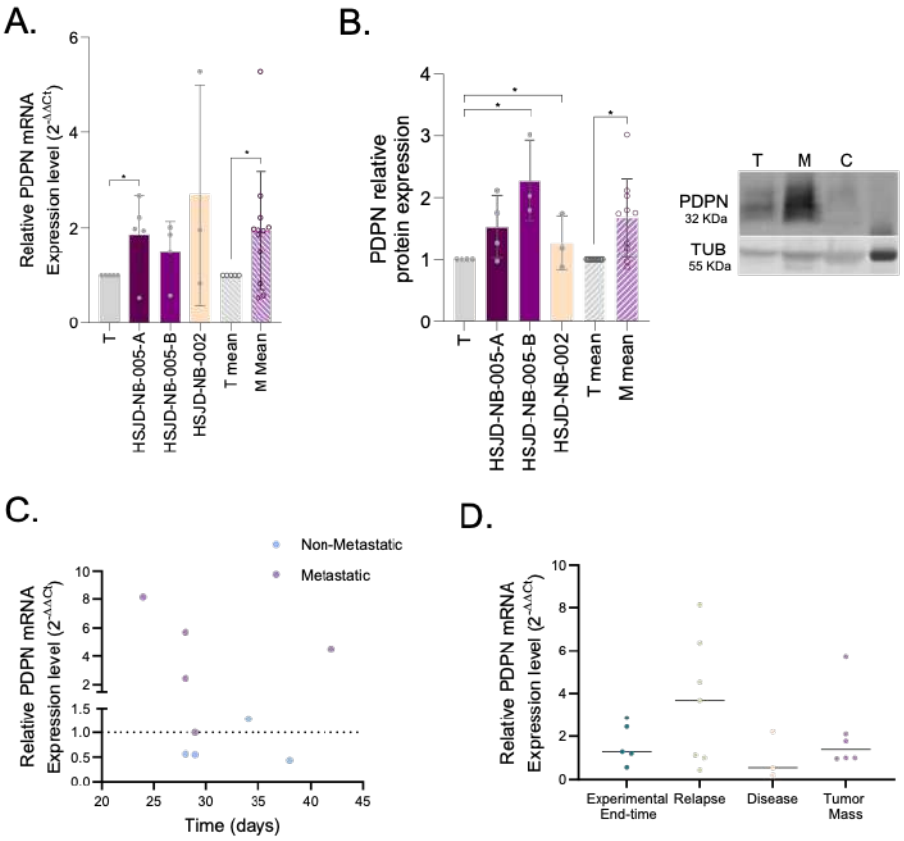

Figure 44. Validation of PDPN expression in our in vivo models. **A**. Relative mRNA expression levels of PDPN in primary tumors and metastatic masses among the three different *in vivo* models (*p-value < 0.05). **B.** Western Blot analysis revealed higher expression levels of PDPN in the metastatic samples compared to the primary tumor. Each metastatic sample was individually compared to its paired primary tumor. The displayed image is from HSJD-NB-005-B but is representative of all models (*p-value < 0.05). **C.** Analysis was conducted to examine the association between PDPN mRNA expression levels in primary tumors and the time until surgery of the primary tumor, considering both metastatic and non-metastatic animals. **D.** PDPN mRNA expression levels, among different endpoint reasons, exhibited a slight increase in both relapse and metastatic mass conditions compared to other endpoints. These endpoints were categorized into four groups: experimental endpoint (>150 days), local relapse, signs of disease, and metastatic mass.

4.1. The intracellular location of PDPN is associated with metastatic rate in our *in vivo* model

As a transmembrane protein, we expected to find membrane staining of PDPN by immunohistochemistry (IHC). Surprisingly, IHC staining showed an unexpected cellular localization pattern for PDPN in NB. Primary tumors exhibited membrane staining, whereas metastasis displayed diffuse staining (**Figure 45**). According to existing literature, there is no reports of PDPN being expressed at the intracellular level. This observation suggested a potential change of the biological role based on its cellular location and/or tumor status. Our *in vivo* samples have been proven to exhibit a high level of FAP protein expression, indicating the infiltration of CAFs derived from mouse. To determine whether PDPN was specifically being expressed by NB cells or by other cells conforming the TME, we included staining with

different specific markers. Human anti-nuclei staining confirmed human origin of the PDPN+ cells. Conversely, a different staining pattern was observed between PDPN and the different vascular markers LYVE-1 and CD31. Of note, PDPN is frequently used as a specific marker for LECs.

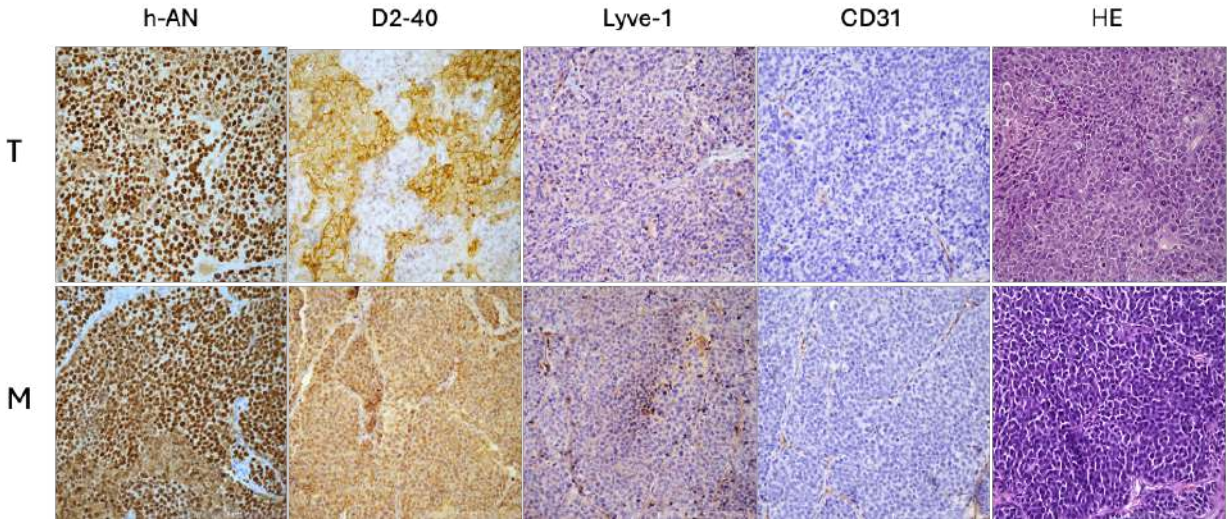

Figure 45. Validation of PDPN protein in our in vivo samples by IHC revealed different PDPN pattern among samples. Analysis was performed for different markers, including h-AN, D2-40 (PDPN), Lyve-1, CD31 and HE in primary tumors (T) and metastatic masses (M).

As a transmembrane protein, the diffuse pattern in the metastasis could be indicative of nonspecific stanning. By confocal immunofluorescence (IF), however, we demonstrated that PDPN translocation within the cell was specific and that most cells expressing PDPN were human (PDPN+; Human anti-Nuclei+; **Figure 46A**). Moreover, we quantified pixel intensity in various cells (N=5) using IF images to determine if the signals from different color channels ($PDPN_{red}$ and human $anti\text{-}nuclei_{green}$) colocalized. The analysis was conducted using a linear approach, whereby the intensity values were measured from a straight line within the cells. The results unveiled different patterns between samples, with no overlap in the primary tumor positioning PDPN at the edge of the analysis, indicating its location in the cellular membrane. In contrast, in the metastasis, there was a noticeable co-localization with human anti-nuclei expression, which allowed for the determination of its intracellular location (**Figure 46B**).

To validate our findings, IHC was conducted on various paired samples from HSJD-NB-005-A and B models to ascertain the specificity and location of PDPN. Our observations revealed that primary tumors exhibited both membrane and intracellular localizations, while metastases only displayed cytoplasmatic expression (**Figure 46C**). Notably, PDPN membrane staining was found mainly in the margins of the tumors, corresponding to the invasive front or regions closer to potential blood vessels, in accordance with previous publications in other tumor types. These findings suggest that specific localizations of PDPN in NB cells might harbor

distinct functions. More importantly, our study reveals new information regarding the intracellular positioning of PDPN in NB, which has not previously been documented.

Moreover, in line with these results, we observed varying PDPN patterns and intensities in primary tumors from mice that developed metastatic masses at endpoint. As shown in **Figure 46D**, PDPN expression was more intense in the primary tumors of metastatic animals compared to non-metastatic animals, exhibiting membrane localization, using the same exposure parameters. The analysis of IF images intensity revealed two-fold increase in metastatic samples, characterized by higher PDPN location in the cellular membrane (p-value < 0.05; **Figure 46E**). As before, specificity of PDPN expression was demonstrated by IHC of different vascular markers (LYVE-1 and CD31). These results suggested that membrane localization of PDPN could be supporting the metastatic capacities of NB cells, which aligns with our previous observations.

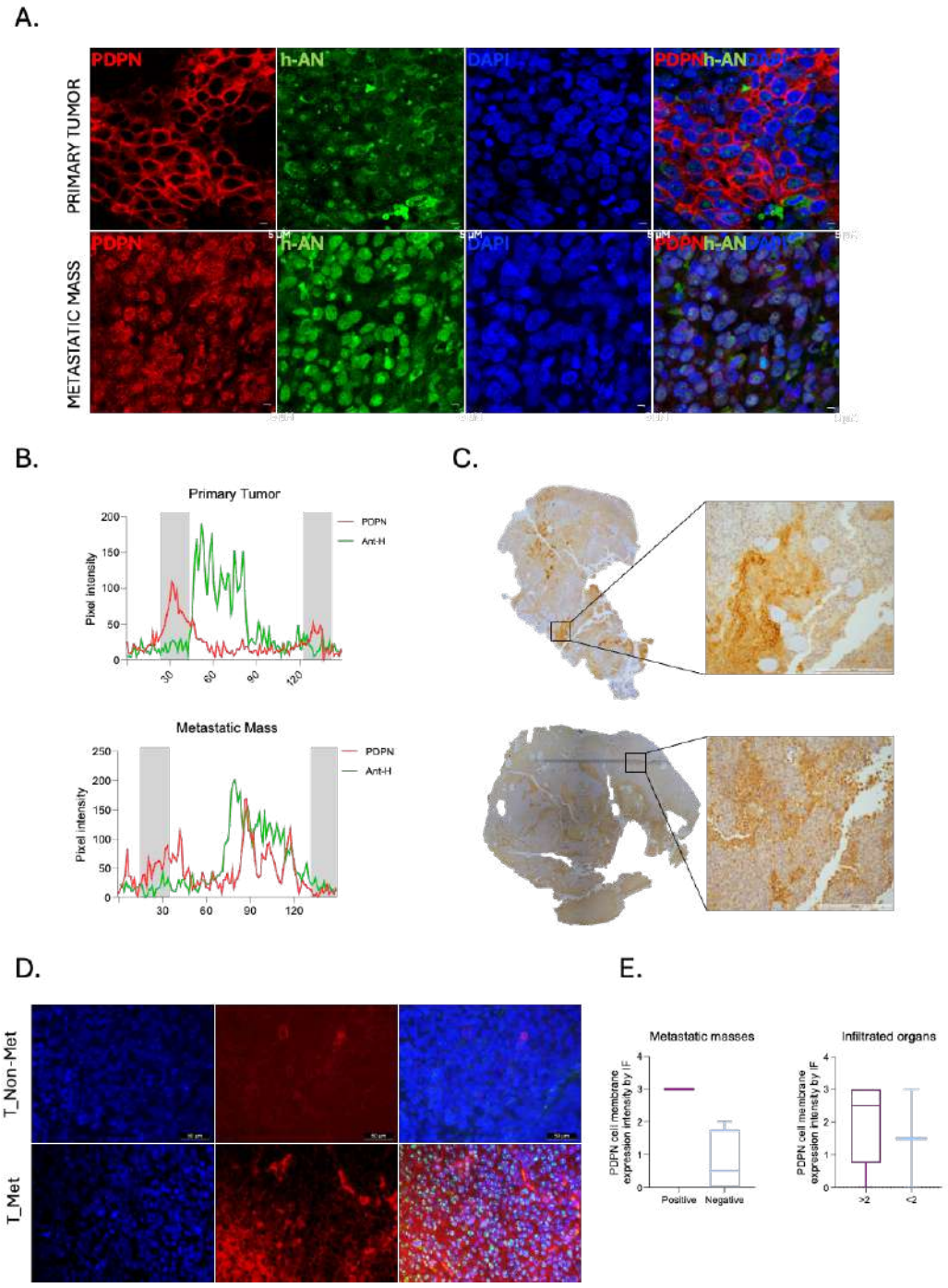

Figure 46. Cellular location of Podoplanin is tissue sample is asssociated with highly metastatic rate. **A**. Representative images of IF stanning revealing different cellular location of PDPN regarding primary tumor or metastatic masses. Human anti-nuclei staining identified NB tumor cells among mouse cells. (Red: PDPN; Green: Human Anti-nuclei; Blue: DAPI). **B.** Analysis of pixel intensity of different color channels showed different location of PDPN (Red) and Human anti-nuclei (Green). **C.** IHC analysis revealed cellular membrane location of PDPN in the edges of primary tumor samples. Scale bars, 200 µm. **D.** IF analysis of primary tumors from metastatic (T_Met) and non-metastatic (T_Non-Met) samples exhibited elevetad PDPN membrane expression in the former. **E.** The association between the occurrence of metastatic masses and the levels of PDPN expression in the membrane of primary tumours was analysed, and a higher proportion of metastatic masses was observed in those samples expressing PDPN in the cell membrane. Furthermore, the association analysis between the number of infiltrated organs and the membrane location of PDPN did not reveal significant differences.

4.2. Neuroblastic tumors exhibit distinct expression levels of PDPN

We sought to ascertain whether the importance of PDPN extends to other neuroblastic tumors, such as GN and GNB, which share similar neural crest cell origins. The primary distinction between neuroblastic tumors lie in their cellular differentiation stage, as previously explained. We used a tissue microarray (TMA) containing over 20 primary NBT samples. It is worth mentioning that TMAs are composed of small biopsies, collected through the *tru-cut* method, from patients who exhibited varying degrees of tumor differentiation and different clinicopathological characteristics. Different intensity and cellular location of PDPN were observed among samples distinguishing 4 different groups (**Figure 47A**). Group 1 and 2 presented intracellular expression of PDPN with high and intermediate intensity, respectively. Notably, group 2 exhibited intense staining in a specific location of the sample. A low intensity expression is found in group 3 within a more homogeneous staining through the tissue sample. Additionally, there were some samples that showed no expression of PDPN, which is classified as group 4. Additionally, a clear vessel staining was observed in group 5. We evaluated the staining intensity by assigning scores from 0 to 3, with 0 indicating absence and 3 the highest intensity. PDPN expression intensity analysis in relation to NBTs type showed NB correlating with the most intense PDPN staining (level 3), suggesting a particular role of PDPN in NB (**Figure 47B**).

Given the association between PDPN and lymph vessel density in NB, we examined vascular staining in our samples to determine whether this was a unique feature of NB (135). In addition, we analyzed if vasculature staining was most frequent in NB. As shown in **Figure 47C**, NB demonstrated a higher incidence of lymphatic vessels than other neuroblastic tumors. However, when considering the number of samples, the ratio of vasculature staining was higher for GN and GNB. Although, additional samples are required to further validate our findings, our results suggest that PDPN expression in tumor cells may be associated with an undifferentiated cellular stage.

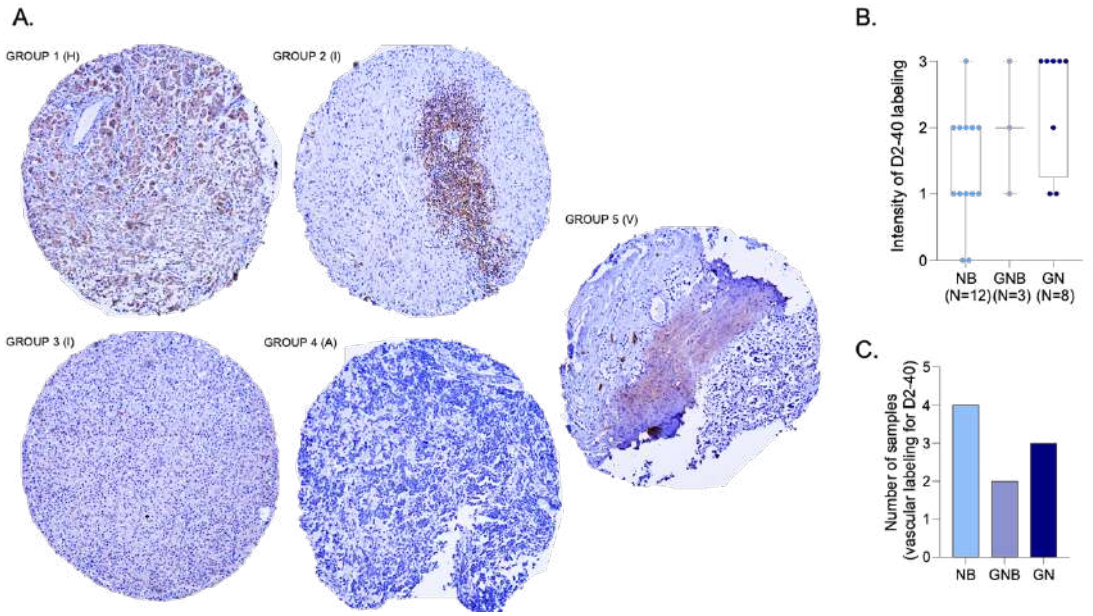

Figure 47. Study of PDPN expression by IHC among neuroblastic tumors using TMA. **A**. Different patterns of expression were observed in the TMA distinguishing between 5 groups. **B.** Intensity of PDPN markers (D2-40) in the neuroblastic tumors conforming our TMA. **C.** Number of neuroblastic tumor samples exhibiting PDPN as a vascular marker.

4.3. PDPN expression is associated with HR-NB patients

Since various expression patterns were identified in the TMA analysis, we decided to expand our patient cohort to investigate PDPN expression patterns in FFPE biopsies of NB patients from our institution (N=16). Biopsies from tumors with different risk factors and stages were included. As anticipated, the primary association of PDPN expression was related to risk stratification (**Figure 48A**). HR-NB patients displayed a membrane pattern of PDPN, whereas LR-NB patients did not express PDPN or, if present, it was intracellular or in the vasculature. NB cells surrounding the vasculature showed a clear membrane staining, which could be associated with the tumor invasive front. Remarkably, similar patterns were observed in loco-regional NB with a membrane location for HR-NB (N=2), and exclusive vascular staining for LR-NB (N=2; **Figure 48B**). A larger sample cohort is necessary to determine the relevance of PDPN expression among NB subtypes.

To determine whether high PDPN expression and cellular location were associated with risk of relapse and tumor aggressiveness, we analyzed PDPN expression in paired samples of patients with relapsed tumors (**Figure 48C**). Of note, only one patient was included in our study at the time of diagnosis, along with several relapsed samples. We evaluated ten pair patients' samples and the analysis revealed an increase in PDPN expression in the relapsed samples, R-I and R-II, consistent with our previous *in vivo* model showing increased PDPN levels in the metastasis. Furthermore, we observed a shift in PDPN cellular location from membrane to intracellular, or from absence to positive expression. Notably, we observed an increase in PDPN expression after each relapse, suggesting a potential association between PDPN upregulation and tumor aggressiveness. Further analysis should consider the potential induction of PDPN of different treatments to understand tumor progression. Specific NB and vascular markers were used to validate specific PDPN expression in NB tumors (**Figure 48D**).

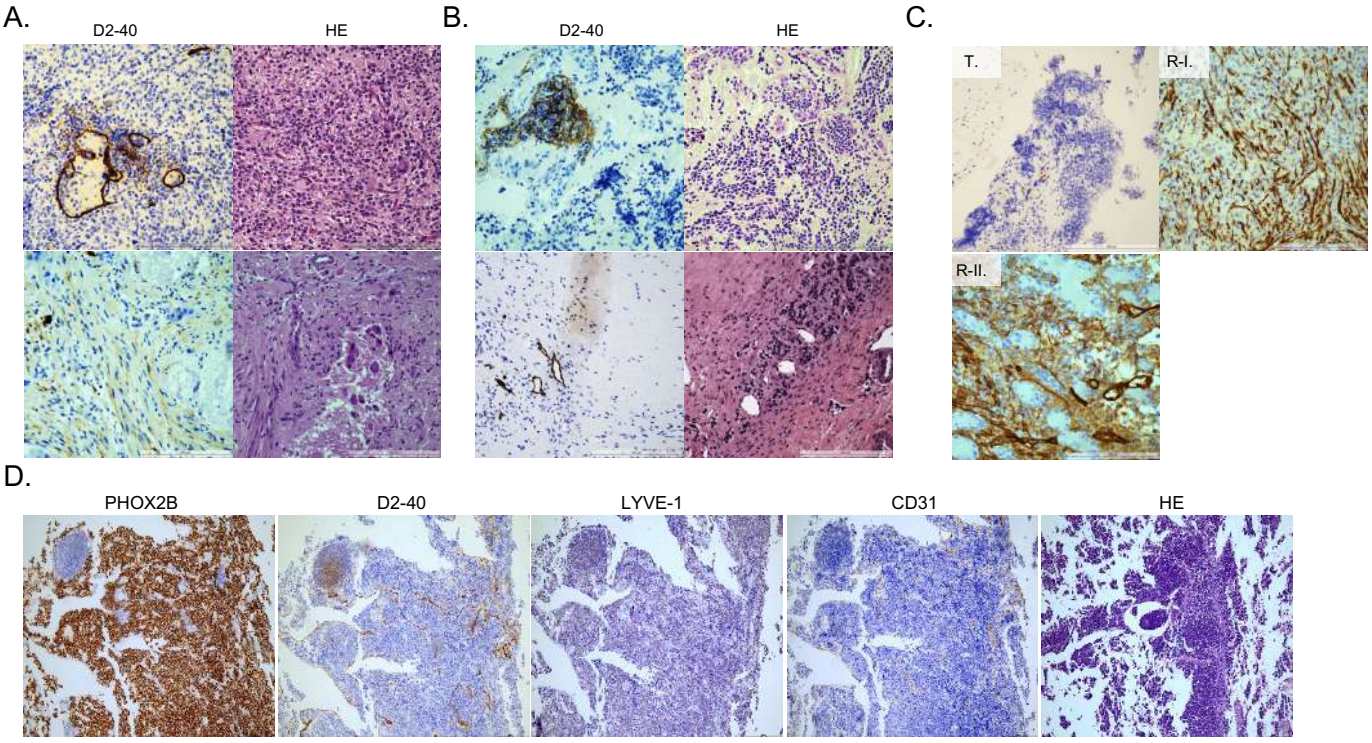

Figure 48. IHC analysis of PDPN (D2-40 Ab) in our cohort of NB patients. A. *PDPN pattern in different risk stratificated NB simples. Top, HR-NB and Bottom, LR-NB**. B.*** *PDPN expression in loco-regional NB with different risk stratifications.* ***C.*** *PDPN expression through patients relapses at different times. Primary tumor: T; first relapse: R-I; and second relapse: R-II.* ***D.*** *Specific IHC staining of NB (PHOX2B) and vascular markers (LYVE-1 and CD31) in patients confirmed specific detection of PDPN. Scale bars, 200 µm.*

4.4. Membrane localization of PDPN in NB at diagnosis correlates with increased lymph node infiltrates in patients

Since distinct intracellular PDPN localizations were observed in our NB cohort correlating with risk stratification, we sought to determine whether PDPN localization at diagnosis (N=20) is associated with outcome. By IHC, distinct subgroups were identified based on expression and cellular localization (**Figure 49A**). No correlations were found with cellular localization (**Figure 49B**). However, a significant increase in lymph node infiltration was observed in the group showing PDPN localized in the cellular membrane, with 85.7% of LN infiltrates, while the cytoplasmic or undetectable expression of PDPN subgroups showed no lymph node invasion (*p-value* < 0.05; **Figure 49C**). These results suggest that membrane location of PDPN may be conforming the invasive front of NB, facilitating its spread towards lymph nodes.

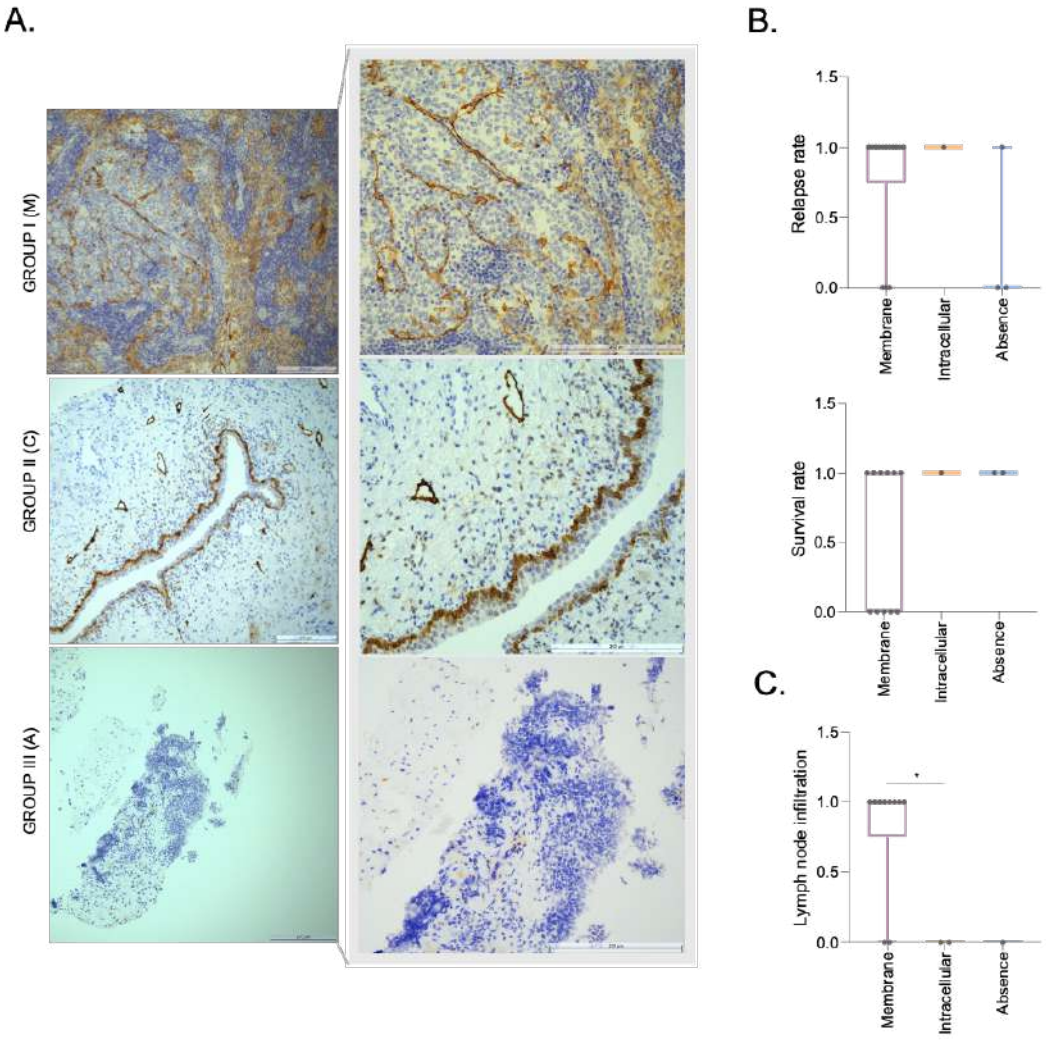

Figure 49. PDPN expression in debut NB patients is associated with lymph node infiltration rate. **A.** IHC showing different cellular location of PDPN in patients' samples: I (membrane location), II (cytoplasmatic location) and III (absence). **B.** Association between cellular location of PDPN in patients and the survival rate and relapse rate. **C.** Lymph node infiltration exhibited a significant difference between group I (membrane location) and II (intracellular location; *p-value < 0.05).

5. The role of PDPN in the metastatic process of NB

5.1. Cell culture expression of PDPN in cell culture is lost through cell passages

Our findings suggest that PDPN may significantly influence the progression of NB by enhancing its metastatic potential to lymph nodes. To better understand this activity, it is essential to conduct functional assays. Since there is no existing literature on PDPN expression *in vitro* for NB cells, we initially examined the basal levels of PDPN in cell lines readily available in the laboratory. Interestingly, no detection was obtained at the mRNA or protein level by RT-qPCR and Western Blot, respectively (**Figure 50A**). As complementary DNA from other established primary cell PDXs were available in our laboratory, we examined mRNA expression of *PDPN*. Notably, a heterogenous expression was observed across models (**Figure 50B**). Nevertheless, the size of the sample set prevented establishing an association between *PDPN* expression and biological characteristic of tumors.

Given the absence of PDPN mRNA expression in NB commercial cell lines and the positive RNA extracts from primary cell cultures derived from PDXs, we suspected that PDPN may become lost during long-term culture. As *PDPN* is known to be stimulated by secreted products like cytokines, among others, we sought to investigate whether the levels of expression changed during *in vitro* maintenance. To do so, we used earlier passages of HSJD-NB-005-A and B since they were established in cell culture. Interestingly, we observed that *PDPN* expression was initially amplified by RT-qPCR, but subsequently lost over time (**Figure 50C**). The results indicate that *PDPN* levels are downregulated as the cells go through serial passages, likely due to lack of expression stimulus. This finding is consistent with previous evidence describing induction of PDPN in response to TME interactions, which are absent when the cells are seeded in plastic. Notably, PDPN expression was detectable in earlier passages because primary cell cultures are likely conformed of various cell types, particularly mouse stromal cells.

Further analyses, using primary cell cultures established from our *in vivo* models, were performed. Therefore, we determined PDPN expression across different sample types, including those established from primary tumor (Tc), and those from metastasis (Mc), from both HSJD-NB-005 models. Unexpectedly, we observed more than 80% reduction of mRNA expression levels in the metastasis (**Figure 50D**). Based on our observations, the location of PDPN varied depending on the type of sample, which intensity is increased when expressed in the cellular membrane of the primary tumors. Therefore, the elevated levels of *PDPN* observed in Tc samples may be attributed to its initial induction in the primary tumor samples, leading to an increase of its transduction. Afterwards, we determined that *PDPN* expression was reduced more than 50% in the samples of Tc that underwent several cell passages when

compared to the initial samples (**Figure 50E**). Overall, our results prompt to speculate that expression of PDPN in NB is mainly triggered by the TME. When these interactions are no longer present, NB cells downregulate the expression of PDPN, in some cases to undetectable levels. Hence, PDPN is translated only under certain conditions to provide specific abilities to tumor cells.

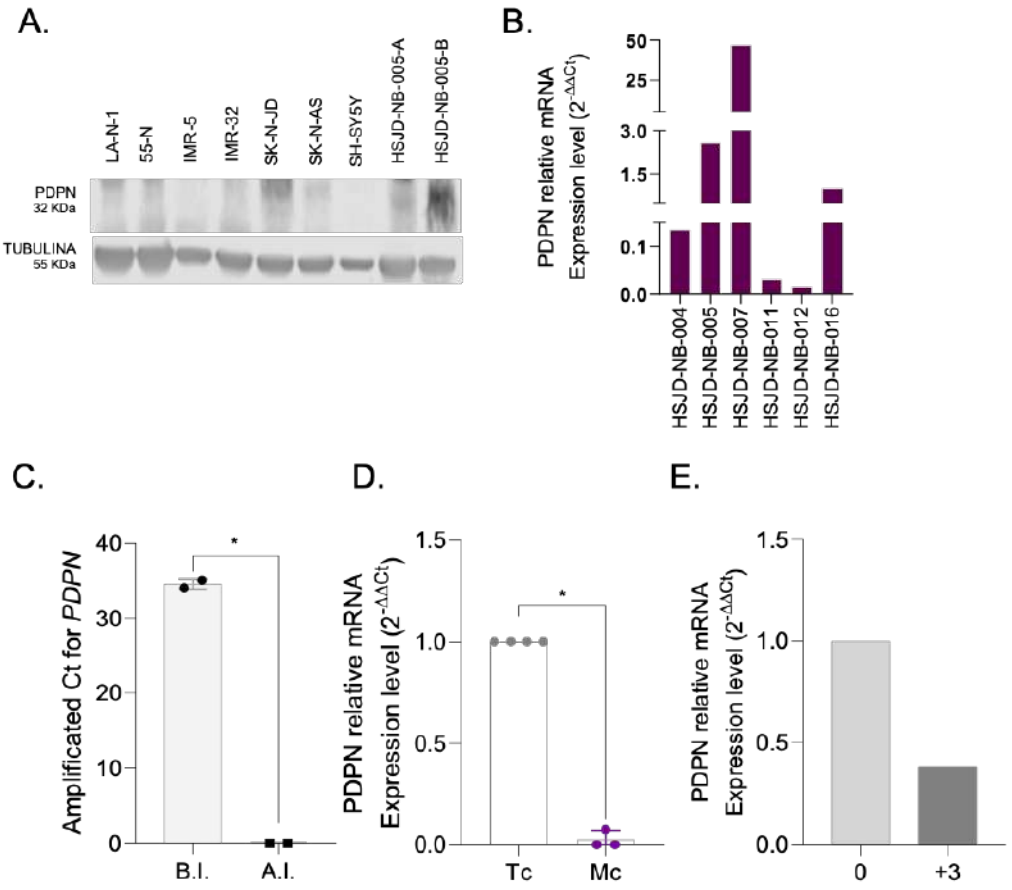

Figure 50. Basal expression of PDPN in NB commercial cell lines, established PDXs NB models and primary cell culture from our in vivo models. **A.** No protein expression of *PDPN* was observed in NB commercial cell lines by Western Blot. However, it was detectable in primary cell culture of HSJD-NB-005-A and -B **B.** mRNA expression levels of *PDPN* was heterogeneous between PDXs models. **C.** PDXs cell culture presented a significant decreased of PDPN mRNA expression levels after mouse inoculation (B.I: before inoculation; A.I: after inoculation; *p-value < 0.005). **D.** Lower levels of PDPN mRNA expression were found in primary cell culture of metastatic samples (Mc) compared to primary cell culture from primary tumors (Tc; *p-value < 0.005). **E.** *PDPN* expression levels were decreased after three passages in the same Tc.)

5.2. Transient inhibition of *PDPN* in primary cell cultures unveils an associated role in proliferation and migration capacities

In an initial attempt to study whether PDPN plays a role in the NB metastatic phenotype, we transiently silenced *PDPN* expression in Tc cells from HSJD-NB-005-A. To validate transfection efficiency, we measured mRNA expression levels at 48- and 72-hours post-transfection. Results show an almost 40% decrease in expression at both time points, with a noticeable loss of siRNA inhibition at 72 hours (*p-value* < 0.03 ; **Figure 51A**).

Subsequently, we performed various functional assays to assess functionality of *PDPN* inhibition. Since we observed different PDPN expression levels associated with the time of tumor resection, we explored its potential role in proliferation capacity as an initial approach. We observed that cells with reduced *PDPN* levels showed higher proliferation rates relative to controls (siCTRL) with most significant difference (50%) observed at 72 hours (**Figure 51B**).

Based on our hypothesis that PDPN may be involved in the process of metastasis in NB, we carried out a migration assay to assess whether there is any difference in this capacity when PDPN is inhibited. To do so, we studied migration using Transwell chambers since tumor cells grow forming spheroids, which make it difficult to analyze given the lack of adherence to transwell membranes. By measuring the number of cells in the bottom of the plate, we observed a reduction of more than 50% of cells with inhibited *PDPN* when compared to control (**Figure 51C**). These preliminary results suggested a potential link between PDPN and the metastatic ability of NB cells *in vitro*.

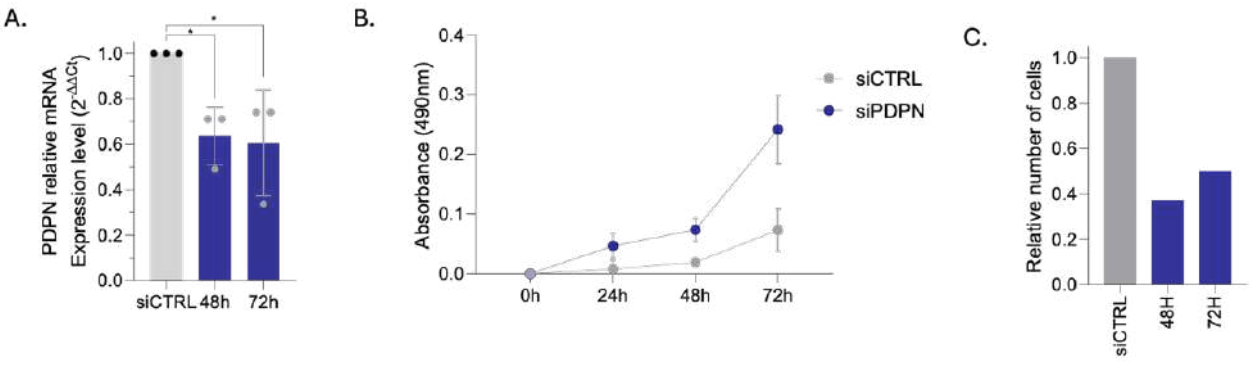

Figure 51. PDPN down-regulation altered proliferation and migration capacities in NB. **A.** mRNA expression levels of transient inhibition of PDPN (siPDPN) after 48 and 72 hours of siRNA transfection (*p-value < 0.04). **B.** Down-regulation of PDPN exhibited an increase proliferation rate compared to control siRNA (siCTRL) in primary cell culture transfected. **C.** Lower number of cells with downregulated PDPN were observed at plate's bottom after 48 and 72 hours in migration transwell assay, compared to siCTRL cells.

5.3. Overexpression of PDPN is associated with cellular localization change in NB cell lines

Since PDPN expression was diminished through cellular passages, it constituted a limitation for functional studies using siRNA. We needed to modulate PDPN levels using stable methods. Since commercial NB cells lines have undetectable levels of PDPN, we decided to overexpress PDPN to determine its role in NB metastasis. Stable overexpression was conducted in LA-N-1 and SH-SY5Y cells by transduction of lentiviral vectors. Control cell lines underwent the same transduction procedure but using an empty vector. The transduction efficiency was confirmed by analysis of GFP signal, with 70% of GFP-positive cells 48 h post-transduction. After selection with puromycin, *PDPN* levels were assessed, showing a significant increase (>100 fold-increase) for both cell lines compared to their empty-vector control (p-value < 0.001; **Figure 52A**). Accordingly, a 50-fold increase of PDPN protein levels was documented by Western blot in ^{High}PDPN cell lines compared to control (**Figure 52B**).

Our previous observations identified distinct cellular localizations for PDPN in various sample types, including the primary tumors and metastasis. Furthermore, we observed PDPN localization on the cellular membrane at the potential invasive front of the tumor. By IF, we investigated PDPN cellular expression in our stable overexpressing cell lines, using wheat germ agglutinin (WGA) staining to identify and visualize the cellular membrane, and to assess whether there was any co-localization of the two markers. As shown in **Figure 52C**, cell lines overexpressing *PDPN* exhibited a clear increase of protein levels and a change in its location compared to control, going from intracellular localization to cellular membrane. The composite image by merging the channels showed a yellow color, indicating an overlap between the red channel (WGA) and the green channel (PDPN).

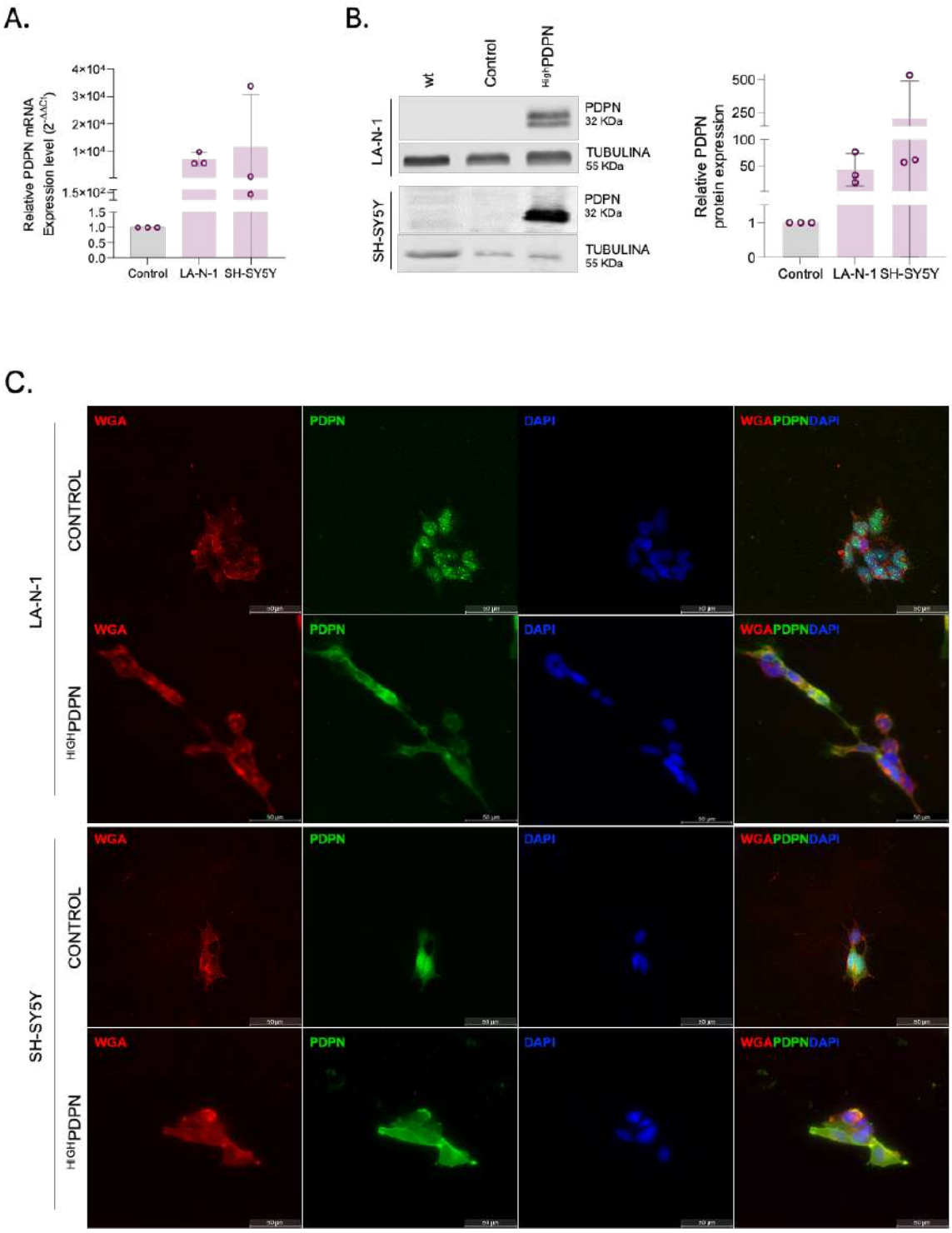

Figure 52. Validation of overexpression of PDPN by lentivirus infection of LA-N-1 and SH-SY5Y cell lines. **A-B.** PDPN mRNA and protein relative expression levels of in LA-N-1 and SH-SY5Y cells stably transfected with PDPN, relative to control (empty-vector) **C.** Increase expression of PDPN is accumulated in the cellular membrane in ^{High}PDPN cell lines (Red: WGA; Green: PDPN; Blue: DAPI).

5.4. Elevated PDPN levels affect proliferation and colony formation capacity in NB cells

Once PDPN expression levels was validated in stable cell lines, we studied whether increased PDPN levels were associated with cellular capacities such as proliferation, as previously observed. Overexpression of *PDPN* was conducted in LA-N-1 and SH-SY5Y cells which exhibited a slower *in vitro* growth, more so in LA-N-1 NB cells (**Figure 53A**).

In agreement with these results, the capacity to form colonies from a single ^{High}PDPN cell was significantly reduced to 75% (LA-N-1) and 50% (SH-SY5Y) after 7 days, compared to controls (*p-value* < 0.005; **Figure 53B**). The results indicate that NB tumor cells may alter their cellular capabilities based upon their phenotypic state adapting to tumor establishment and engraftment, or to migration and invasion.

5.5. The metastatic potential of NB cells is modulated by PDPN expression levels

To get further insight into the role of PDPN in the tumorigenicity of NB, we explored whether stable overexpression of PDPN affected the migratory and invasive abilities. To assess the migration capacity of cells, we employed two different approaches: the wound healing assay (WHA) and the trans-well assay. We evaluated the migration ability of LA-N-1 and SH-SY5Y cells for both control and ^{High}PDPN of each cell line. The healing process of the wound in the WHA-treated LA-N-1 cell line was monitored through photographs taken every 24 hours, until the wound was closed (**Figure 53C**). The open area of the wound was evaluated to determine the percentage of wound closure. After 96 hours, the ^{High}PDPN_LA-N-1 cell line had achieved 60% of closure compared to initial measurement as shown in **Figure 53C**. In contrast, control_LA-N-1 showed 40% of closure at 96 hours compared to initial time. Migration capacity of SH-SY5Y was determined after 48 hours by the trans-well assay. At this point, we quantified the cells attached in the membrane of the trans-well, by measuring the area occupied by cells previously stained with crystal violet. A 60% increase of the stained area was observed in ^{High}PDPN_SH-SY5Y cells compared to control_SH-SY5Y.

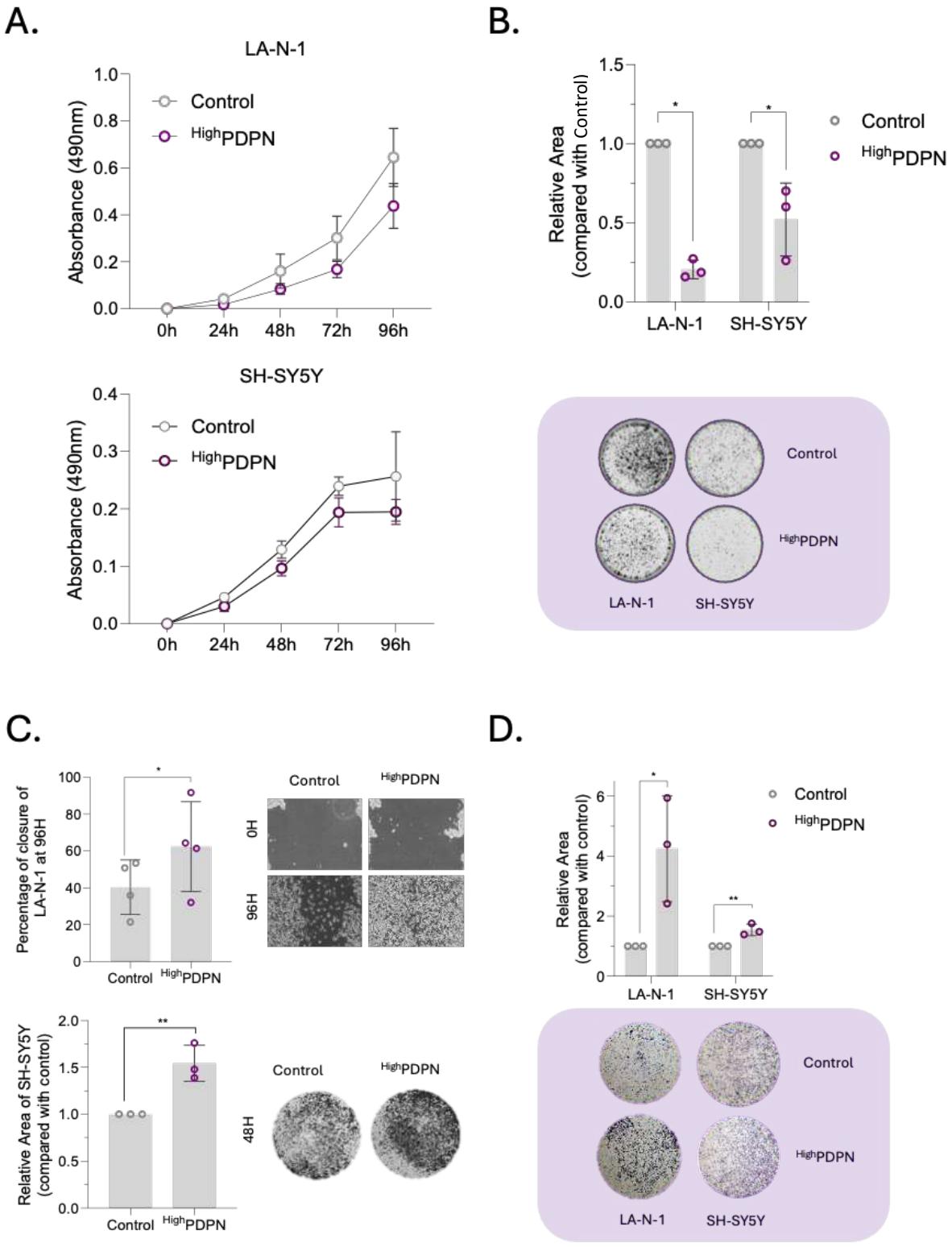

Figure 53. Overexpression of PDPN increases metastatic capacities in NB cell lines. **A**. Proliferation assay showed a decrease on the proliferation rate of LA-N-1 and SH-SY5Y OE_PDPN cells. **B.** Colony formation capacity was significantly decreased when PDPN was overexpressed in both NB cell lines (*p-value < 0.005). **C.** Migration capacity was evaluated differently in NB cell lines, wound healing and transwell assay. In both, cell lines overexpressing PDPN presented significant increase capacity (p-value < 0.005). **D.** Invasion capacity was increased in both cell lines conducting a matrigel matrix transwell analysis *(p-value < 0.005).

To assess the invasive capacity of the two cell lines, we performed a trans-well assay which was distinct from the migration assay performed on SH-SY5Y cells. In this experiment, a matrigel matrix was applied on top of the trans-well membrane. The results showed a notable difference between the two cell lines mainly for LA-N-1 cells (**Figure 53D**). Measurements were obtained by evaluating the stained area of the cells on the trans-well membrane. LA-N-1 cells were evaluated after 72 hours and SH- SY5Y after 48 hours. It should be noted that variations in the endpoint of the assay may be attributed to distinct biological characteristics between cell lines, or even, to differences in PDPN expression. LA-N-1 cell lines showed 400% increase in invasion capacity compared to control (p-value = 0.0067), whereas SH-SY5Y showed a 75% increase when compared to their control cells (p-value = 0.0003). Overall, our results confirm our initial hypothesis whereby increased levels of PDPN expression are associated with enhanced metastatic capacities. These results further support the significance of PDPN in the metastatic process of NB.

6. The interactions of PDPN with the TME

6.1. NB cells expressing PDPN are surrounded by CAFs and TAMs

In order to complete our study, we aimed to investigate which cells within the TME are interacting with PDPN expression in NB cells as it was shown dependent of external stimuli. Our previous spatial transcriptomic analysis demonstrated that primary tumor samples housed CAFs and TAMs, consistent with previous reports. Additionally, our *in vivo* model revealed the presence of FAP with distinct levels of expression between primary tumors from metastatic and non-metastatic animals. Considering that PDPN expression in NB cells seems to require external stimuli and has been linked to interaction with CAFs in other tumors, we sought to investigate the relationship between these populations and PDPN expression. As shown in **Figure 54A**, a diverse distribution of PDPN levels was observed in the samples examined, including primary tumors and metastasis from patients. Expression levels of *PDPN* displayed a range from 0 to 1.6, with the metastasis of patient_1 displaying the highest levels. Noteworthy, the majority of positive spots for PDPN were found at the edges of the tumor, where non-tumor cells were located. In order to acquire more information about the expression of PDPN, we conducted U-MAP clustering to determine the population in which it was expressed (**Figure 54B**). Based on our previous results, low levels of PDPN were expected. However, we observed PDPN positive expression in primary tumors, which were predominantly located in clusters including CAFs, ECs and macrophages, as well as MSC NB phenotype. We conducted a box plot examination to determine whether PDPN levels were elevated in individual NB cluster (**Figure 54C**). Our findings revealed an 80% increase in

PDPN expression in the individual NB cells of patient_1. However, no significant variation was observed in patient_2.

Since the higher levels of PDPN were observed in mixed clusters, we believe PDPN could be expressed by stromal and immune cells conforming the TME but also from MSN NB cells. This observation leads to the hypothesis that MSN NB phenotype, which have shown increased metastatic capacities, may be the subtype of cells expressing PDPN (76).

In this line, we assessed the expression levels of NOR and MSN markers, as well as EMT-TFs, in our stable cell lines, similar to previous analysis performed in primary cell culture from our *in vivo* model. As shown in **Figure 54D**, analysis of both stable cell lines revealed an heterogeneous expression of the various genetic signatures of ^{High}PDPN cells compared to control. Analysis of both cell lines together, we observed a higher increased in MSN markers and a slight increase in NOR markers, although no significant results were obtained (**Figure 54E**). No clear results could be extracted from this study. Neither phenotype was fully defined suggesting a transient NB phenotype.

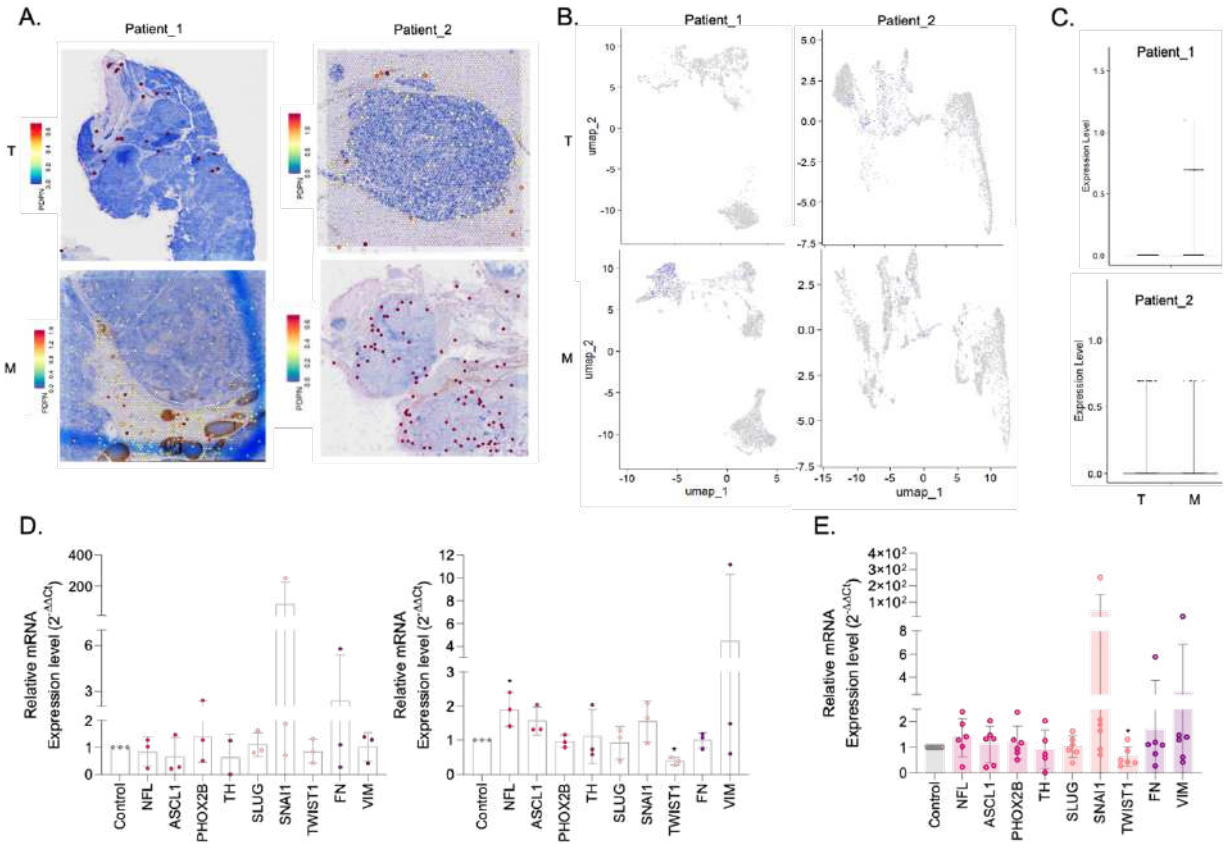

Figure 54. Low expression of PDPN is detected in NB patients. **A.** Spatial distribution of PDPN in primary tumor and metastatic mass in the FFPE samples from two NB patients. **B.** PDPN expression among different cluster of population conforming the tissues, exhibited higher expression in mix population including ECs, CAFs, macrophages and NB-MSN phenotype. **C.** PDPN expression levels in NB-NOR phenotype. **D.** Individual characterization of NOR (*NFL, ASCL1, PHOX2B* and *TH*) and MSN (*FN* and *VIM*) NB phenotype, and EMT-TFs (*SLUG, SNAI1* and *TWIST1*) by gene expression**. (***p-value< 0.004)* **E.** Global characterization of ^{High}PDPN phenotype in both stable NB cell lines.

6.2. Expression of PDPN is induced by TME interactions

Since PDPN expression was found in clusters conformed by different populations, we aimed to determined which cell type was potentially stimulating PDPN expression in NB cells. We explored whether the interaction between fibroblasts and NB cells was inducing PDPN expression or *vice versa*. At first, we aimed to explore whether PDPN expression in NB cells could induce fibroblast polarization of CAFs. Collected media from stable SH-SY5Y cell lines, including control and ^{High}PDPN was exposed to fibroblast culture for 96 hours. Polarization of CAFs was determined by assessing the expression levels of FAP by IF. As shown in **Figure 55A**, an increase of FAP expression was observed in fibroblasts exposed to ^{High}PDPN-CM compared to control-CM. To discard any potential stimulation from the medium, we assessed FAP in fibroblasts cultured in their medium (DMEM supplemented with 15% FBS) and RPMI-1640 used for NB cell cultures, without exposure to NB-CM. No expression of FAP was observed in any of the control groups, suggesting that secreted factors from ^{High}PDPN_SH-SY5Y cells stimulated FAP expression in fibroblasts. Additional analysis determining mRNA and protein levels of specific CAFs are needed to determine its function.

The use of co-culture assays aimed at determining whether the physical interaction between the two cell types, NB and HFF-1 cells, would lead to induction of PDPN and fibroblast polarization. Considering that the proportion of fibroblast is lower than that of tumor cells in NB, a 2:1 ratio (NB: HFF-1) was seeded trying to mimic the tumor stroma condition. Surprisingly, an increase of PDPN expression was observed in empty-vector SH-SY5Y cells (control_SH-SY5Y), as well as a faint signal of FAP in fibroblasts after 48 hours of co-culture (**Figure 55B**). Conversely, ^{High}PDPN_SH-SY5Y co-culture with HFF-1 cells, did not cause alterations in PDPN expression levels. Additionally, higher levels of FAP expression were found in fibroblasts co-cultured with ^{High}PDPN cells compared to controls. These results suggest that an interaction exists between both cell types which may trigger PDPN expression in NB cells and CAF polarization in fibroblasts.

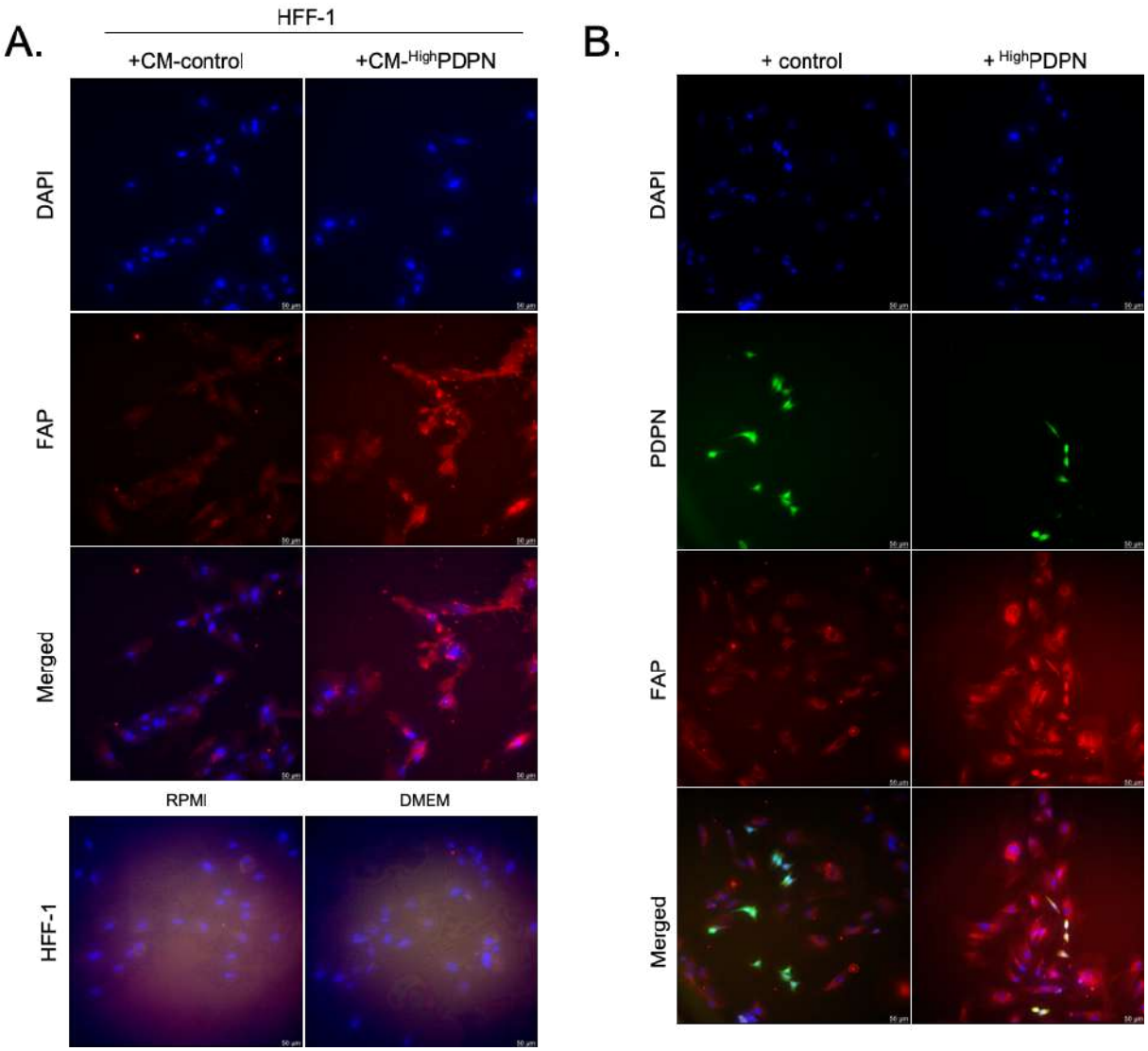

Figure 55. PDPN association with TME interaction in NB. **A.** IF of CM assays in HFF-1 cell lines revealed an increase of FAP expression after 96 hours of exposure to CM from ^{High}PDPN cell culture compared to control. **B.** IF of co-culture assay, distinguishing between HFF-1 with control or ^{High}PDPN cells. Control cells exhibited an increase of PDPN expression after 24 hours of co-culture with HFF-1.

Considering that the control cell line increased PDPN expression when exposed to CAFs, we hypothesized that direct or indirect interactions between CAFs and NB cells triggers PDPN expression. Thus, we aimed to determine whether secreted factors from CAFs could be inducing PDPN expression in NB cells. Therefore, we exposed wild-type SH-SY5Y cells to different cytokines as reported in the literature, to evaluate whether these cytokines induce PDPN expression in NB cells (103, 113). After 16 hours of treatments, including TNF-α, TGF-β_1 and IFN-y, PDPN protein levels were analyzed (**Figure 56A**). We observed 5-fold increased levels for TNF-α, 13-fold increase for TGF-β_1 and 10-fold increase for IFN-y, when compared to non-treated cells. Subsequently, we determined if the exposure to cytokines and subsequent increase of PDPN expression could be regulating metastatic capacities. Hence, we conducted a WHA assay adding the treatment after the wound. As expected, an elevated

percentage of wound closure was observed in cells treated with TGF-β_1 compared to control, after 16 hours, not statistically significant (**Figure 56B**). In contrast, TNF-α and IFN-γ treatments showed more than 20% wound closure compared to non-treated cells, resulting statistically significant (p-value < 0.04).

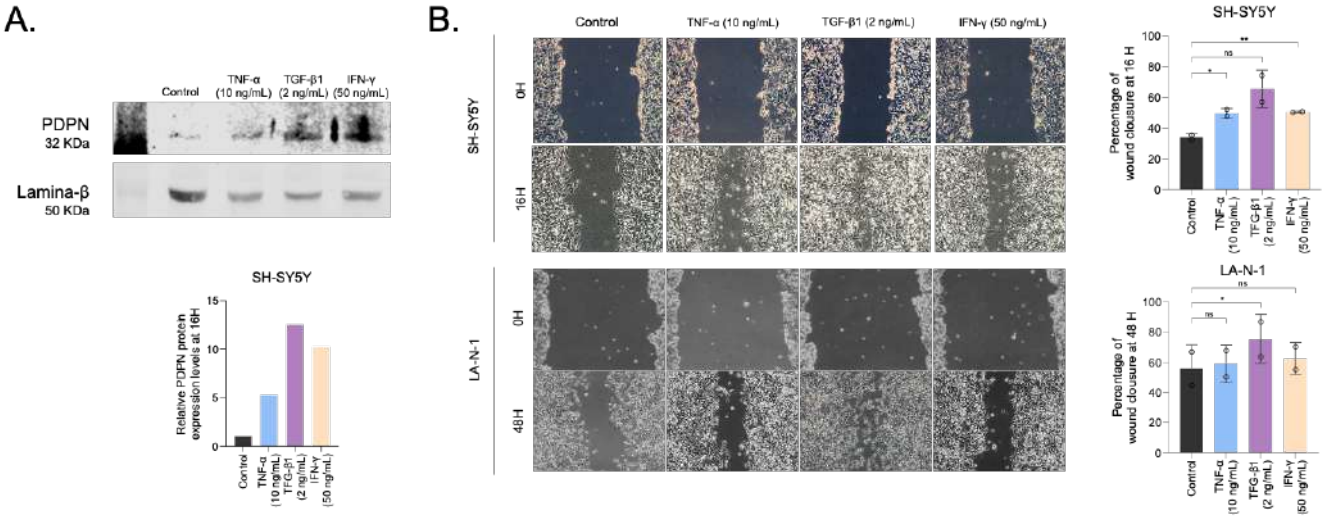

Figure 56. Cytokines treatment induce PDPN expression in SH-SY5Y cell line and enhances metastatic capacities in NB cells A. *Protein quantification of PDPN after 16H treatment with cytokines.* ***B.*** *Treatment with different cytokines increases migration capacity of NB cell lines with different time-points (16H for SH-SY5Y and 48H for LA-N-1)(*p-value < 0.05).*

In summary, our findings suggest that PDPN expression in NB cells may be modulated by TME interactions, particularly fibroblasts, which polarize into CAFs. Moreover, cytokines secreted by CAFs might play a role in stimulating PDPN expression, which could ultimately lead to increased metastatic capacities of NB cells.

6.3. Low oxygen increases PDPN expression in the cellular membrane.

Given that membrane expression of PDPN was observed in the edges of primary tumor tissues in the *in vivo* model, and that it has been previously described in other tumors to form the invasive front, we wondered whether its expression is regulated by other environmental factors, in addition to CAFs and cytokine interactions.

We examined whether PDPN was regulated by the oxygen levels in NB cells by culturing stably transfected cells in a low oxygen (3%) incubator for varying lengths of time. Since metastasis displayed intracellular PDPN, we anticipated a shift in ^{High}PDPN_SH-SY5Y cells similar to that in the core of the tumor. Remarkably, an increase in cell membrane PDPN in control_SH-SY5Y cells was observed, suggesting that low oxygen conditions may trigger the expression of PDPN in the membrane (**Figure 57A**). No significant changes were observed in the overexpressed cell line until after 72 hours when cells displayed a more homogeneous

distribution of PDPN throughout the cell (**Figure 57B**). These findings suggest that NB cells can use the membrane location of PDPN to sense unfavorable conditions such as low oxygen and migrate to other regions.

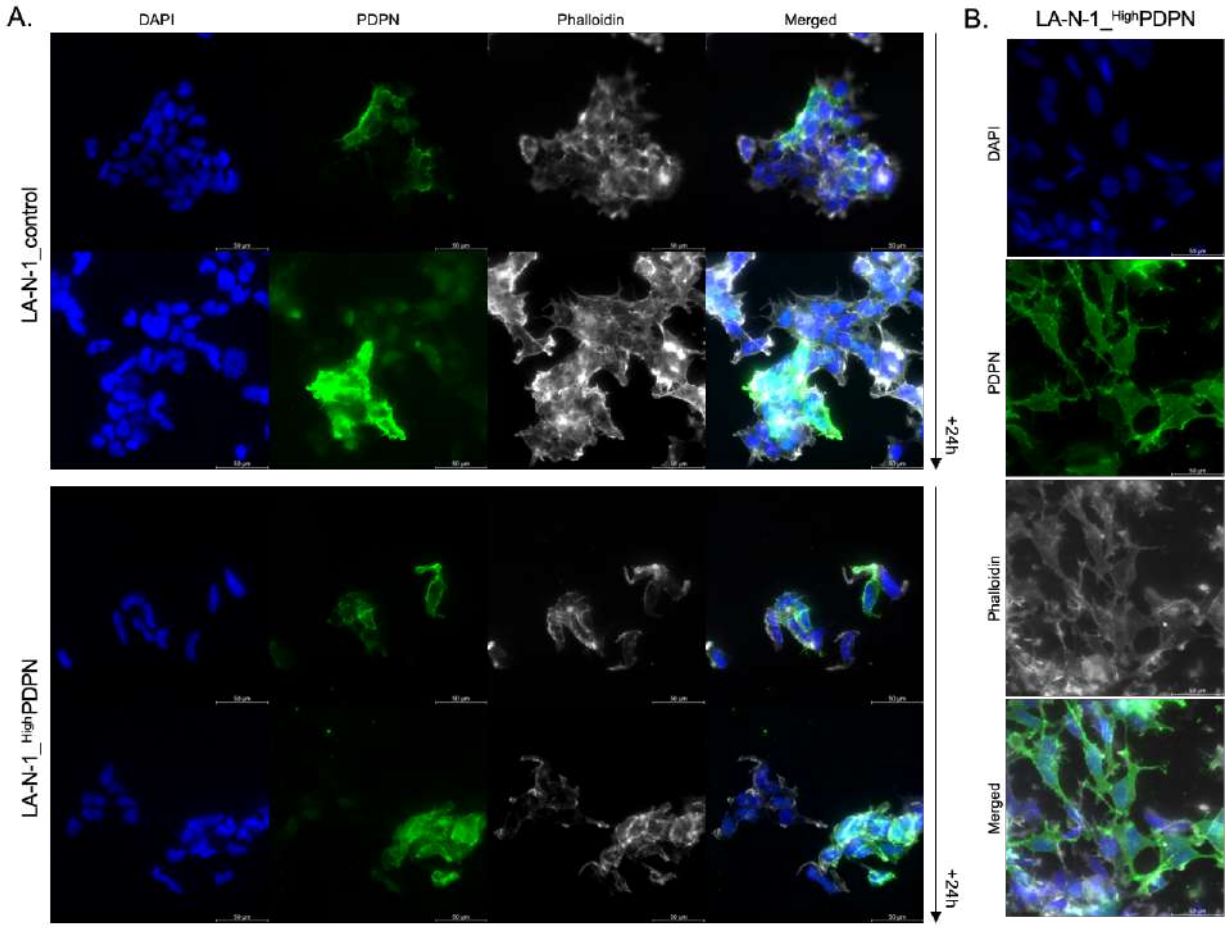

Figure 57. PDPN is regulated by oxygen concentration in LA-N-1 cell line. **A**. PDPN location (green) after 24 h of exposure to low oxygen condition. **B.** Homogeneous PDPN location (green) in HighPDPN_LA-N-1 cell line after 72 h of low oxygen exposure.

To carry out an in-depth analysis of the oxygen levels and its association with PDPN expression in NB, we obtained the previously reported hypoxic signature from our spatial transcriptomic data (173). Among the various genes described upregulated under hypoxic conditions in NB, *DDIT4, ANGPTL4, PGK1* and *PFKFB4* were represented in the U-MAP distinguishing between primary and metastatic samples (**Figure 58A**). The first two genes were expressed in both types of samples, with more spots in the metastasis. Notably, DDIT4 and *ANGPTL4,* were highly expressed in the clusters containing mixed cell type populations, which correlate with positive PDPN expression. Consequently, we explored the spatial location of both genes within the tissue, as shown **Figure 58B**. *DDIT4* was observed homogeneously in both tissue samples, whereas *ANGPTL4* was mostly found in the periphery of NB populations. Further analysis must be performed to establish the relationship between the hypoxic signature and the spatial distribution of PDPN.

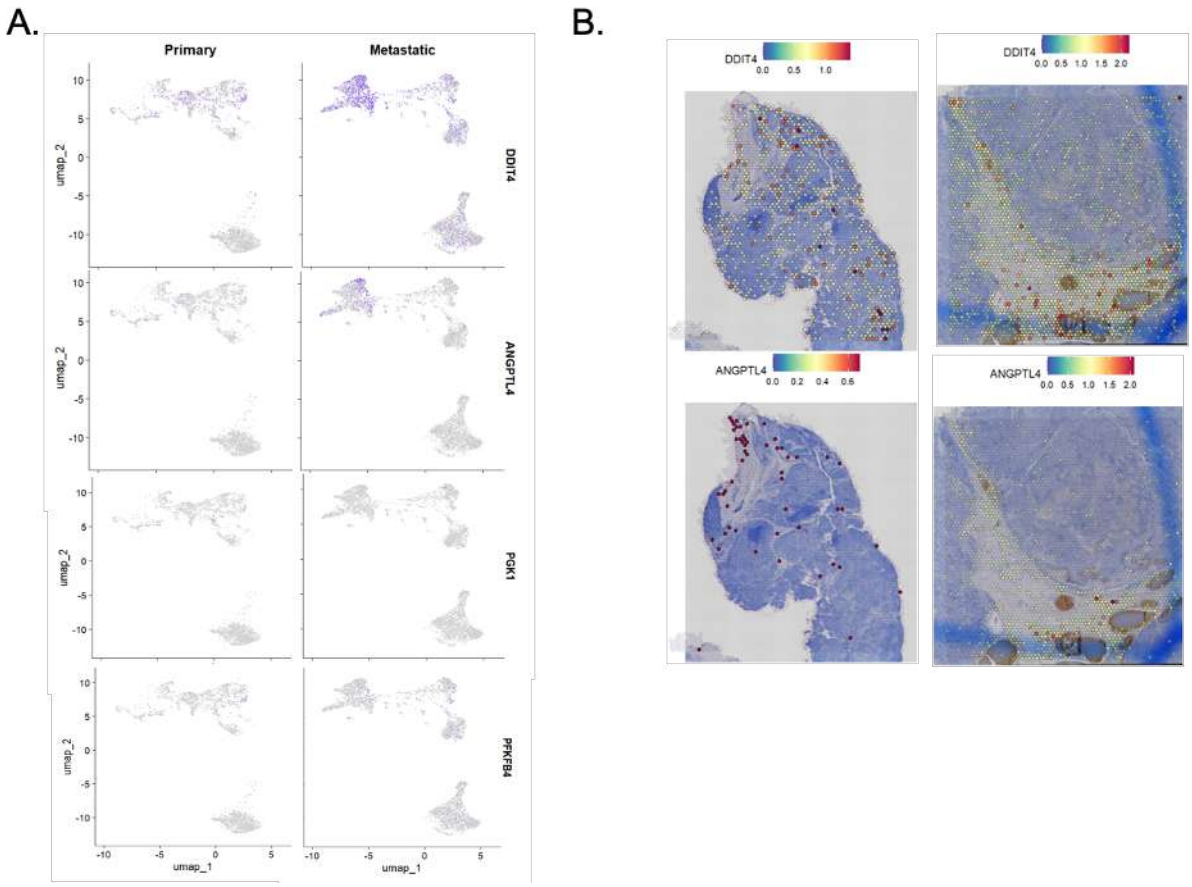

Figure 58. Representative gene expression of hypoxic signature in our spatial transcriptomic data. A. U-map clustering exhibits positive expression of *DDIT4* and *ANGPTL4* in both tissue samples, primary and metastatic tumor. **B.** Spatial distribution of *DDIT4* and *ANGPTL4* in FFPE samples included in spatial transcriptomic analysis.

7. Podoplanin is secreted by NB tumor cells through exosomes

Our results suggest that PDPN plays a role facilitating the metastatic properties of NB cells. Nevertheless, there are many other actors participating in this process. For instance, tumor cells educate the TME to generate a pre-metastatic niche. Among others, exosomes have emerged as important players in tumor progression and metastasis. Since PDPN is secreted via exosomes in melanoma, we evaluated the possibility that PDPN was expressed in NB exosomes (138). First, we analyzed PDPN expression in exosomes *in vitro*. Isolation of exosomes was validated using specific markers like TSG101 and CD9, and by nanosight. Remarkably, exosomes from ^{High}PDPN cell lines cultured under normoxia, including LA-N-1 and SH-Y5Y, showed detectable levels of PDPN compared to controls (**Figure 59A**). We then designed a longitudinal study by collecting blood samples at different time points from our *in vivo* models (**Figure 59B**). Nanosight analysis showed a peak of 100 nm particles which is associated with the presence of exosomes. By protein quantification, we demonstrated that PDPN expression could be detected in exosomes, isolated from serum samples collected at different time points, after NB cell line inoculation, and it is maintained until endpoint (**Figure**

59C). Our results demonstrate the presence of PDPN in NB exosomes when PDPN increases in tumor cells, suggesting a potential role of this protein in early phases of the metastatic process, such as the modulation of the PMN.

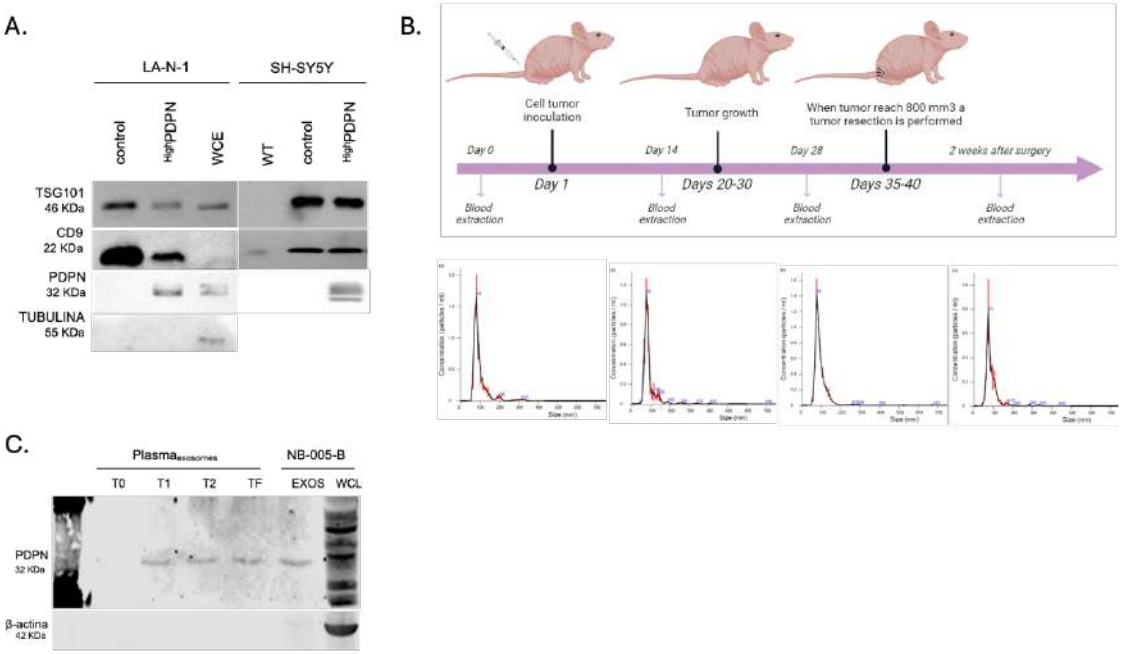

Figure 59. PDPN is secreted by NB tumor cells through exosomes. **A.** Expression levels of exosomes markers and PDPN in isolated exosomes from cell lines supernatant, including whole cell extract (WCE) and isolated exosomes from wild type cells (wt). TSG101 and CD9 are specific markers of exosomes. **B.** Schematic image of the different time points of blood extraction in our in vivo model (Top). Nanosight analysis of isolated exosomes from plasma samples (bottom). **C.** PDPN expression in plasma samples by WB.

7.1. PDPN+ exosomes induce hMSC and HFF-1 polarization

Given the role that exosomes play in modulating the PMN and the ability of PDPN to induce fibroblast polarization into CAFs, we aimed to determine whether the presence of PDPN in NB exosomes serves as a potential regulator of the PMN by inducing fibroblast polarization into CAFs. We treated HFF-1 and hMSC with exosomes isolated from our stable cell lines, given that both cell types have the potential to polarize into CAFs. To determine whether PDPN+ exosomes induced CAF polarization, we evaluated FAP expression by IF. After 24 hours of treatment, hMSCs and HFF-1 showed higher FAP expression (**Figure 60A**). Quantitative analysis demonstrated a significant increase, approximately by 60% of FAP levels (**Figure 60B**). These results suggest a regulatory role of PDPN onto the TME possibly by promoting the polarization of certain organ host cells into CAFs.

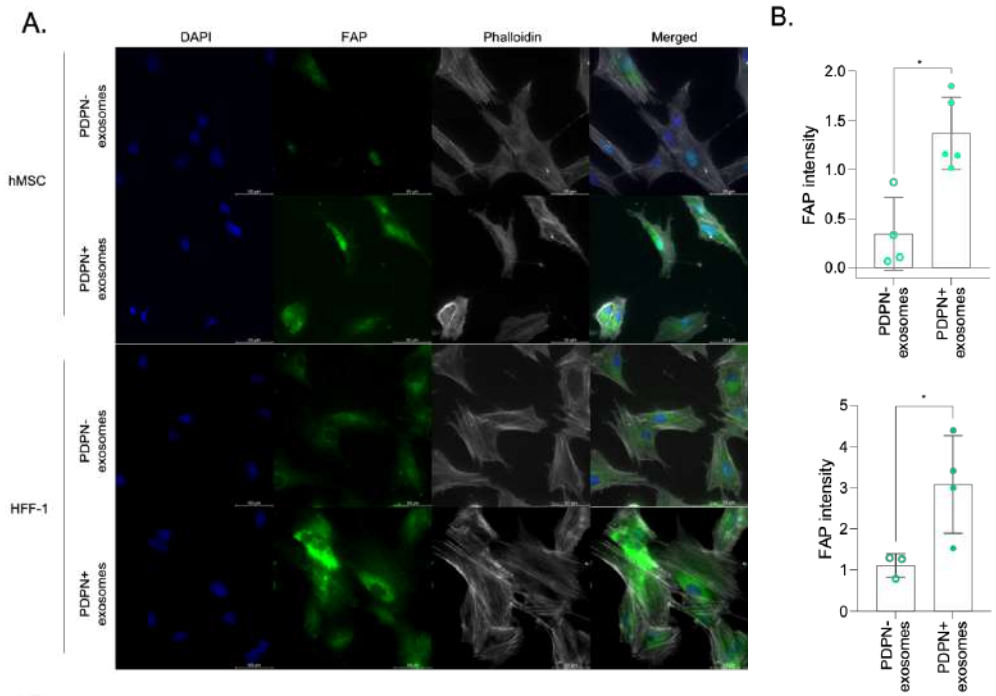

Figure 60. Secretion of PDPN via exosomes induced increase levels of FAP in hMSC and fibroblast. **A.** IF of hMSC and HFF-1 after 24 hours of exosomes treatment. **B.** Signal intensity analysis of IF exhibited a significant increase of FAP levels after 24 hours of treatment with PDPN+ exosomes. Each point represents a biological replicate.

DISCUSSION

NB stands out as an aggressive and highly metastatic tumor, with 50% of patients presenting with metastasis at diagnosis. Survival rates for those with high-risk (HR) disease remain barely above 50% (17). Even though intensive multimodality therapies have been extensively used, HR-NB patients continue to be a clinical challenge, underscoring the need for innovative therapeutic approaches that in turn require a better understanding of NB drivers to target. NB is a developmental tumor originating from neural crest cells, which are multipotent and highly migratory during embryonic development. The analysis of the migratory features of NB cells, particularly those of the cells of origin, offers a promising avenue for understanding and combating the metastatic forms of this aggressive cancer.

Over the years, different theories about the cell of origin of NB have focused on the neural crest development and its potential differentiation trajectories giving rise to various lineages. Recently, single-cell data revealed contradictory information regarding the cell of origin in NB, however, both studies agreed that NB emerged from early differentiation stages of the neural crest thus with inherent migratory capacity (52, 54). Henceforth, the undifferentiated cells could disseminate to different locations of the embryo, and disease emerging apparently as multi-focal Delloye-Bourgeois *et al*. established a chick embryo model to demonstrate migration capacity of NB throughout different locations of the embryo, highlighting sympatho-adrenal territories. Furthermore, they determined that NB cells recapitulate NCC-like initial migratory programs to do it. More importantly, distant metastases were observed only when using cells from patients with metastatic NB (174). Regarding the metastatic capacity of NB cells, numerous studies focus on the different phenotypes described in NB, including ADR or NOR and MSN, and their association to its origin and behavior (52, 175). In addition, transition of phenotypes in NB cells, known as NMT, is associated with different time points and capacities during tumor development, including proliferation and migration capacity, among others (76). Pastushesko *et al.* described in adult tumors, the ability of tumor cells to switch between epithelial and MSN phenotypes as they changed their cellular capabilities (59). Even though both phenotypes present opposite capacities, up- and down-regulated, they described the presence of various transition phenotypes with some cellular abilities simultaneously, resulting in more aggressive phenotypes. Like adult tumors, in 2022, Zhang *et al* identified by single cell RNA-sequencing a transitional phenotype with enhanced aggressiveness in neuroblastic tumors (80). Although NB is potentially a multi-focal disease from its origin, its capacity to interconvert between phenotypes demonstrates its ability to metastasize to distant organs from the primary tumor mass.

Despite all the available studies in NB, there is still a lack of knowledge of the molecular mechanisms driving the metastasis. Different *in vivo* models have been established to study the metastatic process in NB (71). Notably, the same *in vivo* models have been used for

several years including the genetically engineered mouse models for different alterations (*ALK*, *LINB28* and *MYCN*), and the PDX and orthotopic PDX models (71). Nevertheless, these models used to study the metastatic process do not fully replicate all the necessary steps of metastasis, except for the orthotopic PDX models. Therefore, an *in vivo* model that recapitulates all the steps of the process is necessary to fulfill our knowledge of NB metastasis.

We aimed to develop a NB spontaneous metastasis *in vivo* model that recapitulates all the steps that a single pro-metastatic cell undergoes to reach the organ of metastasis. Additionally, we used a multi-omics approach to investigate the molecular mechanisms behind NB progression and metastasis. By combining genetic and epigenetic analyses, we profiled NB primary tumors and metastasis, identifying some altered signaling pathways, like inflammatory response, and specific targets, including *PDPN*, that were relevant for NB development. We also described the role of PDPN in promoting the migratory and invasive properties of NB tumor cells, enabling the escape of the primary tumor and the colonization of distant organs. Furthermore, we sought to understand the potential interaction between NB cells and the most common stromal cells, CAFs, in the TME through PDPN. Additionally, we investigated PDPN's potential role in NB exosomes, which may regulate the PMN by inducing pro-tumoral polarization of host cells.

1. Identifying NB metastatic signature using a novel *in vivo* model

As previously described, various *in vivo* models have been used to investigate the metastatic process in NB. However, it is important to note that most of these models fail to recapitulate all the steps of the metastasis process. Furthermore, NB cells are usually inoculated directly into the bloodstream via intracardiac or intra-venous injections, or into the liver or femur, bypassing initial steps or the metastatic process (83). Consequently, this often leads to high rates of metastatic masses in the animal lungs, which is not frequently observed in patients (85).

We generated a spontaneous metastatic *in vivo* model that recapitulate all the steps of the process, including the resection of the primary tumor in the mouse, simulating the clinical management of NB patients. Moreover, by performing surgical resection of the primary tumor, we were able to assess whether NB cells possessed the ability to undergo the necessary cellular changes to disseminate and initiate the metastatic process. This model takes advantage of the location of the primary tumor that allows for an easy resection of the tumor compared with orthotopic models. Additionally, resection of the primary tumor results in longer survival of the animals, allowing NB cells to settle in secondary organs. Notably, the injection of different NB PDX-derived cells into the gastrocnemius muscle of mice led to a high

incidence of primary tumors. However, it is important to note that the microenvironments of orthotopic injections and our models are different, which could influence the establishment, progression and dissemination pattern of NB cells. Our spontaneous metastasis *in vivo* model provides insights into the mechanisms of primary NB tumors before treatment, but it cannot provide information about the behavior of relapsed tumors after therapy.

Furthermore, numerous studies have emphasized the relevance of the immune system in tumor establishment and progression, including NB tumors (89, 91). Consequently, as an initial approach to generate our *in vivo* model, two mouse strains with different immunocompromised levels were used. Firstly, we showed that selection of mouse strain is essential to spontaneous metastasis model generation in NB, since only the inoculation of NB cells in the gastrocnemius muscle of Athymic Fox $^{nu/nu}$ mice resulted in a high percentage of engraftment. Indeed, both strains were inoculated simultaneously, and mice sacrificed after a period of four months. It is conceivable that the BALB/ c$^{OlaHsd\text{-}Foxn1nu}$ strain needed additional time to develop a primary tumor. Additional experiments are required to elucidate the significance of time in relation to tumor engraftment across different strains.

Additionally, it is noteworthy that the depletion of diverse immune cells between strains could account for the different tumor engraftment results. Contrary to expected, the strain with a more robust immune system, showed the highest engraftment rates. The BALB/ c$^{OlaHsd\text{-}Foxn1nu}$ strain, holds a deficiency of T cells and B cells along with a higher concentration of innate NK cells. In contrast, athymic Fox$^{nu/nu}$ holds a depletion of T cells only, suggesting that the presence or absence of specific immune cells may contribute to NB establishment (176, 177). Considering that different stimuli can affect immune cells inducing pro-tumoral functions, it is also reasonable to speculate that NB cells may be promoting modifications in the phenotype of certain immune cells, such as B cells, NK cells or monocytes, in order to facilitate the formation and growth of tumor cells, as previously described for other tumors (178). It is essential to note the specific immune populations that are diminished in the BALB/ c$^{OlaHsd\text{-}Foxn1nu}$ strain. These observations suggest that NB exploits these immune populations to establish itself. However, it is important to recognize that immunocompromised strains do not exhibit a complete immune response, hindering our ability to comprehensively investigate immune interactions within NB tumors and thus limiting our ability to fully understand these interactions.

Furthermore, the recently described immune atlas of NB by Verhoeven *et al.* the relevance of specific immune cells was highlighted. They identified the NK cells as being more prevalent in LR-NB patients, a favorable prognosis marker which aligns with previous studies that emphasized the relevance of these cells to trigger cytotoxic responses (179, 180). In brief, the

Bassiri's group observed that the absence or the low levels of major histocompatibility complex class I (MHC-I), as observed in NB tumors, promotes the cytotoxic response of NK cells (180). Conversely, recognition of MHC-I through killer cell immunoglobin-like receptor unleashes an inhibition response of this cell type. In NB tumors, the role of NK cells was validated by using NOD/scid mouse strain, which has an impaired function of NK cells. They observed that inoculation of activated NK cells increased the survival time, determining the relevance of this population in NB and its potential use as adjuvant immunotherapy (181). Considering the role of NK cells, their contribution to the lack of tumor development in BALB/c$^{OlaHsd\text{-}Foxn1nu}$ strain could be significant, since this strain has a higher percentage of innate NK cells. Therefore, our *in vivo* model may elicit an anti-tumoral or pro-tumoral response depending on the immune cell population comprising the tumor immune microenvironment (TIME), which is influenced by the distinct immune cell components of each mouse strain. Our results suggest that immune cell populations may be responsible for the absence of tumor growth in BALB/ c$^{OlaHsd\text{-}Foxn1nu}$ mice, or for the promotion of tumor growth in a less immunocompromised mouse strain. Additional analyses are necessary to determine the interactions between TIME, and NB cells, that could be playing an important role in NB engraftment.

Based on our results, the Athymic Fox$^{nu/nu}$ strain was selected to generate the NB spontaneous metastasis model. Despite the direct proportionality observed between the number of inoculated cells and local relapses, we selected an intermediate concentration for further experiments.

The most common sites of metastasis in NB are BM, bone and lymph nodes. In the literature, orthotopic NB *in vivo* models have been reported to spontaneously metastasize to clinically relevant sites including lymph nodes, bone, BM and liver (70, 183). However, the complexity of the technique hinders the use of this model. Another difficulty with NB models is recapitulating the osseous dissemination, thus, systemic injections to the tail vein are widely used to overcome this problem. However, the dissemination pattern of these models do not reproduce the clinical pattern of NB. In our models, the metastasis were found in the peritoneal area or near the spine and micro-metastasis detected in BM, bone and liver, mirroring the clinical spread observed in NB patients. Accordingly, tumor masses in the retroperitoneal area are frequently observed in NB patients (184). Nevertheless, additional experiments should be performed inoculating NB-PDXs with different biological features, like *MYCN* non-amplified cells, to determine whether the spontaneous metastasis *in vivo* model can be used as a generalized model for NB metastasis. Additionally, studying primary tumor engraftment of LR-NB, would teach how to determine the potential aggressiveness of the tumor, and its potential capacity of dissemination. In brief, direct implantation of patient's tumor into the flank of mice is conducted to determine tumor aggressiveness (185, 186). If the implanted tumor

successfully engrafts, it is associated with a high-risk tumor, whereas the absence of tumor engraftment is associated with a low-risk tumor. However, our findings suggest that TME interactions are crucial for NB engraftment in our model. Therefore, it is important to consider that the subcutaneous microenvironment may be playing a role in tumor engraftment, as it has already been described to facilitate tumor vascularization, which could lead to false high-risk tumor classifications (187). Conversely, subcutaneous tumors exhibit a higher infiltration rate of immune cells, which can result in early inhibition of some tumors, as we observed in BALB/ $c^{OlaHsd\text{-}Foxn1nu}$ mice (187). Additionally, it has been shown that the inoculation site of the tumor can determine its pattern of dissemination (187). Consequently, attempting to establish our spontaneous *in vivo* model with other NB tumors with distinct biological features could potentially lead to the development of a new *in vivo* model that provides information about patient outcomes as well as the organs that may be affected by metastasis.

The analysis of metastasis showed consistent pattern across the various *in vivo* models, indicating that NB may exhibit a uniform behavior of dissemination in our spontaneous metastasis model. Additionally, the spontaneous metastasis *in vivo* model generated using Ewing sarcoma cells by our collaborators, did not display the same metastatic pattern, suggesting that this behavior might be specific for NB (***data not shown***). Thus, generated spontaneous metastasis *in vivo* model could be reproducing all the steps of the disease progression. In addition, distinct micro-metastasis patterns were observed among the generated *in vivo* models. These patterns are consistent with the invasion profile documented in the clinical history of the patient (HSJD-NB-005), enhancing the robustness of our models. However, to determine if our *in vivo* model accurately reproduce different patient patterns, new *in vivo* models with different biological features must be generated in the future.

Furthermore, we demonstrated that long time survival mice presented higher metastatic ratios, even when complete resection of the primary tumor was performed, suggesting that NB cells were already migrating and invading distant organs before surgical intervention. Knowing the precise time of metastasis initiation is difficult without tagging tumor cells. Future research using luciferase-labeled cells to track metastasis initiation and studying organ-specific preferences could provide critical insights into the metastatic behavior of NB, helping to determine whether metastasis occurs as a sequential process targeting specific distant organs or as a random dissemination process.

As previously described in the literature, only a small percentage of tumor cells will acquire the necessary characteristics to metastasize (57). Identifying the main genetic and epigenetic features of these cells, will help the understanding of their potential for preferential dissemination. Furthermore, although we anticipated a distinct expression pattern among cells

invading the peritoneal zone, the BM and the brain, we also expected a common metastatic signature compared to non-metastatic cells Initially, we conducted transcriptomic analysis of our samples, including primary tumor and metastasis from our *in vivo* model, HSJD-NB-005-A and -B, and primary cell cultures from each model. As expected, only a small number of DEGs were identified when comparing the two tissue samples, a total of 203. Although both samples had been individually identified, it is important to consider that cells comprising the metastasis originated from small cellular population within the primary tumor. Moreover, it should be noted that the number of DEGs found could vary depending on the origin of each sample, due to the inherent tumor heterogeneity of NB. Unexpectedly, significant differences were observed between the two models when they were analyzed individually. These results suggest that the inoculated cells were differentiated since they were established from different biopsies, even though they were originated from the same patient. Since therapy alters the genetic signature of tumor cells it should be noted that the HSJD-NB-005-B model was obtained from a relapse biopsy sample after therapy, with a higher number of DEGs compared to the HSJD-NB-005-A model, which originated from the diagnostic biopsy of the patient. Furthermore, studies in different pathologies have demonstrated that the microenvironment surrounding tumor cells has an impact in gene expression (188). As anticipated, our findings indicated that the gene expression patterns of cultured cells differed from those of the primary tumors and metastases generated in our *in vivo* model. This occurred, despite using the same cell culture passage to inoculation, suggesting that all differences across samples are due to cellular adaptation and interaction with microenvironment.

Although it has been shown that culturing tumor cells can preserve most of their original features, we use plastic plates which limit the potential interactions with other cells. Moreover, we provide them with an optimal environment to grow without requiring functions such as migration or evasion of the immune system pressure. Additional analyses are necessary to gain a deeper understanding of the key differences between cell culture and tissue samples. This understanding will help to exclude cell culture samples in certain types of analysis conducted to investigate complex processes like interactions with the immune system.

More importantly, different gene expression profiles were observed when comparing primary tumors with metastatic masses, excluding cell lines. This was confirmed by the signaling pathways identified in metastases and tumors. Metastasis were associated with inflammatory response, cytokine signaling and pathways related to the immune system whereas primary tumors were linked to myogenesis. These findings indicate that metastatic NB cells interact intensely with the tumor immune microenvironment, potentially contributing to the formation of the metastatic niche, in line with recent advances, highlighting their pivotal role as a newly recognized hallmark of cancer (11). On the other hand, enrichment of pathways such as

myogenesis, could be attributed to the tissue of origin of our primary tumors, established in the gastrocnemius of mice.

Review of the literature of our most DEGs, including *PDPN*, *GRIK3* and *RUNX1* in the metastasis were relate with lymphatic invasion and immune system interaction (167-169). This observation suggested that the invasion mechanism might involve the lymphatic system.

The epigenetic signature of metastasis by miRNA and methylation patterns showed differential expression patterns when comparing cultured cells to tissue samples. These differences can be attributed to the new TME interactions following inoculation. When the expression of differentially expressed miRNAs was examined, results were consistent with those of the Clariom-D array, indicating their role in metastasis. As miRNA are small non-coding RNAs, its expression levels might be heterogenous across the different sample extractions, resulting in different patterns of expression in our *in vivo* models (66). Notably, results obtained from the same tumor mass exhibited different expression pattern, which highlighted not only the heterogeneity of miRNA, but also, the heterogeneity of NB tumor, as previous studies had already reported (189). Literature search revealed that many of the up-regulated miRNAs including miR-629, miR-1246 or miR-6780 in the metastasis were involved in metastatic processes through conventional and lymphatic pathways (170, 190, 191). For instance, miR-629 has been shown to regulate metastasis and proliferation of prostate cancer cells by targeting multiple pathways (190, 192). Additionally, miR-1246 has been extensively studied in various adult tumor types, particularly in its role of promoting aggressive tumoral behavior (193). Furthermore, it has been demonstrated that miR-1246 is secreted in NB derived EVs, where it plays a crucial role in promoting the formation of the PMN by targeting macrophages in different tissues, including lung and liver (21). In accordance with the transcriptomic analysis, most of the up-regulated miRNAs in the primary tumors were initially associated with muscle-related functions like miR-378 and miR-133, suggesting a potential contamination of the analyzed samples originating in the gastrocnemius.

In light of both transcriptomic and miRNA analyses highlighting the potential role of TME in NB progression, we aimed to investigate whether there were any differences in mouse miRNA expression patterns between primary tumor and metastasis in our *in vivo* model. Given that our model is comprised by human NB cells and mouse stromal and immune cells, we hypothesized that different signaling pathways may be activated in each tumor type, with stromal and immune cells promoting tumor engraftment in the primary tumor. Since the miRNA 4.0 array can detect both human and mouse miRNAs, we conducted the analysis to identify differences in mouse cells infiltrating and surrounding NB, in the distinct tumor masses.

The analysis of mouse miRNAs revealed that the immune system of the mouse was more active in the primary tumors compared to metastasis. The down-regulated miRNA in the metastasis were involved in B cell activation, regulation of innate immune response, and response to cytokines, suggesting that these pathways were relatively more active in the primary tumors. These findings support our hypothesis that immune system interactions are pivotal in NB tumor development and progression, as previously observed in our initial *in vivo* experiments. In addition, we observed the positive regulation of fibroblast signaling, suggesting that cells comprising the stroma may also play a role. In contrast, positively altered pathways were mostly related to cell differentiation and myoblast cell biology, the precursors of muscle cells. To understand why myoblast pathways were increased in the metastasis and not in the primary tumors, we researched the role of miRNAs in these pathways. Among these miRNAs were *mmu-miR-133a* and *mmu-miR-133b*, which, like their human homologues, are principally involved in muscle biogenesis. However, they also play a role in apoptosis and cell proliferation of mouse endocrine cells (194). Despite the limited number of studies of mouse miRNAs, their roles are often associated with their human counterparts. Analysis of the most altered pathways related to their potential target genes was consistent with our previous findings, revealing the presence of EMT, angiogenesis and TFG-β pathways in the targets that were decreased in the metastasis, therefore, increased in the primary tumors. As we are analyzing mouse miRNAs, we anticipated that the surrounding cells of the primary tumors are being modified in order to promote tumor engraftment and metastasis, explaining angiogenesis and TGF-β among the most altered pathways. However, further analysis of the potential regulated targets will provide insight into the actual role of TME interactions, because it is necessary to consider that not all the targets analyzed may play a role in our model. Remarkably, despite the immunocompromised landscape of the mouse model, our findings are in line with previous publications which identified different miRNAs targeting immune system genes in order to facilitate NB tumorigenesis and metastasis (195).

Changes in DNA methylation are related to alterations in tumor cells that confer resistance to therapy. Furthermore, changes in DNA methylation have also been induced by chemotherapy, resulting in altered responses to treatment. Consequently, many studies have examined differences in methylation patterns before and after treatment (196). Additionally, other research efforts have focused on comparing DNA methylation patterns among different tumors, uncovering distinct methylated patterns associated to patient prognosis (197). Therefore, we analyzed the methylation status of our *in vivo* model samples, including cultured cells and tissue samples, to study whether DNA methylation changes contribute to NB metastasis. Surprisingly, methylome analysis results did not reveal significant differences in DMPs, when comparing primary tumors with metastasis. Nevertheless, enrichment analysis

of the DMR within the metastasis revealed genes associated with cytokine signaling pathways, such as *TIAM1* and *IL17RA*, aligning with our prior analyses. However, a more exhaustive analysis of the potential involvement of those genes within the DMR is necessary to gain a deeper understanding of the potential role in the metastatic process. A more comprehensive analysis of the DNA methylation is also necessary to determine whether non-coding genes in the altered regions could be involved in NB metastasis.

Since our study pointed towards the inflammatory response and cytokine pathways as crucial for NB progression, we thought that the TME would be playing a significant role in NB metastasis. Our initial observations where the most immunocompetent strain was the only to allow for a primary tumor to develop in the gastrocnemius also highlighted te relevance of the TME. Furthermore, recent evidence suggests the importance of the TME involvement in NB progression, including stroma and immune cells (179, 200). Among the different interactions, the cooperation of CAFs and macrophages seemed to play a crucial role in disease progression (201, 202). Therefore, this putative role of different cell types should be investigated further to shed some light into NB metastatic process.

To study complex biological processes comprehensively, it is essential to take an integrative approach that combines multi-level data to highlight the interrelationships among the biomolecules involved and their functions. Thus, our multi-omics data integration exhibited common targets, including *PDPN*, *RUNX1* and *GRIK3,* which had been previously associated with conventional and lymphatic dissemination (167-169). Our findings support the hypothesis by which NB can spread via conventional and lymphatic circulation. Although *GRIK3* is not extensively studied in tumors, its expression levels are increased in lymph node metastases of gastric cancer (168). Moreover, increased density of lymph vessels is linked to elevated *PDPN* levels in NB (135). Among the genes differentially expressed, *RUNX1* has been the most thoroughly investigated, and its higher expression associated with increased lymph node metastasis in non-small cell lung cancer (203). Despite no functional assay has been conducted to demonstrate the involvement of these genes to disseminate through the lymphatic system, its high rate of lymph node metastasis and lymphatic vessels density suggest this association. In addition, lymph node infiltration is frequently found in patients with disseminated disease which suggests that NB may be using this pathway quite frequently but not exclusively. Further research is needed to confirm whether NB cells are capable to disseminate via the lymphatic system.

To thoroughly investigate the complex biological processes involved in NB metastasis, pathway enrichment analysis highlighted the TGF-β signaling pathway Once again, the results suggested the interaction with TME through inflammation response and cytokines were

involved in the metastatic process in NB, in accordance with recent articles showing the implication of immune cells in tumorigenesis (204). Additionally, numerous studies are currently providing evidence of the crucial role of different cytokines modulating tumor cells and enabling their metastatic capacity. Considering the low sensitivity of the different techniques to measure cytokine expression, our study revealed distinct cytokine patterns in primary tumors with different metastatic capacities. These cytokines are indeed secreted by cells of the surrounding environment, such as CAFs and TAMs, among other cells including immune cells (205-207). Notably, analyses of mRNA expression revealed an inverse correlation between human and mouse probes. A decreased level of hTGF-β_1 in the metastasis, compared to the primary tumor, indicates that NB cells are expressing, and potentially secreting, this cytokine to interact with the TME of the primary tumor mass. This interaction enables NB cells to induce a pro-tumoral microenvironment, likely through immune modulation, as previously described by Castriconi *et al.* (208). Different roles are attributed to TGF-β_1, including both pro-tumoral functions such as promoting angiogenesis and EMT, as well as tumor suppressive (209). The increased levels of mTGF-β_1 in the metastatic masses may be linked to these roles. However, given that the appearance of the metastasis, it is plausible to suggest that the increase of this cytokine could be contributing to tumor progression. Additionally, a significant decrease in the expression of CAFs and macrophage genes was observed in the metastasis, suggesting that mouse immune cells are likely the ones secreting the mTGF-β_1 in the metastasis. Further analyses of the different populations surrounding or infiltrating the NB tumor masses including metastasis are necessary to comprehend the different roles of TGF-β_1, and to enhance our understanding of TME interactions.

Spatial transcriptomics allows for determining the genetic signature at specific locations within tissues using either FFPE, or frozen, samples. This technology does not permit yet a single-cell resolution, but it can be applied if single-cell transcriptomics is performed instead of next generation sequencing. Furthermore, the spatial transcriptomic technology works with a pre-determined gene probe library, differentiating between human and mouse genes, but not both at the same time, limiting the analysis when studying TME interactions in tumors generated in mouse models. Our spatial transcriptomic analysis revealed a specific distribution of the different stromal and immune cell populations in both primary tumors and metastasis. Notably, the genetic signature of CAFs and TAMs was most significant surrounding NB cells. Our findings are in accordance with previous publications in other tumor types as well as in NB (91).

Recently, a publication from DeClerk's group highlighted the significance of TME interaction in NB, specifically involving TGF-β_1, TNF-α and IFN-γ, suggesting that a slight increase in expression was associated with NB progression (204). Our spatial transcriptomic analysis revealed the lack of expression of these cytokines in the metastasis. Although no significant differences were observed for TNF-α and IFN-γ when comparing primary tumor and metastasis, different expression levels were clear among primary tumors. These differences may be attributed to the inherent heterogeneity of NB, as previously mentioned, or the stage of tumor progression at the time of biopsy acquisition.

Furthermore, the analyses of the NB cells phenotype in the spatial transcriptomics revealed a specific distribution of NOR and MSN phenotypes. Also, a notable reduction in the number of clusters identified as MSN was found in the primary tumors. Additionally, MSN clusters were mostly located near stromal cell clusters including CAFs and TAMs, suggesting a potential interaction between those cell types. Several studies have demonstrated that the NB MSN phenotype correlates with increased metastatic potential, with transition triggered by cytokines (76). Our findings suggest that CAFs and TAMs may interact with NB cells and induce phenotypic transition. Moreover, we observed that MSN phenotype cells tend to localize at the periphery of the tumor, suggesting that this phenotype could be potentially comprising the invasive front.

2. The potential role of PDPN in NB progression

Given that nearly 60% of NB patients present with disseminated disease, and metastasis is the primary cause of cancer-related death, it is essential to identify novel NB metastatic drivers to target. These biomarkers serve as indicators of disease progression, treatment response, and overall patient prognosis. Moreover, the discovery of novel biomarkers can lead to the development of more effective and targeted therapies tailored to individual patients. Throughout our multi-omics study, we selected different targets of interest to validate their putative role in NB metastasis. Of those genes, we paid special attention to *PDPN*, since it has been described as involved in different processes of tumorigenesis promoting tumor cell motility *in vitro* and tumor *(136, 210)*. Even though PDPN has been reported to play a role in the progression of various types of tumors, only two studies discuss its role in NB (134, 135). Both publications described PDPN as a marker for lymphatic endothelial cells (LECs). In the first case, they established an association between the expression of PDPN and the lymphatic density in NB. In addition, higher lymphatic density correlated with adverse clinico-pathological factors and survival. These studies focused on the expression of PDPN in LECs, and did not mention NB cells expressing PDPN. Our results show high mRNA expression of *PDPN* in primary tumors that developed metastasis in our models, suggesting the implication of *PDPN*

in NB metastasis. However, we could not be 100% sure whether this expression belongs to human NB or to mouse stromal cells. Given that our probe and antibody were selected for their specificity in recognizing human tissues, we included mouse samples that had never been inoculated with human cells, to validate their specificity. Notably, neither of the reagents tested positive for these control samples. Consequently, we now can confirm that the expression of PDPN , was indeed of human origin.

As opposed to prior studies of PDPN in NB, our IHC analysis revealed positive PDPN staining in NB cells, previously reported in other tumor cells (211, 212). More importantly, our results revealed an unexpected finding, as we observed different PDPN expression patterns in primary tumors and metastasis. As a transmembrane protein, PDPN is located in the cell membrane, as detected in the primary tumors of our *in vivo* models and patient tissues. Surprisingly, a diffuse cytoplasmatic stanning was observed in the metastasis, which suggested a different role for PDPN. We could not find any description of intracellular expression of PDPN in the literature, except for mRNA expression in the mitochondria (213). Aiming at determining the specificity of PDPN labeling to NB cells, LYVE-1 and CD31 were used as specific markers for LECs and endothelial cells in consecutive sections. No overlapping labeling was observed, confirming the expression of PDPN in NB cells. Similar results were observed in patient samples, with additional positive vasculature labeling comparable to the staining described in NB (134, 135).

Consequently, we aimed to determine whether there was an association between the cellular expression pattern of PDPN and the development of macro-metastasis in our *in vivo* model. Notably, when comparing PDPN cellular localization between animals that developed macro-metastasis and those that did not, we observed a different pattern. Cellular membrane of PDPN was absent in non-metastatic animals, suggesting that membrane localization of PDPN in NB cells may enhance the metastatic process. Our observations align with previous studies that described cell membrane expression of PDPN at the invasive front of different adult tumors (134, 214). Additionally, one of the key benefits of generating a mouse model is the size of the tumor masses, which enables to display an entire section of the tumor on one slide. This is not possible with patient samples, which can limit our study. Through confocal microscopy, we observed different patterns of PDPN expression in primary tumors and metastatic masses. However, when using an optical microscope, it was revealed that the cellular membrane localization of PDPN was unique to the primary tumors, and that this expression pattern was found at the edges of the tumor. In contrast, the cytoplasmic staining was more easily visible inside the tumor mass, both in primary tumors and metastatic masses.

Interestingly, patients with tumors exhibiting a cellular membrane expression of PDPN had a higher incidence of lymph node infiltration, supporting our hypothesis of NB metastasizing via the lymphatic system, and aligning with previous studies (134, 135). However, several studies described the contribution of $PDPN^+$-stroma cells, mainly CAFs, at enhancing the lymphangiogenesis and promoting tumor metastasis, like in breast cancer (136, 215). Therefore, further studies are necessary to determine whether $PDPN^+$-NB cells or $PDPN^+$-stroma cells are contributing to lymph node dissemination. This investigation is crucial for understanding the potential migration of NB through the lymphatic system.

Our previous approach showed PDPN overexpression at the metastasis, however, it lacked information about the spatiotemporal dynamics of PDPN which could be critical for effective interventions. Thus, we studied PDPN expression levels at different times during disease progression. Remarkably, we observed an increase of PDPN expression throughout the disease progression. This suggests a relationship of tumor aggressiveness and PDPN expression. Additionally, the persistent overexpression over time could be partially attributed to the ability of NB cells expressing PDPN to migrate prior to tumor resection. In other words, PDPN expression in the invasive front, may provide an advantage to certain cells that manage to escape the primary tumor before surgical resection. A change in PDPN cellular localization is expected once the tumor cells settle at the secondary sites, as previously observed in the *in vivo* model.

Alternatively, the expression of PDPN at the cellular membrane could be induced by drugs, since aggressive treatments can lead to modifications in the microenvironment, and the tumor cells, that could potentially trigger PDPN induction, thereby enabling tumor cells to spread and survive as they no longer feel comfortable within the tissue. Studies have demonstrated how cancer therapies can lead to the selection of subclones that may potentially give rise to more aggressive tumors (216, 217). Notably, the intensity of PDPN ranges from low to high levels when assessing chemoradiotherapy-sensitive or resistant ovarian cancer cells. Furthermore, this study showed that, in resistant tissues, the intensity of PDPN increases following treatment, suggesting that certain therapies may induce the expression of this protein (213). Remarkably, PDPN continues to mark the cellular membrane in this context, which may suggest a more aggressive tumor phenotype. To determine whether PDPN expression is being induced by the therapies applied in NB patients, we increased the number of patients adding new samples. We observed heterogenous expression post-treatment, from absence of expression to cytoplasmatic or membrane localizations. This suggests that the way PDPN expression is induced may depend on different variables, such as the location of the primary tumor and the type of treatment received. Unfortunately, we cannot extract conclusions due to the limited number of samples analyzed.

Considering all our findings, we would suggest that PDPN has a role in promoting metastasis in NB. Consequently, we explored PDPN levels in NB cell lines. Surprisingly, the levels of PDPN were undetectable at both the mRNA and protein levels in all our NB cell lines. However, positive mRNA expression was observed in the PDX extracts, suggesting the possibility of PDPN loss in NB cell lines due to the absence of stimuli. Our hypothesis was subsequently validated through primary cell cultures derived from our *in vivo* model and cultured PDXs, which exhibited decreased PDPN expression with successive passages. Since primary cell cultures initially consisted of mixed populations, it is possible that the loss of expression in certain cells over passages may be related to PDPN induction, as previously described. Notably, the first primary cell culture passage, considered as pure, derived from our in vivo model still expressed PDPN, albeit at low levels. Further analyses are required to determine the loss or absence of PDPN at the protein level during cell culturing.

Due to undetectable endogenous expression levels of PDPN in wildtype NB cells, we subsequently generated a stable cell line that overexpressed PDPN. As expected, an increase of PDPN expression in the cellular membrane was observed by IF, more prominently in SH-SY5Y cell lines, where PDPN signal overlapped with WGA, suggesting a membrane location of PDPN. Notably, the controls of both cell lines showed intracellular expression of PDPN, which appeared to be inside the nucleus, as in parental cell lines. However, it should be mentioned that NB cell lines have autofluorescence that is observed in the green channel, and our cells were infected with a plasmid containing GFP which also appears in green. Nevertheless, the initial approaches to determine PDPN expression involved conjugating PDPN to red fluorophore, and the same pattern was observed. Subsequently, the color of the fluorophore was changed to green to investigate PDPN location using WGA that had already been conjugated with a red fluorophore. Additionally, GFP expression was lost in both cell lines during cell culture passages.

Importantly, we did not observe alterations in the expression levels or the location of the endogenous PDPN in parental cell lines. Endogenous PDPN was assessed by IF without WGA to avoid interferences with the GFP signal and autofluorescence of NB cells, which exhibited an overlap of DAPI location, but no of the channels. Of note, the NB cells were transfected with the functional isoform, isoform 2, which is expressed in the cellular membrane (218). Therefore, no alterations on the endogenous levels of PDPN after transfections suggests that endogenous PDPN could be another isoform, that can be detected with our antibody. To determine whether the endogenous PDPN is another isoform, additional analysis may be necessary.

It is worth noting that ^{High}PDPN cell lines exhibited PDPN in the cellular membrane, like the primary tumor samples from our *in vivo* model. This suggests that NB cells may upregulate PDPN expression and promote its location in the cellular membrane, potentially contributing to cellular spread. A study published in 2013 demonstrated that esophageal cancer cells expressing PDPN in their membrane are found at the invasive front of the tumors, which aligns with our observations (214). In patient samples, we observed that cells with PDPN in their membrane were not only at the edges but also close to the vasculature. Moreover, our functional analyses revealed an increase in the metastatic capacities for both migration and invasion in ^{High}PDPN cell lines. These results align with those of numerous studies that demonstrated the correlation between elevated PDPN levels and more aggressive tumors, leading to worse patient outcome (219, 220). Understanding whether this condition is the underlying cause of NB cells initiating metastasis could help prevent this process in patients or even to discern whether it had already begun, despite the absence of any evident clinical signs. Undoubtedly, additional *in vivo* experiments inoculating our stable cell lines are necessary to assess whether the membrane expression of PDPN might provide an advantage in initiating metastasis. Furthermore, it would be beneficial to inhibit its expression in the ^{High}PDPN cell line to determine whether the loss of membrane expression levels affects the metastatic capacities in these cells.

Most research on the cellular capacities of tumor cells has been conducted in adult tumors with an epithelial phenotype and the ability to transition into MSN phenotype (221). As previously described by *Pastushenko and Blanpain*, cellular capacities varied between epithelial and MSN phenotypes in adult tumors, leading to a natural balance between them (59). Researchers identified certain abilities that were unique to each phenotype. For instance, the epithelial phenotype demonstrates enhanced abilities typically associated with the early stages of tumorigenesis, such as proliferation. On the other hand, MSN phenotypes exhibit heightened metastatic capacities, including migration or invasion, which are essential to the progression of cancer. More importantly, they determine that transient stages of the cell could harbor different capacities simultaneously. NB tumors, however, are developmental tumors. NB cells have the ability to undergo NMT transition, which is similar to the EMT observed in epithelial cells. For instance, the cellular capacities of the NOR phenotype are similar to those of the epithelial phenotype, with increased abilities linked to tumor establishment, whereas MSN phenotype in both cell types is associated with increased metastatic capacities (59, 75). Notably, in a recent study, Yuan *et al.* described the different phenotypes that a neuroblastic tumor can achieve during tumor progression, relating those phenotypes to different cellular capacities similar to those found in adult tumors, including proliferation, invasion and migration (80). This study incorporated ADR and MSN tumor identities, as well as various transient

stages between them, which were associated with a more aggressive cellular phenotype in neuroblastic tumors, since these tumors can increase their migration capacity without losing their proliferative ability. In other words, neuroblastic tumor cells can simultaneously exhibit different capacities. In this context, our functional results indicate that the expression of PDPN may be inducing a transient phenotype in the NB cell lines. This could potentially explain why we did not observe any significant changes in proliferation with a significant decrease in colony formation ability between ^{High}PDPN and control cell lines.

Our spatial transcriptomic results provided PDPN expression and genetic signature of both NB phenotypes. We observed that NB cells expressing the MSN signature were located at the edges of the tumor tissue according to the spatial transcriptomic analysis, along with *PDPN* expression, as previously hypothesized. These findings suggest an association between *PDPN* and the MSN phenotype or possibly a transient phenotype. However, PDPN was also detected in the NB-NOR phenotype clusters, potentially indicating the initiation of the transition towards the NB-MSN phenotype. Further analysis using a technique with higher cellular resolution would be needed to validate our hypothesis, since the spatial transcriptomic analysis lacks single-cell resolution, we have been analyzing spots containing various cell types. In this line, it is crucial to consider that several spots expressing specific markers for CAFs and TAMs have been observed in NB-NOR clusters. Therefore, PDPN expression could also be present in these cell types or may be induced in NB cells by cellular interactions with them, as described in other tumor types (89) .

Our results indicate that the expression of PDPN in NB cell lines is likely to be initiated by interactions with the TME. This hypothesis is supported by previous *in vitro* experiments that showed the loss of PDPN expression during consecutive cell passages of primary cell cultures. Additionally, the idea of PDPN expression being triggered by TME interactions is also implied in the analysis of the tumors. Our spatial transcriptomic analysis revealed a higher PDPN expression in mix populations including ECS, CAFs, macrophages and NB-MSN phenotype. Nevertheless, some positive spots were observed in NB-NOR clusters, which do not present any other genetic signature. As previously, the examination of specific phenotype markers revealed no evident pattern of expression for either of the two phenotypes, NOR and MSN, when assessing the cell lines individually, LA-N-1 and SH-SY5Y. However, when analyzed simultaneously, a significant increase in MSN markers was observed in ^{High}PDPN cells compared to control. It is important to note that heterogeneous patterns were observed between replicates, probably because cells were harvested at different passages which could be affecting their differentiation states. Notably, both cell lines exhibited a significant increase in SNAI1, which has a crucial role in metastasis, particularly for epithelial tumors, although it has also been previously described in non-epithelial tumors, particularly NB (76). Over the

years, several studies demonstrated that higher levels of SNAI1 are linked to the induction of MSN phenotype and poor prognosis in adult tumors (222, 223). Considering its role, increased levels in ^{High}PDPN cells may be an indicative of NB cells transitioning into MSN phenotype, reinforcing our hypothesis of PDPN inducing a transient phenotype, which is associated with more aggressive tumors (80). Moreover, high levels of SNAI1 have also been demonstrated to play a role in tumor evasion and immune suppression, which is in accordance with our hypothesis of NB cells expressing PDPN in the invasive front to move towards bloodstream and secondary organs (222, 223). During this process, tumor evasion and immune suppression are crucial for NB cells to achieve its mission, thus the increase of both genes simultaneously may provide NB cells with the necessary advantage for success in the metastatic process. This presents an opportunity to examine whether the expression of both genes is interconnected in NB cells. It is important to note that both genes present a common signaling pathway, the TGF-β/Smad axis (223). In addition, it is important to note that no enzymatic domains have been described for PDPN, and thus, its induction must be through different ligand interactions, such as cytokines, which are the most altered pathways observed in our multi-omic analyses (224). Consequently, we aimed to investigate whether any of these populations were responsible for triggering PDPN expression in NB cells. To achieve this, we conducted conditioned medium (CM) experiments and co-culture assays to explore their interactions and effects on PDPN expression levels.

A previous study in oral squamous cell carcinoma described that normal fibroblasts polarize into CAFs leading to the induction of PDPN expression in tumor cells. We aimed to investigate the relevance of this loop in NB cells (225). Our findings demonstrated that ^{High}PDPN-CM increased FAP, indicating the polarization of normal fibroblast into CAFs. Moreover, co-culture experiments showed that close exposure of control cells and fibroblast prompted PDPN expression in NB cells and CAFs polarization. Based on these results, we propose that NB cells expressing PDPN on their cellular membranes secrete cytokines essential for fibroblast polarization. Furthermore, the physical proximity between both cell types induces PDPN expression and promotes CAFs polarization, suggesting that the TME plays a critical role in elevating PDPN levels, thereby facilitating tumor progression. Further analysis is necessary to ascertain the specific cytokines secreted by cells expressing PDPN on their membranes compared to those that do not. Additionally, these analyses will help understand and identify the cross-talk between fibroblast and PDPN induction in NB cells. In this context, the research study by Gao Y *et al* determined that the loop triggering PDPN expression was regulated by TGF-β, aligning with our previous findings from multi-omics analysis that highlighted the involvement of TGF- β in the metastatic process of NB (225). Additionally, Kunita *et al.* demonstrated that cells expressing PDPN (+PDPN) constitute the invasive front due to the

presence of cytokines such as TGF-β1, IFN-γ and TNF-α, which trigger the expression of PDPN (113). Our findings are consistent with theirs, as we observed the induction of PDPN expression following cytokine treatment, along with an enhanced migration capacity. Considering all our results, we hypothesize that CAFs are essential for metastasis initiation and that induction of PDPN expression in NB cells enhance their migration capacity. Additionally, this process is orchestrated by the secretion of TGF-β by both cell types. Furthermore, we observed increased levels of FAP in the primary tumor samples from our *in vivo* model compared to macro-metastasis, supporting our hypothesis regarding the role of CAFs as a metastasis promoter in NB.

Additionally, PDPN expression in our *in vivo* models exhibited different cellular location according to the spatial distribution of tumor cells within the tumor masses, particularly in the primary tumor samples. Specifically, cells located in the central part of the mass displayed intracellular expression of PDPN, whereas cellular membrane location of PDPN was observed at the tumor edges, corresponding to the invasive front. Based on this observation, we hypothesized that necrosis in the center of the tumor masses due to hypoxic conditions may induce PDPN expression in NB cells to facilitate their evasion from the hypoxic microenvironment. To explore this hypothesis, we exposed our stable cell lines to low oxygen conditions, expecting a shift in the cellular location of PDPN. Our data, after 24 hours of exposure, show an increase of PDPN in the cellular membrane of transfected NB cells, suggesting that hypoxia may be triggering the expression of PDPN. In addition, and surprisingly, after 72 hours of low oxygen levels, we observed a shift in the distribution of PDPN in the ^{High}PDPN cell line, with a uniform staining across the cellular membrane. To validate our findings, an IF using WGA must be conducted. To confirm the subcellular location of PDPN, protein cell fractionation was performed. A higher PDPN expression in the nucleus and chromatin fractions of wild-type cell lines was observed (***data not shown***). For ^{High}PDPN cell lines, we observed lower levels of PDPN expression in the nuclear fraction compared to control, with no expression in the cytoplasmic fraction, likely attributable to the loss of membrane protein during the extraction process. To date, there has been no prior description of PDPN in the nucleus, which may possess distinct functions compared to its expression on the cellular membrane, which seems to change based on TME stimuli. Notably, the absence of nuclear signals for PDPN in IF suggest that the nuclear signal had relocated to the cellular membrane, potentially implying the involvement of a distinct isoform in response to oxygen levels.

Numerous studies have been performed to investigate the hypoxic conditions in NB, leading to a genetic signature specific for hypoxia in NB (173). Several genes were established, and some were analyzed in our spatial transcriptomic analysis. To our surprise, increased levels

of various genes altered under hypoxic conditions were observed in NB cells, and in mixed population clusters at the edges of the tumor mass. These findings contradict our initial hypothesis, which supported that hypoxia is found mainly in the center of the tumor mass. The exact location of the analyzed sample within the entire resected tumor is a challenge which could potentially have introduced a bias in our study. Nevertheless, the expression of hypoxic genes was found to align with the same clusters that exhibited higher expression of PDPN, supporting our hypothesis that hypoxia trigger the expression of PDPN. Further analysis is required to determine the relationship between hypoxia and expression of PDPN in NB cells, as the spatial transcriptomic analysis lacks single-cell resolution. At this point we cannot conclude that the NB cells expressing PDPN are those expressing the hypoxic signature

The intricate nature of the metastatic process, involve the tumor cells and their interactions with their surrounding TME, with the different mediators of such interaction like EVs secreted by both tumor and non-tumoral cells (97, 98). (79, 80). EVs have emerged as key players in tumor progression, facilitating cell-to-cell communication and participating in the cross-talk within the TME. Furthermore, exosomes, a specific EVs, have been shown to play a key role in the formation of PMN, enabling tumor cells to colonize distant organs (97, 98). Therefore, we proposed that NB-derived exosomes might play a role in metastasis. Additionally, in 2018, PDPN was described as a component of EVs with an important role in tumor progression in melanoma (140).

Experiments isolating exosomes from our stable cell lines revealed a high expression of PDPN in ^{High}PDPN cell lines. Since the final step of exosome biogenesis involves the fusion of late endosomes with the plasma membrane, we hypothesized that the increased levels of PDPN in these cells might be related to its subcellular localization in the membrane (226). Based on our results, we envisioned cells expressing PDPN on their membranes, particularly those at the invasive front, utilizing the exosomes to modulate the PMN. This idea was reinforced when isolated exosomes from the plasma of our mouse model revealed PDPN only following tumor cell injection, demonstrating the secretion of PDPN by NB cells. The detection of PDPN in exosomes even before the formation of the primary tumor strengthens the potential role of PDPN in the formation of PMN, in accordance with previous studies showing the involvement of exosomes in this process (227).

Recent findings indicate that exosomes derived from ^{High}PDPN cells can stimulate the polarization of stroma cells within the TME, thereby promoting tumor progression (228). However, additional experiments are necessary to understand how these exosomes influence PMN cells, as previous studies have demonstrated the involvement of tumor exosomes in PMN modulation (21). Several studies have already demonstrated the tumor-derived

exosomes driving the PMN formation by regulating immune and stromal cells (229-231). Additionally, altered stromal cells contribute to tumor promotion by modulating the immune microenvironment in distant tissues (229).

In recent years, significant advancements have been made in the field of nanoparticles for the development of new therapeutic approaches. Research has demonstrated that exosomes can be potentially used as nanocarriers for delivering therapeutic agents and as potential targets for immunotherapy, avoiding direct targeting of tumor cells, thereby potentially reducing the risk of inducing mutations (232-234). The identification of +PDPN as a modulator of PMN suggests that inhibiting intracellular communication by targeting exosomes could prevent the formation of PMN, thus hindering the progression of NB.

In addition to potentially targeting NB tumors with exosomes, in 2022, Takemoto *et al.* generated a humanized anti-PDPN antibody (160). In their *in vivo* study, they demonstrated the efficacy by reducing tumor growth and metastasis. In light of the current state of knowledge, to determine the role of PDPN in the bloodstream could provide valuable insights in the understanding of the metastatic process. Since PDPN's physiological function is platelet aggregation, tumor cells may exploit this mechanism to evade immune response.

PDPN promotes intravascular arrest, which is one of the final stages of metastasis (235). Currently, we are exploring this *in vitro* by exposing our stable cell lines to platelets derived from healthy donors to determine whether the presence of PDPN facilitates platelet aggregation in NB cells. Preliminary results appear to support our hypothesis, suggesting that PDPN expression on the cellular membrane may persist until the secondary organ is reached. Therefore, conducting *in vivo* experiments targeting PDPN would be advantageous to determine its potential role in reducing NB metastasis. This approach would help determine whether NB cells not only express PDPN to enhance its migration capacity, but also to promote subsequent stages of the metastatic process in the bloodstream. In addition, if the involvement in intravascular arrest is validated, it would be worth to investigate whether intravenous inoculation of ^{High}PDPN cells avoids intravascular arrest when treated in parallel with the anti-PDPN antibody.

In summary, we performed a multi-omics approach to determine the metastatic signature of NB cells. We established for the first time a spontaneous metastasis mouse model for NB displaying a dissemination pattern similar to patients. By analyzing the genetic and epigenetic differences between primary tumors and metastasis, we identified pathways that NB cells could be exploiting for disease progression and genes and miRNAs involved in the metastatic process. Our results show the relevance of the immune system and the inflammatory response in the tumorigenesis and metastasis of NB, particularly through the involvement of cytokines.

Based on these results, we identified PDPN as a strong biomarker of NB metastasis. We show how PDPN provides of metastatic capacities to NB tumor cells. We describe the intracellular localization of PDPN for the first time, suggesting a different role in tumor cells depending on its cellular localization. In addition, our *in vitro* experiments suggest that interactions between fibroblast and NB cells trigger the polarization of CAFs, as well as PDPN expression. Moreover, we find that NB cells secrete PDPN through exosomes, which are potentially involved in PMN formation, particularly inducing CAFs polarization. More broadly, our results suggest PDPN as a therapeutic target for the treatment of HR-NB.

CONCLUSIONS

In this thesis, we provided further insight into the mechanisms underlying of NB metastasis. By multi-omics analyses we identified signaling cascades and targets enriched in metastases that could be modulating aggressiveness in NB. Notably, our findings highlight the identification of PDPN as a promising therapeutic target that can improve patient outcomes. The main conclusions related to this study are summarized as follows:

1. We have successfully established a NB spontaneous metastasis mouse model that accurately recapitulates all the steps of the metastatic process, displaying an infiltration pattern closely resembling that observed in NB patientS
2. Through transcriptomic analysis, we identify DEGs in metastatic masses associated with lymphatic dissemination across various tumors, highlighting *PDPN* as a potential metastatic marker in NB.
3. Epigenetic analysis revealed different miRNAs expression profile in the metastatic masses compared to primary tumors, whereas methylation status remained unaltered. Additionally, analysis of mouse miRNAs highlighted the involvement of stromal cells in NB progression.
4. Analysis of the most significantly altered pathways in the multi-omics data enhanced the crucial role of cytokines and inflammatory response in NB metastasis. Further supported by data integration of transcriptomic and miRNA array.
5. By multi-omics analysis, we observed a slight elevation in cytokines levels within the primary tumor that might be fostering NB progression.
6. The spatial transcriptomic analysis of patient samples outlined different TME composition between primary tumors and metastatic masses. Additionally, it highlighted the interactions between stromal cells and NB-MSN phenotype, which is associated with heightened metastatic capacities.
7. For the first time, we demonstrated different cellular locations of PDPN in NB cells, including membrane location observed in primary tumor samples and cytoplasmic location found in both primary tumors and metastatic samples. Analysis of PDPN expression in our cohort of debut NB patients demonstrated an association between membrane location of PDPN and lymph node infiltration rate. Additionally, PDPN expression may be induced during treatment administration to NB patients.
8. By generating stable cell lines overexpressing PDPN, we demonstrated its functional role enhancing metastatic capacities, such as migration and invasion *in vitro*. Conversely, we observed a decreased in cellular capacities associated to early stages of tumorigenesis, such as proliferation and colony formation.

9. Increased levels of PDPN could be inducing a transition NB phenotype from NOR to MSN phenotype, which is characterized by a more aggressive tumor behavior.
10. PDPN is induced by TME, including cytokines treatment with TNF-α, TGF-β_1 and IFN-γ, low oxygen exposure and direct interaction with fibroblast cell line (HFF-1).
11. PDPN overexpression in NB cells led to higher levels of FAP in fibroblast cell lines through both direct (co-culture) and indirect (conditioned medium) interactions, implying a role in the polarization of CAFs. CAFs might be facilitating NB progression by direct induction of PDPN expression in NB cells.
12. The PDPN protein is secreted by exosomes in ^{High}PDPN cell lines, exhibiting a membrane location, and inducing an increase of FAP protein in fibroblast and hMSC cells, suggesting a potential role in PMN formation.
13. We detect exosomes with elevated levels of PDPN in serum samples from our *in vivo* model, after tumor cell inoculation exclusively.

Bibliography

1. Yin W, Wang J, Jiang L, James Kang Y. Cancer and stem cells. Exp Biol Med (Maywood). 2021;246(16):1791-801.
2. Kattner P, Strobel H, Khoshnevis N, Grunert M, Bartholomae S, Pruss M, et al. Compare and contrast: pediatric cancer versus adult malignancies. Cancer Metastasis Rev. 2019;38(4):673-82.
3. Fearon ER, Vogelstein B. A genetic model for colorectal tumorigenesis. Cell. 1990;61(5):759-67.
4. Imyanitov EN, Kuligina ES, Sokolenko AP, Suspitsin EN, Yanus GA, Iyevleva AG, et al. Hereditary cancer syndromes. World J Clin Oncol. 2023;14(2):40-68.
5. Mora J. What is a pediatric tumor? Clinical Oncology in Adolescents and Young Adults. 2012.
6. Organization WH. CureAll framework: WHO global initiative for childhood cancer: increasing access, advancing quality, saving lives.; 2021.
7. Baliga S, Yock TI. Pediatric Cancer. Hematol Oncol Clin North Am. 2020;34(1):143-59.
8. Matthay KK, Maris JM, Schleiermacher G, Nakagawara A, Mackall CL, Diller L, et al. Neuroblastoma. Nat Rev Dis Primers. 2016;2:16078.
9. Zhang L, Nesvick CL, Day CA, Choi J, Lu VM, Peterson T, et al. STAT3 is a biologically relevant therapeutic target in H3K27M-mutant diffuse midline glioma. Neuro Oncol. 2022;24(10):1700-11.
10. He WG, Yan Y, Tang W, Cai R, Ren G. Clinical and biological features of neuroblastic tumors: A comparison of neuroblastoma and ganglioneuroblastoma. Oncotarget. 2017;8(23):37730-9.
11. Shimada H, Ikegaki N. Genetic and Histopathological Heterogeneity of Neuroblastoma and Precision Therapeutic Approaches for Extremely Unfavorable Histology Subgroups. Biomolecules. 2022;12(1).
12. van Heerden J, Abraham N, Schoeman J, Reynders D, Singh E, Kruger M. Reporting Incidences of Neuroblastoma in Various Resource Settings. JCO Glob Oncol. 2021;7:947-64.
13. Steliarova-Foucher E, Colombet M, Ries LAG, Moreno F, Dolya A, Bray F, et al. International incidence of childhood cancer, 2001-10: a population-based registry study. Lancet Oncol. 2017;18(6):719-31.
14. Tas ML, Nagtegaal M, Kraal K, Tytgat GAM, Abeling N, Koster J, et al. Neuroblastoma stage 4S: Tumor regression rate and risk factors of progressive disease. Pediatr Blood Cancer. 2020;67(4):e28061.
15. Zeineldin M, Patel AG, Dyer MA. Neuroblastoma: When differentiation goes awry. Neuron. 2022;110(18):2916-28.
16. Qiu B, Matthay KK. Advancing therapy for neuroblastoma. Nat Rev Clin Oncol. 2022;19(8):515-33.
17. Kushner BH, Cheung NK. Neuroblastoma--from genetic profiles to clinical challenge. N Engl J Med. 2005;353(21):2215-7.
18. Maris JM. Recent advances in neuroblastoma. N Engl J Med. 2010;362(23):2202-11.
19. Maris JM, Hogarty MD, Bagatell R, Cohn SL. Neuroblastoma. Lancet. 2007;369(9579):2106-20.
20. Delloye-Bourgeois C, Castellani V. Hijacking of Embryonic Programs by Neural Crest-Derived Neuroblastoma: From Physiological Migration to Metastatic Dissemination. Front Mol Neurosci. 2019;12:52.
21. Blavier L, Nakata R, Neviani P, Sharma K, Shimada H, Benedicto A, et al. The capture of extracellular vesicles endogenously released by xenotransplanted tumours induces an inflammatory reaction in the premetastatic niche. J Extracell Vesicles. 2023;12(5):e12326.
22. Morgenstern DA, London WB, Stephens D, Volchenboum SL, Hero B, Di Cataldo A, et al. Metastatic neuroblastoma confined to distant lymph nodes (stage 4N) predicts outcome in patients with stage 4 disease: A study from the International Neuroblastoma Risk Group Database. J Clin Oncol. 2014;32(12):1228-35.

23. Iavarone A, Lasorella A, Servidei T, Riccardi R, Mastrangelo R. Uptake and storage of m-iodobenzylguanidine are frequent neuronal functions of human neuroblastoma cell lines. Cancer Res. 1993;53(2):304-9.
24. Geatti O, Shapiro B, Sisson JC, Hutchinson RJ, Mallette S, Eyre P, et al. Iodine-131 metaiodobenzylguanidine scintigraphy for the location of neuroblastoma: preliminary experience in ten cases. J Nucl Med. 1985;26(7):736-42.
25. Hero B, Hunneman DH, Gahr M, Berthold F. Evaluation of catecholamine metabolites, mIBG scan, and bone marrow cytology as response markers in stage 4 neuroblastoma. Med Pediatr Oncol. 2001;36(1):220-3.
26. Whittle SB, Smith V, Doherty E, Zhao S, McCarty S, Zage PE. Overview and recent advances in the treatment of neuroblastoma. Expert Rev Anticancer Ther. 2017;17(4):369-86.
27. Shimada H, Chatten J, Newton WA, Jr., Sachs N, Hamoudi AB, Chiba T, et al. Histopathologic prognostic factors in neuroblastic tumors: definition of subtypes of ganglioneuroblastoma and an age-linked classification of neuroblastomas. J Natl Cancer Inst. 1984;73(2):405-16.
28. Sano H, Bonadio J, Gerbing RB, London WB, Matthay KK, Lukens JN, et al. International neuroblastoma pathology classification adds independent prognostic information beyond the prognostic contribution of age. Eur J Cancer. 2006;42(8):1113-9.
29. Cohn SL, Pearson AD, London WB, Monclair T, Ambros PF, Brodeur GM, et al. The International Neuroblastoma Risk Group (INRG) classification system: an INRG Task Force report. J Clin Oncol. 2009;27(2):289-97.
30. Nakazawa A, Haga C, Ohira M, Okita H, Kamijo T, Nakagawara A. Correlation between the International Neuroblastoma Pathology Classification and genomic signature in neuroblastoma. Cancer Sci. 2015;106(6):766-71.
31. Matsui A, Ihara T, Suda H, Mikami H, Semba K. Gene amplification: mechanisms and involvement in cancer. Biomol Concepts. 2013;4(6):567-82.
32. Huang M, Weiss WA. Neuroblastoma and MYCN. Cold Spring Harb Perspect Med. 2013;3(10):a014415.
33. Trigg RM, Turner SD. ALK in Neuroblastoma: Biological and Therapeutic Implications. Cancers (Basel). 2018;10(4).
34. Passoni L, Longo L, Collini P, Coluccia AM, Bozzi F, Podda M, et al. Mutation-independent anaplastic lymphoma kinase overexpression in poor prognosis neuroblastoma patients. Cancer Res. 2009;69(18):7338-46.
35. Molenaar JJ, Domingo-Fernandez R, Ebus ME, Lindner S, Koster J, Drabek K, et al. LIN28B induces neuroblastoma and enhances MYCN levels via let-7 suppression. Nat Genet. 2012;44(11):1199-206.
36. Fetahu IS, Taschner-Mandl S. Neuroblastoma and the epigenome. Cancer Metastasis Rev. 2021;40(1):173-89.
37. Janoueix-Lerosey I, Schleiermacher G, Michels E, Mosseri V, Ribeiro A, Lequin D, et al. Overall genomic pattern is a predictor of outcome in neuroblastoma. J Clin Oncol. 2009;27(7):1026-33.
38. Henrich KO, Schwab M, Westermann F. 1p36 tumor suppression--a matter of dosage? Cancer Res. 2012;72(23):6079-88.
39. Schleiermacher G, Janoueix-Lerosey I, Ribeiro A, Klijanienko J, Couturier J, Pierron G, et al. Accumulation of segmental alterations determines progression in neuroblastoma. J Clin Oncol. 2010;28(19):3122-30.
40. Rivera Z, Escutia C, Madonna MB, Gupta KH. Biological Insight and Recent Advancement in the Treatment of Neuroblastoma. Int J Mol Sci. 2023;24(10).
41. Mora J. Autologous Stem-Cell Transplantation for High-Risk Neuroblastoma: Historical and Critical Review. Cancers (Basel). 2022;14(11).
42. Mora J, Castaneda A, Colombo MC, Gorostegui M, Gomez F, Mane S, et al. Clinical and Pathological Evidence of Anti-GD2 Immunotherapy Induced Differentiation in Relapsed/Refractory High-Risk Neuroblastoma. Cancers (Basel). 2021;13(6).

43. Morandi F, Sabatini F, Podesta M, Airoldi I. Immunotherapeutic Strategies for Neuroblastoma: Present, Past and Future. Vaccines (Basel). 2021;9(1).
44. Munoz JP, Larrosa C, Chamorro S, Perez-Jaume S, Simao M, Sanchez-Sierra N, et al. Early Salvage Chemo-Immunotherapy with Irinotecan, Temozolomide and Naxitamab Plus GM-CSF (HITS) for Patients with Primary Refractory High-Risk Neuroblastoma Provide the Best Chance for Long-Term Outcomes. Cancers (Basel). 2023;15(19).
45. Kennedy PT, Zannoupa D, Son MH, Dahal LN, Woolley JF. Neuroblastoma: an ongoing cold front for cancer immunotherapy. J Immunother Cancer. 2023;11(11).
46. Heczey A, Courtney AN, Montalbano A, Robinson S, Liu K, Li M, et al. Anti-GD2 CAR-NKT cells in patients with relapsed or refractory neuroblastoma: an interim analysis. Nature medicine. 2020;26(11):1686-90.
47. Del Bufalo F, De Angelis B, Caruana I, Del Baldo G, De Ioris MA, Serra A, et al. GD2-CART01 for Relapsed or Refractory High-Risk Neuroblastoma. The New England journal of medicine. 2023;388(14):1284-95.
48. Sun J, Huye LE, Lapteva N, Mamonkin M, Hiregange M, Ballard B, et al. Early transduction produces highly functional chimeric antigen receptor-modified virus-specific T-cells with central memory markers: a Production Assistant for Cell Therapy (PACT) translational application. J Immunother Cancer. 2015;3:5.
49. Pinto NR, Albert CM, Taylor M, Wilson A, Rawlings-Rhea S, Huang W, et al. Effect of bispecific B7H3 x CD19 CAR T cells on host CD19 expression and CAR T cell engraftment. Journal of Clinical Oncology. 2023;41(16_suppl):10043-.
50. Ponzoni M, Bachetti T, Corrias MV, Brignole C, Pastorino F, Calarco E, et al. Recent advances in the developmental origin of neuroblastoma: an overview. J Exp Clin Cancer Res. 2022;41(1):92.
51. Cheung NK, Dyer MA. Neuroblastoma: developmental biology, cancer genomics and immunotherapy. Nat Rev Cancer. 2013;13(6):397-411.
52. Kameneva P, Artemov AV, Kastriti ME, Faure L, Olsen TK, Otte J, et al. Single-cell transcriptomics of human embryos identifies multiple sympathoblast lineages with potential implications for neuroblastoma origin. Nat Genet. 2021;53(5):694-706.
53. Dong R, Yang R, Zhan Y, Lai HD, Ye CJ, Yao XY, et al. Single-Cell Characterization of Malignant Phenotypes and Developmental Trajectories of Adrenal Neuroblastoma. Cancer Cell. 2020;38(5):716-33 e6.
54. Jansky S, Sharma AK, Korber V, Quintero A, Toprak UH, Wecht EM, et al. Single-cell transcriptomic analyses provide insights into the developmental origins of neuroblastoma. Nat Genet. 2021;53(5):683-93.
55. Furlan A, Dyachuk V, Kastriti ME, Calvo-Enrique L, Abdo H, Hadjab S, et al. Multipotent peripheral glial cells generate neuroendocrine cells of the adrenal medulla. Science. 2017;357(6346).
56. Tsubota S, Kadomatsu K. Origin and initiation mechanisms of neuroblastoma. Cell Tissue Res. 2018;372(2):211-21.
57. Fares J, Fares MY, Khachfe HH, Salhab HA, Fares Y. Molecular principles of metastasis: a hallmark of cancer revisited. Signal Transduct Target Ther. 2020;5(1):28.
58. Massague J, Obenauf AC. Metastatic colonization by circulating tumour cells. Nature. 2016;529(7586):298-306.
59. Pastushenko I, Brisebarre A, Sifrim A, Fioramonti M, Revenco T, Boumahdi S, et al. Identification of the tumour transition states occurring during EMT. Nature. 2018;556(7702):463-8.
60. De Craene B, Berx G. Regulatory networks defining EMT during cancer initiation and progression. Nat Rev Cancer. 2013;13(2):97-110.
61. Lee CK, Jeong SH, Jang C, Bae H, Kim YH, Park I, et al. Tumor metastasis to lymph nodes requires YAP-dependent metabolic adaptation. Science. 2019;363(6427):644-9.
62. Peinado H, Zhang H, Matei IR, Costa-Silva B, Hoshino A, Rodrigues G, et al. Pre-metastatic niches: organ-specific homes for metastases. Nat Rev Cancer. 2017;17(5):302-17.

63. Moore LD, Le T, Fan G. DNA methylation and its basic function. Neuropsychopharmacology. 2013;38(1):23-38.
64. Kravitz CJ, Yan Q, Nguyen DX. Epigenetic markers and therapeutic targets for metastasis. Cancer Metastasis Rev. 2023;42(2):427-43.
65. Greger V, Passarge E, Hopping W, Messmer E, Horsthemke B. Epigenetic changes may contribute to the formation and spontaneous regression of retinoblastoma. Hum Genet. 1989;83(2):155-8.
66. Sole C, Lawrie CH. MicroRNAs in Metastasis and the Tumour Microenvironment. Int J Mol Sci. 2021;22(9).
67. O'Carroll D, Schaefer A. General principals of miRNA biogenesis and regulation in the brain. Neuropsychopharmacology. 2013;38(1):39-54.
68. Treiber T, Treiber N, Meister G. Regulation of microRNA biogenesis and its crosstalk with other cellular pathways. Nat Rev Mol Cell Biol. 2019;20(1):5-20.
69. Hill M, Tran N. miRNA interplay: mechanisms and consequences in cancer. Dis Model Mech. 2021;14(4).
70. Ara T, DeClerck YA. Mechanisms of invasion and metastasis in human neuroblastoma. Cancer Metastasis Rev. 2006;25(4):645-57.
71. Nolan JC, Frawley T, Tighe J, Soh H, Curtin C, Piskareva O. Preclinical models for neuroblastoma: Advances and challenges. Cancer Lett. 2020;474:53-62.
72. Biedler JL, Helson L, Spengler BA. Morphology and growth, tumorigenicity, and cytogenetics of human neuroblastoma cells in continuous culture. Cancer research. 1973;33(11):2643-52.
73. Boeva V, Louis-Brennetot C, Peltier A, Durand S, Pierre-Eugene C, Raynal V, et al. Heterogeneity of neuroblastoma cell identity defined by transcriptional circuitries. Nat Genet. 2017;49(9):1408-13.
74. Verly IRN, Leen R, Meinsma JR, Hooijer GKJ, Savci-Heijink CD, van Nes J, et al. Catecholamine excretion profiles identify clinical subgroups of neuroblastoma patients. European journal of cancer (Oxford, England : 1990). 2019;111:21-9.
75. Thirant C, Peltier A, Durand S, Kramdi A, Louis-Brennetot C, Pierre-Eugene C, et al. Reversible transitions between noradrenergic and mesenchymal tumor identities define cell plasticity in neuroblastoma. Nat Commun. 2023;14(1):2575.
76. Gautier M, Thirant C, Delattre O, Janoueix-Lerosey I. Plasticity in Neuroblastoma Cell Identity Defines a Noradrenergic-to-Mesenchymal Transition (NMT). Cancers (Basel). 2021;13(12).
77. Sehgal M, Nayak SP, Sahoo S, Somarelli JA, Jolly MK. Mutually exclusive teams-like patterns of gene regulation characterize phenotypic heterogeneity along the noradrenergic-mesenchymal axis in neuroblastoma. Cancer Biol Ther. 2024;25(1):2301802.
78. Mabe NW, Huang M, Dalton GN, Alexe G, Schaefer DA, Geraghty AC, et al. Transition to a mesenchymal state in neuroblastoma confers resistance to anti-GD2 antibody via reduced expression of ST8SIA1. Nat Cancer. 2022;3(8):976-93.
79. Asgharzadeh S, Salo JA, Ji L, Oberthuer A, Fischer M, Berthold F, et al. Clinical significance of tumor-associated inflammatory cells in metastatic neuroblastoma. J Clin Oncol. 2012;30(28):3525-32.
80. Yuan X, Seneviratne JA, Du S, Xu Y, Chen Y, Jin Q, et al. Single-cell profiling of peripheral neuroblastic tumors identifies an aggressive transitional state that bridges an adrenergic-mesenchymal trajectory. Cell Rep. 2022;41(1):111455.
81. Aygun N. Biological and Genetic Features of Neuroblastoma and Their Clinical Importance. Curr Pediatr Rev. 2018;14(2):73-90.
82. Veeraraghavan VP, Jayaraman S, Rengasamy G, Mony U, Ganapathy DM, Geetha RV, et al. Deciphering the Role of MicroRNAs in Neuroblastoma. Molecules. 2021;27(1).
83. Braekeveldt N, Bexell D. Patient-derived xenografts as preclinical neuroblastoma models. Cell Tissue Res. 2018;372(2):233-43.
84. Majidpoor J, Mortezaee K. Steps in metastasis: an updated review. Med Oncol. 2021;38(1):3.

85. Kamili A, Atkinson C, Trahair TN, Fletcher JI. Mouse models of high-risk neuroblastoma. Cancer Metastasis Rev. 2020;39(1):261-74.
86. Ziegler MM, Ishizu H, Nagabuchi E, Takada N, Arya G. A comparative review of the immunobiology of murine neuroblastoma and human neuroblastoma. Cancer. 1997;79(9):1757-66.
87. Lode HN, Dreier T, Xiang R, Varki NM, Kang AS, Reisfeld RA. Gene therapy with a single chain interleukin 12 fusion protein induces T cell-dependent protective immunity in a syngeneic model of murine neuroblastoma. Proc Natl Acad Sci U S A. 1998;95(5):2475-80.
88. Chen Q, Wang J, Liu WN, Zhao Y. Cancer Immunotherapies and Humanized Mouse Drug Testing Platforms. Transl Oncol. 2019;12(7):987-95.
89. de Visser KE, Joyce JA. The evolving tumor microenvironment: From cancer initiation to metastatic outgrowth. Cancer Cell. 2023;41(3):374-403.
90. Liu Y, Cao X. Characteristics and Significance of the Pre-metastatic Niche. Cancer Cell. 2016;30(5):668-81.
91. Blavier L, Yang RM, DeClerck YA. The Tumor Microenvironment in Neuroblastoma: New Players, New Mechanisms of Interaction and New Perspectives. Cancers (Basel). 2020;12(10).
92. Orimo A, Gupta PB, Sgroi DC, Arenzana-Seisdedos F, Delaunay T, Naeem R, et al. Stromal fibroblasts present in invasive human breast carcinomas promote tumor growth and angiogenesis through elevated SDF-1/CXCL12 secretion. Cell. 2005;121(3):335-48.
93. Erez N, Truitt M, Olson P, Arron ST, Hanahan D. Cancer-Associated Fibroblasts Are Activated in Incipient Neoplasia to Orchestrate Tumor-Promoting Inflammation in an NF-kappaB-Dependent Manner. Cancer Cell. 2010;17(2):135-47.
94. Kennel KB, Bozlar M, De Valk AF, Greten FR. Cancer-Associated Fibroblasts in Inflammation and Antitumor Immunity. Clin Cancer Res. 2023;29(6):1009-16.
95. Hashimoto O, Yoshida M, Koma Y, Yanai T, Hasegawa D, Kosaka Y, et al. Collaboration of cancer-associated fibroblasts and tumour-associated macrophages for neuroblastoma development. The Journal of pathology. 2016;240(2):211-23.
96. Borriello L, Nakata R, Sheard MA, Fernandez GE, Sposto R, Malvar J, et al. Cancer-Associated Fibroblasts Share Characteristics and Protumorigenic Activity with Mesenchymal Stromal Cells. Cancer Res. 2017;77(18):5142-57.
97. Kok VC, Yu CC. Cancer-Derived Exosomes: Their Role in Cancer Biology and Biomarker Development. Int J Nanomedicine. 2020;15:8019-36.
98. Dai J, Su Y, Zhong S, Cong L, Liu B, Yang J, et al. Exosomes: key players in cancer and potential therapeutic strategy. Signal Transduct Target Ther. 2020;5(1):145.
99. Zhou Y, Zhang Y, Gong H, Luo S, Cui Y. The Role of Exosomes and Their Applications in Cancer. Int J Mol Sci. 2021;22(22).
100. Cooks T, Pateras IS, Jenkins LM, Patel KM, Robles AI, Morris J, et al. Mutant p53 cancers reprogram macrophages to tumor supporting macrophages via exosomal miR-1246. Nat Commun. 2018;9(1):771.
101. Fonseka P, Liem M, Ozcitti C, Adda CG, Ang CS, Mathivanan S. Exosomes from N-Myc amplified neuroblastoma cells induce migration and confer chemoresistance to non-N-Myc amplified cells: implications of intra-tumour heterogeneity. J Extracell Vesicles. 2019;8(1):1597614.
102. Colletti M, Petretto A, Galardi A, Di Paolo V, Tomao L, Lavarello C, et al. Proteomic Analysis of Neuroblastoma-Derived Exosomes: New Insights into a Metastatic Signature. Proteomics. 2017;17(23-24).
103. Quintanilla M, Montero-Montero L, Renart J, Martin-Villar E. Podoplanin in Inflammation and Cancer. Int J Mol Sci. 2019;20(3).
104. Breiteneder-Geleff S, Matsui K, Soleiman A, Meraner P, Poczewski H, Kalt R, et al. Podoplanin, novel 43-kd membrane protein of glomerular epithelial cells, is down-regulated in puromycin nephrosis. Am J Pathol. 1997;151(4):1141-52.
105. Suzuki H, Kaneko MK, Kato Y. Roles of Podoplanin in Malignant Progression of Tumor. Cells. 2022;11(3).

106. Pradhan S, Guddattu V, Solomon MC. Association of the co-expression of SOX2 and Podoplanin in the progression of oral squamous cell carcinomas - an immunohistochemical study. J Appl Oral Sci. 2019;27:e20180348.
107. Meng D, Luo M, Liu B. The Role of CLEC-2 and Its Ligands in Thromboinflammation. Front Immunol. 2021;12:688643.
108. Martin-Villar E, Megias D, Castel S, Yurrita MM, Vilaro S, Quintanilla M. Podoplanin binds ERM proteins to activate RhoA and promote epithelial-mesenchymal transition. J Cell Sci. 2006;119(Pt 21):4541-53.
109. Ugorski M, Dziegiel P, Suchanski J. Podoplanin - a small glycoprotein with many faces. Am J Cancer Res. 2016;6(2):370-86.
110. Wicki A, Lehembre F, Wick N, Hantusch B, Kerjaschki D, Christofori G. Tumor invasion in the absence of epithelial-mesenchymal transition: podoplanin-mediated remodeling of the actin cytoskeleton. Cancer Cell. 2006;9(4):261-72.
111. Schacht V, Dadras SS, Johnson LA, Jackson DG, Hong YK, Detmar M. Up-regulation of the lymphatic marker podoplanin, a mucin-type transmembrane glycoprotein, in human squamous cell carcinomas and germ cell tumors. Am J Pathol. 2005;166(3):913-21.
112. Shimada Y, Ishii G, Nagai K, Atsumi N, Fujii S, Yamada A, et al. Expression of podoplanin, CD44, and p63 in squamous cell carcinoma of the lung. Cancer Sci. 2009;100(11):2054-9.
113. Kunita A, Baeriswyl V, Meda C, Cabuy E, Takeshita K, Giraudo E, et al. Inflammatory Cytokines Induce Podoplanin Expression at the Tumor Invasive Front. Am J Pathol. 2018;188(5):1276-88.
114. Ito T, Ishii G, Nagai K, Nagano T, Kojika M, Murata Y, et al. Low podoplanin expression of tumor cells predicts poor prognosis in pathological stage IB squamous cell carcinoma of the lung, tissue microarray analysis of 136 patients using 24 antibodies. Lung Cancer. 2009;63(3):418-24.
115. Longatto-Filho A, Pinheiro C, Pereira SM, Etlinger D, Moreira MA, Jube LF, et al. Lymphatic vessel density and epithelial D2-40 immunoreactivity in pre-invasive and invasive lesions of the uterine cervix. Gynecol Oncol. 2007;107(1):45-51.
116. Durchdewald M, Guinea-Viniegra J, Haag D, Riehl A, Lichter P, Hahn M, et al. Podoplanin is a novel fos target gene in skin carcinogenesis. Cancer research. 2008;68(17):6877-83.
117. Krishnan H, Rayes J, Miyashita T, Ishii G, Retzbach EP, Sheehan SA, et al. Podoplanin: An emerging cancer biomarker and therapeutic target. Cancer science. 2018;109(5):1292-9.
118. Inoue H, Miyazaki Y, Kikuchi K, Yoshida N, Ide F, Ohmori Y, et al. Podoplanin promotes cell migration via the EGF-Src-Cas pathway in oral squamous cell carcinoma cell lines. J Oral Sci. 2012;54(3):241-50.
119. Toyoshima M, Nakajima M, Yamori T, Tsuruo T. Purification and characterization of the platelet-aggregating sialoglycoprotein gp44 expressed by highly metastatic variant cells of mouse colon adenocarcinoma 26. Cancer Res. 1995;55(4):767-73.
120. Watanabe M, Okochi E, Sugimoto Y, Tsuruo T. Identification of a platelet-aggregating factor of murine colon adenocarcinoma 26: Mr 44,000 membrane protein as determined by monoclonal antibodies. Cancer Res. 1988;48(22):6411-6.
121. Watanabe M, Sugimoto Y, Tsuruo T. Expression of a Mr 41,000 glycoprotein associated with thrombin-independent platelet aggregation in high metastatic variants of murine B16 melanoma. Cancer Res. 1990;50(20):6657-62.
122. Sugimoto Y, Watanabe M, Oh-hara T, Sato S, Isoe T, Tsuruo T. Suppression of experimental lung colonization of a metastatic variant of murine colon adenocarcinoma 26 by a monoclonal antibody 8F11 inhibiting tumor cell-induced platelet aggregation. Cancer Res. 1991;51(3):921-5.
123. Kato Y, Kaneko MK, Kunita A, Ito H, Kameyama A, Ogasawara S, et al. Molecular analysis of the pathophysiological binding of the platelet aggregation-inducing factor podoplanin to the C-type lectin-like receptor CLEC-2. Cancer Sci. 2008;99(1):54-61.
124. Mehta P. Potential role of platelets in the pathogenesis of tumor metastasis. Blood. 1984;63(1):55-63.

125. Reymond N, d'Agua BB, Ridley AJ. Crossing the endothelial barrier during metastasis. Nat Rev Cancer. 2013;13(12):858-70.
126. Hughes CE, Pollitt AY, Mori J, Eble JA, Tomlinson MG, Hartwig JH, et al. CLEC-2 activates Syk through dimerization. Blood. 2010;115(14):2947-55.
127. Senbanjo LT, Chellaiah MA. CD44: A Multifunctional Cell Surface Adhesion Receptor Is a Regulator of Progression and Metastasis of Cancer Cells. Front Cell Dev Biol. 2017;5:18.
128. Martin-Villar E, Fernandez-Munoz B, Parsons M, Yurrita MM, Megias D, Perez-Gomez E, et al. Podoplanin associates with CD44 to promote directional cell migration. Mol Biol Cell. 2010;21(24):4387-99.
129. Martin-Villar E, Borda-d'Agua B, Carrasco-Ramirez P, Renart J, Parsons M, Quintanilla M, et al. Podoplanin mediates ECM degradation by squamous carcinoma cells through control of invadopodia stability. Oncogene. 2015;34(34):4531-44.
130. Li YY, Zhou CX, Gao Y. Podoplanin promotes the invasion of oral squamous cell carcinoma in coordination with MT1-MMP and Rho GTPases. Am J Cancer Res. 2015;5(2):514-29.
131. Zhao P, Xu Y, Wei Y, Qiu Q, Chew TL, Kang Y, et al. The CD44s splice isoform is a central mediator for invadopodia activity. J Cell Sci. 2016;129(7):1355-65.
132. de Winde CM, George SL, Crosas-Molist E, Hari-Gupta Y, Arp AB, Benjamin AC, et al. Podoplanin drives dedifferentiation and amoeboid invasion of melanoma. iScience. 2021;24(9):102976.
133. Tozluoglu M, Tournier AL, Jenkins RP, Hooper S, Bates PA, Sahai E. Matrix geometry determines optimal cancer cell migration strategy and modulates response to interventions. Nat Cell Biol. 2013;15(7):751-62.
134. Ribatti D, Nico B, Cimpean AM, Raica M. Podoplanin and LYVE-1 expression in lymphatic vessels of human neuroblastoma. J Neurooncol. 2010;100(1):151-2.
135. Ramani P, Somerville MS, May MT. Podoplanin lymphatic density and invasion correlate with adverse clinicopathologic and biological factors and survival in neuroblastomas. Am J Surg Pathol. 2012;36(6):908-15.
136. Bieniasz-Krzywiec P, Martin-Perez R, Ehling M, Garcia-Caballero M, Pinioti S, Pretto S, et al. Podoplanin-Expressing Macrophages Promote Lymphangiogenesis and Lymphoinvasion in Breast Cancer. Cell Metab. 2019;30(5):917-36 e10.
137. Neri S, Ishii G, Hashimoto H, Kuwata T, Nagai K, Date H, et al. Podoplanin-expressing cancer-associated fibroblasts lead and enhance the local invasion of cancer cells in lung adenocarcinoma. Int J Cancer. 2015;137(4):784-96.
138. Yamanashi T, Nakanishi Y, Fujii G, Akishima-Fukasawa Y, Moriya Y, Kanai Y, et al. Podoplanin expression identified in stromal fibroblasts as a favorable prognostic marker in patients with colorectal carcinoma. Oncology. 2009;77(1):53-62.
139. Komohara Y, Jinushi M, Takeya M. Clinical significance of macrophage heterogeneity in human malignant tumors. Cancer Sci. 2014;105(1):1-8.
140. Carrasco-Ramirez P, Greening DW, Andres G, Gopal SK, Martin-Villar E, Renart J, et al. Podoplanin is a component of extracellular vesicles that reprograms cell-derived exosomal proteins and modulates lymphatic vessel formation. Oncotarget. 2016;7(13):16070-89.
141. Cimini M, Kishore R. Role of Podoplanin-Positive Cells in Cardiac Fibrosis and Angiogenesis After Ischemia. Front Physiol. 2021;12:667278.
142. Fujita N, Takagi S. The impact of Aggrus/podoplanin on platelet aggregation and tumour metastasis. J Biochem. 2012;152(5):407-13.
143. Tawil N, Bassawon R, Meehan B, Nehme A, Montermini L, Gayden T, et al. Glioblastoma cell populations with distinct oncogenic programs release podoplanin as procoagulant extracellular vesicles. Blood Adv. 2021;5(6):1682-94.
144. Fonseca P, Vardaki I, Occhionero A, Panaretakis T. Metabolic and Signaling Functions of Cancer Cell-Derived Extracellular Vesicles. Int Rev Cell Mol Biol. 2016;326:175-99.

145. Kim SB. Function and therapeutic development of exosomes for cancer therapy. Arch Pharm Res. 2022;45(5):295-308.
146. Sharma P, Schiapparelli L, Cline HT. Exosomes function in cell-cell communication during brain circuit development. Curr Opin Neurobiol. 2013;23(6):997-1004.
147. Retzbach EP, Sheehan SA, Nevel EM, Batra A, Phi T, Nguyen ATP, et al. Podoplanin emerges as a functionally relevant oral cancer biomarker and therapeutic target. Oral Oncol. 2018;78:126-36.
148. Kato Y, Kaneko MK, Kuno A, Uchiyama N, Amano K, Chiba Y, et al. Inhibition of tumor cell-induced platelet aggregation using a novel anti-podoplanin antibody reacting with its platelet-aggregation-stimulating domain. Biochem Biophys Res Commun. 2006;349(4):1301-7.
149. Abe S, Kaneko MK, Tsuchihashi Y, Izumi T, Ogasawara S, Okada N, et al. Antitumor effect of novel anti-podoplanin antibody NZ-12 against malignant pleural mesothelioma in an orthotopic xenograft model. Cancer science. 2016;107(9):1198-205.
150. Takagi S, Sato S, Oh-hara T, Takami M, Koike S, Mishima Y, et al. Platelets promote tumor growth and metastasis via direct interaction between Aggrus/podoplanin and CLEC-2. PLoS One. 2013;8(8):e73609.
151. Chang YW, Hsieh PW, Chang YT, Lu MH, Huang TF, Chong KY, et al. Identification of a novel platelet antagonist that binds to CLEC-2 and suppresses podoplanin-induced platelet aggregation and cancer metastasis. Oncotarget. 2015;6(40):42733-48.
152. Krishnan H, Retzbach EP, Ramirez MI, Liu T, Li H, Miller WT, et al. PKA and CDK5 can phosphorylate specific serines on the intracellular domain of podoplanin (PDPN) to inhibit cell motility. Exp Cell Res. 2015;335(1):115-22.
153. Ashour AE, Jamal S, Cheryan VT, Muthu M, Zoheir KM, Alafeefy AM, et al. CARP-1 functional mimetics: a novel class of small molecule inhibitors of medulloblastoma cell growth. PLoS One. 2013;8(6):e66733.
154. Cheriyan VT, Wang Y, Muthu M, Jamal S, Chen D, Yang H, et al. Disulfiram suppresses growth of the malignant pleural mesothelioma cells in part by inducing apoptosis. PLoS One. 2014;9(4):e93711.
155. Kato T, Furusawa A, Okada R, Inagaki F, Wakiyama H, Furumoto H, et al. Near-Infrared Photoimmunotherapy Targeting Podoplanin-Expressing Cancer Cells and Cancer-Associated Fibroblasts. Mol Cancer Ther. 2023;22(1):75-88.
156. Ishikawa A, Waseda M, Ishii T, Kaneko MK, Kato Y, Kaneko S. Improved anti-solid tumor response by humanized anti-podoplanin chimeric antigen receptor transduced human cytotoxic T cells in an animal model. Genes Cells. 2022;27(9):549-58.
157. Shiina S, Ohno M, Ohka F, Kuramitsu S, Yamamichi A, Kato A, et al. CAR T Cells Targeting Podoplanin Reduce Orthotopic Glioblastomas in Mouse Brains. Cancer Immunol Res. 2016;4(3):259-68.
158. Kaneko MK, Yamada S, Nakamura T, Abe S, Nishioka Y, Kunita A, et al. Antitumor activity of chLpMab-2, a human-mouse chimeric cancer-specific antihuman podoplanin antibody, via antibody-dependent cellular cytotoxicity. Cancer Med. 2017;6(4):768-77.
159. Zhang Z, Zhang N, Yu J, Xu W, Gao J, Lv X, et al. The Role of Podoplanin in the Immune System and Inflammation. J Inflamm Res. 2022;15:3561-72.
160. Takemoto A, Takagi S, Ukaji T, Gyobu N, Kakino M, Takami M, et al. Targeting Podoplanin for the Treatment of Osteosarcoma. Clin Cancer Res. 2022;28(12):2633-45.
161. Schneider CA, Rasband WS, Eliceiri KW. NIH Image to ImageJ: 25 years of image analysis. Nat Methods. 2012;9(7):671-5.
162. Bengtsson H, Wirapati P, Speed TP. A single-array preprocessing method for estimating full-resolution raw copy numbers from all Affymetrix genotyping arrays including GenomeWideSNP 5 & 6. Bioinformatics. 2009;25(17):2149-56.
163. Ritchie ME, Phipson B, Wu D, Hu Y, Law CW, Shi W, et al. limma powers differential expression analyses for RNA-sequencing and microarray studies. Nucleic Acids Res. 2015;43(7):e47.

164. Xie Z, Bailey A, Kuleshov MV, Clarke DJB, Evangelista JE, Jenkins SL, et al. Gene Set Knowledge Discovery with Enrichr. Curr Protoc. 2021;1(3):e90.
165. Huang HY, Lin YC, Cui S, Huang Y, Tang Y, Xu J, et al. miRTarBase update 2022: an informative resource for experimentally validated miRNA-target interactions. Nucleic Acids Res. 2022;50(D1):D222-D30.
166. Lopez-Alemany R, Tirado OM. Metastasis Assessment in Ewing Sarcoma Using Orthotopic Xenografts. Methods Mol Biol. 2021;2226:201-13.
167. Arimoto S, Hasegawa T, Takeda D, Saito I, Amano R, Akashi M, et al. Lymphangiogenesis and Lymph Node Metastasis in Oral Squamous Cell Carcinoma. Anticancer Res. 2018;38(11):6157-62.
168. Gong B, Li Y, Cheng Z, Wang P, Luo L, Huang H, et al. GRIK3: A novel oncogenic protein related to tumor TNM stage, lymph node metastasis, and poor prognosis of GC. Tumour Biol. 2017;39(6):1010428317704364.
169. Zhai T, Muhanhali D, Jia X, Wu Z, Cai Z, Ling Y. Identification of gene co-expression modules and hub genes associated with lymph node metastasis of papillary thyroid cancer. Endocrine. 2019;66(3):573-84.
170. Cai J, Gong L, Li G, Guo J, Yi X, Wang Z. Exosomes in ovarian cancer ascites promote epithelial-mesenchymal transition of ovarian cancer cells by delivery of miR-6780b-5p. Cell Death Dis. 2021;12(2):210.
171. Wang J, Song C, Tang H, Zhang C, Tang J, Li X, et al. miR-629-3p may serve as a novel biomarker and potential therapeutic target for lung metastases of triple-negative breast cancer. Breast Cancer Res. 2017;19(1):72.
172. Ghafouri-Fard S, Khoshbakht T, Hussen BM, Kadkhoda S, Taheri M, Tafrishinejad A. A Review on the Role of miR-149-5p in the Carcinogenesis. Int J Mol Sci. 2021;23(1).
173. Fardin P, Barla A, Mosci S, Rosasco L, Verri A, Versteeg R, et al. A biology-driven approach identifies the hypoxia gene signature as a predictor of the outcome of neuroblastoma patients. Mol Cancer. 2010;9:185.
174. Delloye-Bourgeois C, Bertin L, Thoinet K, Jarrosson L, Kindbeiter K, Buffet T, et al. Microenvironment-Driven Shift of Cohesion/Detachment Balance within Tumors Induces a Switch toward Metastasis in Neuroblastoma. Cancer Cell. 2017;32(4):427-43 e8.
175. van Groningen T, Koster J, Valentijn LJ, Zwijnenburg DA, Akogul N, Hasselt NE, et al. Neuroblastoma is composed of two super-enhancer-associated differentiation states. Nat Genet. 2017;49(8):1261-6.
176. Radaelli E, Santagostino SF, Sellers RS, Brayton CF. Immune Relevant and Immune Deficient Mice: Options and Opportunities in Translational Research. ILAR J. 2018;59(3):211-46.
177. Chen J, Liao S, Xiao Z, Pan Q, Wang X, Shen K, et al. The development and improvement of immunodeficient mice and humanized immune system mouse models. Front Immunol. 2022;13:1007579.
178. Xu Y, Mao Y, Lv Y, Tang W, Xu J. B cells in tumor metastasis: friend or foe? Int J Biol Sci. 2023;19(8):2382-93.
179. Verhoeven BM, Mei S, Olsen TK, Gustafsson K, Valind A, Lindstrom A, et al. The immune cell atlas of human neuroblastoma. Cell Rep Med. 2022;3(6):100657.
180. McNerney KO, Karageorgos SA, Hogarty MD, Bassiri H. Enhancing Neuroblastoma Immunotherapies by Engaging iNKT and NK Cells. Front Immunol. 2020;11:873.
181. Castriconi R, Dondero A, Cilli M, Ognio E, Pezzolo A, De Giovanni B, et al. Human NK cell infusions prolong survival of metastatic human neuroblastoma-bearing NOD/scid mice. Cancer Immunol Immunother. 2007;56(11):1733-42.
182. DuBois SG, Macy ME, Henderson TO. High-Risk and Relapsed Neuroblastoma: Toward More Cures and Better Outcomes. Am Soc Clin Oncol Educ Book. 2022;42:1-13.
183. Braekeveldt N, Wigerup C, Gisselsson D, Mohlin S, Merselius M, Beckman S, et al. Neuroblastoma patient-derived orthotopic xenografts retain metastatic patterns and geno- and phenotypes of patient tumours. Int J Cancer. 2015;136(5):E252-61.

184. Vo KT, Matthay KK, Neuhaus J, London WB, Hero B, Ambros PF, et al. Clinical, biologic, and prognostic differences on the basis of primary tumor site in neuroblastoma: a report from the international neuroblastoma risk group project. J Clin Oncol. 2014;32(28):3169-76.
185. Aschero R, Castillo-Ecija H, Baulenas-Farres M, Resa-Pares C, Jimenez-Cabaco A, Rodriguez E, et al. Prognostic value of xenograft engraftment in patients with metastatic high-risk neuroblastoma. Pediatr Blood Cancer. 2023;70(6):e30318.
186. Castillo-Ecija H, Pascual-Pasto G, Perez-Jaume S, Resa-Pares C, Vila-Ubach M, Monterrubio C, et al. Prognostic value of patient-derived xenograft engraftment in pediatric sarcomas. J Pathol Clin Res. 2021;7(4):338-49.
187. Fernandez JL, Arbogen S, Sadeghinia MJ, Haram M, Snipstad S, Torp SH, et al. A Comparative Analysis of Orthotopic and Subcutaneous Pancreatic Tumour Models: Tumour Microenvironment and Drug Delivery. Cancers (Basel). 2023;15(22).
188. Hinshaw DC, Shevde LA. The Tumor Microenvironment Innately Modulates Cancer Progression. Cancer Res. 2019;79(18):4557-66.
189. Gomez RL, Ibragimova S, Ramachandran R, Philpott A, Ali FR. Tumoral heterogeneity in neuroblastoma. Biochim Biophys Acta Rev Cancer. 2022;1877(6):188805.
190. Liu Y, Zhao S, Wang J, Zhu Z, Luo L, Xiang Q, et al. MiR-629-5p Promotes Prostate Cancer Development and Metastasis by Targeting AKAP13. Front Oncol. 2021;11:754353.
191. Wu L, Zuo N, Pan S, Wang Y, Wang Q, Ma J. miR-1246 Promotes Laryngeal Squamous Cell Carcinoma Progression by Interacting with THBS1. J Environ Pathol Toxicol Oncol. 2022;41(3):65-75.
192. Li Y, Zeng S, Cao L. Mir-629 Repressed LATS2 Expression and Promoted the Proliferation of Prostate Cancer Cells. Horm Metab Res. 2023;55(8):573-9.
193. Ghafouri-Fard S, Khoshbakht T, Hussen BM, Taheri M, Samadian M. A Review on the Role of miR-1246 in the Pathoetiology of Different Cancers. Front Mol Biosci. 2021;8:771835.
194. Pan C, Fei Q, Jin J, Zheng J, Wu D, Li H, et al. MicroRNA profiling reveals the role of miR-133b-3p in promoting apoptosis and inhibiting cell proliferation and testosterone synthesis in mouse TM3 cells. In Vitro Cell Dev Biol Anim. 2023;59(1):63-75.
195. Wang J, Xiao D, Wang J. A 16-miRNA Prognostic Model to Predict Overall Survival in Neuroblastoma. Front Genet. 2022;13:827842.
196. Gomez S, Castellano G, Mayol G, Queiros A, Martin-Subero JI, Lavarino C. DNA methylation fingerprint of neuroblastoma reveals new biological and clinical insights. Genom Data. 2015;5:360-3.
197. Sugino RP, Ohira M, Mansai SP, Kamijo T. Comparative epigenomics by machine learning approach for neuroblastoma. BMC Genomics. 2022;23(1):852.
198. Iswariya GT, Paital B, Padma PR, Nirmaladevi R. microRNAs: Epigenetic players in cancer and aging. Front Biosci (Schol Ed). 2019;11(1):29-55.
199. Saviana M, Le P, Micalo L, Del Valle-Morales D, Romano G, Acunzo M, et al. Crosstalk between miRNAs and DNA Methylation in Cancer. Genes (Basel). 2023;14(5).
200. Jahangiri L. Neuroblastoma Interaction with the Tumour Microenvironment and Its Implications for Treatment and Disease Progression. Curr Oncol. 2023;30(10):9116-40.
201. Zhang SM, Wei CY, Wang Q, Wang L, Lu L, Qi FZ. M2-polarized macrophages mediate wound healing by regulating connective tissue growth factor via AKT, ERK1/2, and STAT3 signaling pathways. Mol Biol Rep. 2021;48(9):6443-56.
202. Asif PJ, Longobardi C, Hahne M, Medema JP. The Role of Cancer-Associated Fibroblasts in Cancer Invasion and Metastasis. Cancers (Basel). 2021;13(18).
203. Ma H, Jiang S, Yuan Y, Li J, Li Y, Lv Y, et al. RUNX1 promotes proliferation and migration in non-small cell lung cancer cell lines via the mTOR pathway. FASEB J. 2023;37(11):e23195.
204. Louault K, Porras T, Lee MH, Muthugounder S, Kennedy RJ, Blavier L, et al. Fibroblasts and macrophages cooperate to create a pro-tumorigenic and immune resistant environment via activation of TGF-beta/IL-6 pathway in neuroblastoma. Oncoimmunology. 2022;11(1):2146860.
205. Smith HA, Kang Y. The metastasis-promoting roles of tumor-associated immune cells. J Mol Med (Berl). 2013;91(4):411-29.

206. Hussain S, Peng B, Cherian M, Song JW, Ahirwar DK, Ganju RK. The Roles of Stroma-Derived Chemokine in Different Stages of Cancer Metastases. Front Immunol. 2020;11:598532.
207. Naleskina LA, Kunska LM, Chekhun VF. Modern views on the role of main components of stroma and tumor microinvironment in invasion, migration and metastasis. Exp Oncol. 2020;42(4):252-62.
208. Castriconi R, Dondero A, Bellora F, Moretta L, Castellano A, Locatelli F, et al. Neuroblastoma-derived TGF-beta1 modulates the chemokine receptor repertoire of human resting NK cells. J Immunol. 2013;190(10):5321-8.
209. Perera M, Tsang CS, Distel RJ, Lacy JN, Ohno-Machado L, Ricchiuti V, et al. TGF-beta1 interactome: metastasis and beyond. Cancer Genomics Proteomics. 2010;7(4):217-29.
210. Raica M, Cimpean AM, Ribatti D. The role of podoplanin in tumor progression and metastasis. Anticancer Res. 2008;28(5B):2997-3006.
211. Sharma G, Kumar R, Singh HP, Gupta M, Gupta M. Expression of podoplanin in tumor cells and lymphatic vessels in both tumoral and peritumoral areas and correlation with metastatic potential of oral squamous cell carcinoma. J Oral Maxillofac Pathol. 2021;25(1):131-5.
212. Sasano T, Gonzalez-Delgado R, Munoz NM, Carlos-Alcade W, Cho MS, Sheth RA, et al. Podoplanin promotes tumor growth, platelet aggregation, and venous thrombosis in murine models of ovarian cancer. J Thromb Haemost. 2022;20(1):104-14.
213. Liu Z, Zeinalzadeh Z, Huang T, Han Y, Peng L, Wang D, et al. Mitochondria-related chemoradiotherapy resistance genes-based machine learning model associated with immune cell infiltration on the prognosis of esophageal cancer and its value in pan-cancer. Transl Oncol. 2024;42:101896.
214. Nakashima Y, Yoshinaga K, Kitao H, Ando K, Kimura Y, Saeki H, et al. Podoplanin is expressed at the invasive front of esophageal squamous cell carcinomas and is involved in collective cell invasion. Cancer Sci. 2013;104(12):1718-25.
215. Friedman G, Levi-Galibov O, David E, Bornstein C, Giladi A, Dadiani M, et al. Cancer-associated fibroblast compositions change with breast cancer progression linking the ratio of S100A4(+) and PDPN(+) CAFs to clinical outcome. Nat Cancer. 2020;1(7):692-708.
216. van Malenstein H, Dekervel J, Verslype C, Van Cutsem E, Windmolders P, Nevens F, et al. Long-term exposure to sorafenib of liver cancer cells induces resistance with epithelial-to-mesenchymal transition, increased invasion and risk of rebound growth. Cancer Lett. 2013;329(1):74-83.
217. Pisco AO, Huang S. Non-genetic cancer cell plasticity and therapy-induced stemness in tumour relapse: 'What does not kill me strengthens me'. Br J Cancer. 2015;112(11):1725-32.
218. Martin-Villar E, Yurrita MM, Fernandez-Munoz B, Quintanilla M, Renart J. Regulation of podoplanin/PA2.26 antigen expression in tumour cells. Involvement of calpain-mediated proteolysis. Int J Biochem Cell Biol. 2009;41(6):1421-9.
219. Wang X, Li W, Bi J, Wang J, Ni L, Shi Q, et al. Association of high PDPN expression with pulmonary metastasis of osteosarcoma and patient prognosis. Oncol Lett. 2019;18(6):6323-30.
220. Modrek AS, Eskilsson E, Ezhilarasan R, Wang Q, Goodman LD, Ding Y, et al. PDPN marks a subset of aggressive and radiation-resistant glioblastoma cells. Front Oncol. 2022;12:941657.
221. Pastushenko I, Blanpain C. EMT Transition States during Tumor Progression and Metastasis. Trends Cell Biol. 2019;29(3):212-26.
222. Kaufhold S, Bonavida B. Central role of Snail1 in the regulation of EMT and resistance in cancer: a target for therapeutic intervention. J Exp Clin Cancer Res. 2014;33(1):62.
223. Tang X, Sui X, Weng L, Liu Y. SNAIL1: Linking Tumor Metastasis to Immune Evasion. Front Immunol. 2021;12:724200.
224. Astarita JL, Acton SE, Turley SJ. Podoplanin: emerging functions in development, the immune system, and cancer. Front Immunol. 2012;3:283.
225. Li YY, Zhou CX, Gao Y. Interaction between oral squamous cell carcinoma cells and fibroblasts through TGF-beta1 mediated by podoplanin. Exp Cell Res. 2018;369(1):43-53.

226. Krylova SV, Feng D. The Machinery of Exosomes: Biogenesis, Release, and Uptake. Int J Mol Sci. 2023;24(2).
227. Yang X, Zhang Y, Zhang Y, Zhang S, Qiu L, Zhuang Z, et al. The Key Role of Exosomes on the Pre-metastatic Niche Formation in Tumors. Front Mol Biosci. 2021;8:703640.
228. Wu M, Shi Y, Liu Y, Huang H, Che J, Shi J, et al. Exosome-transmitted podoplanin promotes tumor-associated macrophage-mediated immune tolerance in glioblastoma. CNS Neurosci Ther. 2024;30(3):e14643.
229. Wang M, Qin Z, Wan J, Yan Y, Duan X, Yao X, et al. Tumor-derived exosomes drive pre-metastatic niche formation in lung via modulating CCL1(+) fibroblast and CCR8(+) Treg cell interactions. Cancer Immunol Immunother. 2022;71(11):2717-30.
230. Jia W, Liang S, Lin W, Li S, Yuan J, Jin M, et al. Hypoxia-induced exosomes facilitate lung pre-metastatic niche formation in hepatocellular carcinoma through the miR-4508-RFX1-IL17A-p38 MAPK-NF-kappaB pathway. Int J Biol Sci. 2023;19(15):4744-62.
231. Gu J, Chu X, Huo Y, Liu C, Chen Q, Hu S, et al. Gastric cancer-derived exosomes facilitate pulmonary metastasis by activating ERK-mediated immunosuppressive macrophage polarization. J Cell Biochem. 2023;124(4):557-72.
232. Srivastava A, Babu A, Filant J, Moxley KM, Ruskin R, Dhanasekaran D, et al. Exploitation of Exosomes as Nanocarriers for Gene-, Chemo-, and Immune-Therapy of Cancer. J Biomed Nanotechnol. 2016;12(6):1159-73.
233. Kim H, Kim EH, Kwak G, Chi SG, Kim SH, Yang Y. Exosomes: Cell-Derived Nanoplatforms for the Delivery of Cancer Therapeutics. Int J Mol Sci. 2020;22(1).
234. Di C, Zhang Q, Wang Y, Wang F, Chen Y, Gan L, et al. Exosomes as drug carriers for clinical application. Artif Cells Nanomed Biotechnol. 2018;46(sup3):S564-S70.
235. Sheng M, Sun R, Fu J, Lu G. The podoplanin-CLEC-2 interaction promotes platelet-mediated melanoma pulmonary metastasis. BMC Cancer. 2024;24(1):399.